UNIVERSITÉ DE SHERBROOKE
Faculté de génie
Département de génie civil

PUNCHING SHEAR BEHAVIOR OF GFRP-RC EDGE SLAB COLUMN CONNECTIONS WITH AND WITHOUT SHEAR STIRRUPS REINFORCEMENT

COMPORTEMENT AU POINCONNEMENT DE JONCTIONS DALLE-POTEAU DE RIVE EN BETON ARME DE PRFV AVEC OU SANS ÉTRIERS ARMATURES DE CISAILLEMENT

Thèse de doctorat
Spécialité: génie civil

Ahmed El-Sayed Salem Ahmed SALAMA
(Ahmed Salama)

A dissertation submitted in partial fulfillment
of the requirements for the degree of
Doctor of Philosophy
(Civil Engineering)

MEMBRES DU JURY : Prof. Mathieu ROBERT (Président du jury)
Prof. Brahim BENMOKRANE (Directeur de recherche)
Prof. Adel EL-SAFTY (Examinateur)
Prof. PV VIJAY (Examinateur)
Prof. Nathalie ROY (Examinateur)

Sherbrooke (Québec) Canada
October 2019

DEDICATION

I dedicate this dissertation to my mom, she was my greatest teacher, a teacher of compassion, love and fearlessness. If love is sweet as a flower, then my mother is that sweet flower of love. I got to grow up with a mother who taught me to believe in myself, even when nobody else does.

ABSTRACT

Flat plates are commonly used in parking garages due to their functional and economic advantages. Slabs in parking garages are susceptible to accelerated deterioration due to harsh environment exposure as diffusion of de-icing salts, which, in turn, causing steel-corrosion problems. The use of Glass Fiber-Reinforced Polymers (GFRP) bars has yielded a great interest as an innovative solution to overcome such problems. However, flat plate structural system is vulnerable to a type of brittle failure known as a punching-shear failure. This failure exaggerated more in the case of edge slab connections due to the lack of symmetry of the portion of the slab resisting the punching action and relatively large unbalanced moments to be transferred between the slab and column may produce significant shear stresses that increase the likelihood of brittle failure. Experimental and analytical investigations are carried out to examine the punching-shear strength and behavior of reinforced concrete (RC) edge slab-column connections totally reinforced in flexure with GFRP bars. The experimental work included edge slab-column connections without and with GFRP stirrups as shear reinforcement. Nine full-scale connections—one reinforced with steel bars for comparison, five reinforced solely with GFRP bars in flexural, and three reinforced with GFRP bars and stirrups—were constructed and tested to failure under combined vertical shear force and unbalanced moment. All slabs had identical geometries of 2500×1350×200 mm with a 300-mm square column stub protruding 700 mm above and below the slab surfaces. The investigated parameters are: (1) GFRP stirrups type (closed and spiral); (2) stirrups extension (1.75d and 4.25d); (3) flexural reinforcement ratio (1.04% and 1.55%) and type (steel and GFRP); (4) concrete strength (normal and high-strength concretes); and (5) moment-to-shear (*M/V*) ratios (0.3 m and 0.6 m). The analytical investigation is conducted through two phases. Phase I, focused on design codes assessment and proposing simplified design approaches for connections without and with shear reinforcement, respectively. Assessment of the available punching-shear equations provided by FRP design provisions , ACI 440.1R-15; CSA S806-12; and JSCE-97, is conducted by comparing their predictions against the experimental results for the tested connections and other specimens in the literature. Phase II focused on a 3D non-linear finite element analysis (FEA) using ANSYS software to simulate the behavior of the tested connections with shear reinforcement. Then, a comprehensive parametric study was performed to investigate the key parameters influencing

the shear capacity of such connections. The test results revealed that the final mode of connections without shear reinforcement was punching shear failure with no signs of concrete crushing. However, existence of GFRP stirrups shear reinforcement was shown to be essential for significant warning before failure. GFRP stirrups shear reinforcement extended to 4.25d yielded a significant effect in enhancing the shear strength, deformation capacity and leading to mixed flexure/punching shear failure with considerable deformability. High-strength concrete directly enhanced punching-shear capacity, load-deflection response, initial stiffness as well as evidenced fewer and narrower cracks compared to their counterparts constructed with normal-strength concrete. Meanwhile, increasing the *M/V* ratio for normal and high strength concrete connections evidenced significant punching shear stresses causing reduction in the strength and limits the deformation capacity with subsequent brittle punching shear failure. On the other hand, the numerical results from the FEAs simulation adequately predicted the experimental responses for the tested GFRP edge connections with and without shear reinforcement and confirm the accuracy of the finite element model. Based on the results, a simplified design approache is proposed to estimate the punching capacity for GFRP-reinforced edge connections with shear stirrups. The model yielded good yet conservative predictions with respect to the experimental results as well as the available results in the literature. The recommendations presented herein may support the work of the North American technical committees engaged in the development of standards and design provisions for GFRP-RC slab-column connections columns subjected to combined vertical load and unbalanced moment.

keywords: Edge slab-column connections, Punching shear, unbalanced moment, GFRP bars, stirrups, shear reinforcement, high strength concrete, FEM, design codes, shear strength.

RÉSUMÉ

Les planchers-dalles ou dalles pleines sur poteaux sont couramment utilisés dans les stationnements en raison de leurs avantages fonctionnels et économiques. Les dalles de stationnements sont exposées à la dégradation accélérée due à l'exposition aux environnements rigoureux, comme la diffusion de sels de déverglaçage qui provoque des problèmes de corrosion de l'acier. L'utilisation de barres en polymère renforcé de fibres de verre (PRFV) a suscité un grand intérêt en tant que solution innovante pour résoudre de tels problèmes. Cependant, le système planchers-dalles est vulnérable à un type de rupture fragile appelée rupture par poinçonnement. Cette défaillance est encore plus amplifiée dans le cas des jonctions dalle-poteau de rive en raison de l'absence de symétrie de la partie de la dalle résistant au poinçonnement et des moments de transfert ou moments non équilibrés relativement importants à transférer entre la dalle et le poteau, pouvant produire des contraintes de cisaillement importantes, augmentant ainsi la probabilité de rupture fragile. Des études expérimentales et analytiques sont effectuées pour examiner la résistance au poinçonnement et le comportement des jonctions dalle-poteau de rive en béton armé, totalement renforcés en flexion avec des barres d'armature en PRFV. Le travail expérimental comprend des jonctions dalle-poteau de rive sans et avec des étriers en PRFV comme armature de cisaillement. Neuf (9) jonctions pleine grandeur (une jonction avec des barres d'armature en acier à des fins de comparaison, cinq jonctions avec uniquement des barres d'armature en flexion en PRFV et trois jonctions avec des barres et des étriers en PRFV) ont été fabriquées et testées jusqu'à la rupture sous une combinaison d'effort de cisaillement vertical et d'un moment non équilibré. Toutes les dalles avaient une géométrie identique de 2500 × 1350 × 200 mm avec un poteau de section carré de 300 mm de côté et ayant une saillie de 700 mm au-dessus et au-dessous des surfaces de la dalle. Les paramètres étudiés sont les suivants : (1) le type d'étrier en PRFV (fermé et en spirale) (2) – la longueur de prolongement des étriers (1,75d et 4,25d) (3) le taux d'armature en flexion (1,04 % et 1,55 %) et leur type (acier et PRFV) (4) la résistance en compression du béton (béton de résistance normale et béton à haute résistance) ; et (5) les rapports moment/cisaillement (*M/V*) (0,3 m et 0,6 m). L'étude analytique a été réalisée en deux phases. La phase I comportait l'évaluation des codes de conception et la proposition de méthodes de calcul simplifiées pour les jonctions sans

et avec armatures de cisaillement. L'évaluation des équations de poinçonnement disponibles dans les dispositions de conception à l'aide des PRF, ACI 440.1R-15; CSA S806-12; and JSCE-97, est effectuée en comparant leurs prévisions aux résultats expérimentaux des jonctions testées et d'autres spécimens dans la littérature. La phase II s'est concentrée sur une analyse 3D non linéaire par éléments finis (FEA) à l'aide du logiciel ANSYS pour simuler le comportement des jonctions testées. Ensuite, une étude paramétrique complète a été réalisée pour étudier les paramètres clés influençant la résistance au cisaillement de telles jonctions. Les résultats des essais ont montré que le dernier mode de jonction avec et sans armatures de cisaillement était la rupture par poinçonnement sans aucun signe d'écrasement du béton ou de rupture par glissement des barres d'armature. Cependant, la présence d'armatures de cisaillement constituées d'étriers en PRFV s'est avérée être un signe avant-coureur d'une rupture. Les armatures de cisaillement constituées d'étriers en PRFV prolongés de 4,25d ont eu un effet significatif sur l'amélioration de la résistance au cisaillement, sur la capacité de déformation et ont conduit à un mode de rupture par poinçonnement adouci, avec une déformabilité considérable. Le béton à haute résistance a directement contribué à améliorer la résistance au poinçonnement, la réponse charge-flèche, la rigidité initiale avec des fissures moins nombreuses et plus étroites par rapport aux spécimens construits avec du béton de résistance normale. Entre-temps, l'augmentation du rapport *M/V* pour les jonctions en béton normal et en béton à haute résistance s'est traduite par des contraintes de poinçonnement importantes, entraînant une réduction de la résistance et une limitation de la capacité de déformation, avec une rupture par poinçonnement fragile. D'autre part, les résultats numériques de la simulation par éléments finis ont permis de prédire de manière adéquate les réponses expérimentales pour les jonctions de rive en PRFV testées avec et sans armatures de cisaillement et de confirmer la précision du modèle par éléments finis. Sur la base des résultats, deux méthodes simplifiées de calcul sont proposées pour estimer la résistance au poinçonnement des jonctions de rive avec et sans étriers de cisaillement en PRFV. Les modèles ont montré de bonnes prédictions, mais prudentes par rapport aux résultats expérimentaux et aux résultats disponibles dans la littérature. Les recommandations présentées dans le présent document peuvent soutenir les travaux des comités techniques nord-américains chargés de l'élaboration des normes et des dispositions de conception des jonctions dalle-poteau en béton armé de PRFV soumises à une charge verticale et à un moment non équilibré.

Mots clés : Jonctions dalle-poteau de rive, poinçonnement, moment non équilibré, barres en PRFV, étriers, armatures de cisaillement, béton à haute résistance, FEM, codes de conception, résistance au cisaillement.

ACKNOWLEDGEMENT

First and foremost, thanks to Almighty ALLAH to whom I attribute all my knowledge and success in my life.

The author would like to express his gratefulness to his research director, **Prof. Brahim BENMOKRANE**, for his inspiration, motivation, guidance, and constructive criticism. It is due to his confidence in me, as well as his seemingly boundless patience that I have been able to do my best work; for this I am truly thankful. I cannot thank you enough for the limitless meetings, late-night conversations and technical brainstorming. This is beside the hand-by-hand work with dedication and devotion throughout this research program. Many thanks also go to my jury **Prof. Adel EL-SAFTY**, **Prof. PV VIJAY**, and **Prof. Nathalie ROY**.

The author is grateful to our group technical staff; **Mr. Jérôme LACROIX** and **Mr. Steven MACEACHERN** for their technical assistance in the experimental program during the laboratory work. The author also would like to thank all his colleagues in Prof. Benmokrane research group especially **Dr. Fareed ELGABBAS** and **Dr. Ahmed ABDELDAYEM** for their assistance and encourage.

I gratefully acknowledge scholarship granted to me by the Canada Research Chair in Advanced Composite Materials for Civil Structures and Natural Sciences and Engineering Research Council of Canada (**NSERC-Industry Research Chair program**). The author also would like to acknowledge **Pultrall Inc**. (Thetford Mines, Québec) which generously provided the FRP materials for the project.

I would like to express my deep appreciation and thanks to my father, my brothers, my sister and my wife's family, for their unlimited love, support, encouragement, duas, and prayers.

Finally, my words stand helpless, and cannot express my deep love and appreciation to my wife (**Eman**) for her continuous encouragement, steadfast support and typing of the manuscript. I cannot present this work without expressing my love to my little daughter (**Hana**) who enlightened my life with her smile.

Ahmed Salama

October 2019

TABLE OF CONTENTS

LIST OF TABLES

LIST OF FIGURES

CHAPTER 1
INTRODUCTION

1.1. General Background

Reinforced concrete flat plate structures are defined as uniform thicknesses slabs supported directly on columns without drop panels or column capitals. They are used commonly in parking structure as main structural systems. Other applications of flat plate structures are multi-story industrial buildings, warehouses, office buildings, public halls, and offshore structures. Flat plate structures provide architectural flexibility, more clear space, easier formwork and shorter construction time. In spite of their advantages, the ultimate strength of such structures is governed by the ultimate capacity of their connections. However, their connections are vulnerable to local brittle failure in the column periphery, known as a punching-shear failure. Punching failure can arise in such system when the column with a surrounding portion of the slab is pushed through the slab under the transfer of shear or combined shear and unbalanced moments. The combination of shear and unbalanced moment is inevitable at edge and comer column-plate connections and may occur at interior column-plate connections as the result of unequal spans, unequal loads on adjacent panels, or as a result of lateral loads (Shahab 1997). Unbalanced moments transferred between slabs and columns produces additional shear stresses leads to minimizing the strength of slab-column connection and increasing the likelihood of brittle punching failure. In addition, such failure is more critical at edge columns owing to the presence at the free edge of a smaller resisting section combined with a large bending moment (Dilger and shatila). To protect slab-column connections from such failures, caution is clearly needed in shear strength calculation and attention should be given to increase the punching shear strength (Hassan 2013).

Many parking structures in northern climates are deficient due corrosion of steel reinforcement and delamination of the concrete at the level of the top mat of reinforcement. Some conditions, such as, significant temperature fluctuations, use of deicing salts, and chlorides have created harsh environment conditions and make the hazard more severe. This can lead to a premature punching shear failure and redistribution of the forces to adjacent supports, causing additional

failures and possibly resulting in progressive collapse of the slab (Julie et al. 2014). There have been several cases of progressive collapse due to punching shear failure and steel corrosion problems include a parking garage collapse in Ville St. Laurent, Québec in 2008 (Fig 1.1), Hôtel de Ville parking garage deterioration in Québec, Canada, in 2010 (Hassan et al. 2013), and La Chancelière parking garage deterioration in Québec, Canada, in 2011 (Benmokrane et al. 2012).

Various solutions have been implemented to mitigate the accelerated deterioration of parking structures resulted from corrosion problems as using galvanized-steel bars and epoxy-coated steel bars. None of these techniques, however, has been proven to be cost-effective or a long-term solution. On the other hand, using fiber reinforced Polymer (FRP) bars as internal reinforcement for concrete structures in aggressive environment has emerged as an innovative solution to eliminate corrosion problems. Glass FRP (GFRP) reinforcing bars have recently gained wide acceptance as a viable construction material for sustainable new constructions due to the lower costs compared to the other FRP types.

(a) Corrosion of steel reinforcement (b) Catastrophic collapse of flooring slabs

Figure 1.1 – Punching shear failure in Ville St. Laurent parking garage (Julie et al. 2014)

GFRP reinforcing bars advantages paved the way to successful field applications as concrete reinforcement, especially in concrete parking structures. The implementation of GFRP bars in parking structures ago with an extensive research project conducted at the University of Sherbrooke. The experimental work presented in this dissertation extends that extensive research project. The first phase of this project has been completed (Dulude et al. 2013; Hassan et al. 2013a, b; and Hassan et al. 2014 a, b). A total of 30 GFRP-RC interior slab-column

connections were tested under concentric loading. This phase contributed to first field implementation of GFRP bars in flat slab parking structures in a demonstration area of 350 m^2 at Hôtel de Ville parking garage (Quebec, Canada, 2010). In addition to this achievement, it helped in designing the world' first flat-slab parking garage totally reinforced with GFRP bars: La Chancelière parking garage (Québec, Canada, 2011) (Benmokrane et al. 2012).

That notwithstanding, very limited research has been conducted on edge slab-column connections reinforced with FRP bars or grids (Zaghloul 2007, El Gendy and El-Salakawy 2016, Mostafa and El-Salakawy 2018). There is also the potential for FRP-shear reinforcement in the form of stirrups, shear studs, or shear bands to improve the punching-shear strength of two-way slabs reinforced with GFRP bars (Hassan et al. 2014 a, b; El-Gendy and El-12 Salakawy 2016; Mostafa and El-Salakawy 2018). To the authors' knowledge, no experimental or analytical investigations have been conducted to examine the effectiveness of GFRP-stirrup as shear reinforcement in GFRP edge slab-column connections. In addition, no research has been conducted to investigate the effect of different *M/V* ratios on GRRP-reinforced edge connections constructed with HSC. This has been the main impetus to carry out the current study to fill the gap of knowledge and provide information about these effects on the behavior of GFRP edge slab column connections. Then design provisions and recommendations for engineers in designing FRP edge slab-column connections were established.

1.2. Objectives and Scope

Experimental and analytical investigations on full-scale GFRP-RC edge slab–column connections with and without GFRP shear stirrups reinforcement under combined vertical shear and unbalanced moment were conducted. The punching shear strength and behavior of such connections is the main scope of this study.

Basically, the objectives of the current study can be summarized as follows:

1. Study the effectiveness of the GFRP stirrups, considering the effects of GFRP-stirrup type and extension within the slab in a crucifix layout around the column faces;

2. Investigates the punching strength of normal and high strength GFRP edge slab-column connections tested under different *M/V* ratios;
3. Evaluate the accuracy of the available punching-shear equations in different FRP codes and guides under shear force and unbalanced moment transfer;
4. Propose design provisions as an extension to CSA S806-12 and ACI 440.1R-15 to account the contribution of FRP shear stirrups and predict the ultimate capacity of such connections;
5. Perform a finite element parametric study using ANSYS software to expand the range of investigated parameters affecting the punching shear strength of GFRP edge slab-column connections with shear stirrups reinforcement ; and
6. Establish new punching-shear design equation to reasonably predict the ultimate shear strength for edge slab column connections with shear reinforcement on the basis of the finite element results.

1.3. Methodology

To achieve the foregoing objectives, a set of test specimens that comprised nine full scale specimens were fabricated and tested under combined vertical shear and unbalanced moment up to failure. The test specimens represented edge slab-column connections from a prototype of flat-plate parking structure with 5 × 5 m^2 square panels. One reinforced was reinforced with steel bars as a control specimen, five were reinforced with GFRP bars in flexural, and the remaining three were reinforced with GFRP bars and shear stirrups in different configurations and reinforcement ratios according to the studied parameters. The total ultimate factored loads on the prototype, including the slab weight, was estimated according to national building code of Canada (NBCC 2015). The prototype is analysed using Equivalent Frame Method in CSA A23.3-14 to determine the straining action on the selected connection. Then, the flexural design was conducted according to the CSA A23.3-14 for steel RC connection and the CSA S806 for GFRP RC edge connections, considering the requirement for structural integrity reinforcement in CSA A23.3-14. Given the absence of shear reinforcement provisions in the CSA S806-12; however, similar philosophies that are being used in the companion code, CSA A23.3-14, were adopted.

Analysis of the experimental results in terms of strength, deformability, slab–column rotation, concrete strains, and flexural and shear-reinforcement strains facilitate a better understanding of the behavior of GFRP edge slab–column connections with GFRP stirrups. Evaluation of the influence of shear stirrups type and extension was discussed. The experimental results were also analyzed, identifying the effect of different moment -to-shear ratios on the behavior of normal and high strength edge connections without shear reinforcement in terms of crack pattern, failure mode, deformability, cumulative energy absorption, ultimate strength. Documentation of the strain distribution in flexural reinforcement bars was also presented.

The experimental measurements captured the strain distribution in shear stirrups along perpendicular and parallel directions to the free edge of the slab to assist in a reasonable estimation of their contribution to punching shear capacity. As a result, a new design provisions as an extension to CSA S806-12 and ACI 44.1R-15 equations was proposed to account the contribution of FRP shear stirrups and predict the ultimate capacity of such connections. Evaluation of the ultimate capacity of tested edge connections without shear reinforcement according to the ACI 44.1R-15, CSA S806-12 codes and JSCE-97 punching shear equations was also introduced. Finally, Three-dimensional non-linear finite element analysis (FEA) is used to simulate tested edge slab-column connections with shear stirrups reinforcement using ANSYS software. The results from the finite element analysis validated against the experimental results to confirm the accuracy of the finite element model. Then, a comprehensive finite element parametric study is presented to expand the range of investigated parameters influencing the shear capacity of such connections. Based on the results, a simplified design approach is proposed to estimate the punching capacity for FRP-RC edge connections with shear reinforcement.

1.4. Organization of Dissertation

The dissertation consists of seven chapters. The contents of each chapter can be summarized as follows:

Chapter 1 of this dissertation presents background information on the research topic, the work objectives and the adopted methodology.

Chapter 2 introduces a literature review reporting the pertinent studies on FRP-RC edge slab column connections to this work in a chronological order. Some aspects such as failure modes and the most decisive parameters that affect the FRP slab-column connections' behavior are presented.

Chapter 3 gives the details of the experimental program and the testing procedure. The geometry and reinforcement details of the test specimens, shear reinforcement configuration, test setup and procedure, and the instrumentation details are presented.

The subsequent three chapters respectively correspond to three technical papers have submitted for publication in scientific journals:

Chapter 4: (Article 1) Salama, A. E., Hassan, M., and Benmokrane, B., 2018 (Published) "Effectiveness of GFRP Stirrups as Shear Reinforcement in GFRP-RC Edge Slab–Column Connections," *ACI Structural Journal, V. 116, No. 5*.

Chapter 5: (Article 2) Salama, A. E., Hassan, M., and Benmokrane, B., 2019 (Reviewed) "Behavior of Concrete Edge Column-Slab- Connections Reinforced with GFRP Bars Subjected to Different Moment-to-Shear Force Ratios," *Journal of Composites for Construction, ASCE*.

Chapter 6: (Article 3) Salama, A. E., Hassan, M., and Benmokrane, B., 2019 (Accepted) "Effect of GFRP Shear Stirrups on the Strength of Two-Way GFRPRC Edge Slabs: Experimental and Finite-Element Investigations," *Journal of Structural Engineering, ASCE.*

Chapter 7 presents a general conclusion of the results obtained from the experiments and analyses with respect to the problems and observations discussed throughout the dissertation in addition to recommendations for future work.

CHAPTER 2
LITERATURE REVIEW

2.1. Introduction

In this chapter, a survey of relevant previous works related to this research study is presented. A review for the behavior of steel edge slab column connections under moment and shear is first presented. Emphasis is given on the identifications of failure modes and main factors that affect the behavior. Afterwards, it presents a brief summary about FRP material constituents, manufacturing, and properties as well as previous studies pertinent to the subject under investigation.

2.2. Steel RC Edge Slab column connections

2.2.1. General Background

Reinforced concrete flat plates are commonly used as a main structural system in the buildings of North America and Europe since the beginning of the 20th century. Compared to beam-slab floor structure, the main advantages that can be rendered by flat slabs are reduction of floor height, easy construction and formwork and reduction of the construction cost. Slabs without column capitals and/or drop panels appeared in the 1950s. These slabs developed high shear stresses near the column and thus they were considered as vulnerable to the punching shear failure. The first flat slabs were designed by George M. Hill in 1901, however, the most famous contributors were C.A.P. Turner (1869-1955) in USA and R. Maillart (1872-1940) in Switzerland. Flat plate structures are employed in the construction of many multi-story buildings; such as parking garages, offices, hotels, and apartments (Fig. 2.1)

(a) Hotel building

(b) Office building

(c) Parking structures

(d) Commercial building (Dubai Tower)

Figure 2.1 – Flat plate structure applications (Salama 2016)

In flat plate structure, relatively large shear stresses are generated around the column periphery resulted from vertical shear forces or vertical shear forces combined with unbalanced moments transferred between the slab, that are sufficient to cause a local brittle failure around the column, known as a punching-shear failure. The unbalanced moment transfer occurs at edge slab column connections subjected to gravity loads due to the discontinuity of the slab. The existence of the unbalanced moment produces more shear stresses led to minimizing the strength and ductility of the connection. When designing edge slab column connections, the lack of symmetry of the portion of slab resisting this punching action and the large unbalanced moment to be resisted, must also be considered. Therefore, edge slab column connections behavior is generally dominated by punching shear stresses from shear and moment and its punching shear capacity constitutes a major concern in their design. Numerous experimental and analytical investigations have been devoted to study the behavior of edge steel RC slab-column

connections under shear and moment. Based on these studies; failure modes, punching shear behavior as well as the main parameters affecting the behavior and ultimate shear strength were identified. These issues will be discussed in the following subsections.

2.2.2. Mode of Failures

An edge slab-column connection transferring vertical shear and unbalanced moment may fail by flexure, punching or a combination of both modes. A slab with low flexural reinforcement ratio will fail in a ductile manner by developing complete yield lines (Park and Gamble 1980). If the slab shear strength is reached in a critical section, the slab will fail in diagonal tension near the side of the column where the vertical shear stresses are the highest. This will result in the column punching through the slab and the top flexural reinforcement splitting off the concrete cover near the side of the column.

Figures 2.3 and 2.4 show cracking patterns on the tension sides and along the free edge of specimens with shear reinforcement failing in punching shear under high and low eccentricities, respectively (Sherif 1996). On the tension side, the radial and circumferential flexure cracks appear first as the top flexural steel start to yield in the column vicinity, especially the bars crossing the column. The diagonal shear cracks will form at about 50 to 70% of the ultimate load, near the column side where shear stresses are maximum. The shear cracks will appear near the inner corners of the column and then towards the free edge.

The eccentricity, *M/V* ratio, of the shear force from critical section centroid near the column, is usually high edge. Thus, the shear stresses produced by the moment on the critical section near the free edge are larger and opposite to the stresses caused by the vertical shear force (Figure 2.2a). Therefore, the net vertical shear stresses on the critical section near the free edge are in the opposite direction to the applied vertical force. This causes the shear cracks across the free edge will propagate from the tension sides of the slab towards the compression side (Figure 2.3). For a critical section near the column subjected to low eccentricity, the direction of the vertical shear stresses on the critical section near the free edge will be in the direction of applied shear force (Figure 2.2b). Thus, the cracks across the free edge will propagate from compression side of the slab towards the tension side of the slab (Figure 3.4). Test results demonstrated that the formation of these inclined cracks across the free edge are usually dominant the form of final

punching surface regardless the value of eccentricity. It should be noted that this crack propagation is the same in the case of slabs without shear reinforcement.

The third mode of failure is the combination of flexure and punching; this is the case for slabs with well anchored shear reinforcement. The main role of shear reinforcement is to control the opening of the diagonal shear crack and consequently allow more load to be carried by the concrete and the transverse reinforcement. Thus, more flexural steel can yield before failure and the ductility of the connection is enhanced. The transverse reinforcement will increase the ductility by allowing more flexural steel to yield. Punching may happen after extensive yielding of flexural reinforcement in the column vicinity, or as a secondary phenomenon after the flexure failure.

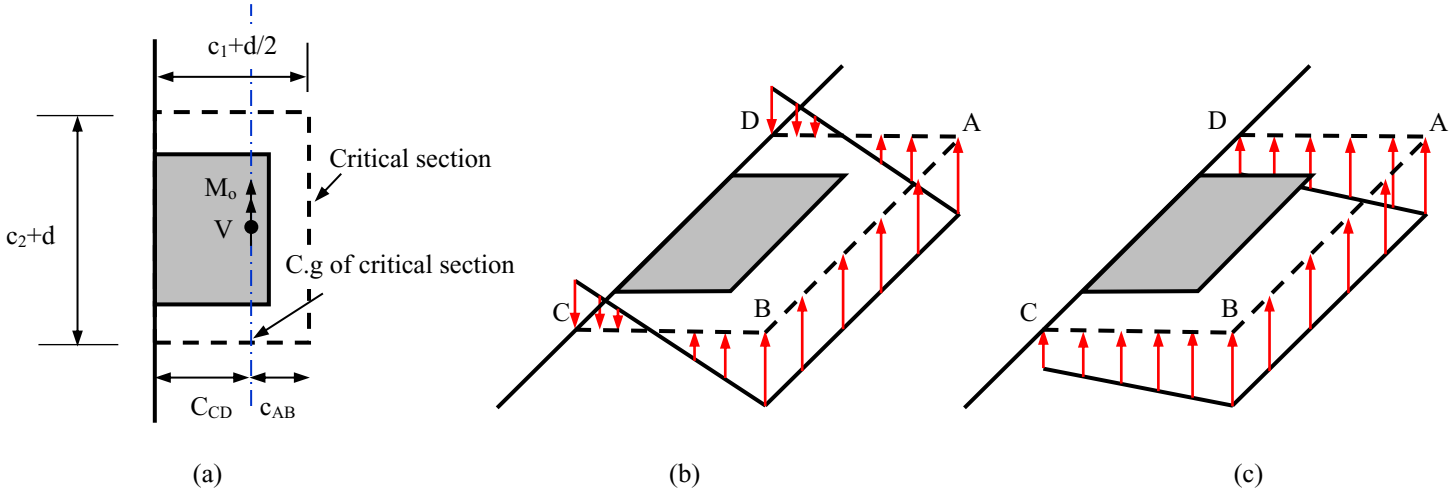

Figure 2.2 – Shear stress distribution due to shear and unbalanced moment: (a) Critical shear section; (b) High *M/V* ratio; (c) Low *M/V* ratio (Sherif 1996)

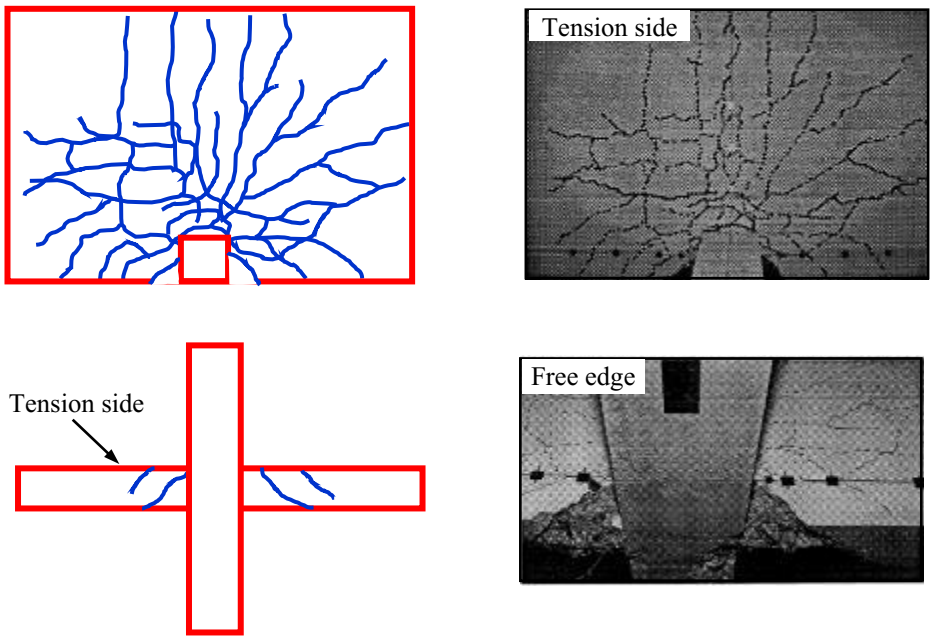

Figure 2.3 – Punching shear failure under high *M/V* ratio of 800 mm: (a) Schematic detail; (b) Photo (Sherif 1996)

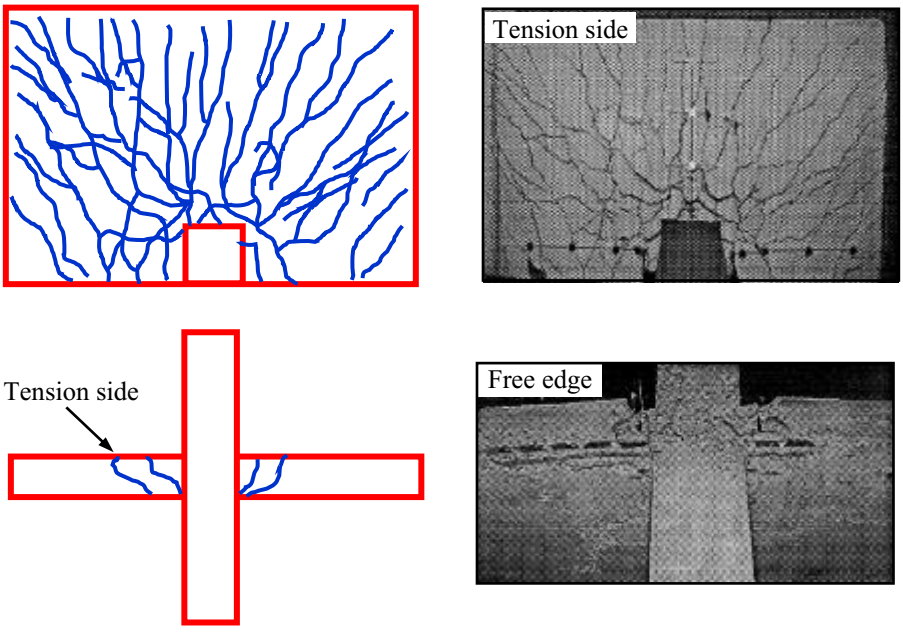

Figure 2.4 – Punching shear failure under low *M/V* ratio of 350 mm: (a) Schematic detail; (b) Photo (Sherif 1996)

2.2.3. Factors Affecting Edge Slab Column Connections Behavior

The experimental database compiled from previous experimental and analytical researches revealed that the punching shear behavior of edge slab column connections was governed by many factors such as flexural reinforcement ratio, shear reinforcement, *M/V*, and concrete strength. Summary about the effect of each parameter is briefly presented in the following subsections.

2.2.3.1. Flexural Reinforcement Ratio

There is an agreement that flexural reinforcement ratio is one of the most crucial parameters that affects the punching shear strength, ductility and mode of failure of slab column connections. Marzouk et al 1992 studied experimentally the effect of flexural reinforcement ratio (ranging between 0.6 to 2.4%) on punching shear capacity for high strength interior slabs with thickness ranging from 120 and 150 mm. They concluded the punching shear capacity increased by 63 % for slabs with 150 mm thickness when the reinforcement ratio was increased by threefold while, increased by 78% with an increase in reinforcement ratio from 0.9 to 2.3% for the slabs with 120-mm thickness. (Stein et al.2007) studied experimentally the effect of the flexural reinforcement ratio and Concluded that increasing the flexural reinforcement ratio controls flexural cracks so, the mode of failure changes from ductile flexural mode to brittle punching shear failure. Stein et al 2007 reported that the two main modes of failure of slab column connections are flexure and punching failures. Rizk et al 2011 tested ten full-scale interior slab-column connections with different reinforcement ratios to examine the effect of reinforcement ratio on punching shear capacity. Rizk et al. (2011) reported that increase of reinforcement ratio from 0.52% to 2.17% increases maximum punching shear capacity by 40% and punching capacity is not linearly proportional to the reinforcement ratio. The importance of including the effect of flexural reinforcement ratio on punching shear capacity equations is well recognized by many researchers. However, in current North American codes didn't consider the flexure reinforcement ratio as a variable in the design equations that predict punching shear capacity. The best power function for the reinforcement ratio is one third power based on extensive experimental analytical studies (Richart 1948, Regan and Bræstrup 1985; Gardner 1990; Takahashi et al. 1992; Sherif and Dilger 2000; Dilger 2000).

2.2.3.2. Shear Reinforcement

The use of shear reinforcement is an efficient solution that enhances both the ductility and punching shear. There are many types of shear reinforcement as closed stirrups, shear studs, shear bands, U-shaped stirrups, single leg stirrups, lattice reinforcement to avoid punching shear failure. These types have been tested seeking to evaluate their efficiency. Figure 2.5 shows the different types of shear reinforcement. The efficiency of shear reinforcement refers to many aspects such as the used type in addition to the ratio, distribution, spacing, anchorage which is usually critical in thin flat plates. Previous studies concluded that shear stirrups, is not fully effective, because it does not reach its yield strength before slab failure (Kinnunen and Nylander (1960), Franz (1963), Wantur (1969), Carpenter, et al (1970). On the other hand, Shear Stud provides ease in installation process around column zone; fully anchorage at top and bottom that develop yield in studs before failure and consequently increase ultimate capacity and ductility of the connection (Dilger et al 1978; Seible et al 1980; Dilger and Ghali 1981; Mokhtar et al 1985; Elgabry and Ghali 1987; Birkle and Dilger 2008; El Salakawy 1998; Heinzman et al 2012). Stein et al (2007) concluded that when the flexural capacity exceeds the punching shear capacity, the ultimate capacity of the connection will increase and the failure mode changes from brittle punching shear failure into ductile failure mode.

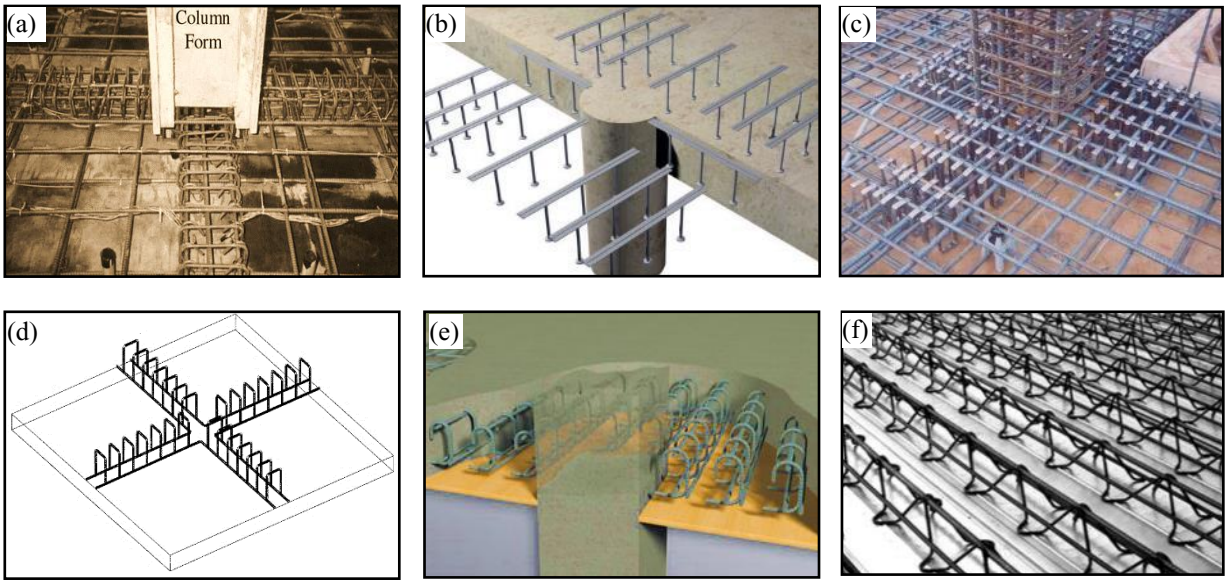

Figure 2.5 – Shear reinforcement types: (a) Closed stirrups; (b) Shear studs; (c) Shear bands; (d) U-shaped stirrups; (e) Single leg stirrups; (f) Lattice reinforcement (Salama 2016)

The work conducted by Mortin and Ghali (1991) is one of the early investigations that studied effect of shear studs on the behavior of edge connections under shear and moment. Mortin and Ghali (1991) reported tests on six edge connections loaded in shear and moment. Four of them contained stud shear reinforcement and two had no shear reinforcement. The tests showed a considerable improvement in shear strength and ductility when studs were provided. Increases in strength between 43 and 64 percent were noticed. Deflections at failure for specimens with studs were twice as much as those with no shear reinforcement. The two specimens with no shear reinforcement failed in punching. On the other hand, all four specimens with stud reinforcement failed in flexure. The stud reinforcement changed the failure mode from brittle punching shear failure to the more ductile flexural failure. Besides, Elgabry (1991) studied experimentally the effect of shear stud configuration on five full scale interior slab column connections under gravity loads associated with unbalanced moment. They concluded that increase in punching shear capacity up to 200% depended on shear stud configuration. El-Salakawy et al. **(**2000) investigated the influence of shear stud existence on the behavior of reinforced concrete edge slab column connections with openings in order to present and discuss the results of large-scale tests on slabs with shear stud reinforcement and compare these test results with those of tests on identical slabs but without shear reinforcement. The slabs had dimensions of 1540 × 1020 ×120 mm with square exterior column stub of side length 250 mm extending 700 mm above and below the slab. All specimens were subjected to a constant *M/V* of 0.3 m. El-Salakawy et al. (2000) concluded that using shear studs increases stiffness; shear capacity; and ductility of connections and the opening located at the side of the column affects the behavior less than the opening located in front of the column.

2.2.3.3. Moment-to-Shear Ratio (*M/V)*

Previous investigations on steel RC slab column connections have confirmed that increasing the *M/V* ratio decreases the ultimate capacity of the connection (Zaghlool and Rawdon de Paiva 1973; Marzouk et al. 1996, 2000; El-Salakawy et al. 1998; Ozden et al. 2006). The work conducted by Rosenthal (1959) is one of the early investigations that studied this parameter. Rosenthal (1959) reported the results of tests on simply supported circular reinforced concrete slabs. Rosenthal (1959) interior slab-column connections, three of these specimens were loaded eccentrically to produce the combined effect of shear and moment acting on the connections. For one of the latter three specimens, which were found to have failed in punching, a clear

unsymmetrical crack pattern was observed, accompanied by a 15% reduction in the connection capacity. This reduction was attributed to the effect of the moment induced in the connection by the eccentrically applied axial load. El-Salakawy et al. (1998) studied experimentally the effect of high *M/V* ratio on punching shear for eight full scale edge slab column connections reinforced with shear studs. The shear studs were arranged in six lines around the column as shown in Figure 2.12. El Salakawy et al. 1998 concluded that the mode of failure is changed from ductile flexural failure to more brittle flexural failure because of higher stresses for specimens subjected to high *M/V* ratio of 0.66 m, besides increase in punching shear capacity outside shear reinforced zone. Edge slab column connections subjected to high *M/V* ratio the shear stresses at the free edge reverse their direction . Consequently, the inclined cracks at the free edge propagate approximately perpendicular to the case of low *M/V* ratio (El-Salakawy et al. 1998).

2.2.3.4. Concrete Compressive Strength

Very limited researches have been devoted to study the influence of high strength concrete on the punching shear capacity of slab column connections under moment and shear. Marzouk et al. (1992) tested seventeen interor slabs with different grades of concrete where , fifteen slabs with high strength and two with normal strength . Based on the test results, a mechanical model was adopted and developed for high-strength concrete slab applications. The formulation takes into account the actual behavior of the high-strength concrete and steel. The proposed model gives a fairly good agreement between the predicted and experimental punching loads. Marzouk et al. (1998) tested six slabs with compressive strength varying from 35 to 75 MPa; the test result showed 7 to 15% increase in the shear strength when the concrete compressive strength was increased by 114%. In addition, these pervious investigations concluded that using the cubic root of the concrete compressive strength to predict the punching resistance of the slab-column connections generally yielded better results than the square root expression used in North American codes.

Ozden et al (2006) carried out a comprehensive experimental program involving twenty-six circular slab column connections, twelve six fabricated with normal strength concrete while the others constructed with high-strength concrete. The connections were tested under concentric and eccentric loads. The slab plates had a 1500 mm diameter circular geometry and 120 mm

thickness with a concentric 200 mm square central column stub, extending above and below the slab. The results indicate that concrete strength has a direct influence on the punching behavior and punching capacity of concrete slabs. The initial and post cracking stiff nesses of HSC specimens tested were higher than those of NSC specimens.CSA-A23.3-04 (CSA 2004) expressions result in conservative punching shear capacity predictions for concentrically loaded slabs and provide good agreement with the experimentally observed punching shear capacities for eccentrically loaded slabs.

2.3. FRP Composite Materials

In the last decades, steel corrosion is one of the major factors that leads to the accelerated deterioration for concrete infrastructures such as parking garages and bridges. This is typically due to significant temperature fluctuations, deicing salts, and chlorides have created harsh environment conditions accelerating the corrosion of steel. Solutions have been proposed to reduce the potential for corrosion and related degradation such as using galvanized-steel bars waterproofing membranes, epoxy-coated steel bars. None of these techniques, however, has been proven to be cost-effective or a long-term solution. The added cost of repairing deteriorated structures with replacement costs commonly more than twice the original cost of construction, led to the adoption of stricter specifications in some building codes and more stringent limits of chloride ions in construction materials. It also stimulated the recent major research efforts in design and construction techniques to improve the durability of reinforced concrete (Arafa 2017).

The use of fiber-reinforced polymer (FRP) bars provides a suitable solution for eliminating the potential of corrosion and the related deterioration. In addition, FRP can result in significant benefits related to the service life and reduce maintenance costs of concrete structures. Other advantages include high-strength and stiffness to-weight ratios, chemical attack resistance, thermal expansion control and electromagnetic neutrality. Due to the lower costs of glass FRP (GFRP) compared to the other FRP types, GFRP bars have been used widely in concrete bridge decks (Nanni and Faza 2002; Benmokrane et al. 2006), bridge barriers (El-Salakawy et al. 2003; Matta and Nanni 2009, bridge piers (De Luca et al. 2010) and recently parking garages (Ahmed

et al 2017, Hassan et al. 2013 a,b). A brief summary for FRP material Constituents, manufacturing process and properties is presented in the following subsections.

2.3.1. FRP Constituents

FRP products are composite materials consisting of reinforcing fibers impregnated with a matrix (resin). The fibers provide the mechanical strength and stiffness to the composite, while the resins transfer shear stresses between the fibers, protect the fibers from mechanical abrasion, and prevent the fibers from buckling. In order to provide the reinforcing function, the fiber-volume fraction should be more than 55 percent for FRP bars and rods and 35 percent for FRP grids (ISIS Product Certification #1, 2006).

Fibers

The most commonly used fibers for FRPs are aramid, carbon, glass, and recently basalt fibers. The performance of fibers is affected by their length, cross-sectional shape and chemical composition. Since glass FRP (GFRP) is more economical than the available types (carbon and aramid) of FRP bars, it is more attractive for the construction industry. GFRP characterized with high strength-to-weight ratio, low cost, electromagnetic neutrality, and chemical resistance. Nevertheless, the disadvantages are relatively low tensile modulus, sensitive to abrasion, and relatively low fatigue resistance. Glass fibers are classified as fiber drawn from an inorganic product of fusion that has cooled without crystallizing. The types of glass fibers commonly used are E-glass, S-glass and C-glass. E-glass has the lowest cost among all commercially available reinforcing fibers, which is the reason for its widespread use in the FRP industry (ISIS 2007).

Matrix (Resin)

The selection of the proper matrix (resin) significantly affects the final mechanical properties of the FRP product. In order to exploit the full strength of the fibers, the matrix should be able to develop a higher ultimate strain than the fibers (Phillips, 1989). There are two types of polymeric matrices widely used for FRP composites; namely, thermosetting and thermoplastic. However, thermosetting polymers are used more often than thermoplastic in FRP industry. They are low

molecular-weight liquids with very low viscosity, and their molecules are joined together by chemical cross-links. Hence, they form a rigid three-dimensional structure that once set, cannot be reshaped by applying heat or pressure.

2.3.2. Manufacturing Process

There are three common manufacturing techniques for FRP materials: pultrusion, braiding, and filament winding. Pultrusion is a common technique for manufacturing straight FRP bars. In this technique, Continuous strands of reinforcing material are drawn from creels, through a resin tank, where they are saturated with resin, and then through a number of wiper rings into the mouth of a heated die as shown in Figure 2.6. Before the FRP bars are cut to the required lengths, the bars surface must be treated in the form of spirals or with sand coating to create rough surface that creates a strong bond with concrete (ISIS 2007).

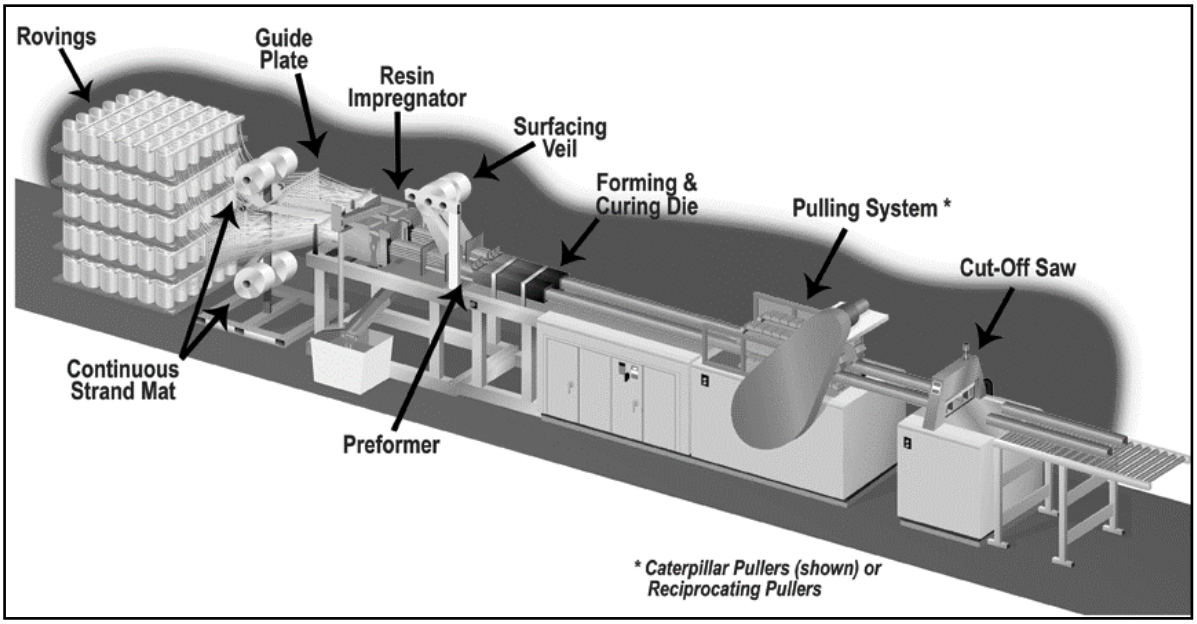

Figure 2.6 – Pultrusion process (www.strongwell.com, 2018)

2.3.3. Mechanical Properties

2.3.3.1. Tensile Strength

When loaded in tension, FRP bars do not exhibit any plastic behavior (yielding) before rupture. The tensile behavior of FRP bars consisting of one type of fiber material is characterized by a

linearly elastic stress-strain relationship until failure with a general lack of ductility, very high tensile strength and relatively low modulus of elasticity (Figure 2.7). The tensile strength and stiffness of an FRP bar are dependent on several factors. The most significant factors are fiber type and fiber-volume fraction that is defined as the ratio of the volume of fiber to the overall volume of the bar over the unit length. The rate of curing, the manufacturing process, and the manufacturing quality control also affect the mechanical characteristics of the bar (ACI 440.1R-15 and Wu 1990).

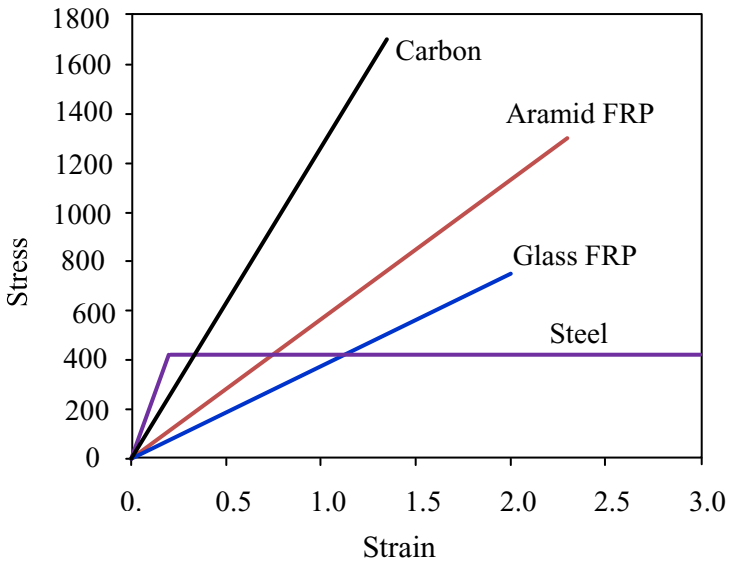

Figure 2.7 – Typical stress strain for steel and FRP bars (Ahmed 2009)

Unlike steel, the unit tensile strength of an FRP bar can vary with diameter. For example, GFRP bars from three different manufacturers show tensile strength reductions of up to 40% as the diameter increases proportionally from 0.375 to 0.875 in. (9.5 to 22.2 mm) (Faza and GangaRao 1993b). On the other hand, similar cross section changes do not seem to affect the strength of twisted CFRP strands (Santoh 1993). The sensitivity of AFRP bars to cross section size has been shown to vary from one commercial product to another. For example, in braided AFRP bars, there is a less than 2% strength reduction as bars increase in diameter from 0.28 to 0.58 in. (7.3 to 14.7 mm) (Tamura 1993). The strength reduction in a unidirectionally pultruded AFRP bar with added aramid fiber surface wraps is approximately 7% for diameters increasing from 0.12 to 0.32 in. (3 to 8 mm) (Noritake et al. 1993). The FRP bar manufacturer should be contacted for particular strength values of differently sized FRP bars.

2.3.3.2. Compression Strength

The ACI 440.1R-15 do not recommended to rely on FRP bars to resist compressive stresses, while the CSA S806-12 neglect the compressive contribution of FRP longitudinal reinforcement is design. Nevertheless, very limited research has been devoted to study the behavior of FRP bars under compression load. Wu 1990 reported that tests on FRP bars with a length-diameter ratio from 1:1 to 2:1 have shown that the compressive strength is lower than the tensile strength. The compressive modulus of elasticity of FRP bars depends on length-to-diameter ratio; bar size and type; and other factors, such as boundary conditions. In the reported results from compression tests, it is generally agreed that compressive stiffness ranges from 77 to 100% of the tensile stiffness (Bedard. 1992, Chaallal and Benmokrane 1993, Tavassoli et al. 2015), while the compressive strength is around 50% of the tensile strength. Experimental test results (De Luca et al. 2009; ; Issa et al. 2011, Deiveegan and Kumaran 2009) on the behavior of concrete columns entirely reinforced with glass fiber RC polymer (GFRP) reinforcement have also demonstrated the feasibility of such structural element.

2.3.3.3. Flexural Strength

The behavior of FRP RC sections is different compared to sections reinforced with traditional steel reinforcement. This is due to the different mechanical behavior between the two types of reinforcements. FRP bars exhibit linear stress-strain behavior up to failure without any yielding. Therefore, tension failure in FRP RC section is sudden and catastrophic; hence, it should be avoided (Jaeger et al. 1997, Theriault and Benmokrane 1998). On the other hand, compression failure of FRP RC sections offers more favorable response, as concrete ductility is utilized in giving ample warnings before failure (Nanni 1993).

Most of current codes and guidelines require FRP RC section to be design for compression failure. According to ACI 440.1R-15, a large amount of FRP reinforcement to be provided in the tension zone of flexural members in order to obtain compression failure mode which is the most ductile failure mode, as well as, for controlling crack width and deflection. The CSA S6-14 and CSA S806-12 , on the other hand, recommends that the moment of resistance of flexure member cross section reinforced with FRP should be at least 50% greater than the cracking moment, to avoid brittle failure.

2.3.3.4. Shear Strength

As identified by Joint ACI-ASCE Committee 445 (ACI-ASCE 1998), cracked reinforced concrete members resist the applied shear stresses by the following five mechanisms: (1) shear stresses in uncracked concrete; (2) aggregate interlock; (3) dowel action of the longitudinal reinforcing bars; (4) arch action; and (5) residual tensile stresses transmitted directly across the cracks. Aggregate interlock results from the resistance to relative slip between the two rough interlocking surfaces of the crack, much like frictional resistance. As long as the crack is not too wide, this action can be significant (Razaqpur et al. 2001). Dowel forces generated by longitudinal bars crossing the crack partially resist shearing displacements along the crack. Arching action occurs in deep members or in members having shear span-to-depth ratio less than 2.5 (Razaqpur et al. 2004). The residual tension in cracked concrete is reported to be present for cracks less than 0.15 mm in width (ACI-ASCE Committee 445-98).

Due to the relatively low modulus of elasticity of FRP bars, concrete members reinforced with FRP will develop wider and deeper cracks than members reinforced with steel. Deeper cracks decrease the contribution to shear strength from the uncracked concrete due to the lower depth of concrete in compression. Wider cracks, in turn, decrease the contributions from aggregate interlock and residual tensile stresses. Additionally, due to the relatively small transverse strength of FRP bars and the relatively wider cracks, the contribution of dowel action may be negligible. Eventually, the overall shear capacity of concrete members reinforced with FRP bars as flexural reinforcement is lower than that of concrete members reinforced with steel bars.

2.3.3.5. Bent Portion Strength

Currently-available FRP reinforcing bars are fabricated using thermosetting resin matrices and consequently cannot be bent on site. Bends and hooks, when required, must be produced by the bars' manufacturer during the fabrication process. It is possible to obtain bends and hooks in virtually any geometry from current FRP rebar manufacturers (Figure 2.8), although minimum bend radius is typically larger than for steel bars due to significant weakening of FRP bars around tight corners. Typical minimum allowable bend radius for FRP bars are 3.5 to 4 times the bars' diameter and these bends are accompanied by up to 50 percent reduction in the tensile strength of the bar at the bend (ISIS 2007).

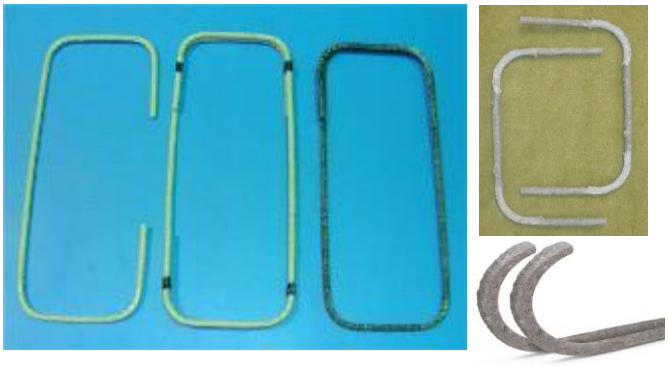

Figure 2.8 – Bends in GFRP bars reinforcement (Arafa 2017)

Many studies have reported a significant reduction in the tensile strength of bent FRP bars and stirrups at the location of the bend. For instance, Shehata et al. (2000) reported that the bend strength generally decreases with decreasing bend radius and can be as low as 35% of the tensile capacity of straight portions of the bar. Other investigation conducted by Morphy et al. (1997) on 16 specimens with different types of CFRP stirrups, it was recommended limiting the strength of CFRP stirrups to 50% of the ultimate straight bar capacity for design. The CSA S806-12 recommends that bend portion strength shall be taken equal to 40% of the straight portion tensile strength while the ACI 440.1R-15 gives the following equation for bend portion strength estimation (SI units):

$$f_{fb} = \frac{(0.05 r_b/d_b + 0.3) E_{fv}}{1.5} \leq f_{fu} \quad (2.1)$$

where f_{fb} is the bend portion strength, r_b is the bend portion's radius, d_b is the bar diameter, f_{fu} is the ultimate tensile strength for straight portion.

2.4. FRP RC Edge Slab Column Connections

Recent years have seen a great interest in testing concrete slab-column connections reinforced with GFRP bars. In addition, there has been a growing effort to improve design guidelines for concrete structures reinforced with FRP, especially with respect to punching shear equations. However, there is a need for more experimental work that systematically studies the effect of some factors, such as the different shapes of shear reinforcement; HSC edge connections under different *M/V* ratios; column aspect ratio and shear perimeter-to- slab depth ratio, openings on the punching shear strength of FRP edge slab column connections.

Because of the elastic nature of FRP up to failure, the contribution of shear resisting mechanisms in FRP-reinforced edge slab column connections is believed to be different from that in steel-reinforced concrete beams. For instance, FRP reinforced concrete members typically develop wider and deeper cracks than those in concrete members reinforced with steel. Because of such deeper cracks, the contribution of the uncracked concrete compression zone, dowel action, and aggregate interlock to punching shear strength is reduced. Moreover, the dowel action for FRP bars is always less than that of steel bars because of its lower transverse strength (El-Sayed et al. 2006).

The use FRP bars in RC slab column connections can extend the service life, reduce maintenance cost and improve-life cycle cost efficiency. Moreover, FRP bars may also reduce construction costs by eliminating the need for membrane and pavement items (Benmokrane et al. 2006). The direct implementation of FRP instead of steel bars, however, is not possible due to the differences in the mechanical and bond properties compared to steel bars. This results development of wider and deeper cracks affected the shear strength from the uncracked concrete compression zone below the neutral axis (N.A) depth and the contribution of aggregate interlock to decrease which, in turn, the ultimate punching-shear capacity to decrease. A brief summary for the implemented works, ordered chronologically, is given as following.

Zaghloul 2007 was the first who conducted a study to investigate the behavior of CFRP reinforced edge slab column connections subjected to shear and unbalanced moment . The test includes 10 half-scale slab-column edge connections in which three connections reinforced with steel bars and seven reinforced with CFRP NEFMAC grids. All tested specimens were reinforced with top and bottom meshes of CFRP grids or steel bars . It was found that increasing the reinforcement ratio by 46% increased the ultimate capacity by 21% without an increase in the post-cracking stiffness. Two connections were assigned to study the effect of CFRP shear reinforcement on the punching shear behavior of such connections. A typical CFRP shear rails consisted of four legs 90 mm apart were used. The rails were placed orthogonally parallel to the column faces. For the interior connection, it was found that the shear reinforcement increased the ultimate capacity by 24.6 and 30.4% when the first leg of the rail was located at a distance of 0.5d and 0.85d from the column face, respectively. For the edge connection, the increase was

only 9% with the first leg of the rail located 0.5d from the column face. Also, it was reported that the shear reinforcement increased the deformability of the connections.

The second attempt was done by El-Gendy and El-Salakawy (2016) by investigate the behavior of edge slab column connections reinforced internally with GFRP bars. The test connections included two series with three connections each. The connections of Series 1 investigated the effect of a new type of GFRP shear reinforcement on the punching shear behavior of slab-column edge connections, while those of Series 2 investigated the effect of *M/V*. For Series 1, one connection did not have shear reinforcement, while the other two connections had ribbed-deformed GFRP shear studs with headed ends at different radial spacing (120 and 80 mm). For Series 2, three different *M/V* ratios were applied to the connections (0.2, 0.4, and 0.6 m). The typical dimensions of the slabs were 2,800 × 1,550 × 200 mm with a 300-mm square column extending above and below the slab. Details of connections tested by El-Gendy and El-Salakawy (2016) shown in Figure 2.9.

The results indicated that, as shown in Figure 2.10, the punching shear capacity of the specimens decreased as the *M/V* ratio increased. Increasing the *M/V* ratio from 0.2 (SC-XX-L)to 0.4 (SC-XX-M) and 0.6 m (SC-XX-H) decreased the punching capacity by 7 and 33%, respectively, and the ultimate deflections by 21 and 62%, respectively. The headed ends of the shear studs provided adequate anchorage, which allowed the studs to reach their recommended design strains with no apparent signs of slippage. Thus, the studs were capable of controlling the propagation of diagonal shear cracks, which increased the loading capacities of the connections. The presence of studs spaced at 120 mm (0.75d) changed the mode of failure to a mixed flexural-punching mode, while reducing the spacing to 80 mm (0.50d) allowed the connection to reach its full flexural capacity. Connections RD-75-M (studs spaced at 120 mm, 0.75d) and RD-50-M (studs spaced at 80 mm, 0.50d) showed 34 and 46% higher capacity than connection RD-XX-M (without shear studs). Also, connections RD-75-M and RD-50-M showed a considerable ample warning before failure with ultimate deflections of 48 and 75 mm, respectively. These values are 55 and 142% higher than that of connection RD-XX-M (38 mm), respectively.

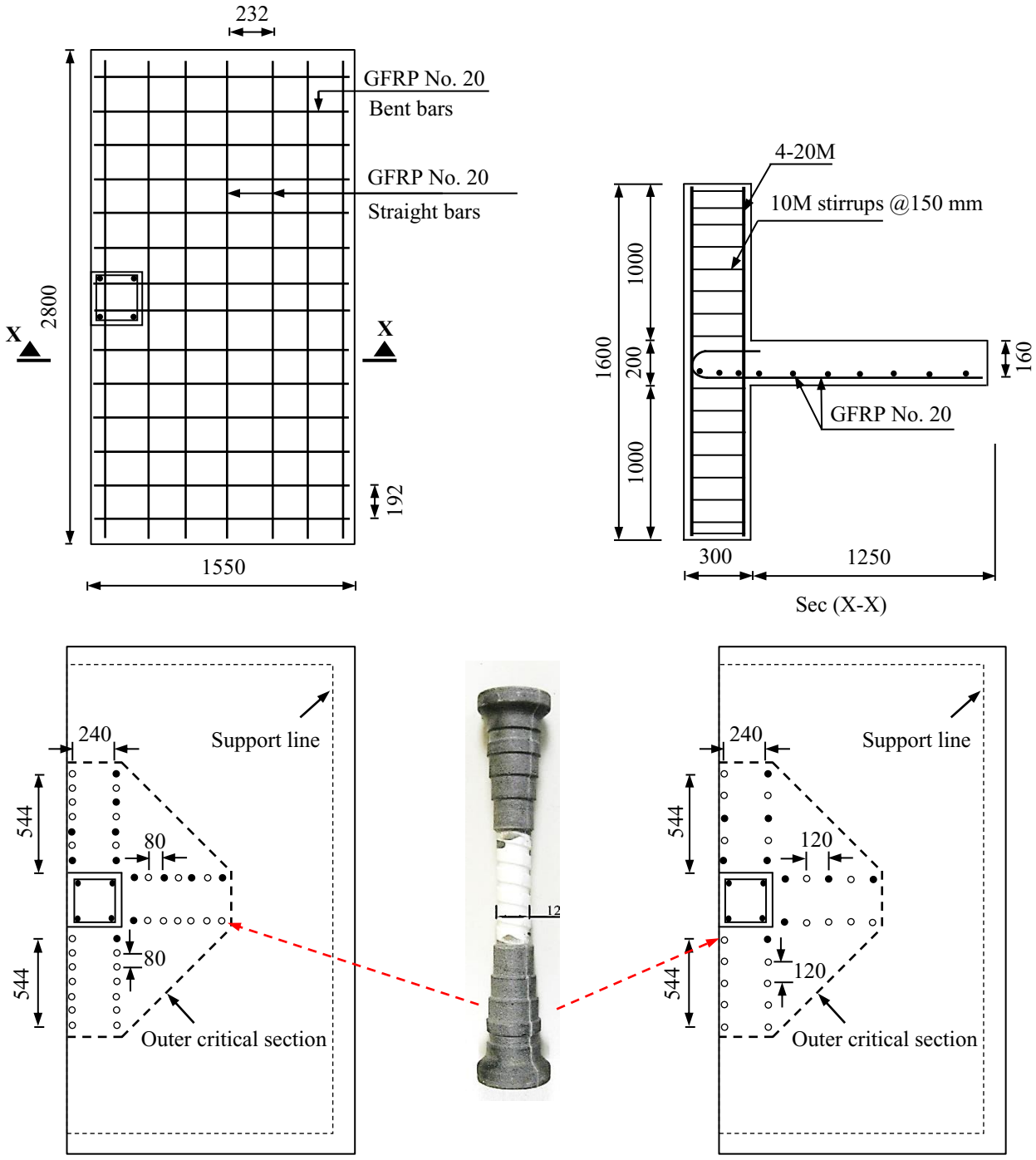

Figure 2.9 – Geometry and reinforcement for edge connections (El-Gendy and El-Salakawy 2016)

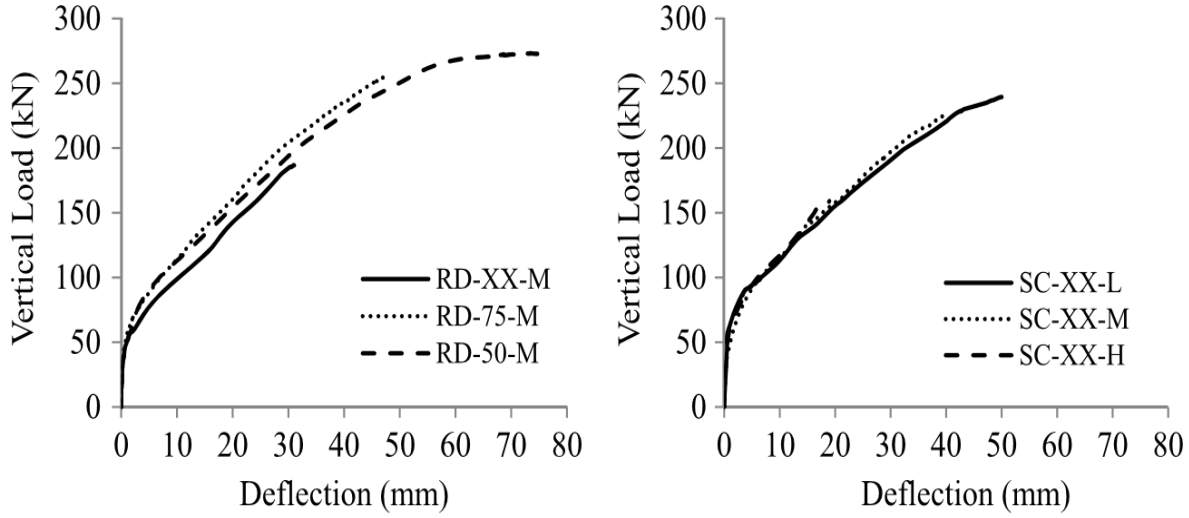

(a) Effect of using GFRP shear studs (b) Effect of *M/V* ratio

Figure 2.10 – Deflection response of specimens (El-Gendy and El-Salakawy 2016)

In an attempt to quantify the effect of other types shear reinforcements, sand coated studs and corrugated bars (refer to Fig. 2.11), as well as high strength concrete, Mostafa and El-Salakawy (2018) conducted punching shear tests on 7 GFRP-RC edge slab-column connections with and without shear reinforcement. The test connections were divided into two series. Series 1 included three high-strength concrete (HSC) connections, investigating the effect of the flexural reinforcement ratio (0.90, 1.35, and 1.80%); and Series 2 included four normal-strength concrete (NSC) connections, investigating the effect of the GFRP shear-reinforcement type (headed studs or corrugated bars) and pattern (six or eight lines of shear reinforcement). The flexural details are the same of the test specimens tested by El-Gendy and El-Salakawy with changing the concrete type, types of shear reinforcements, and shear reinforcement layouts. Shear reinforcement layout of connections tested by Mostafa and El-Salakawy (2018) shown in Figure 2.12.

As shown in Figure 2.13, all the connections were tested in an upside-down position, in comparison with the position of a real structure, with the vertical column load applied downward; consequently, tension cracks appeared on the bottom surface of the slab. Stiff steel I-beams were used to simply support the connections at three edges through the 20-mm-wide steel bearing plates, and the fourth edge was left free. Neoprene strips were placed between the slab and the bearing plates to allow a uniform load distribution along the supported edges. Three

heavy steel angles were placed on top of each supported edge of the slab to prevent any slab movement. C-clamps were used to tighten the steel angles to the supporting I-beams, while the two corners of the slab were kept free to lift. A hydraulic actuator and two hydraulic jacks, all attached to a rigid steel frame, were used to apply the vertical shear force and the lateral forces causing the unbalanced moment, respectively. The actuator and one hydraulic jack were placed at the tip of the upper column, and the other hydraulic jack was placed at the tip of the lower column. To maintain a *M/V* ratio of 0.4 m during the test, the loads were applied simultaneously in a monotonic mode with small increments (10 and 2.3 kN for the vertical and horizontal loads, respectively). The loading was paused every 20 kN to mark the propagation of cracks.

The main findings of this investigation can be summarized as follows:

- The HSC connections without shear reinforcement failed in a brittle punching shear mode characterized by a sudden drop in the load accompanied by column penetration through the slab.
- The flexural reinforcement ratio had a considerable effect on the punching shear capacity and the post-cracking stiffness of the HSC connections. Increasing the flexural reinforcement ratio by 50 and 100% increased the punching shear capacity by 7 and 15% and the post-cracking stiffness by 65 and 129%, respectively. This increase in the post-cracking stiffness resulted in a decrease in the deflection at service by 35 and 67%, respectively.
- The use of HSC enhanced the uncracked stiffness and the punching shear capacity of the connections and decreased the deflection at service. Doubling the concrete compressive strength from 40 to 80 MPa resulted in 83 and 10% increases in the uncracked stiffness and the punching shear capacity.
- With the use of eight lines of shear reinforcement, both the GFRP headed studs and corrugated bars managed to control the propagation of shear cracks and prevented the brittle punching shear failure in the column vicinity. However, in reducing the shear reinforcement ratio by the use of six lines of shear reinforcement, only the headed studs were able to fully control the shear cracks and to prevent the brittle punching shear failure. A minimum shear reinforcement ratio of 0.4% is recommended to ensure

flexural failure. Further investigation is required to examine the efficiency of corrugated bars with larger bar diameters.

- The use of shear reinforcement enhanced the deformability and the punching capacity of the connections. The connections N-0.9-S8, N-0.9-C8, N-0.9-S6, and N-0.9-C6 had 60, 41, 68, and 15% higher deformability; 66, 75, 62, and 17% higher deflection at failure; and 26, 23, 27, and 8% higher capacity, respectively, than the counterpart connection N-0.9-XX* without shear reinforcement.

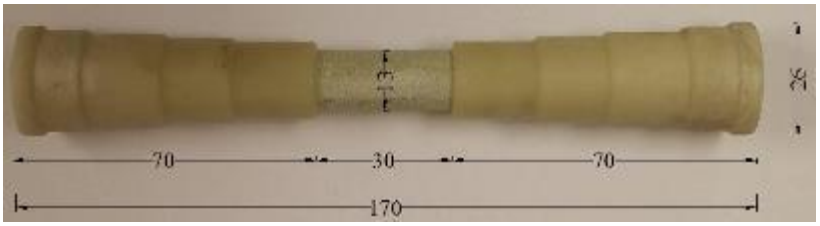

(a) Headed bars

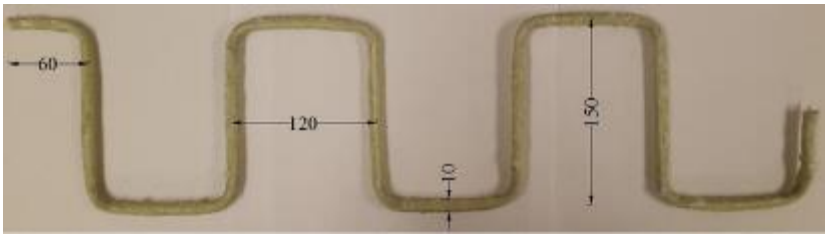

(b) Corrugated bars

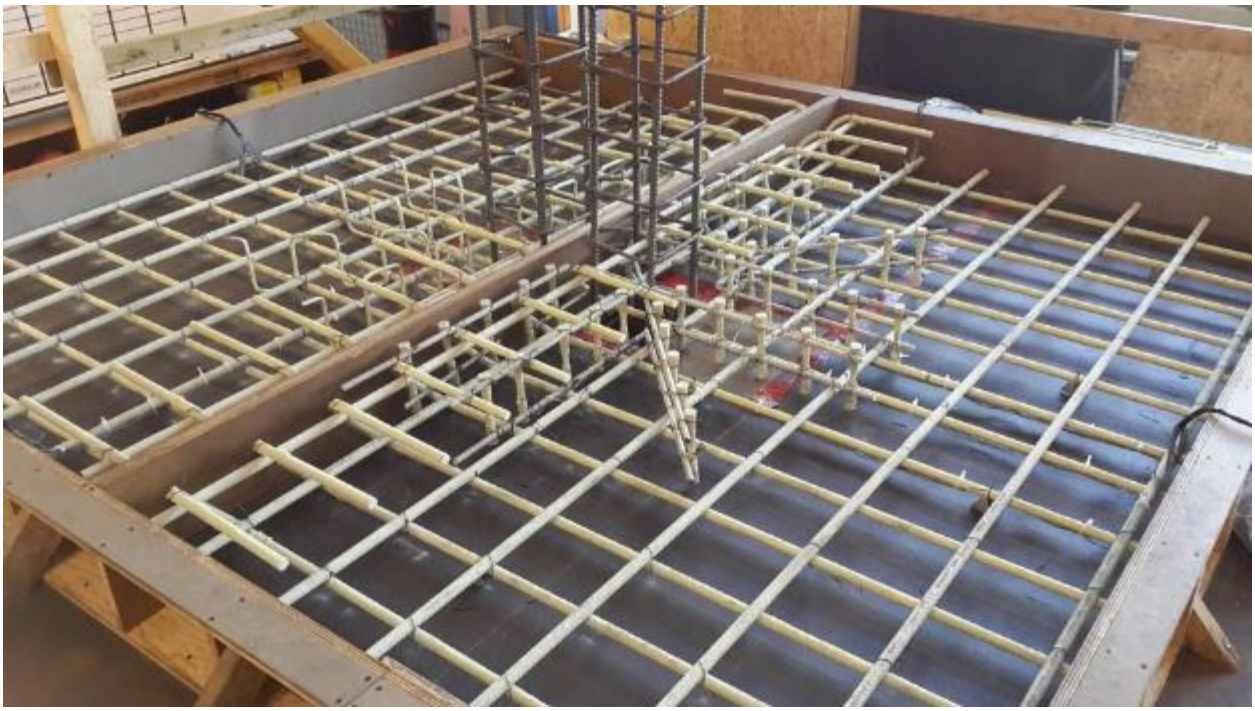

(c) Connections N-0.9-S8 and N-0.9-C8

Figure 2.11– Details of GFRP shear reinforcement (Mostafa and El-Salakawy 2018)

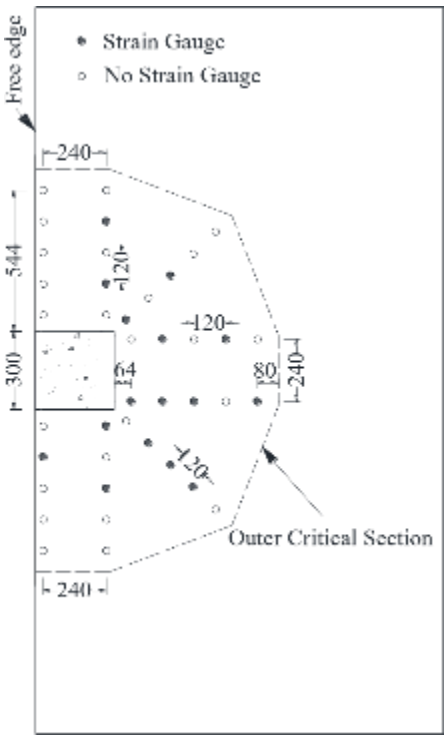

(a) Connection N-0.9-S8

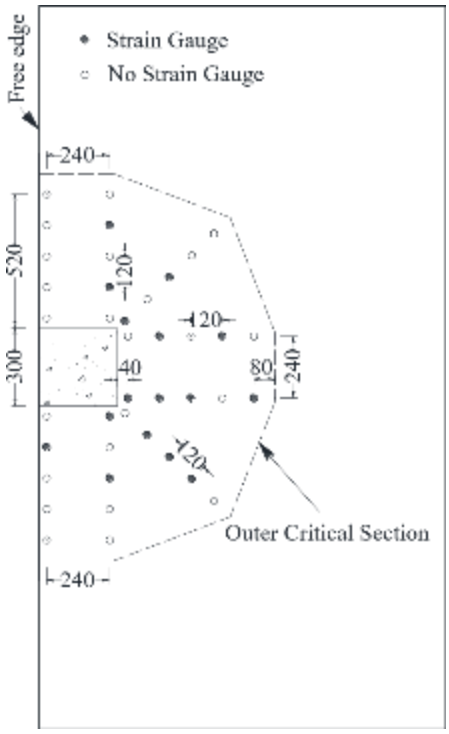

(b) Connection N-0.9-C8

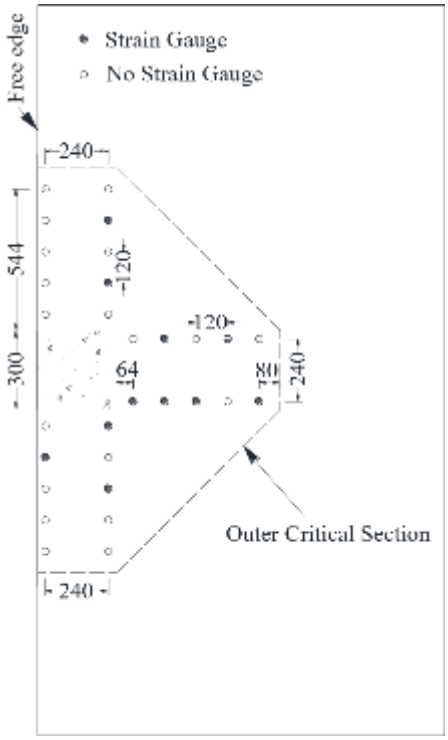

(c) Connection N-0.9-S6

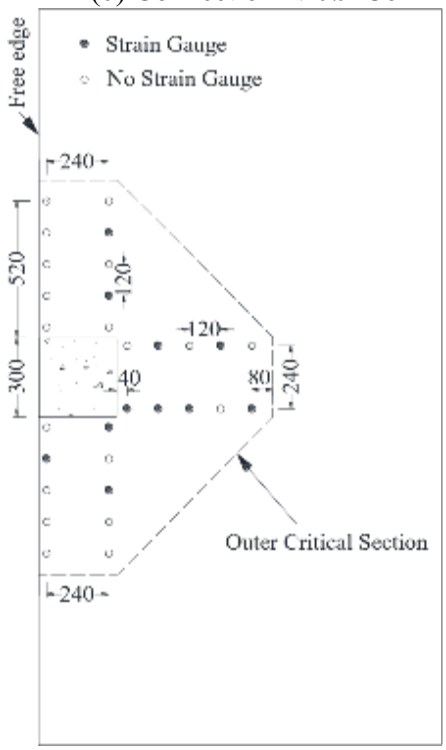

(d) Connection N-0.9-C6

Figure 2.12 – Details of shear reinforcement (Mostafa and El-Salakawy 2018)

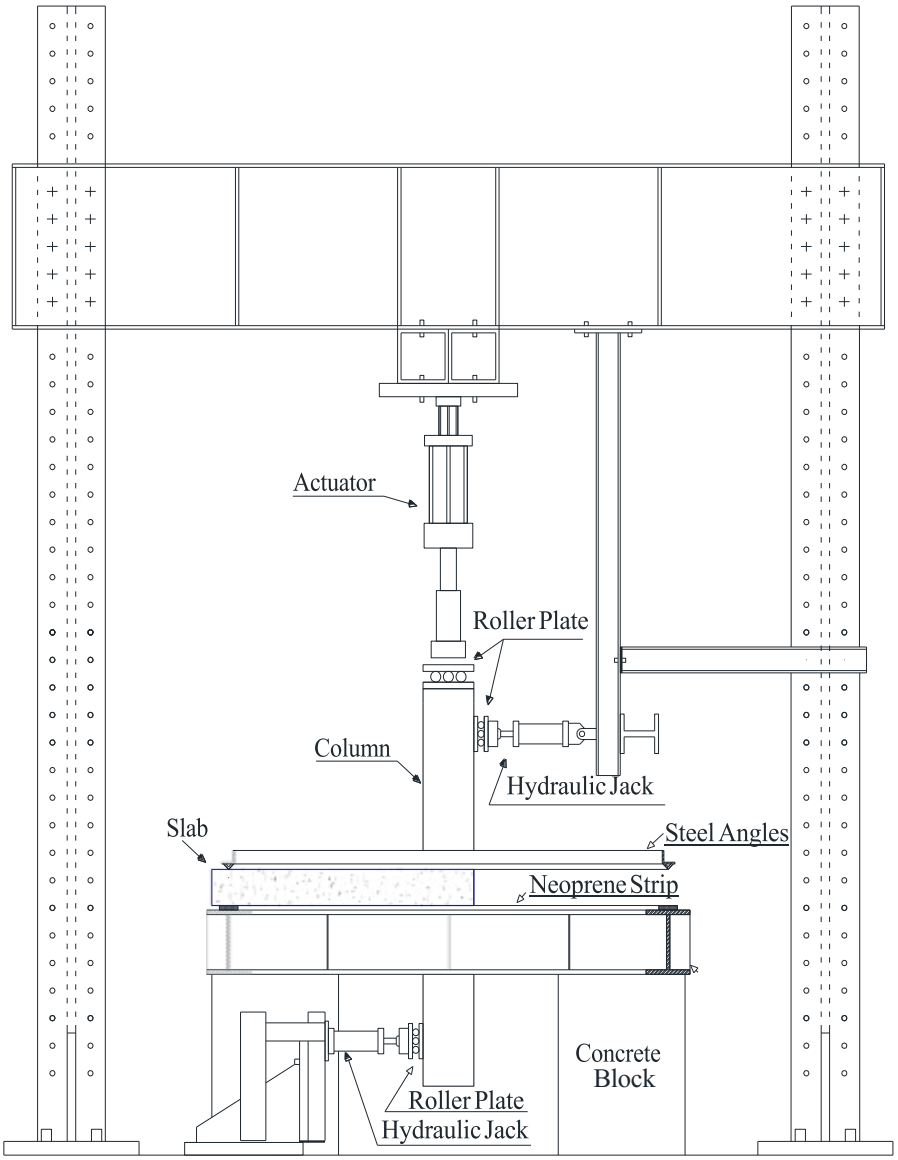

Figure 2.13 – Test setup (Mostafa and El-Salakawy 2018)

2.5. Summary

The available literature on steel-RC edge slab-column connections and their strength is quite large. On the other hand, very limited research has been devoted to the problem of shear-moment transfer at GFRP-RC edge slab-column connections. These investigations have been directed to investigate some variables affecting the punching capacity as discussed in this chapter. The main variables affecting the punching capacity are the *M/V* ratio, concrete strength, FRP flexural reinforcement type and ratio, and shear reinforcement type. In this regard, this study aims at

investigating the punching-shear behavior of GFRP-RC edge slab-column connections reinforced with and without FRP shear stirrups reinforcement, which contributes to understand the general behavior of such connections. In addition, tests are needed to examine and modify the current design equations in ACI 440.1R-15 and CSA S806-12 to insure safe and practical design of such connections with FRP shear stirrups. The test parameters in the current experimental program are described in the following chapter.

CHAPTER 3
EXPERIMENTAL PROGRAM

3.1. Introduction

The details of the experimental program that includes nine large-scale edge slab-column connections are presented in this chapter. The design, construction and testing of the specimens at the Structural Engineering Laboratory at the University of Sherbrooke are discussed in detail.

3.2. Test Matrix

Nine full-scale edge slab-column connections were fabricated and tested to failure under combined vertical load and unbalanced moment. Of the nine specimens, one specimen was reinforced with conventional steel bars and served as a control specimen; five were reinforced with GFRP bars in flexural, and the remaining three were reinforced with GFRP bars and shear stirrups. The design and details have been conducted according to according to CSA A23.3-14 and CSA S806-12 for test connections. It should be noted that since there is no design provision for FRP shear reinforcement in the CSA S806-12, similar methodologies that are being using in the companion code was adapted and followed. All slabs measured 2500 mm in length, 1350 mm in width, and 200 mm in thickness with a 300 mm square column stub protruding 700 mm above and below the slab surfaces. Figure 3.1 shows the concrete dimensions of the test specimens. The slabs' thickness satisfied the CSA A23.3-14 Clause 13.2.3 requirement for the minimum thickness. The test matrix was designed to investigate the influence of the following parameters on the punching shear behavior and strength of edge slab connections:

1. GFRP stirrups type (closed and spiral);
2. Stirrups extension (1.75d and 4.25d);
3. Flexural reinforcement ratio (1.04% and 1.55%);
4. Reinforcement type (GFRP and steel);
5. Concrete strength (normal and high-strength concretes); and

6. Different *M/V* ratios (0.3 m and 0.6 m).

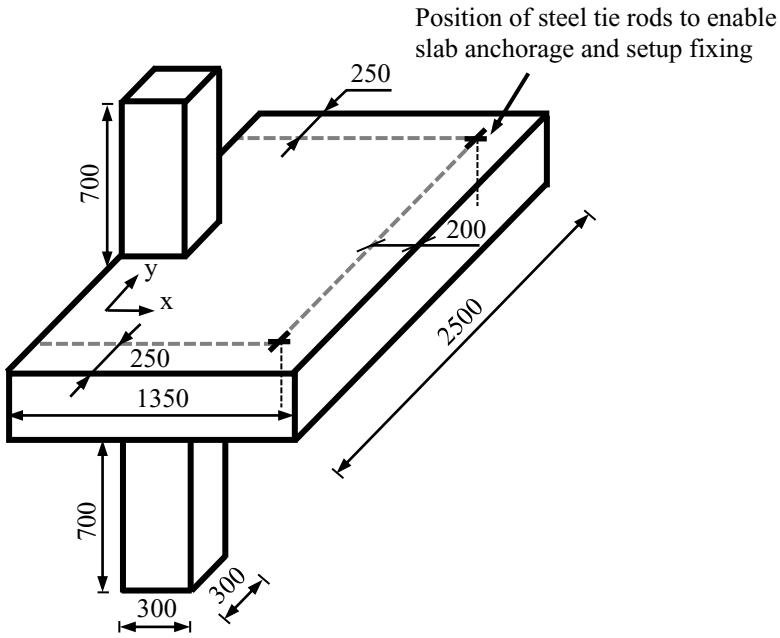

Figure 3.1 – Overall dimensions of test edge connections (Unit: mm)

The first specimen G was designed to have high flexural reinforcement ratio. The flexural tension reinforcement in the bottom side consisted of 10 and 20 No. 20 bars in the short and long directions. Whereas, the flexural tension reinforcement in the compression (top) side consisted of 7 and 10 No. 15 bars in the short and long directions with at least two bars passing through the column core to satisfy the requirement for structural integrity reinforcement in CSA A23.3 (2014).Three specimens; G-CS-1.75d, G-CS-4.25d and G-SS-4.25d were reinforced identically in flexure to G; however, with different types of transverse-reinforcement systems and extension from the column faces. Figure 3.2 and Figure 3.3 show the flexural and shear reinforcement details of the tested specimens with shear reinforcement, respectively. It should be mentioned that these three specimens were designed to have high amounts of flexural and transverse reinforcement such that punching-shear failure would be expected to occur prior flexural failure. Two connections (G-CS-1.75d and G-CS-4.25d) were reinforced in shear with No. 10 closed GFRP stirrups extended to 1.75d and 4.25d away from the column face, respectively, where d is the slab effective depth equal to 160 mm. These connections were designed to fail outside and within the punching-shear zone to evaluate the effect of stirrup extension on the punching behavior and to quantify the concrete contribution (v_c) outside the

punching-shear zone. The third connection (G-SS-4.25d) was reinforced No.10 spiral GFRP stirrups extended to 4.25d away from the column face to study the influence of stirrup type on the punching strength and deformation capacity and to compare its behavior with the counterpart slab (G-CS-4.25d) with discrete closed stirrups. The shear-reinforcement stirrups were arranged in a cruciform pattern according to ACI 318-14 and CSA A23.3-14. The number of peripheral lines of shear reinforcement varied between four and nine in both directions among the specimens; the spacing between the consecutive lines was 0.5*d*. The first perimeter was offset *d*/4 from the column face for all slabs with shear reinforcement, as specified in CSA A23.3-14.

Four other specimens, G-N-0.3, G-H-0.3, G-N-0.6, and G-H-0.6, were constructed using normal and high strength concretes and tested under different *M/V* ratios ranged between 0.30 to 0.6 to investigate the effect of different *M/V* ratios on the behavior. These specimens were reinforced in flexure without shear stirrups as shown in Figure 3.4. Each specimen was reinforced in the short and long directions, respectively, with 7 and 14 No. 20 bars as a flexural tension reinforcement in the bottom side and 5 and 8 No. 15 bars in the compression (top) side. Two bars in the compression side passing through the column core to satisfy the requirement for structural integrity reinforcement in CSA A23.3-14. The steel RC edge connection (S-N-0.3) served as a control specimen for G-N-0.3, so both had identical reinforcement configurations and ratios. In all test specimens, the tension reinforcement (bottom) in the long direction had double bent ends to provide the required anchorage and avoid any unexpected mode of failure, such as slippage failure rather than punching failure. The anchorage length was equal to the development length specified in CSA S806-12 and CSA A23.3-14 for GFRP and steel edge connections, respectively. It should be mentioned that connection G-N-0.3 was compared to connection G to study the effect of different flexural reinforcement on the behavior and strength. Each slab was monolithic with square column stub, which was designed to transfer shear force and lateral moment to the slab without any premature column failure. The nominal concrete cover both on the top and bottom faces of the slabs was 21 mm. Table 3.1 shows the reinforcement details of all tested specimens.

Table 3.1 – Flexural and shear reinforcement details

Test Specimen	f'_c, (MPa)	$f't$, (MPa)	Flexural-Reinforcement Ratio		Stirrup Layout Parameters					
			Bottom	Top	ρ_{fv}, (%)	Shape	d_s, (mm)	S_o; (mm)	S_{fv}; (mm)	Extent
			ρ_b, (%)	ρ_t, (%)						
G	41.4	3.6	1.55	0.65	0.90	------	------	------	----	----
G-CS-1.75d	47.6	3.9	1.55	0.65	0.90	Closed	9.5	0.25d	0.5d	1.75d
G-CS-4.25d	51.3	3.9	1.55	0.65	0.90	Closed	9.5	0.25d	0.5d	4.25d
G-SS-4.25d	52.5	3.5	1.55	0.65	0.90	Spiral	9.5	0.25d	0.5d	4.25d
S-N-0.3	39.2	3.73	1.09	0.34	------	------	------	----	----	----
G-N-0.3	37.1	3.73	1.04	0.34	------	------	------	----	----	----
G-H-0.3	85.8	6.54	1.04	0.34	------	------	------	----	----	----
G-N-0.6	38.8	3.56	1.04	0.34	------	------	------	----	----	----
G-H-0.6	86.0	6.54	1.04	0.34	------	------	------	----	----	----

f_c' = concrete compressive strength; ft' = concrete tensile strength; s_{fv} = stirrup spacing; ρ_b = average tensile flexural reinforcement ratio within effective widths; ρ_t = average compression flexural reinforcement ratio within effective widths; ρ_{fv} = shear-reinforcement ratio at a perimeter of 0.5d from column face = $(n_s * A_{fv} / S_{fv}\, b_o)$; d_s = stirrup diameter.

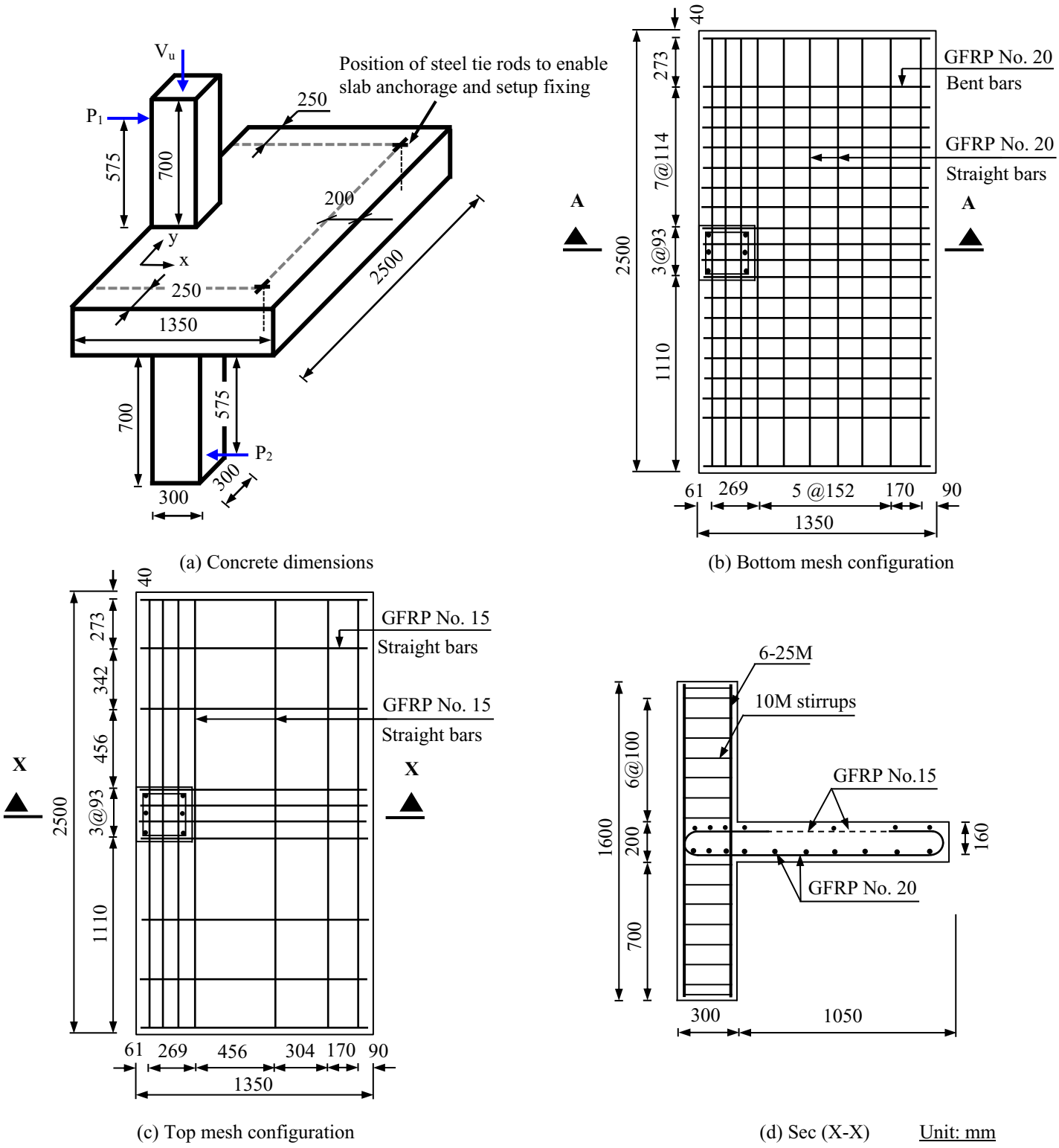

Figure 3.2 – Flexural reinforcement details of specimens with shear reinforcement

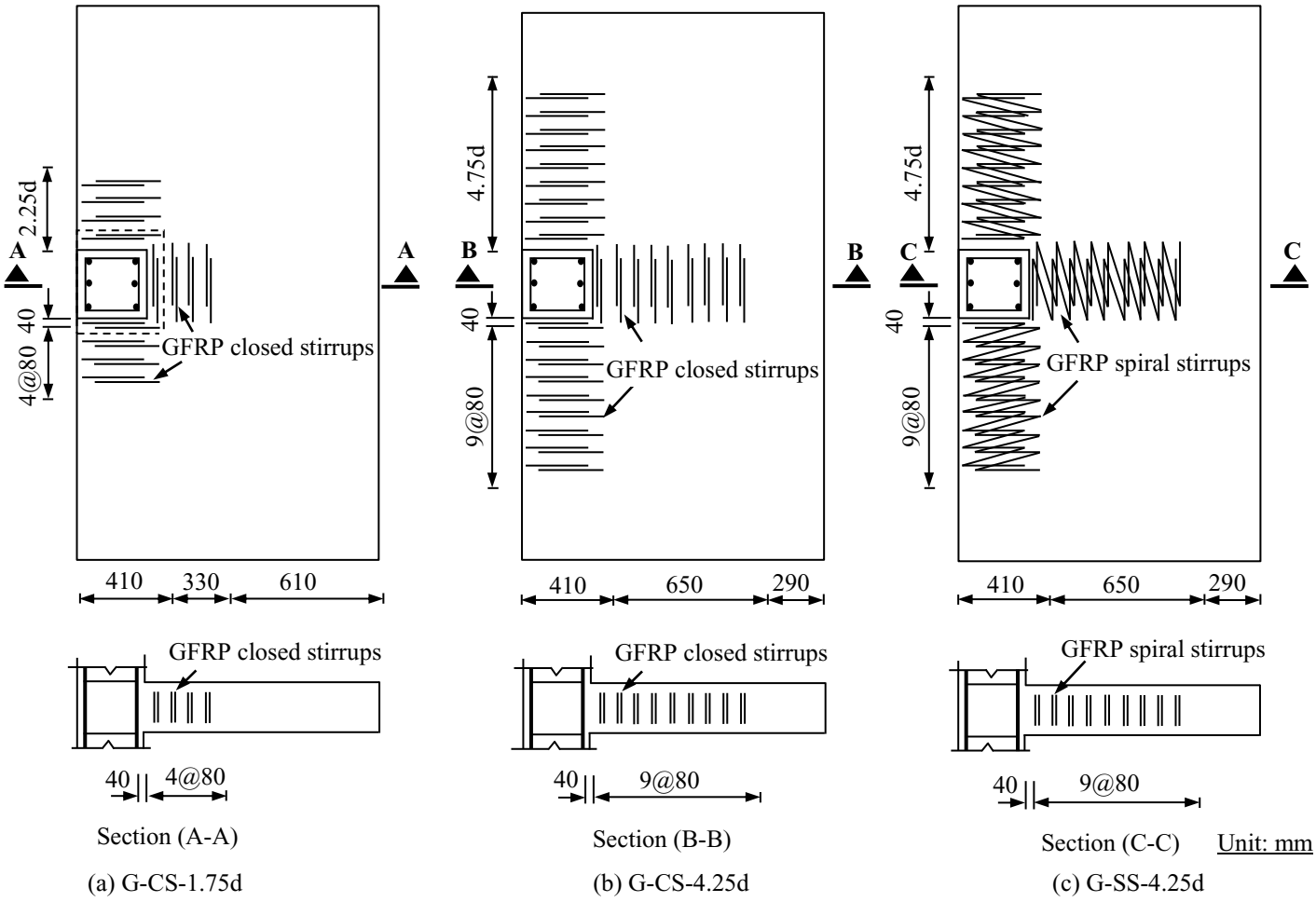

Figure 3.3 – Arrangement of GFRP stirrups shear reinforcement

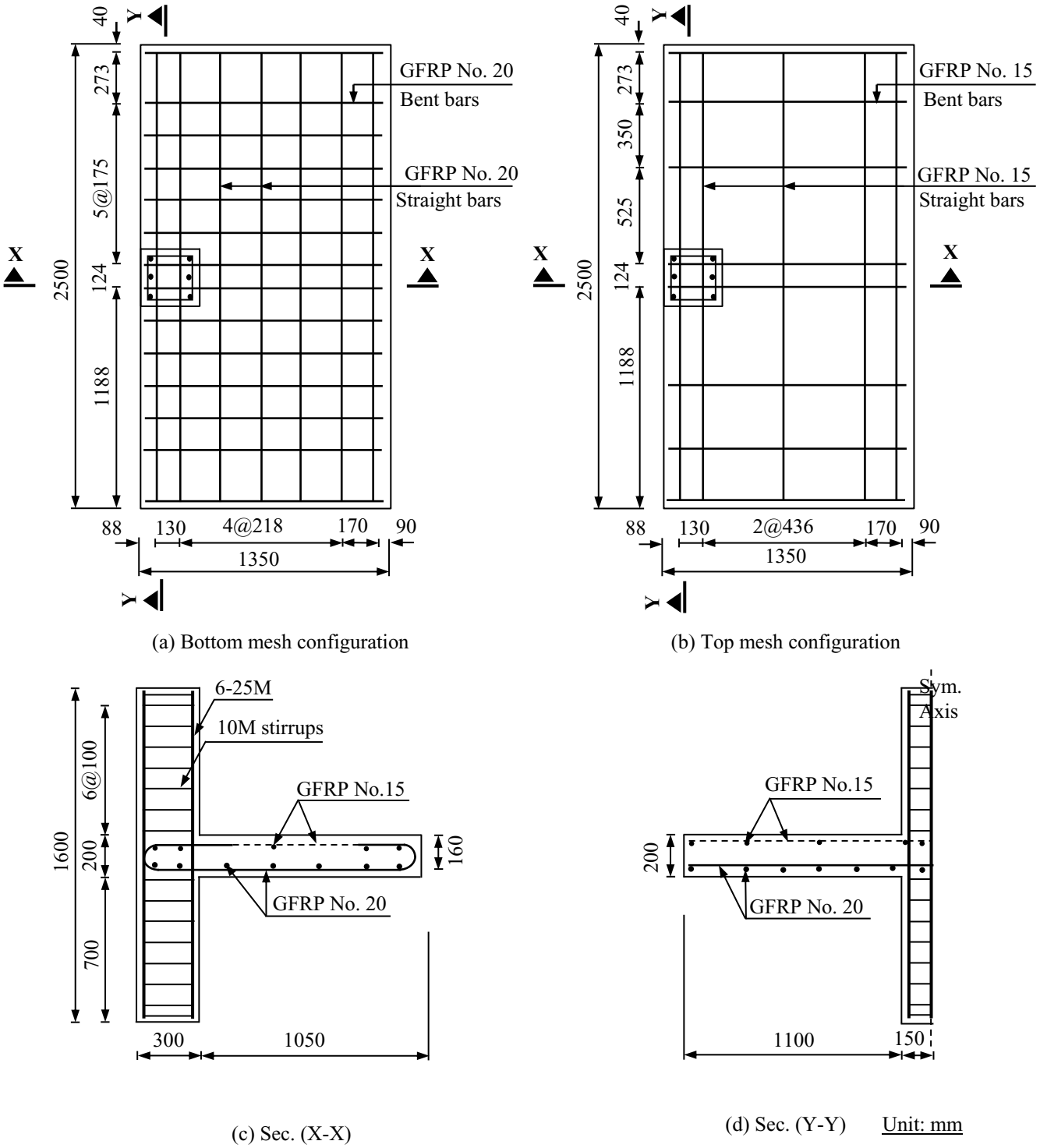

Figure 3.4 – Flexural reinforcement details of specimens without shear reinforcement

3.3. Material Properties

All specimens were cast using ready-mixed normal and high concrete with a targeted 28-day concrete compressive strength of 35 MPa and 75 MPa, respectively. The slab and the bottom and top column stubs were cast monolithically on the same day. Table 3.1 also gives the actual concrete compressive (fc′) and tensile (ft′) strengths based on the average of at least three 100 × 200 mm cylinders for each of the compression and splitting tests on the day of testing. The concrete compressive strength ranged from 37.1 to 52.5 MPa, whereas the tensile strength ranged from 3.5 to 6.54 MPa. Two types of reinforcing bars were used as flexural reinforcements; sand-coated GFRP and deformed steel bars. Sand-coated GFRP bars of Grade II and III compliant with CSA S807-15, were used in all GFRP specimens. The GFRP bars were manufactured by combining the pultrusion process with an in-line sand-coating process for the bar surface. This sand coating was designed to improve bonding between the GFRP bars and surrounding concrete. The bottom flexural reinforcement bars were bent and straight GFRP bars No.20 (#20) in the direction perpendicular and parallel to the free edge, respectively. Straight GFRP bars of size No.15 (#15) were used as top flexural reinforcement in both orthogonal directions. The tensile properties of the straight and bent GFRP bars were determined from testing five representative specimens according to ASTM D7205M (2011) and the B.5 test method in ACI 440.3R-12, respectively. Deformed steel bars 15M and 20M (Type 44W) were used in top and bottom reinforcements for the reference connection. The column stub was reinforced with steel bars of 25M and 10M as longitudinal and transverse reinforcements, respectively. The steel-bar properties were provided by the manufacturer. Discrete No. 10 closed and rectilinear sand-coated spiral GFRP stirrups were used as shear reinforcement. The tensile strengths of the straight and bent portions of the stirrups were determined by testing five representative specimens according to ASTM D7205M (2011) and the B.5 test method in ACI 440.3R-12, respectively. Table 3.2 summarizes the tensile properties of the used reinforcing bars. Figure 3.5 depicts the GFRP bars and shear-reinforcement stirrups.

Table 3.2 – Tensile properties of the reinforcing bars and shear reinforcement

Bar Designation[a]	Nominal Cross-Sectional Area[a]	Ultimate Tensile Strength (MPa)	Elastic Tensile Modulus (GPa)	Ultimate Tensile Strain (%)
GFRP straight flexural bars				
No. 15 GFRP bar	199	1323 ±12	64.8±0.5	2.04 ±0.05
No. 20 GFRP bar	285	1334 ±85	64.9±0.6	2.06 ±0.13
GFRP bent flexural bars				
No. 20 straight portion	285	1210±63	53±0.48	2.28±0.15
No. 20 bent portion		f_{fvb} [b]= 490±44	------	------
GFRP-stirrup shear reinforcement				
No. 10 straight portion	71	967±39	45.7±0.5	2.12±0.08
No. 10 bent portion		f_{fvb} [b]= 489±38	------	------
Steel bars				
10M	100	f_y [c]= 420	200	ε_y = 0.21
20M	300	f_y [c]= 460	200	ε_y = 0.23
25M	500	f_y [c]= 470	204	ε_y = 0.23

[a] According to CSA S807 (2015).
[b] f_{fvb} = ultimate tensile bend strength obtained from the B.5 test method (ACI 440.3R 2012)
[c] f_y steel yielding strength and ε_y steel yielding strain, as provided by the manufacturer.

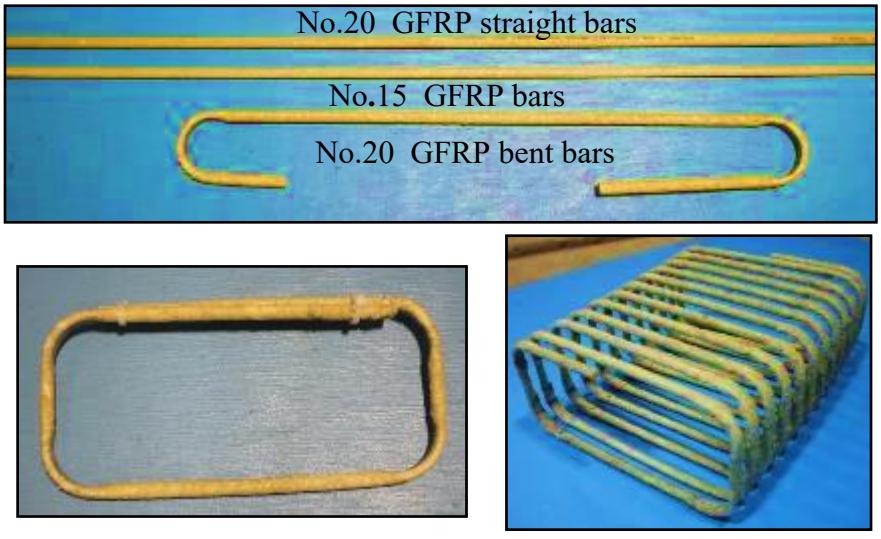

Closed stirrups (No.10 GFRP)

Spiral stirrups (No.10 GFRP)

Figure 3.5 – GFRP bars and shear stirrups reinforcement

3.4. Specimens Construction

The cages were assembled in the Structural Laboratory at the University of Sherbrooke and then moved for casting at Les Coffrages Carmel, inc. upon completion. A wooden formwork was manufactured by Les Coffrages Carmel, inc. from plywood plates of 19 mm thickness. The top and bottom column stubs were fabricated in the wooden formwork 700 mm beyond the slab. The formwork was supported on Thirteen aluminum I beams of 4 m long, 9 beams in the long direction and 3 beams in the short direction, which were supported in turn on steel supports. Before installing the reinforcing cages, the vertical level of the column was adjusted, and the formwork was lubricated to provide ease in formwork removal. The construction started with mounting the steel column cage without top column stub stirrups in the wooden formwork. Then the instrumented slab cages were placed in the formwork and the stirrups of the top column stub were installed (Figure 3.6) followed by the installation of the wooden formwork of the top column stub (Figure 3.7). Two 10 mm-diameter holes were cast close to the slab edges to enable anchorage during testing by fixing PVC pipe at those locations. Two vertical steel hooks were placed at 450 mm from the free edge of the slab to carry the slabs after removing from the formwork.

Batch plant delivered ready-mixed concrete and slump test was performed for each delivered mix. The orientation of the specimens during casting was the same as during testing. The column stub was cast simultaneously with the slab (Figure 3.8). The concrete was internally vibrated, and the surface of the concrete slab was adjusted when casting had been completed. Nine plastic standard cylinders of 100 x 200 mm were moulded for each delivered mix to determine concrete compressive strength and splitting tensile strength. One day after casting, the cylinders and the external sides of the formworks were stripped and then the slabs, column stubs and the concrete cylinders were covered with moist burlap (Figure 3.9). After one week, the specimens were moved out from the formwork, and transported to the Structural Laboratory at the University of Sherbrooke for testing using 10-ton capacity crane (Figure 3.10).

(a) S-N-0.3

(b) G-N-0.3, G-H-0.3, G-N-0.6, G-H-0.3

(c) G-CS-1.75d

(d) G-CS-4.25d

Figure 3.6 – Assembly of the slab and column cages to the formwork

Figure 3.7 – Assembly and alignment of column formwork

(a) Casting the column stub

(b) Casting the slab

(c) Surfacing the slab surface

(d) Connection just after casting

Figure 3.8 – Casting the test specimen

Figure 3.9 – Curing of concrete

Figure 3.10 – Lifting test specimen for testing

3.5. Design of Test Specimens

The test specimens represented edge slab-column connections from a prototype of flat plate parking structure. The prototype consisted of four-square panels with 5 m long in both directions. Figure 3.11 depicts the position of the test specimens relative to a prototype slab. All slabs had identical geometries of 2500 × 1350 × 200 mm with a 300-mm square column stub protruding 700 mm above and below the slab surfaces. The slabs were simply supported on a 2000 × 1150 mm perimeter on the bottom face of the slab. The prototype structure was analysed using Equivalent Frame Method in CSA A23.3-14 to determine the straining action on the selected connection and the *M/V* ratio (Appendix). Then, the flexural design was conducted according to the CSA A23.3-14 for steel RC connection and the CSA S806-12 for GFRP RC

edge connections. Each specimen was simply supported on three edges, simulating lines of contra flexure in the prototype floor, and monolithic with a column at the middle of the fourth edge. The lines of contra flexure were assumed to be 0.2*L* away from the column centerlines, where *L* is the span between the column centerlines. The prototype had a gravity live service load of 2.40 kN/m^2, a super-imposed dead load of 1.0 kN/m^2 and a self-weight of 4.80 kN/m^2, resulting in a *M/V* ratio of 0.3 m.

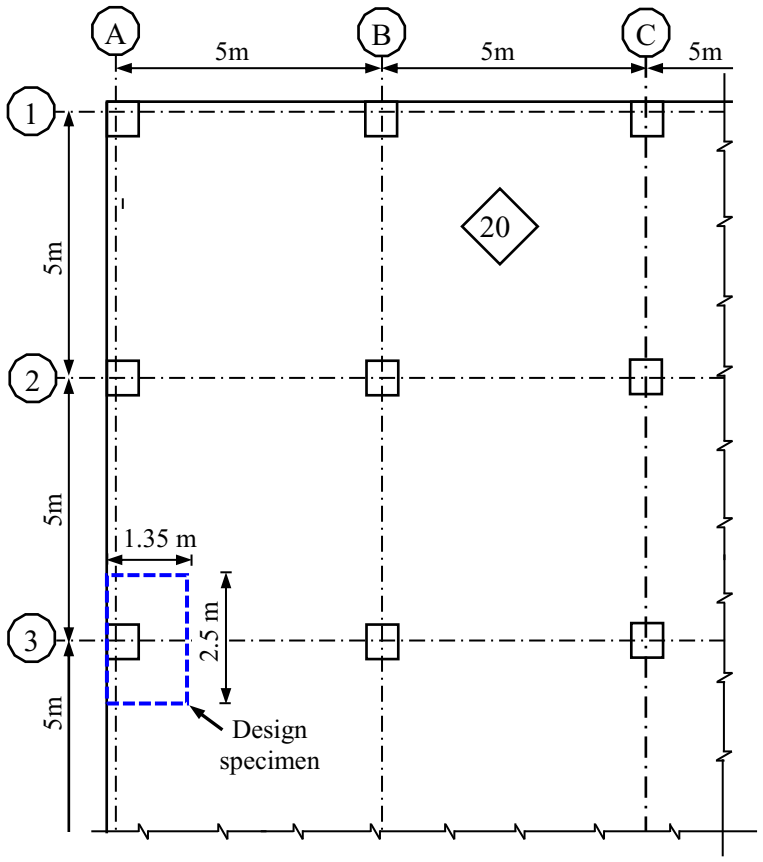

Figure 3.11 – Design specimen location relative to prototype structure

The predicted shear strength for the investigated GFRP edge connections without shear reinforcement was calculated based on the available punching-shear equations provided in CSA S806-12, ACI 440.1R-15, and JSCE-97. These equations are forms of the original equations for steel that have been modified to account for the difference in mechanical properties between FRP and steel reinforcement, especially the lower modulus of elasticity.

ACI 440.1R-15

The punching-shear stress provided by concrete (v_c) for two-way slabs reinforced with FRP bars or grids is simply the ACI 318-14. Punching-shear equation for steel-reinforced slabs modified to account for the shear transfer in two-way slabs. The v_c equation for steel modified by the factor ([5/2] k) accounts for the axial stiffness of the FRP reinforcement through the neutral-axis-depth term (kd), as shown in Eq. (3.1).

$$v_c = \frac{4}{5}\, k \sqrt{f_c'} \tag{3.1a}$$

$$k = \sqrt{2\rho_f\, n_f + (\rho_f\, n_f)^2} - \rho_f n_f \tag{3.1b}$$

Where: $n_f = {E_f}/{E_C}$, $E_c = 4700\sqrt{f_c'}$

where f_C' = concrete compressive strength (MPa); $b_{o,0.5d}$ = perimeter of the critical section for slabs at a distance of effective depth (d)/2 from the column face (mm); k = neutral-axis depth to reinforcement depth ratio (mm); and ρ_f = average of the FRP reinforcement ratio in both directions.

CSA S806-12

v_c can be calculated as the smallest of Eq. (3.2) to (3.4), which are essentially the CSA A23.4-14 equations with modifications to account for FRP bars instead of steel. A critical perimeter nearest a column equal to 0.5 times the effective depth (0.5d) from the column face was taken

$$v_c = 0.028\,\lambda\,\emptyset_c \left(1 + \frac{2}{\beta_c}\right)\left(E_f\,\rho_f\;\, f_c'\right)^{\frac{1}{3}} \tag{3.2}$$

$$v_c = 0.147\,\lambda\,\emptyset_c \left(0.19 + \frac{\alpha_s\, d}{b_{o;0.5d}}\right)\left(E_f\,\rho_f\;\, f_c'\right)^{\frac{1}{3}} \tag{3.3}$$

$$v_c = 0.056\,\lambda\,\emptyset_c\,(E_f\,\rho_f\,\,f_c')^{\frac{1}{3}} \tag{3.4}$$

where λ= concrete density factor (1 for normal weight and 0.85 for semi-lightweight); $\emptyset_c$ = concrete resistance factor (0.65); β_C = ratio of long side to short side of column; α_S = 4 for interior columns, 3 for edge columns, and 2 for corner columns; and f_C' shall not exceed 60 MPa. If d exceeds 300 mm, the v_C obtained from the equations shall be multiplied by $(300/d)^{0.25}$.

JSCE-97

v_c can be calculated as given in Eq. (3.5).

$$v_c = \beta_d\,\beta_p\,\beta_r\,f_{pcd}\,/\gamma_b \tag{3.5a}$$

$$\beta_d = (1000/d)^{0.25} \leq 1.5\,, \tag{3.5b}$$

$$\beta_p = (100\rho_f E_f/E_S)^{\frac{1}{3}} \leq 1.5\,, \tag{3.5c}$$

$$\beta_r = 1 + 1/(1 + 0.25\,u_o/d)\,, \tag{3.5d}$$

$$f_{pcd} = 0.2\sqrt{f_c'} \leq 1.2 \tag{3.5e}$$

where u_o =perimeter of reaction area of supporting column; ρ_f = average flexural reinforcement ratio in both orthogonal direction; γ_b = partial safety factor equal to 1.3 or 1.5 for concrete strengths below and above 50 MPa, respectively, that was set to 1.0 to get an un factored prediction of capacity; f_{pcd} = concrete compressive strength (MPa), and d = effective slab depth (mm).

Due to the lack of provisions in CSA S806-12 and ACI 440.1R-15 for calculating ultimate capacity of FRPRC two-way slabs with FRP shear reinforcement, we opted to propose design provisions as an extension to CSA S806-12 and ACI 440.1R-15. Regarding steel-reinforced two-way slabs with shear reinforcement, ACI 318-14 and CSA A23.3-14 require that the shear stresses be checked either inside or outside the shear-reinforced zone. The critical shear section inside the shear-reinforced zone is located at d/2 from the column faces, while the critical section outside the shear reinforcement lies at d/2 from the outermost shear reinforcement. Within the shear reinforced zone, the factored shear-stress resistance, computed as (v_c + v_s), where v_c and

v_s are the summations of concrete and shear-reinforcement contributions to the shear strength inside the punching zone. Design codes, ACI 318-14 and CSA A23.3-14, calculated the concrete contribution inside and outside the region reinforced with shear stirrups as 50% of the punching-shear strength of slabs without shear reinforcement. Accordingly, the concrete contribution inside and outside the shear-reinforced zone for FRP-reinforced two-way slabs is proposed to have a value equal to 50% of the least of Eqs. (3.2) to (3.4) according to CSA S806-12 or Eq. (3.1) according to ACI 440.1R-15.

In order to calculate the FRP-stirrup contribution, steel stirrups equation has been modified by replacing, f_y (yielding strength) with a specific stress (f_{fv}) at a limiting strain value (ε_{fv}) of 5000 or 4000 μs according to CSA S806-12 and ACI 440.1R-15, respectively, where f_{fv} equals ε_{fv} multiplied by the FRP-stirrup modulus of elasticity (E_{fv}). It should be noted that the f_{fv} should be less than the stress corresponding to the failure of the stirrup corners or bends as determined with the appropriate procedure in accordance with ACI 440.1R-15 and CSA S806-12. The proposed design equations can be summarized as follows.

Proposed design provisions for CSA S806-12 with the shear-reinforced zone

$$v_{c\ inside} = v_{c_{outside}} = 0.028\lambda\phi_c\left(E_f\rho_f f_c'\right)^{\frac{1}{3}} \tag{3.6}$$

$$v_{fv} = \frac{\phi_f A_{fv}(0.005E_{fv})}{b_0\, S_{fv}} \tag{3.7}$$

Proposed design provisions for ACI440.1R-15 with the shear-reinforced zone

$$v_{c\ inside} = v_{c\ outside} = \frac{2}{5}k\sqrt{f_c'} \tag{3.8}$$

$$v_{fv} = \frac{\phi_f A_{fv}(0.004E_{fv})}{b_0 S_{fv}} \tag{3.9}$$

3.6. Test-Setup and Procedure

The specimens were tested in the structural laboratory at the University of Sherbrooke under monotonic vertical shear force and lateral static unbalanced moment until failure. The test setup included three main parts: (1) the testing frame, (2) reaction frames, and (3) the supporting bed and top restrain beams. The testing frame consisted of two main frames and a stiff connecting steel I-beam on top. A 1500-kN vertical hydraulic jack was installed at the center of the I beam

to apply a constant vertical load at the top of the concrete column. During testing, a steel pan with rollers was placed between a vertical jack and the top of upper concrete column to free horizontal movement of the column during lateral loading while maintaining the vertical load. Two 1000 kN horizontal hydraulic jacks were installed on two very rigid reaction frames fixed firmly to the laboratory strong floor to apply lateral loads. The vertical and lateral jacks were controlled using three manual hydraulic pumps. The loads were monitored with three load cells on each pump and connected to the data-acquisition system.

The specimens were simply supported on the bottom surface along three sides during testing with a new fabricated supporting steel bed, which was designed to ensure adequate strength and stiffness under the testing load of the specimens. The supporting bed consisted of four-square steel beams [HSS 250 × 150 × 8 mm] supported on four square columns [HSS 152 × 100 × 6 mm] laterally stiffened with back-to-back double steel angles [102 × 102 × 7.9 mm] in both directions. It is worth mentioning that, before placing the test specimen in the setup, the supporting bed was prestressed directly on the laboratory strong floor with four 38 mm diameter steel tie rods to prevent the supporting bed from moving laterally. On the slab top face, three supported edges were restrained by steel reaction beams to prevent slab lifting. Each end of the reaction beam was held in position by four steel nuts and plates attached to the steel tie rods. In addition, 20 mm thick neoprene pads were placed between the slab and supporting bed and between the slab and top restrain beams along the support lines to simulate slab rotation at the line of contra flexure and ensure uniform stress distribution along the edges. The test setup details are depicted in Figure 3.12 to 3.14. The specimens were tested under varied unbalanced moment (M_{un}) to vertical load (V) ratios between 0.3 to 0.6 m. The unbalanced moments were calculated by multiplying the two lateral forces, applied to each column by the distance from the application point to the center of the slab: 675 mm. The vertical load was applied monotonically at a load-controlled rate of 5 kN/min, whereas the horizontal forces were simultaneously applied with the vertical force in small increments to maintain a constant *M/V* ratio of 0.3 or 0.6 m throughout the test until failure.

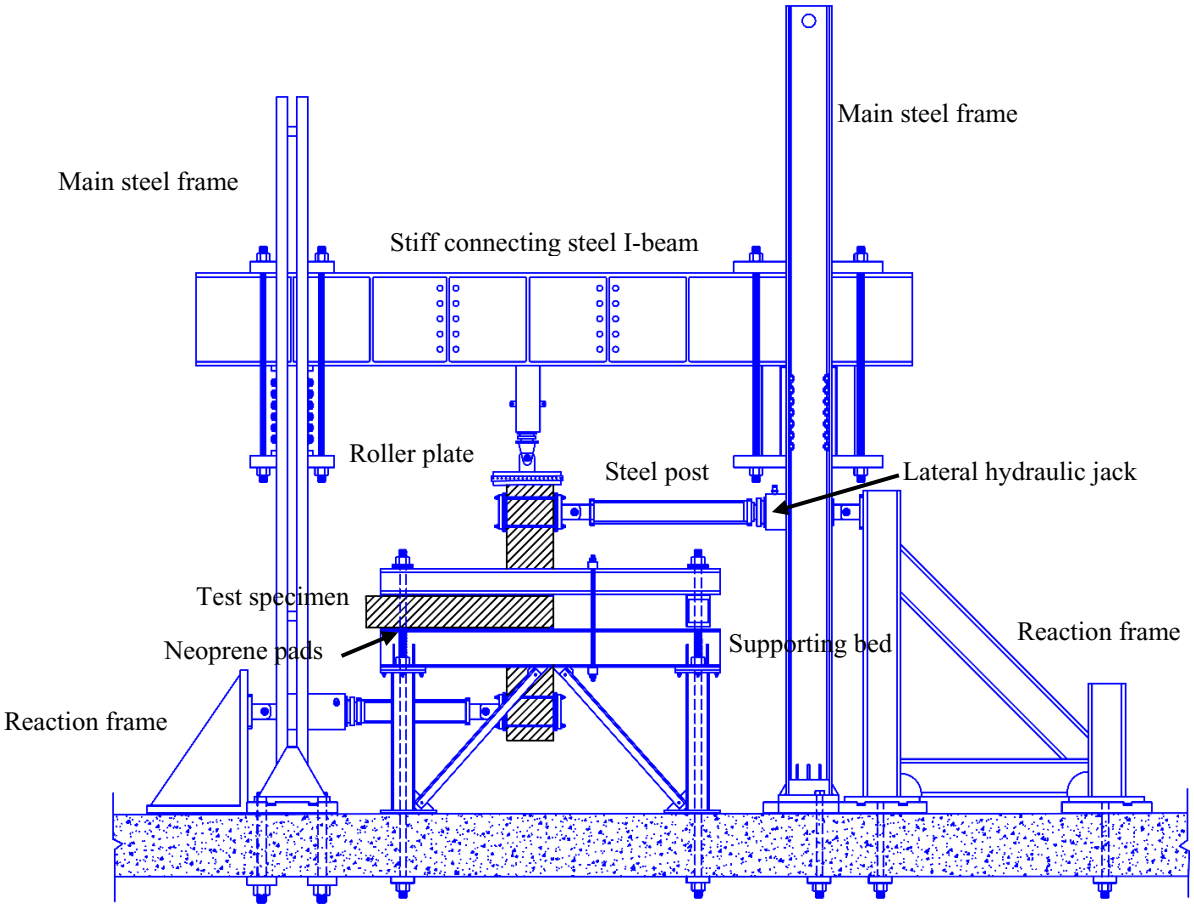

Figure 3.12 – Elevation view of test setup

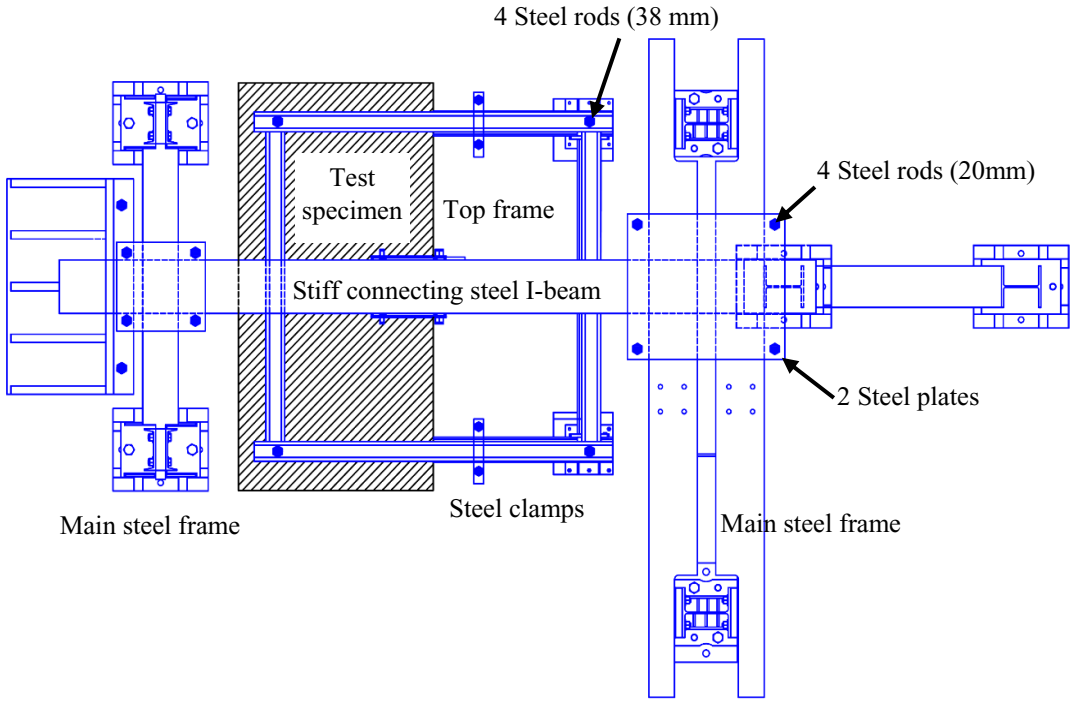

Figure 3.13 – Plan view of test setup

Figure 3.14 – Overview of test setup

Instrumentation

Strains in the bottom flexural reinforcement (tension side) were measured with 11 electrical resistance strain gauges [6 mm long] at different locations in both orthogonal directions (Fig. 3.15). The strain gauges were located at a distance of 0, 75, 225, 450, and 750 mm from the column face on one bar in each direction. In addition, one electrical strain gauge was glued at the bend location of the GFRP bar at the column location (see Fig. 3.15). The strains in the FRP stirrups were monitored using six strain gauges mounted at mid-height of the vertical legs of the FRP stirrups and bend location in each orthogonal direction, as shown in Figure 3.16. In addition, five concrete electrical strain gauges —labeled C1 to C5—were glued before testing to the slab's top surface (compression side) at 0 and 200 mm from the column face (see Fig. 3.17).

Sixteen string potentiometers (pots) were used at different locations to measure the displacements. Eleven pots (P1 to P11) were placed on the top slab face along two orthogonal directions at a distance of 80, 250, 550, and 850 mm from the column face to measure the slab-deflection profile while one pot (P15) was located at the column centerline to measure the central deflection. Two pots (P12 and P16) were installed horizontally on the top and bottom column ends to measure column lateral displacements. To monitor any possible shifting of the specimen or test setup, two pots (P13 and P14) were installed in the horizontal loading directions at the center of slab thickness and frame test setup. All instruments were installed onto rigid steel frames, separated from the testing frame and attached directly to the laboratory floor, to prevent any frame deformations from affecting the measurements. Moreover, two linear variable differential transformers (LVDTs) were placed throughout slab testing to monitor flexural-crack widths in each direction. The strain gauges, pots, and LVDTs were connected to a data-acquisition system to record the readings. Figures 3.15 to 3.17 show the position of several instrumentation details of the test specimen. During the test, crack propagation was marked, and the corresponding loads were recorded.

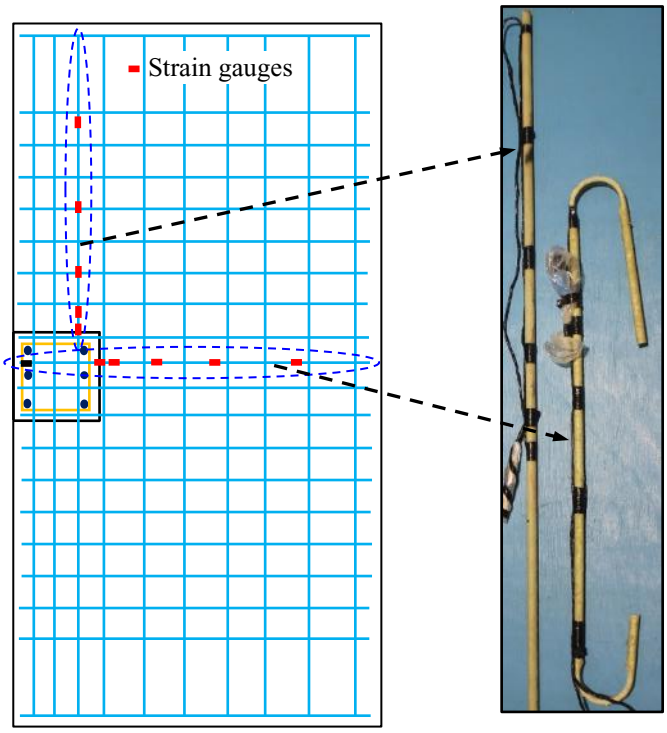

(a) Slabs with shear reinforcement

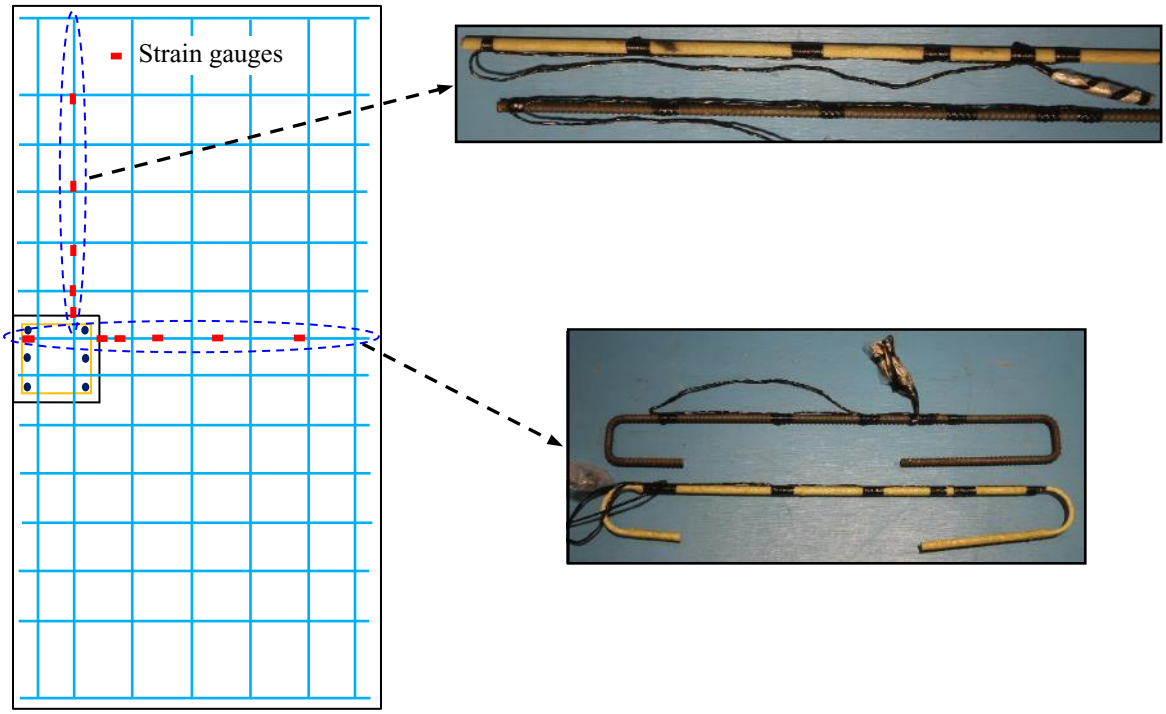

(b) Slabs without shear reinforcement

Figure 3.15 – Strain gauges instrumentation for flexural reinforcement

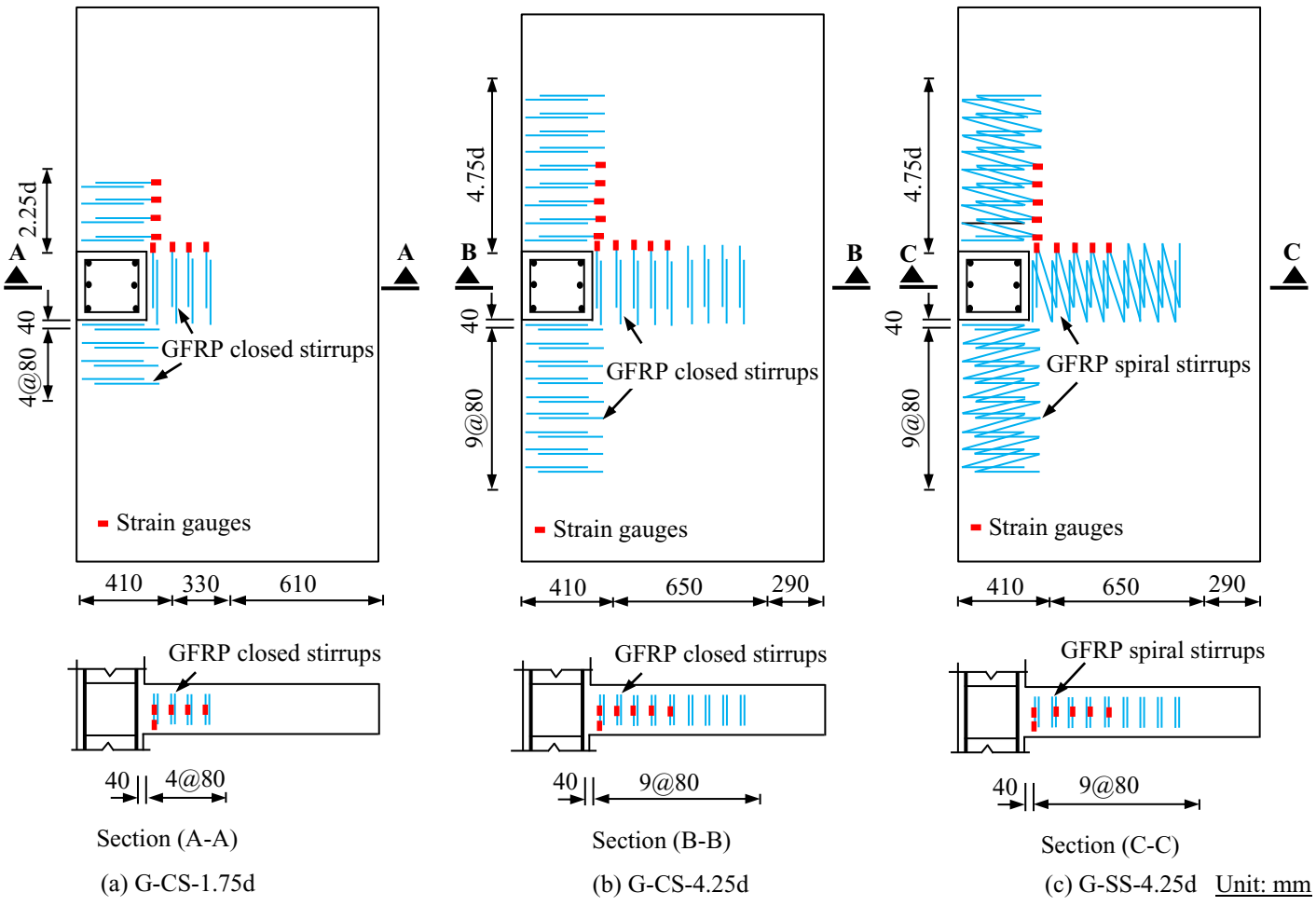

Figure 3.16 – Strain gauges instrumentation for shear reinforcement

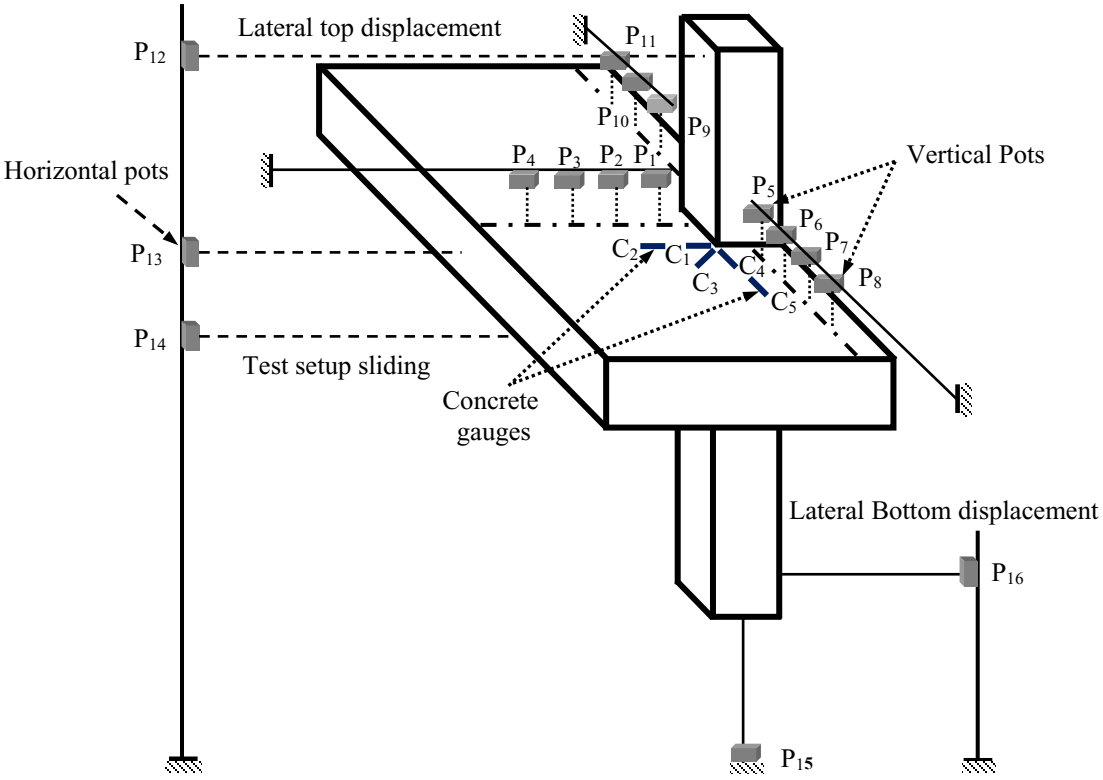

Figure 3.17 – String potentiometers and concrete gauges instrumentation

CHAPTER 4

Article 1: EFFECTIVENESS OF GFRP STIRRUPS AS SHEAR REINFORCEMENT IN GFRP-RC EDGE SLAB–COLUMN CONNECTIONS

Foreword

Authors and Affiliation

- Ahmed E. Salama: PhD Candidate, Department of Civil Engineering, University of Sherbrooke, Quebec, Canada J1K 2R1, E-mail: Ahmed.Salama@USherbrooke.ca

- Mohamed Hassan: Postdoctoral Fellow, Department of Civil Engineering, University of Sherbrooke, Quebec, Canada J1K 2R1, E-mail: Mohamed.Hassan@USherbrooke.ca.

- Brahim Benmokrane: **FACI**, is professor of civil engineering and NSERC Research Chair in FRP Reinforcement for Concrete Infrastructure. He is a member of ACI Committee 440 FRP Reinforcement and serves as co-chair of Canadian Standard Association (CSA) committees on FRP structural reinforcing materials for building design code (CSA S806), and bridge design code (CSA S6).
  Corresponding author, E-mail: Brahim.Benmokrane@USherbrooke.ca.

Paper submitted to ACI structural journal on September 9, 2018

Paper status: Published on September 1, 2019 (DOI: 10.14359/51716757)

Reference: Salama , A. E. , Hassan , M., and Benmokrane, B., 2019, "Effectiveness of GFRP Stirrups as Shear Reinforcement in GFRP RC Edge Slab–Column Connections," *ACI Structural Journal, V. 116, No. 5.*

Abstract

Recent years have seen a great interest in testing concrete slab-column connections reinforced with glass-fiber-reinforced-polymer bars (GFRP-RC). Yet, current FRP codes and guidelines have not addressed the design of slab-column connections with FRP shear reinforcement. Results from an experimental investigation aimed at evaluating the effectiveness of glass-fiber-reinforced-polymer (GFRP) stirrups as shear reinforcement in edge slab–column connections reinforced with GFRP bars are presented. Four full-sized slabs with and without stirrups as shear reinforcement were tested to failure under combined vertical load and unbalanced moment. The effect of the GFRP-stirrup type and extension on the punching shear response of the tested slab–column connections are analyzed and discussed. In addition, simplified design provisions to predicate the ultimate shear capacity of the tested specimens are proposed. The test results revealed that the presence of GFRP shear reinforcement as either closed or spiral stirrups within the slab around the column perimeter improved the punching-shear response of the tested connections. The results also indicated that the performance of the spiral stirrups was equivalent to or better than that of the closed stirrups in reducing the brittleness of the tested specimens with the same amounts of flexural and shear reinforcement. The proposed design provisions as extensions to those in CSA S806 design code yielded good yet conservative predictions with an average V_{test}/V_{pred} of 1.28 ± 0.24 for test specimens with FRP shear stirrups as well as others with different types of FRP shear reinforcement found in the literature. This represents a step forward for engineers in designing two-way concrete slabs reinforced with FRP stirrups.

Keywords: Punching Shear, FRP, Flat Slab, Edge Slab, Parking Garages, Design Codes, Stirrups, Shear Reinforcement, Unbalanced Moment.

4.1. Introduction

The construction industry has expressed great demand for innovative and durable structural members. Glass-fiber-reinforced-polymer (GFRP) reinforcing bars have recently gained wide acceptance as a viable construction material for sustainable new constructions. Reduced material costs—coupled with labor savings inherent with its light weight and comparatively simple installation, its high tensile strength, and immunity to corrosion and chemical attack—have made GFRP reinforcing bars an attractive alternative to steel reinforcement in concrete members subjected to severe environmental conditions. Code writing bodies in the USA and Canada have tasked several technical committees to produce standards and guidelines for elements reinforced with GFRP, including AASHTO (2009), ACI 440-1R (2015), CSA S806 (2012), and CSA S6 (2014). Field applications over the last years have shown excellent performance and durability of GFRP-reinforced structures (Benmokrane et al. 2007; Ahmed et al. 2014, etc.). Only limited work, however, has been conducted on implementing GFRP reinforcement in two-way concrete flat-slab parking structures (Ahmed et al. 2017).

Reinforced-concrete (RC) two-way flat-slab systems are very popular in construction because of their functional and economic advantages. Yet this type of structural system is not very efficient in terms of energy dissipation and is vulnerable to a type of brittle failure known as a punching-shear failure. When designing edge slab–column connections, the lack of symmetry of the portion of the slab resisting the punching action and relatively large unbalanced moments to be transferred between the slab and column may produce significant shear stresses that increase the likelihood of brittle failure, which must be considered. The avoidance of such a failure is of paramount importance. Various solutions have been used in the past to mitigate punching-shear failure at a slab–column connection. This can be achieved by simply (1) increasing the slab thickness by providing a drop panel or capital or increasing the column dimensions; (2) using higher-strength concrete; or (3) providing additional shear strength through shear reinforcement in the form of stirrups, shear studs, shear heads, or shear bands within the slab around the column perimeter. The latter solution is more effective and practical than the other two methods in increasing the punching-shear strength and deformation capacity of slab–column connections (Megally and Ghali 2000), which is one of the primary motivations of this research.

Despite the increasing demand to use GFRP reinforcing bars in two-way flat slabs (Dulude et al. 2013; Hassan et al. 2013 a, b; Gouda and El-Salakawy 2015; Hassan et al. 2017), very limited research has been conduced on FRP edge slab–column connections (Zaghloul 2007; El-Gendy and El-Salakawy 2016, 2018; Mostafa and El-Salakawy 2018). Most of the existing studies have been focused on the behavior of two-way slabs reinforced solely with GFRP bars as flexural reinforcement. There is also the potential for FRP-shear reinforcement in the form of stirrups, shear studs, or corrugated GFRP bars to improve the punching-shear strength of two-way slabs reinforced with GFRP bars (Hassan et al. 2014 a, b; El-Gendy and El-Salakawy 2016; Mostafa and El-Salakawy 2018).

New types of FRP shear reinforcement for slabs have been tested at the University of Sherbrooke (Hassan et al. 2014 a, b): sand-coated carbon- and glass-FRP shear reinforcement in the form of discrete closed and spiral stirrups. The stirrup shear reinforcement proved quite effective in tests on GFRPRC interior connections. The use of FRP stirrups significantly increased the punching-shear strength and deformation capacity on average by 27% and 107%, respectively, particularly when the flexural reinforcement ratio was high. El-Gendy and El-Salakawy (2016) tested two GFRP edge connections with another type of FRP shear reinforcement, headed studs, which consisted of ribbed GFRP bars with double heads. The studs were placed in an orthogonal layout with 0.5d and 0.75d spacing between the rows of studs. Decreasing the spacing of the shear studs from 0.75d to 0.5d increased the punching-shear strength by 34% and 46%, respectively, and the maximum deflections by 55% and 142%, respectively, compared to connections without shear reinforcement. Mostafa and El-Salakawy (2018) examined two types of GFRP shear reinforcement, specifically, sand-coated double-headed GFRP studs and corrugated GFRP bars in tests on edge slab–column connections reinforced with GFRP bars. The test results indicate that both types of shear reinforcement can be highly satisfactory in preventing brittle punching-shear failure in the column vicinity. The average increases in the ultimate shear strength were 27% and 16% and the deformation capacity were 64% and 46% for the shear studs and corrugated GFRP bars, compared to their counterparts without shear reinforcement, respectively.

Based on these earlier studies, FRP shear reinforcement has demonstrated its ability to develop substantial increases in punching-shear and deformation capacities, making it an attractive

alternative to traditional methods, such as drop panels and column capitals, for the construction of two-way GFRPRC slabs, especially when there are constraints on slab thickness. It is worth mentioning that the current North American codes for FRP—ACI 440.1R (2015) and CSA S806 (2012)—do not have provisions for designing GFRP-reinforced connections with FRP shear reinforcement. This is mainly due to a lack of experimental research, particularly on edge connections. Given the increase use of FRP as flexural and transverse shear reinforcement in different structural elements such as beams, beam–column joints, and piles, similar code provisions are urgently needed for two-way flat-slab structures reinforced with FRP flexural and shear reinforcement.

This paper presents experimental tests on GFRP edge slab–column connections with the aim of investigating the influence of GFRP-stirrup type (closed and spiral) and extension inside the slab around the column perimeter on the punching-shear strength and failure within or outside the shear-reinforced zone. Detailed measurements on deflections, slab–column rotation, concrete strains, and flexural- and shear-reinforcement strains facilitate a better understanding of the behavior of GFRP edge slab–column connections with GFRP stirrups.

4.2. Research Significance

The purpose was to assess the effectiveness of the GFRP stirrups, considering the effects of GFRP-stirrup type and extension within the slab in a crucifix layout around the column faces. The paper also establishes design provisions and recommendations for engineers in designing two-way flat slabs with GFRP stirrups as shear reinforcement. The recommendations herein may support the work of the North American technical committees engaged in the development of standards and design provisions for GFRP-RC slab-column connections columns subjected to combined vertical load and unbalanced moment.

4.3. Experimental Program

4.3.1. Overall Specimen Configuration and Design

In this study, a total of four full-size specimens were constructed and tested to failure under combined vertical load and unbalanced moment. The test specimens represented edge

connections from a prototype RC flat-slab structure with 5 × 5 m^2 (196.9×196.9 in^2) square panels. Each specimen was simply supported on three edges, simulating lines of contra flexure in the prototype floor, and monolithic with a column at the middle of the fourth edge. The lines of contra flexure were assumed to be 0.2*l* away from the column centerlines, where *l* is the span between the column centerlines. All slabs had identical geometries of 2500 × 1350 × 200 mm (98.4 ×53.1×7.9 in.) with a 300-mm (11.8 in.) square column stub protruding 700 mm (27.6 in.) above and below the slab surfaces. The slabs were simply supported on a 2000 × 1150 mm (78.7 × 45.3 in.) perimeter on the bottom face of the slab. The nominal concrete cover both on the top and bottom faces of the slabs was 21 mm (0.83 in.). Figure 4.1 shows the typical geometry and reinforcement details of the test specimens.

All slabs had identical reinforcement in the tension and compression sides as well as similar material properties but different types of transverse-reinforcement systems and extension from the column faces. Each specimen was reinforced in the short and long directions, respectively, with 10 and 20 No. 20 bars (20 mm (0.79 in.) in diameter) as a flexural tension reinforcement in the bottom side and 7 and 10 No. 15 bars (15 mm (0.6 in.) in diameter) in the compression (top) side with at least two bars passing through the column core to satisfy the requirement for structural integrity reinforcement in CSA A23.3 (2014). The average bottom reinforcement ratio (ρ_b) was 1.55%, while the average compression (top) reinforcement (ρ_t) was 0.68%. Table 4.1 presents the test matrix and characteristics for each specimen.

Specimens with shear reinforcement were designed to have high amounts of flexural reinforcement such that punching-shear failure would be expected to occur prior to flexural failure. That would allow for measuring the shear-strength contribution of the GFRP stirrups and for the shear-reinforcement system to achieve its maximum strength and deformation capacity. Two connections (G-CS-1.75d and G-CS-4.25d) were reinforced in shear with discrete four branches of closed GFRP stirrups (No. 10, 10 mm in diameter) extended to 1.75d and 4.25d away from the column face, respectively, where d is the slab effective depth equal to 160 mm. Slabs G-CS-1.75d and G-CS-4.25d were designed to evaluate the effect of stirrup extension on the punching behavior and to quantify the concrete contribution (v_c) to shear strength outside the shear reinforced zone. The third connection (G-SS-4.25d) was reinforced with four branches of spiral GFRP stirrups (No. 10) extended to 4.25d away from the column face to study the

influence of stirrup type on the punching strength and deformation capacity and to compare its behavior with the counterpart slab (G-CS-4.25d) with discrete closed stirrups. The remaining slab (G) served as the control with no shear reinforcement. The shear-reinforcement ratio (ρ_{fv}) at the perimeter of 0.5d from the column face was maintained constant at 0.9%.

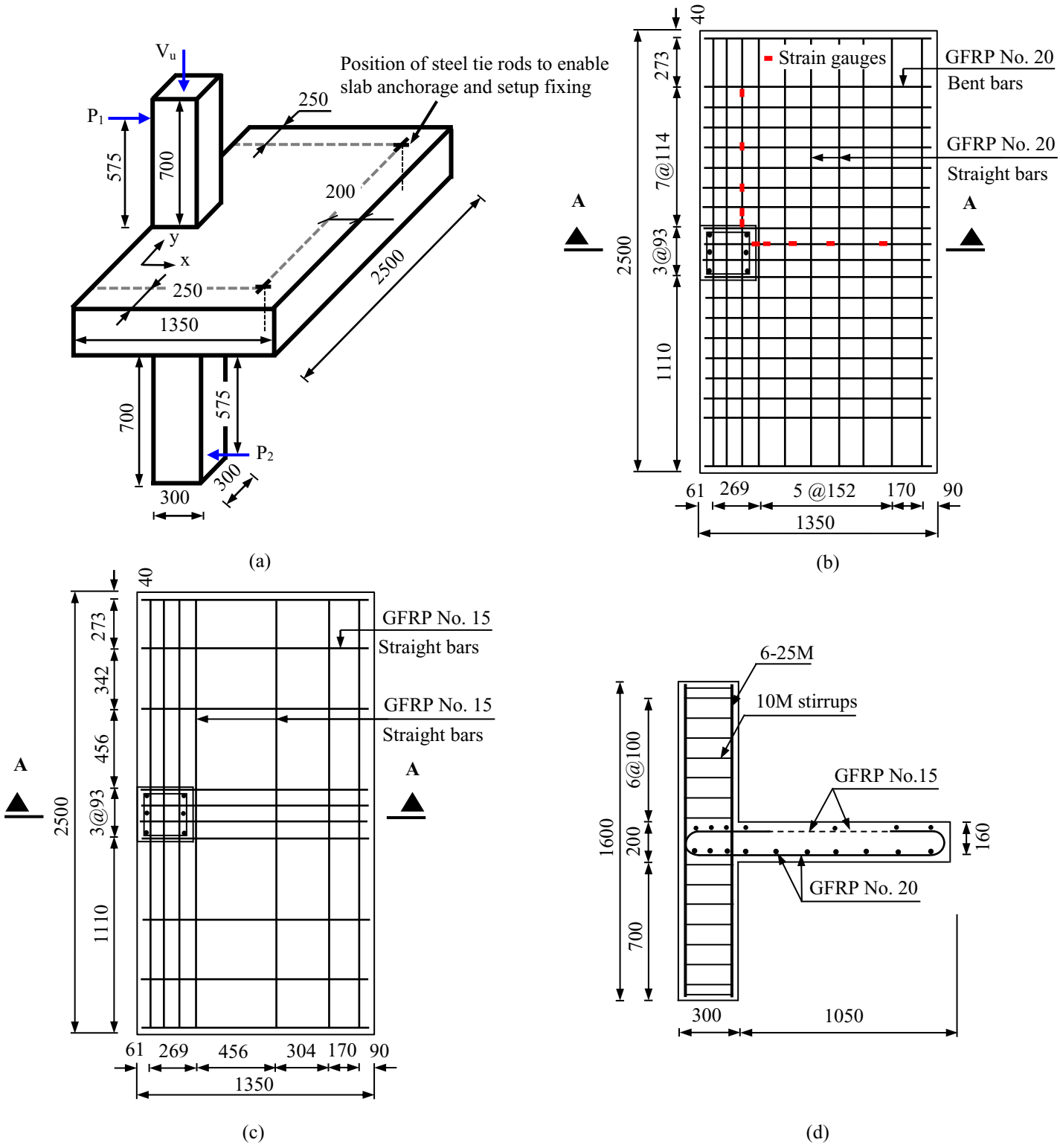

Figure 4.1 – Typical slab geometry and reinforcement details: (a) Concrete dimension; (b) Bottom mesh configuration; (c) Top mesh configuration; (d) Sec (A-A) (Note: 1 mm = 0.0394 in.)

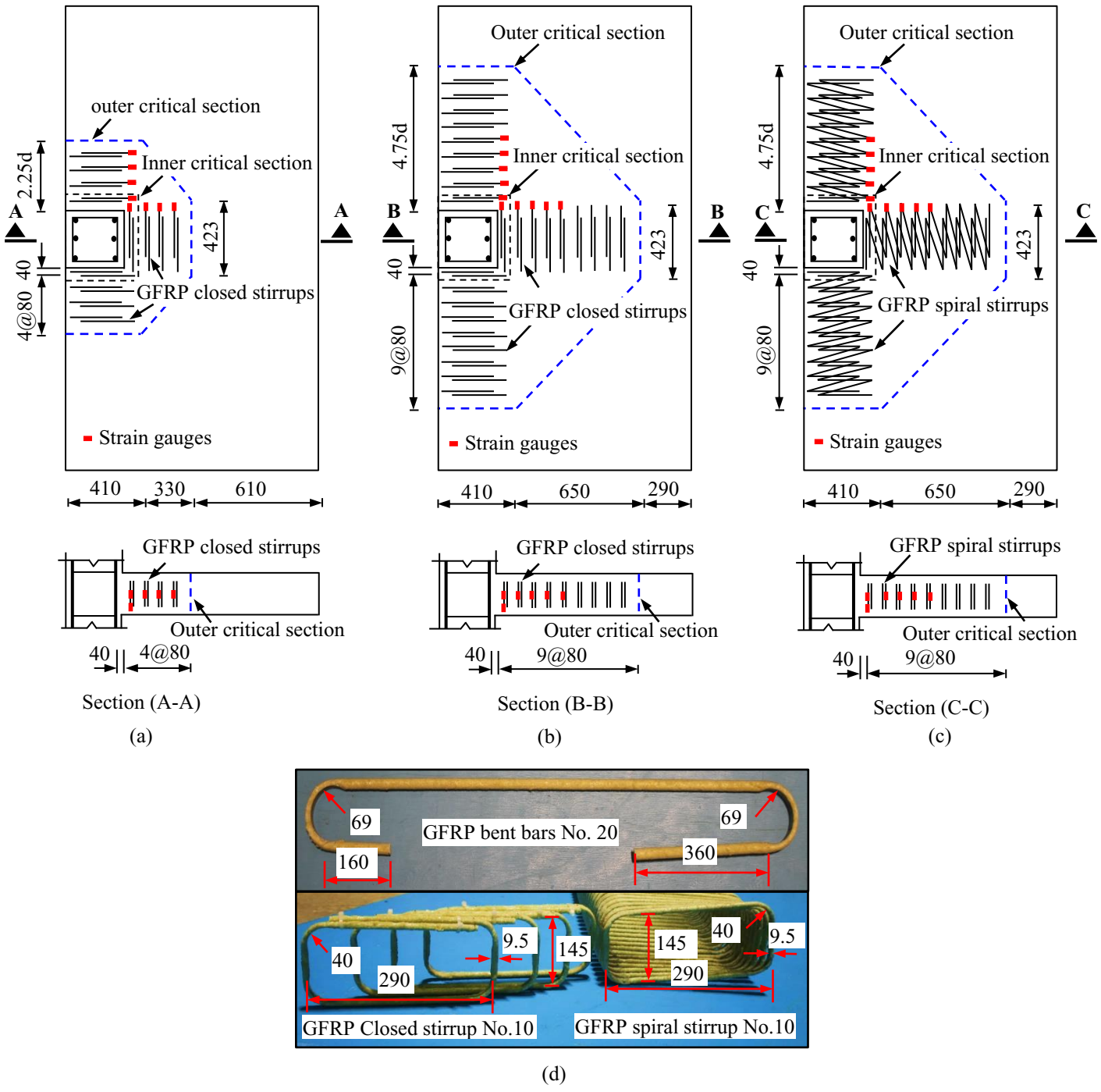

Figure 4.2 – Shear stirrups configuration: (a) Closed stirrups arrangement (G-CS-1.75d); (b) Closed stirrups arrangement (G-CS-4.25d); (c) Spiral stirrups arrangement (G-SS-4.25d); and (d) Typical dimensions of bent bars and stirrups (Note: 1 mm = 0.0394 in.)

The shear-reinforcement stirrups were arranged in a cruciform pattern according to ACI 318 (2014) and CSA A23.3 (2014). The number of peripheral lines of shear reinforcement varied

between four and nine in both directions among the specimens; the spacing between the consecutive lines was 0.5d. The first perimeter was offset 0.25d from the column face for all slabs with shear reinforcement, as specified in CSA A23.3 (2014). Figure 4.2 shows the shear-stirrup layout and arrangement. Each slab was monolithic with a square column stub, which was designed to transfer shear force and lateral moment to the slab without any premature column failure. The column reinforcement consisted of six 25M deformed steel bars (three bars on each face) with 10M deformed closed steel ties at 100 mm (3.9 in.). Figure 4.1 provides the details of the reinforcement used in the test specimens.

Table 4.1 – Details of test specimens

Test Specimen [a]	f_c' [b], MPa	f_t' [b], MPa	Average Flexural-Reinforcement Ratio		Stirrup Layout Parameters				
			Bottom	Top	Shape	Width × height, mm× mm	S_o, mm	S_{fv}, mm	Extent
			ρ_b, %	ρ_t, %					
G	41.4	3.6	1.55	0.65	------	------	------	----	----
G-CS-1.75d	47.6	3.9	1.55	0.65	Closed	290×145	0.25	0.5d	1.75d
G-CS-4.25d	51.3	3.9	1.55	0.65	Closed	290×145	0.25	0.5d	4.25d
G-SS-4.25d	52.5	3.5	1.55	0.65	Spiral	290×145	0.25	0.5d	4.25d

[a] G-aa-xd: G for GFRP tension reinforcement, aa for stirrup configuration (CS for closed stirrups; SS for spiral stirrups); and xd for stirrup distance from the column faces relative to the average effective depth, if any.
[b] Cylinder strength at day of testing [100×200mm cylinders (3.9×7.9 in.)].
1MPa = 145 psi; 1 mm = 0.0394 in.

4.3.2. Material Properties

Concrete—All specimens were cast using normal-weight, ready-mixed concrete with a targeted 28-day concrete compressive strength of 35 MPa and 5% to 8% of entrained air. The slab and the bottom and top column stubs were cast monolithically on the same day. The concrete compressive (f_c') and tensile strength (f_t') of each specimen were determined, on the day of testing, using six 100 × 200 mm (3.9 × 7.9 in.) concrete cylinders for each of the compression and splitting tests. The concrete compressive strength ranged from 41.4 to 52.5 MPa (6 to 7.6 ksi), whereas the tensile strength ranged from 3.5 to 3.9 MPa (0.51 to 0.57 ksi). Table 4.1 provides the concrete strengths.

Flexural Reinforcement—Grade II and III sand-coated GFRP bars—classified in CSA S807 (2015) as No. 15 and No. 20—were used as flexural reinforcement in all specimens. Each specimen was reinforced with layers of straight GFRP bars, except for the tension reinforcement

(bottom) in the short direction, which had double bent ends. That was to provide the required anchorage and avoid any unexpected mode of failure, such as slippage failure rather than punching failure. Table 4.2 reports the tensile properties of the GFRP bars, which were determined by testing five representative specimens in accordance with ASTM D7205M (2011) as shown in Figure 4.3. The tensile properties were calculated with nominal cross-sectional areas.

Transverse shear reinforcement—Discrete No. 10 closed and rectilinear sand-coated spiral GFRP stirrups [290 mm (11.4 in.) wide × 145 (5.7in.) mm high] were used as shear reinforcement. The tensile strength and elastic modulus of the straight portions were determined in accordance with ASTM D7205M using five samples cut from the FRP stirrups. The bend strength of the GFRP stirrups was determined by testing five specimens according to the B.5 test method (concrete blocks) in accordance with ACI 440.3R-04 (2012). Figure 4.3 also shows specimen preparation and testing as well as the mode of failure, whereas Table 4.2 presents the tensile properties of the GFRP stirrups. Figure 4.2 also depicts the FRP bent bars and shear-reinforcement stirrups used herein.

Table 4.2 – Tensile properties of the reinforcing bars and shear reinforcement

Bar Designation [a]	Nominal Cross-Sectional Area [a] (mm^2)	Ultimate Tensile Strength (MPa)	Elastic Tensile Modulus (GPa)	Ultimate Tensile Strain (%)
GFRP straight flexural bars				
No. 15 GFRP bar	199	1323 ±12	64.8±0.5	2.04 ±0.05
No. 20 GFRP bar	285	1334 ±85	64.9±0.6	2.06 ±0.13
GFRP bent flexural bars				
No. 20 straight portion	285	1210±63	53.0±0.48	2.28±0.15
No. 20 bent portion		f_{fvb} [b]= 490±44	------	------
GFRP-stirrup shear reinforcement				
No. 10 straight portion	71	967±39	45.7±0.5	2.12±0.08
No. 10 bent portion		f_{fvb} [b]= 489±38	------	------
Steel bars				
10M	100	f_y [c]= 420	200	ε_y = 0.21
25M	500	f_y [c]= 470	204	ε_y = 0.23

[a] According to CSA S807 (2015).

[b] f_{fvb} = ultimate tensile bend strength obtained from the B.5 test method according to ACI 440.3R (2012).

[c] f_y steel yielding strength and ε_y steel yielding strain, as provided by the manufacturer.

Note:1 MPa = 145 psi; 1 GPa = 145 psi; 1 mm^2 = 0.00155 $in.^2$

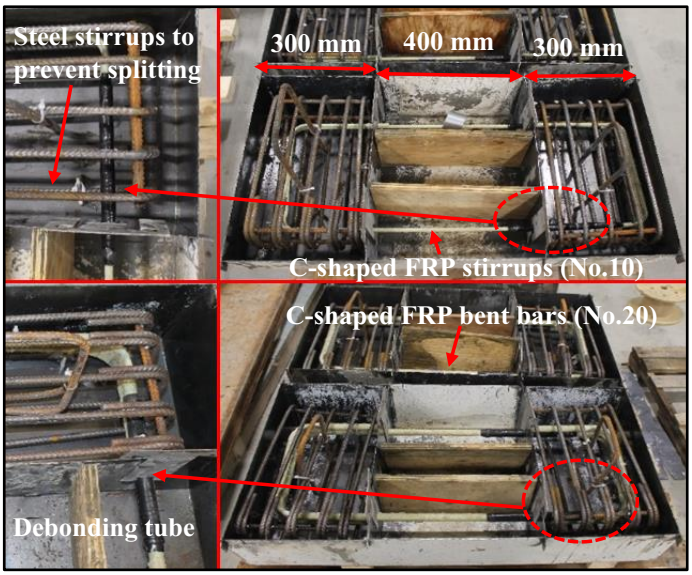

(a)

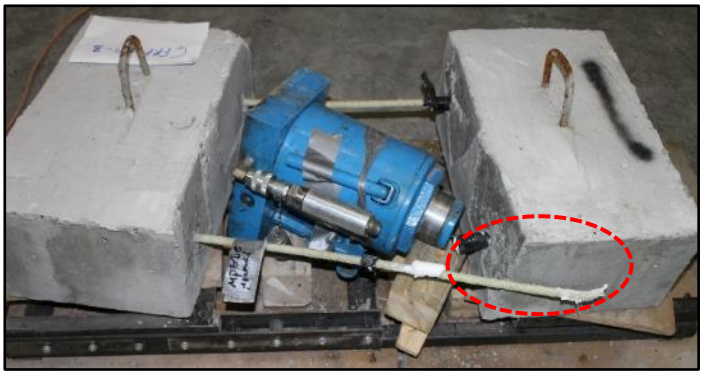

(b)

Figure 4.3 – B5 test method: (a) B5 test specimens; (b) Typical mode of failure at bend portion

(Note: 1 mm = 0.0394 in.)

4.3.3 Instrumentation

Strains in the bottom flexural reinforcement (tension side) were measured with 11 electrical resistance strain gauges [6 mm (0.24 in.) long] at different locations in both orthogonal directions (Fig 4.1). The strain gauges were located at a distance of 0, 75, 225, 450, and 750 mm (0, 3, 8.9, 17.7, 29.5 in.) from the column face on one bar in each direction. In addition, one electrical strain gauge was glued at the bend location of the GFRP bar at the column location (see Fig. 4.1). Strains in the GFRP stirrups were measured through 6 mm (0.24 in) strain gauges mounted at mid-height of the vertical legs and bend location in each orthogonal direction as shown in Fig. 2. In addition, five concrete electrical strain gauges [60 mm (23.6 in.) long]—

labeled C1 to C5—were glued before testing to the slab's top surface (compression side) at 0 and 200 (7.9 in.) mm from the column face (see Fig. 4.4).

Sixteen string potentiometers (pots) were used at different locations to measure the displacements. Eleven pots (P_1 to P_{11}) were placed on the top slab face along two orthogonal directions at a distance of 80, 250, 550, and 850 mm (3.1, 9.8, 21.6, 33.5 in.) from the column face to measure the slab-deflection profile while one pot (P_{15}) was located at the column centerline to measure the central deflection. Two pots (P_{12} and P_{16}) were installed horizontally on the top and bottom column ends to measure column lateral displacements. To monitor any possible shifting of the specimen or test setup, two pots (P_{13} and P_{14}) were installed in the horizontal loading directions at the center of slab thickness and frame test setup. All instruments were installed onto rigid steel frames, separated from the testing frame and attached directly to the laboratory floor, to prevent any frame deformations from affecting the measurements. The strain gauges, and pots were connected to a data-acquisition system to record the readings. Figures 4.1, 4.2, and 4.4 show the position of several instrumentation details of the test specimen. During the test, crack propagation was marked, and the corresponding loads were recorded.

4.3.4. Experimental Setup

The specimens were tested in the structural laboratory at the University of Sherbrooke under monotonic vertical shear force and lateral static unbalanced moment until failure, as shown in Fig. 4.5. The test setup included three main parts: (1) the testing frame, (2) reaction frames, and (3) the supporting bed and top restrain beams. The testing frame consisted of two main frames (labeled number 1 in Fig. 4.5) and a stiff connecting steel I-beam on top. A 1500-kN (337.2 kip.) vertical hydraulic jack was installed at the center of the I beam to apply vertical load at the top of the concrete column. During testing, a steel pan with rollers (connection 5) was placed between the vertical jack and the top of upper concrete column to free horizontal movement of the column during lateral loading while maintaining the vertical load. Two 1000 kN (224.8 kip.) horizontal hydraulic jacks were installed on two very rigid reaction frames (labeled number 2 in Fig. 4.5) fixed firmly to the laboratory strong floor to apply lateral loads. The vertical and lateral jacks were controlled using three manual hydraulic pumps. The loads were monitored with three load cells on each pump and connected to the data-acquisition system.

The specimens were simply supported on the bottom surface along three sides during testing with a new fabricated supporting steel bed (labeled number 3 in Fig. 4.5), which was designed to ensure adequate strength and stiffness under the testing load of the specimens. The supporting bed consisted of four-square steel beams [HSS 250 × 150 × 8 mm (9.8 × 6 × 0.3 in.)] supported on four square columns [HSS 152 × 100 × 6 mm (6 × 3.9 × 0.24 in.)] laterally stiffened with back-to-back double steel angles [102 × 102 × 7.9 mm (4 × 4 × 0.31in.)] in both directions. It is worth mentioning that, before placing the test specimen in the setup, the supporting bed was prestressed directly on the laboratory strong floor with four 38 mm (1.5 in.) diameter steel tie rods to prevent the supporting bed from moving laterally. On the slab top face, the three supported edges were restrained by steel reaction beams (labeled number 4) to prevent slab lifting. Each end of the reaction beam was held in position by four steel nuts and plates attached to the steel tie rods. In addition, 20 mm (0.79 in.) thick neoprene pads were placed between the slab and supporting bed and between the slab and top restrain beams along the support lines to simulate slab rotation at the line of contraflexure and ensure uniform stress distribution along the edges.

4.3.5. Test Procedure

The specimens were subjected to vertical load (V) through the column stub and unbalanced moment (M_{un}) through two opposite horizontal loads (P) applied at the tips of column ends. The unbalanced moments were calculated by multiplying the two lateral loads, applied to each column by the distance from the application point to the center of the slab: 675 mm (26.6 in.) [see Fig. 4.1]. The ratio between the unbalanced moment and vertical load (M_{un}/V) was 0.3 m (11.8 in.). This value was based on analysis of a typical floor-system prototype under gravity loads only according to CSA A23.3 (2014). The vertical load was applied monotonically at a load-controlled rate of 5 kN/min (1.12 kip/min), whereas the horizontal loads were simultaneously applied with the vertical load in small increments to maintain a constant *M/V*

ratio of 0.3 m (11.8 in.) throughout the test until failure.

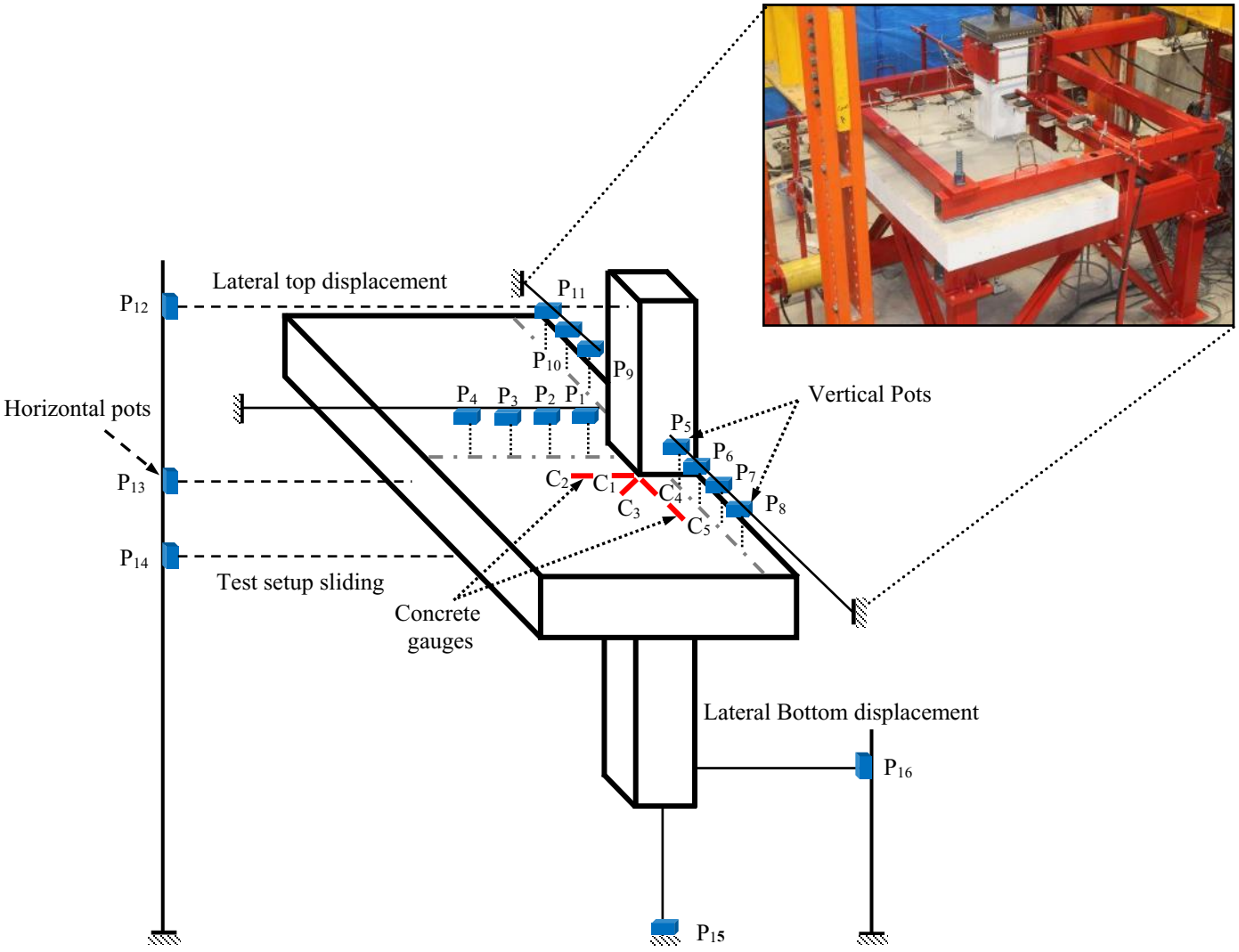

Figure 4.4 – Instrumention details

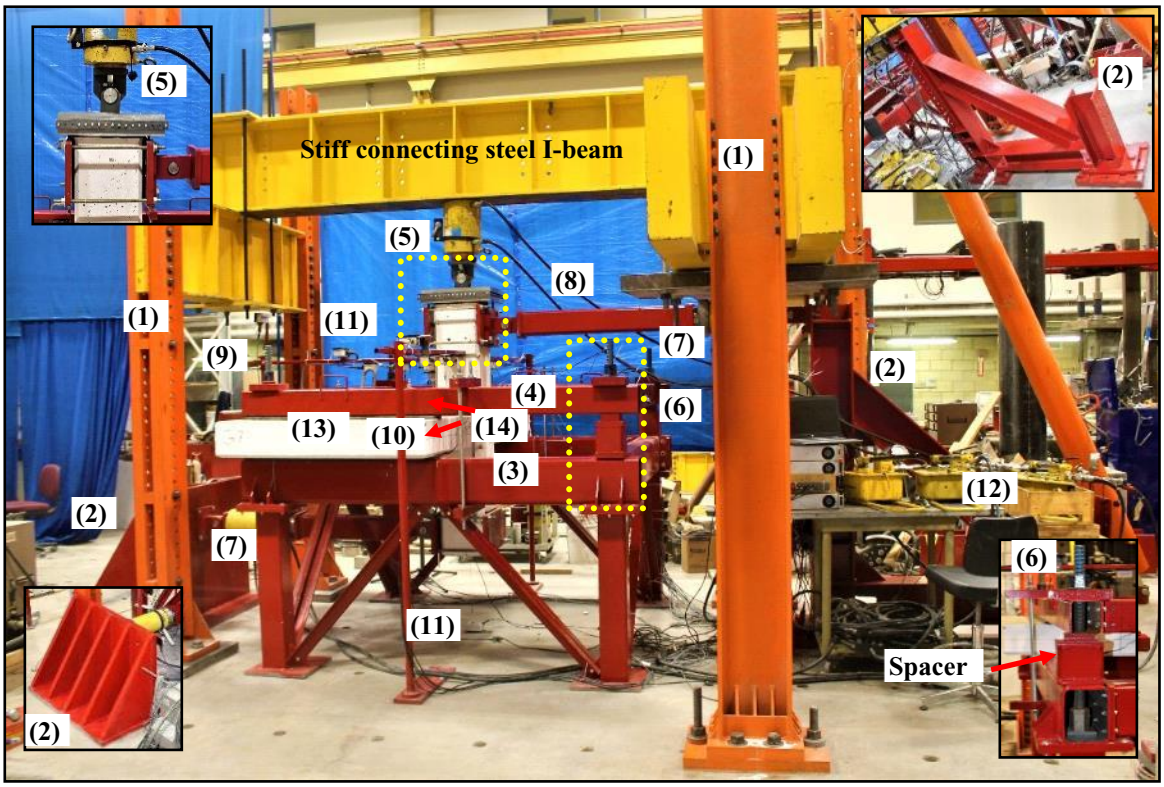

(1) Main steel frames	(2) Reaction frames
(3) Square prestressed supporting bed	(4) Restrain top frame
(5) Steel pan, roller, and column collar joint	(6) Bed connection
(7) Lateral hydraulic jacks	(8) Lateral steel post
(9) 4 Steel tie rods (38 M in diameter)	(10) Steel clamps
(11) Pot supporting frame	(12) Hydraulic pumps and data-acquisition system
(13) Test specimen	(14) Neoprene pads [20 mm (0.79 in.) thick]

Figure 4.5 –Test setup

4.4. Test Results

4.4.1. Overall Response and Cracking Pattern

The tested specimens showed similar cracking propagation on the bottom surface (tension side) and along the slab's free edge during the test. Specimens with shear reinforcement, however, evidenced more intensive cracks with larger punching-shear failure surfaces compared to their counterpart without shear reinforcement. Figure 4.6 shows the cracking patterns for all the test specimens in tension and compression and along the free-edge sides. Generally, three typical kinds of cracks were observed on the tension side, progressing in the following sequence as the applied loads were increased: 1) Radial flexural cracks (fan-shaped) originated from the inner slab–column interface and propagated towards the supports. The cracks began to appear at vertical loads between 51 and 72 kN (11.5 and 16.2 kip) [at about 15% to 16% of the ultimate loads]. (2) Inclined torsion cracks formed at the inner corners of the columns at about 35° form the slab edge. The cracks started to appear at between 23% and 25 % of the ultimate loads. They then propagated upward the slab edge to half of the slab depth at approximately 50% of the ultimate loads and then further extended until reaching the top of the slab. These cracks were normally developed at an angle of approximately 90° to the diagonal shear cracks that formed later when punching occurred. (3) Circumferential (tangential) cracks generated around the column and crossed over the radial cracks at higher loads approximately at 52% to 60% of the test-specimen ultimate loads. As the loads increased, the number of such cracks and their widths in the column vicinity increased. At the same time, new diagonal shear cracks caused by the shear stresses initiated near the slab free edge from the bottom side and then extended toward the top of the slabs. These diagonal cracks propagated with small widths until the test specimen failed. At failure, a major tangential crack was intercepted by the flexural cracks in approximately perpendicular manner forming the punching cone. Figure 4.6 shows the diagonal shear cracks at the free edge of the slabs.

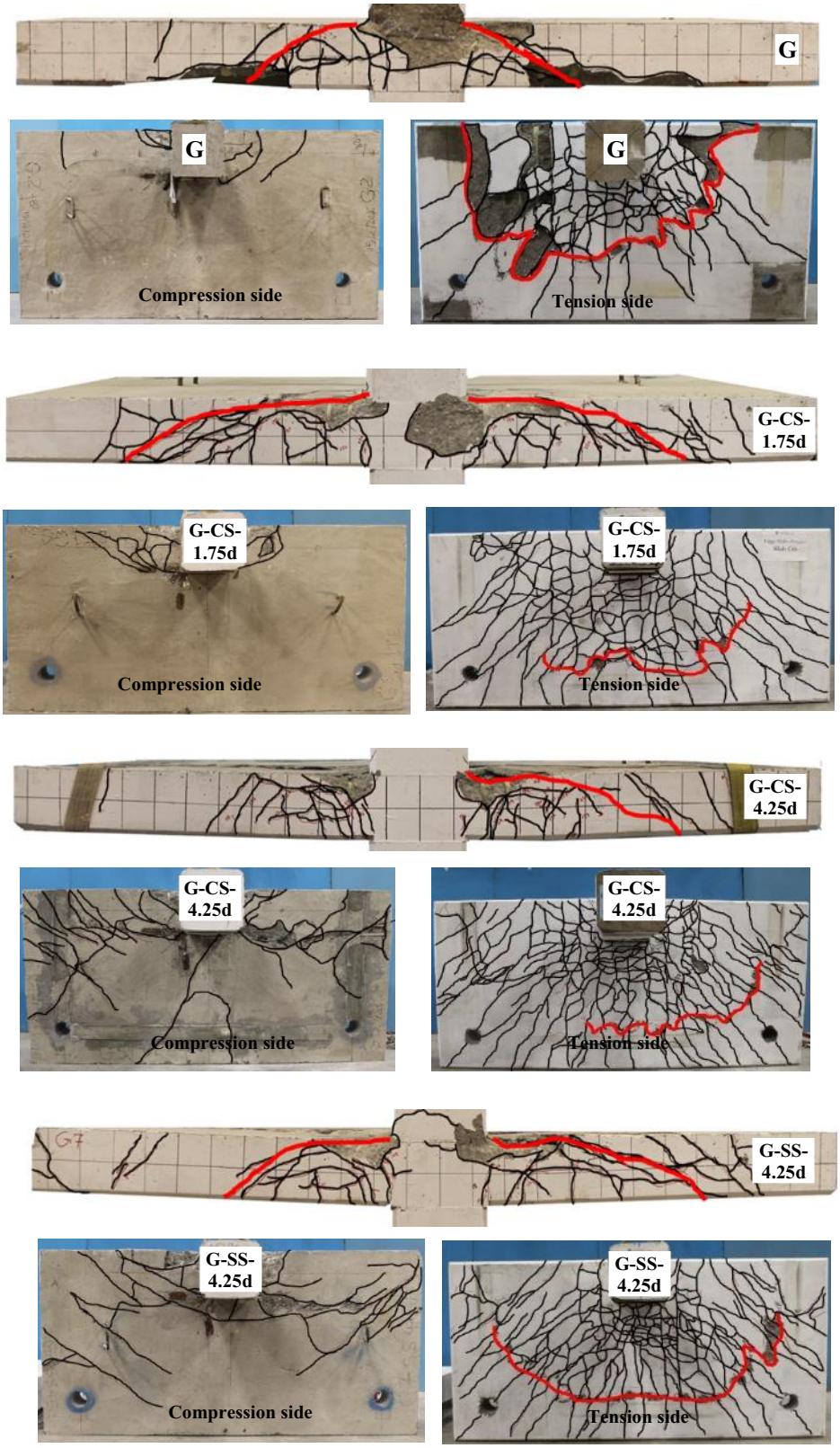

Figure 4.6 – Cracking patterns and punching-shear failure surface for the tested specimens

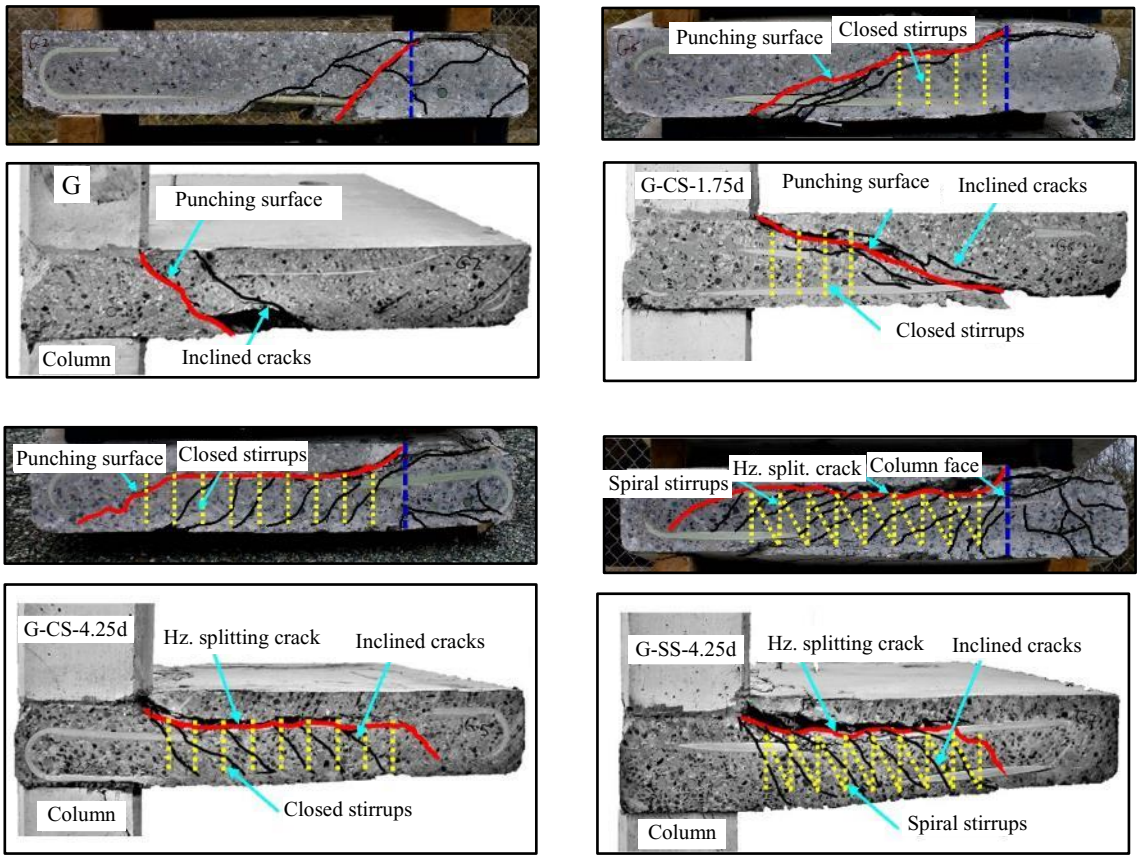

Figure 4.7 – Inclined shear cracks and failure envelope on the two parts of cut sections

4.4.2. Mode of Failure and Envelope

Control specimen G, without shear reinforcement, experienced a typical brittle punching-shear failure without much warning. The punching failure along the slab free edge was characterized by a main diagonal shear crack inclined to the tension side of the slab at an angle of 29º. Spalling of the concrete cover on some parts of the tension side as well as fine torsion cracks on the slab compression side (Fig. 4.6) were also observed. In the case of specimen G-CS-1.75d, with stirrups extended 1.75d, the FRP stirrups effectively contributed in distributing the shearing forces to the uncracked concrete outside the shear-reinforced zone. The mode of failure was punching-shear failure outside the shear zone. Some deformability was, however, achieved before failure compared to the control specimen, G, without shear reinforcement. The slab free edge evidenced horizontal splitting cracks over the top of the shear stirrups near the column top before joining with inclined cracks that developed outside of the shear-reinforced zone. The

angle of the shear crack at the free edge was 25º with respect to the slab tension side. Other torsion cracks on the slab compression side were also observed.

The extension of the FRP stirrups by 4.25d for specimens G-CS-4.25d and G-SS-4.25d offered sufficient resistance and larger deformations before final failure. A similar horizontal splitting crack over the top of the shear reinforcement, as in specimen G-CS-1.75d, was seen at the slab free edge but extended further away from the column face to the sixth line of stirrups before joining with inclined cracks. The increase in the deformation capacity and the concrete crushing in the column vicinity on the compression side of the slabs were considered early warning signs before the punching-shear failure occurred. As a result, the mode of failure was mixed flexural–punching-shear failure within the shear-reinforced zone. This behavior has been observed with interior steel-reinforced slab–column connections reinforced with shear studs (Grander et al. 1996 and Dam et al. 2017).

Figure 4.7 shows sawn sections for all specimens with and without shear reinforcement through a line perpendicular to the free edge and adjacent to the column. This figure shows a clear view of the cracks within the slabs. Specimen G had a single shear crack with an inclination angle of 39.5º. The radius of the punching failure surface extended 2.9d [464 mm (18.3 in.)] from the lower column face. Specimen G-CS-1.75d had a horizontal splitting crack over the top of the stirrups. This splitting crack became an inclined shear crack beyond the outermost set of shear stirrups, which confirms that the punching shear occurred outside the shear-reinforced zone. The angle of the inclined shear crack was about 25º with respect to the slab tension side and the radius of the failure surface extended 3.9d [624 mm (24.6 in.)] from the bottom column face. For the other specimens, several inclined shear cracks were observed within the regions reinforced with shear stirrups as well as horizontal splitting cracks located above the shear stirrups. The formation of the horizontal splitting cracks near the columns is assumed to have caused the slight gradual drops in load capacity. Finally, these inclined and splitting cracks created the failure surfaces. This observation confirmed the occurrence of the mixed flexural–punching-shear failure.

4.4.3. Vertical Load–Deflection Characteristics

Figure 4.8 plots the applied vertical load versus deflection relationships at 80 mm from the column face in both directions for all the tested specimens. Table 4.3 provides the maximum

applied vertical load (V_u) and corresponding ultimate deflection (Δ_{Vu}) for each specimen. In general, the initial uncracked stiffness for all specimens was similar, regardless of the presence of shear reinforcement. The slabs with shear reinforcement, however, exhibited slightly higher post-cracking stiffness compared to their counterparts without shear reinforcement. In the case of control specimen G and specimen G-CS-1.75d, including limited stirrups around the column produced similar bilinear load–deflection responses until the punching failure occurred abruptly, as shown in Fig. 4.8. Specimens G and G-CS-1.75d failed, respectively, at 314 and 370 kN (70.6 and 83 kip) ultimate loads and at 21 and 28 mm (0.83 and 0.31 in.), corresponding to ultimate deflections along the moment direction. In comparison to specimen G, specimen G-CS-1.75d achieved 18% and 34% increases in failure load and deflection, respectively.

Specimens G-CS-4.25d and G-SS-4.25d, with shear reinforcement extending 4.25d, showed different responses compared to G and G-CS-1.75d, specifically gradual failure with considerable post-peak deformations. The addition of FRP stirrups resulted in flexure mechanism due to the mobilization of the shear reinforcement before punching-shear failure. Specimens G-CS-4.25d and G-SS-4.25d failed at ultimate loads of 444 and 486 kN (99.8 and 109.3 kip), respectively, and at corresponding ultimate deflections along the moment direction of 36 and 46 mm (1.4 to 1.8 in.), respectively. As shown in Fig. 4.8, the load–deflection curves for the two specimens were similar in both directions. Nevertheless, the load–deflection curves perpendicular to the free edge expanded horizontally in the opposite direction after the peak (see Fig. 4.8 a). This might be due to separation of the concrete over the stirrups in top surface of the slab because of opening the horizontal splitting cracks during the test and the deflection readings were not affected. The load–deflection curves parallel to the free edge showed post-peak softening behavior with large deformations (Fig. 4.8 b). The resulting maximum deformations of G-CS-4.25d and G-SS-4.25d at failure were 1.8 and 2.4 times that of G, respectively. This confirms the effectiveness of closed and spiral stirrups in achieving substantial deformations before slab collapse.

Table 4.3 – Summary of the test results

Specimen	Cracking		Ultimate Load				Δ_{vu}, mm		Strains at Ultimate Load (μs)					Deformability Factor, J_Δ	Energy Absorption		Failure Modes [b]
	V_{cr}, kN	M_{cr}, kN.	V_u, kN	M_u, kN.	$v_{u,\ inside}$, MPa	$v_{u,}$ outside, MPa	⊥ [a]	// [a]	Concrete, μs	Flexural ⊥ [a]	Flexural // [a]	FRP stirrups ⊥ [a]	FRP stirrups // [a]		Due to deflection	Due to rotation	
G	51	16	314	98	2.44	---	20.5	18.95	784	6432	5387	-----	-----	12.15	4.23	1.64	P
G-CS-	53	18	370	115	2.87	1.21	28.0	26.19	979	8661	7683	3918	3402	16.40	6.86	3.44	P *
G-CS-	63	20	444	133	3.38	0.88	35.8	33.36	2444	13,226	9141	6412	5899	32.59	10.54	6.60	P †
G-SS-4.25d	72	24	486	146	3.70	0.97	46.1	45.29	2696	13,947	9602	7035	6525	36.68	14.34	7.20	P †

[a] Position perpendicular (⊥) or parallel (//) to the free edge.

[a] P (punching failure).

* Brittle punching failure occurred outside the shear-reinforced zone.

† Flexure- punching failure occurred inside the shear-reinforced zone.

Note: 1 kN = 0.2248 kip, 1 kN.m = 8.86 kip.in., 1 mm = 0.0394 in.

4.4.4. Moment–Rotation Relationships

Figure 4.8 c gives the applied unbalanced moment versus column rotation relationships for all tested specimens. The column rotation was calculated as the ratio of the sum of measured displacements at the column ends by means of potentiometers P_{12} and P_{16} to the distance between the two loading rams (see Fig. 4.4). As seen in Fig. 4.8c, the measured rotations of the columns at failure increased with the use of stirrup shear reinforcement. The ultimate rotations for specimens G, G-CS-1.75d, G-CS-4.25d, and G-SS-4.25d were 0.0182, 0.0352, 0.0444, and 0.0515 radians, respectively. The ultimate moment increased by 17%, 36%, and 49% and rotation capacities increased by 93%, 144%, and 183% for specimens G-CS-1.75d, G-CS-4.25d, and G-SS-4.25d, respectively, compared to the control specimen G. It is also important to note that, in maintaining the same amounts of flexural and shear reinforcement in specimens G-SS-4.25d and G-CS-4.25d, spiral stirrups performed better than closed stirrups, with the ultimate moment and rotation capacities increased by 10% and 16%, respectively. On the other hand, increasing the stirrup extension around the column from 1.75d to 4.25d increased the moment and rotation capacities of the connection by 16% and 26%, respectively.

4.4.5. Flexural Reinforcement and Concrete Strains

Figure 4.9 plots the applied vertical load versus the flexural tension reinforcement and concrete strains for all tested specimens. The flexural-reinforcement strains were measured at 75 mm from the column face perpendicular and parallel to the free edge, whereas the concrete strains were recorded at the column face with gauge C1 (Fig. 4.4). Table 4.3 reports the maximum reinforcement and concrete strains. Specimen G, without shear reinforcement, showed the least tensile strain compared to its counterparts with GFRP-stirrup reinforcement. The maximum reinforcement strain was 6430 μs, which represents 35% of the ultimate tensile strength. Besides, the maximum concrete strains around the column region were low and below the concrete crushing strain of 3500 and 3000 μs, as per CSA S806 (2012) and ACI 440.1R (2015), respectively. Upon punching-shear failure, however, no concrete crushing in the compression zone was observed.

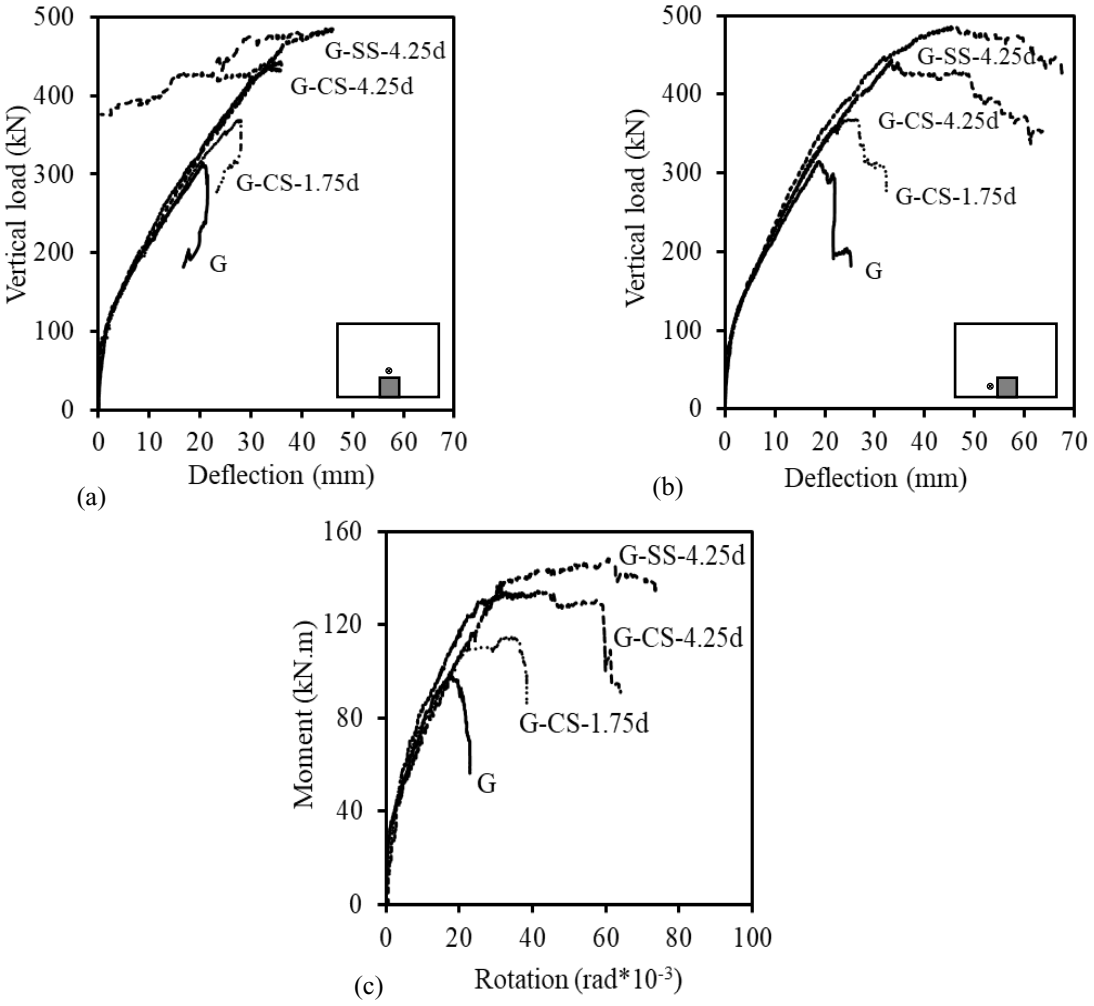

Figure 4.8 – Vertical load–deflection relationships: (a) Perpendicular to the free edge; (b) Parallel to the free edge; and (c) Moment–rotation relationships (Note: 1 mm = 0.0394 in.; 1 kN = 0.2248 kip; 1 kN.m = 8.86 kip.in.)

Specimens G-CS-1.75d, G-CS-4.25d and G-SS-4.25d, with shear reinforcement, exhibited higher strains in the GFRP reinforcing bars and higher concrete strains values compared to control specimen G at ultimate. The maximum reinforcement strains were 8700, 13200, and 13900 μs, respectively, representing 47%, 71%, and 75% of the ultimate tensile strength, respectively. The maximum recorded concrete strains were 979, 2444, and 2696 μs (< 3000 or 3500) for G-CS-1.75d, G-CS-4.25d, and G-SS-4.25d, respectively. It is important to report that the mode of failure of specimen G-CS-1.75d was triggered by brittle punching-shear failure occurring outside the shear-reinforced zone with no signs of concrete crushing in the compression zone (see Figs. 4.6 and 4.7). In contrast, for specimens G-CS-4.25d and G-SS-

4.25d, the achieved higher concrete strains indicated concrete crushing in the column vicinity on the compression side of the slabs, which exhibited the mixed flexure–punching-shear failure. Figure 4.10 shows the flexural-reinforcement-strain distribution along selected bars at different load levels. Figure 4.10 shows that the reinforcement strains decayed in both orthogonal directions toward the supported slab edge until reaching very low strain values at 750 mm from the column face. This implies that the sand-coated GFRP bars used adequately transferred loads with no signs of bar slippage or bond failure during the tests.

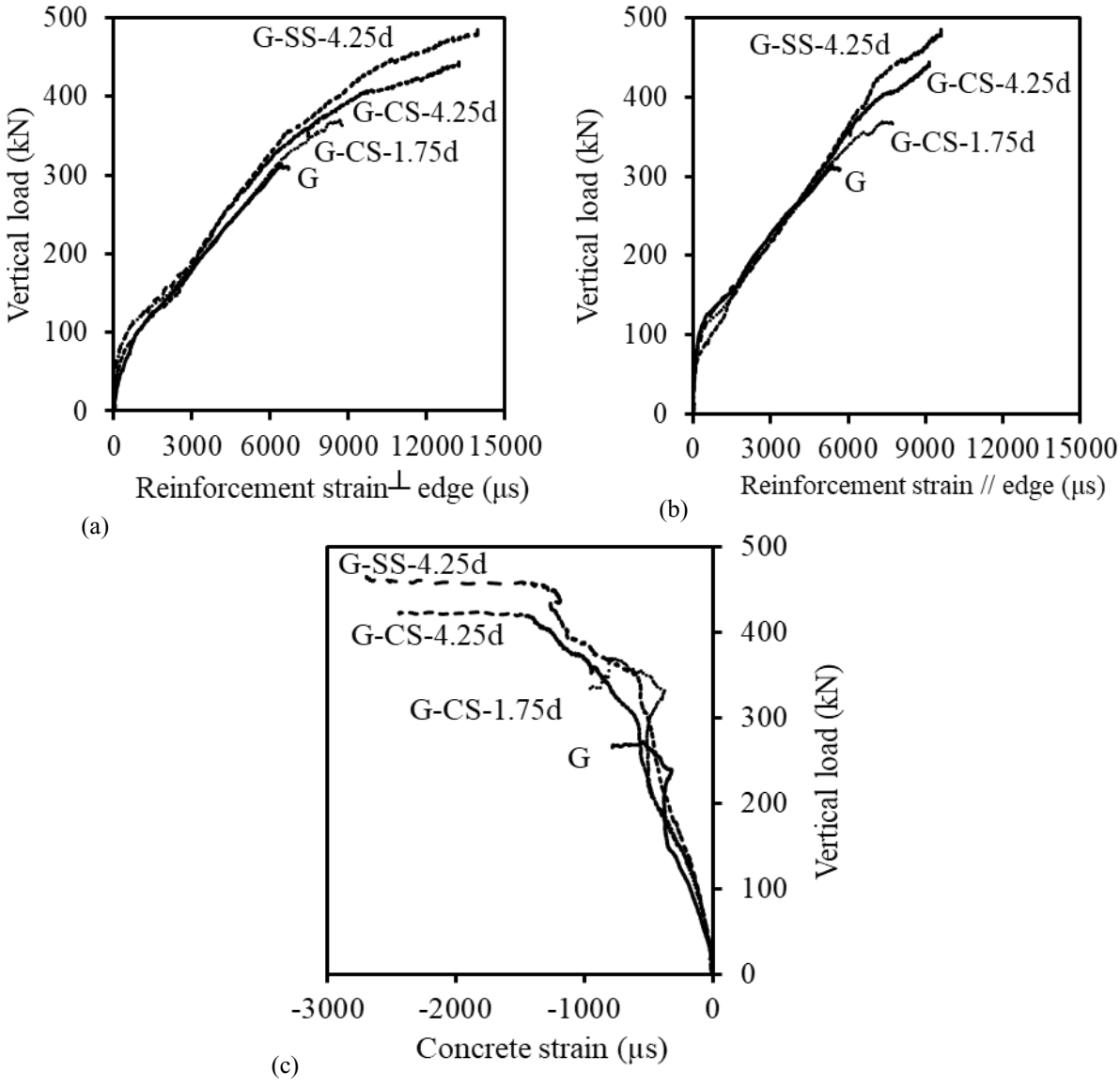

Figure 4.9 – Vertical load–strain relationships: (a) Reinforcement strain perpendicular to the free edge; (b) Reinforcement strain parallel to the free edge; (c) Concrete strain (Note: 1 kN = 0.2248 kip)

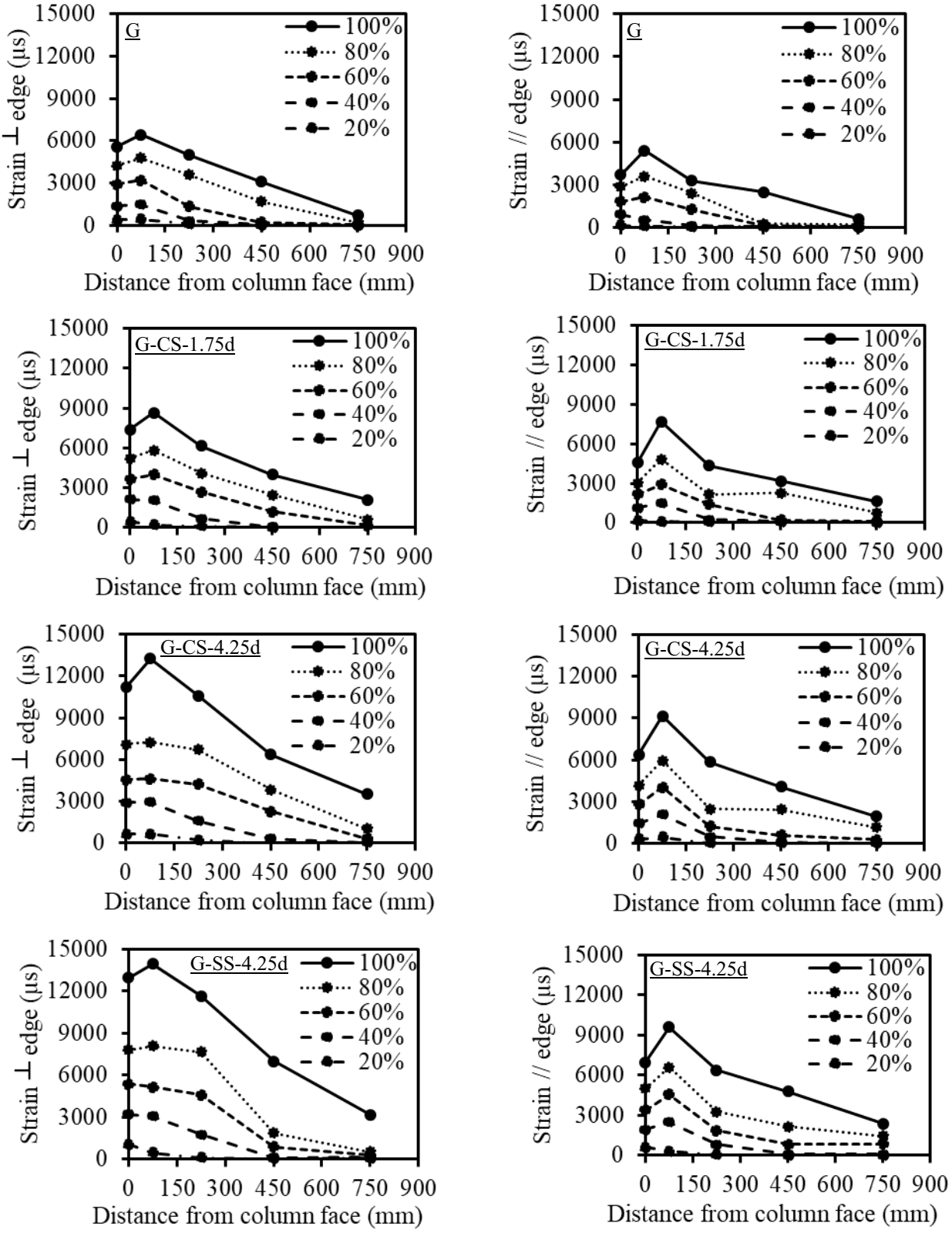

Figure 4.10 – Distribution of flexural-reinforcement strains in both directions (Note: 1 mm = 0.0394 in.)

4.4.6. Shear-Reinforcement Strains

Figure 4.11 depicts the vertical-strain distributions in the stirrups versus the distance from the column face divided by d at different load levels in both orthogonal directions. As shown, the stirrup strains decreased as the distance from the column face increased. In all the specimens, the strains in the stirrups increased rapidly beyond the 80% of the ultimate loads. The maximum strains were recorded in the FRP stirrups for up to a distance of 0.25d to 1.25d from the column faces without any apparent signs of rupture in the vertical or bent portions of the stirrups. The maximum recorded strains at 95% of the ultimate loads in both directions were 7035 and 6412 μs for specimens G-SS-4.25d and G-CS-4.25d, respectively, representing 33% and 30% of the ultimate tensile strain, respectively. For specimens G-CS-1.75d, G-CS-4.25d, and G-SS-4.25d, the average strains in the vertical portions of the FRP stirrups in both directions were 2867, 5305, and 5163 μs, respectively, which represents 53%, 106%, and 103%, of the CSA S806 (2012) strain limit, respectively, and 72%, 132%, and 129% of the ACI 440.1R (2015) strain limit. Thus, the FRP shear reinforcement might be designed with a strain value of 4000 or 5000 μs, as recommended in ACI 440.1R (2015) and CSA S806 (2012) (Hassan et al 2014). Table 4.3 lists the maximum recorded strains in the FRP stirrups.

It is worth mentioning that the FRP shear stirrups along the moment direction between 1.75d and 2.25d achieved relatively high strains compared to the measured strains at 0.25d at 95% of the ultimate loads. The measured strains at 1.75d for G-CS-1.75d, G-CS-4.25d, and G-SS-4.25d were 2765, 5486, and 4934 μs, respectively, and the strains at 2.25d were 4637 and 3356 μs for G-CS-4.25d and G-SS-4.25d, respectively. This implies that the FRP stirrups were still active up to 2.25d. In addition, limiting the extension of the FRP stirrups in specimen G-CS-1.75d beyond a distance of 1.75d exhibited only limited deformation capacity and occurrence of brittle punching failure. Therefore, more experimental work is needed to determine a minimum extension limit of FRP stirrups for FRP-reinforced slab–column connections to overcome brittle punching failure.

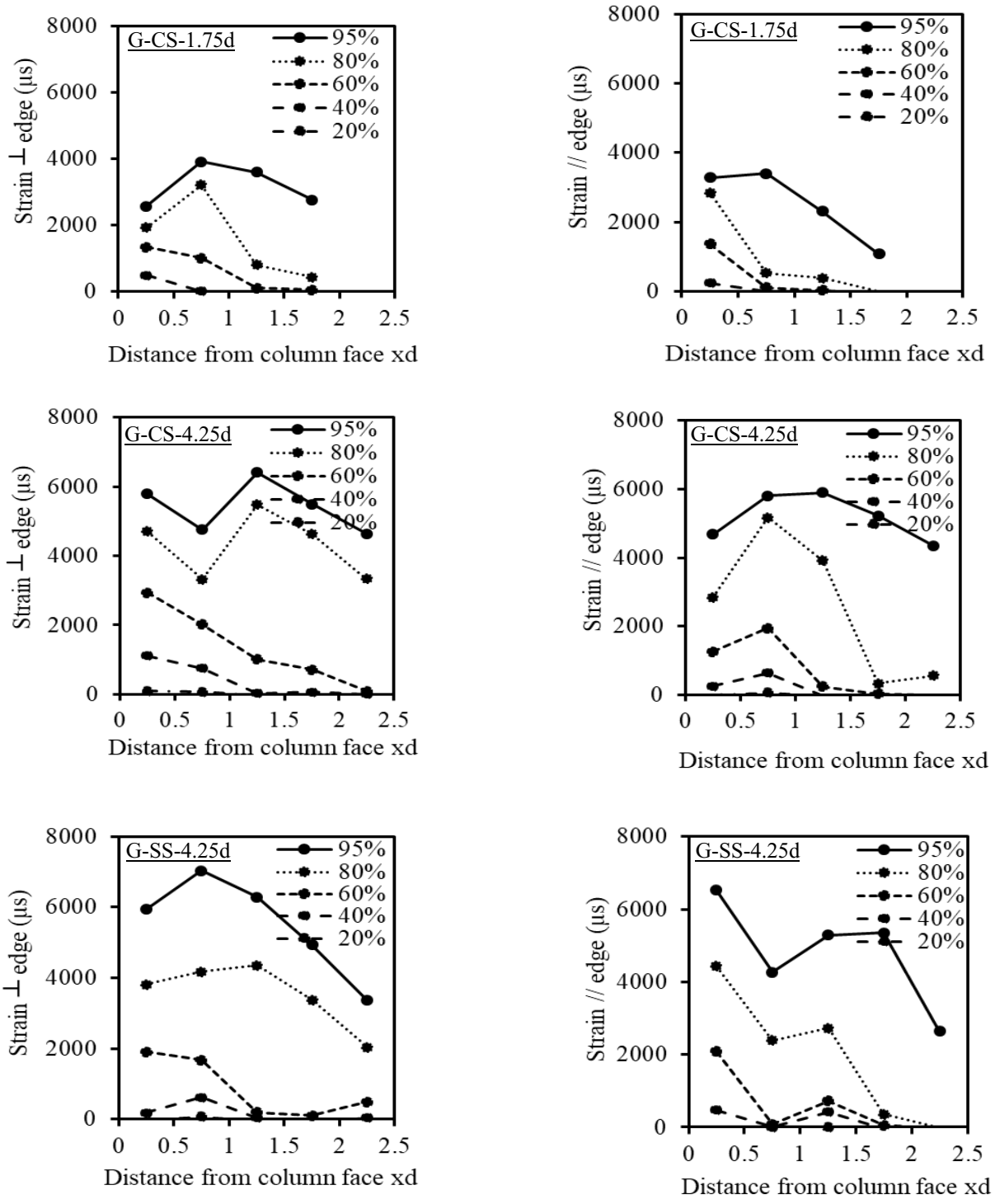

Figure 4.11 – Vertical strain distribution in vertical legs of stirrups

4.4.7. Ultimate Strength

The failure loads were multiplied by $(48/f_c')^{1/3}$ to account for variations in concrete strength, where f_c' (MPa) is the compressive concrete strength of each specimen and 48 (7 ksi) is the average concrete strength for all the tested specimens in MPa. The test results show the effect of the FRP stirrups as shear reinforcement in increasing not only the punching-shear strength but also the deformation capacity of the tested specimens, even with the limited amount of stirrup extension around the column. Specimens G-CS-1.75d, G-CS-4.25d, and G-SS-4.25d evidenced noticeable increases in the normalized vertical shear force at ultimate load by 12%, 32%, and 43%, respectively, compared to specimen G (without shear reinforcement). Besides, increasing the stirrup extension around the column from 1.75d to 4.25d increased the normalized vertical-shear force by 17%. Use of spiral stirrups in specimen G-SS-4.25d showed an increased normalized ultimate capacity of 9% compared to specimen G-CS-4.25d, with closed stirrups, with the same amounts of flexural and shear reinforcement and distribution layout.

4.4.8. Deformability and Energy Absorption

A main concern of slab–column connections is the prevention of brittle failure. Thus, the connection must be able to deform significantly before collapse. In steel-reinforced concrete members, ductility measures the ability of the structural member to undergo significant large deformations before failure, which provides a warning of impending failure. Ductility in steel-reinforced concrete is quantified by the ratio of maximum displacement or rotation to that at yielding of the steel reinforcement. Unlike steel bars, GFRP bars do not exhibit a yielding plateau. GFRPRC members, however, could achieve significant deformations before failure due to the low elastic modulus of GFRP bars. Consequently, the deformability factor (CSA S6 2014) J_Δ was introduced to quantify the deformation property of GFRP-RC structures (Eq. 1), in which P and Δ are the vertical load and deflection and the subscripts u and s refer to the ultimate and service limit states, respectively. The service limit state for GFRP has several definitions, such as the state corresponding to a concrete compressive strain of 1000 με (CSA S6 2014) or a tensile strain of 2000 με in the flexural reinforcement (Design Manual No3, 2007). The service limit state corresponding to a tensile strain of 2000 με was used in this study to compute the deformability factor (El-Gendy and El-Salakawy 2016). Table 4.3 provides the deformability

factors for all specimens.

$$J_{\Delta} = \frac{P_u \ \Delta_u}{P_s \ \Delta_s} \tag{4.1}$$

As shown in Table 4.3, the deformability factors were substantially enhanced by using GFRP stirrups as shear reinforcement around the column at each connection. For specimens G-CS-1.75d, G-CS-4.25d, and G-SS-4.25d, the deformability factors were 1.4, 2.7, and 3 times higher than that of control specimen G without shear reinforcement. In addition, extending the FRP stirrups 4.25d from the column face significantly contributed to reducing slab brittleness, thus increasing slab safety. The deformability factor of G-CS-4.25d was 2 times higher than that of G-CS-1.75d. On the other hand, specimen G-SS-4.25d, which had spiral stirrups in instead of the discrete closed stirrups in specimen G-CS-4.25d, showed an increase of 13%.

Energy absorption of the structural member is of prime importance, particularly in areas of earthquake activity. Two different measurements can be used to evaluate the energy absorption of slab–column connections using slab deflections (U_{Δ}) or slab–column rotations (U_{θ}) (Marzouk et al. 1996). Energy absorption is calculated by integrating the area under the load–deflection (Fig. 4.8a) or moment–rotation (Fig. 4.8c) curves. Table 4.3 gives the calculated values for all tested specimens. The energy absorptions by deflection for specimens G-CS-1.75d, G-CS-4.25d, G-SS-4.25d were about 58%, 149%, and 239% and by rotation were about 110%, 302%, and 339% higher than that of specimen G, respectively. The reported values indicate that, even in limited amounts, GFRP stirrups can be an efficient means for increasing the strength, deformation, and rotation capacity, and the energy absorption of edge flat slab–column connections.

4.5. Discussion

4.5.1. Influence of Stirrup Extension

In general, the presence of GFRP stirrups as shear reinforcement inside the punching-shear zone significantly improves slab behavior. The strength and deformation capacity of shear-reinforced slabs are, however, strongly influenced by the characteristics of the shear reinforcing system (i.e., extension, amount, type, etc.). Increasing the GFRP-stirrup extension from 1.75d to 4.25d

was attributed with achieving large punching strength and deformations before stirrup final failure, regardless of whether closed or spiral GFRP shear reinforcement was used. The GFRP stirrups offered sufficient resistance and confinement to control the development of large shear cracks and effectively distributed the shearing forces around the punching-shear zone to fail inside or outside the shear-reinforced zone. The more significant increase in deformability in specimens G-CS-4.25d and G-SS-4.25d could be attributed to the fact that, unlike in specimens G and G-CS-1.75d, flexure mechanism took place, due to the mobilization of shear reinforcement before punching-shear failure.

The test results indicate that the shear-stress resistance of the concrete contribution decreased outside the shear-reinforced zone. For example, specimen G-CS-1.75d failed—as intended—outside the shear-reinforced zone under an ultimate shear-stress resistance of 1.21 MPa (0.18 ksi) [refer to Table 4.3]. The corresponding normalized shear-stress resistance is 1.21 MPa (0.21 ksi), which is 52% less than the normalized shear-stress resistance of 2.56 MPa (3.7 ksi) for specimen G. It is therefore reasonable to assume the concrete contribution to shear resistance outside the shear-reinforced zone to be reduced by 50% as recommended in ACI 318 (2014) and CSA A23.3 (2014). Further experimental tests are needed to examine the effect of GFRP shear reinforcement with different extensions around the column zone to quantify the concrete-fraction contribution outside the shear-reinforced zone and determinate the minimum extension limit of GFRP stirrups.

4.5.2. Influence of GFRP Stirrup Type

The increase in strength and deformation capacity depends somewhat on the shear-reinforcement system, specifically the good performance of stirrups due to enhanced anchoring. The spiral stirrups clearly afforded superior response as well as fast, easy installation during construction compared to the specimens with discrete closed stirrups and the same amounts of flexural and shear reinforcement. This can be attributed to the better mechanical anchorage of the spiral stirrups, which enhanced concrete confinement in the compression zone and resulted in higher capacity and better post-peak behavior. Both GFRP stirrup shear reinforcement systems can efficiently reduce the brittleness of specimens and provide ample warning before failure.

Like steel shear reinforcement, spiral or discrete closed GFRP stirrups with a large amount of shear reinforcement near the column zone might develop horizontal splitting cracks over the top of the stirrups, as depicted in Fig. 4.7. This can be attributed to a significant portion of the radial compressive force occurring in the concrete near the column, which acts in a nearly horizontal direction and is transmitted to the region around and over the upper part of the shear reinforcement. This radial compressive force changes its direction. Consequently, tensile stresses were produced in a horizontal section through the upper part of the shear reinforcement. In addition, the large amount of shear reinforcement caused an increase in the eccentricity of the radial compressive force in the concrete, which increased the radial tensile stresses in the slab's top surface. This observation coincides with the past experimental findings reported in the literature by Hassan et al. (2014) and Dam et al. (2017) for FRP and steel slab–column connections with a large amount of shear reinforcement, respectively.

4.6. Proposed Design Provisions and Predications

4.6.1. Slabs without Shear Reinforcement

The North American codes—that are, ACI 318 (2014) and CSA A23.3 (2014)—compute the shear stress for steel, v_u, using the moment transfer by eccentricity of shear located at a distance of 0.5d from the column face using the Eq. (4.2).

$$v_u = \frac{V_u}{b_{o;0.5d}\, d} + \frac{\gamma_v M_o}{J_c} \text{ c} \tag{4.2}$$

The North American design codes for FRP-reinforced two-way slabs without shear reinforcement—i.e., CSA S806 (2012) and ACI 440.1R (2015)—are based on the same forms as steel design codes with modifications to consider the effect of FRP-bar axial stiffness. The punching-shear resistance provided by concrete (v_c) in CSA S806 (2012) [the smallest of Eqns. 4.3-4.5] and ACI 440.1R (2015) [Eq. 4.6] are summarized below.

CSA S806 (2012): without shear reinforcement

$$v_c = 0.028\lambda\phi_c\left(1+\frac{2}{\beta_c}\right)\left(E_f\rho_f f_c^{'}\right)^{\frac{1}{3}} \tag{4.3}$$

$$v_c = 0.147\lambda\phi_c\left(\frac{\alpha_s d}{b_o} + 0.19\right)\left(E_f\rho_f f_c'\right)^{\frac{1}{3}} \quad (4.4)$$

$$v_c = 0.056\lambda\phi_c\left(E_f\rho_f f_c'\right)^{\frac{1}{3}} \quad (4.5)$$

ACI 440.1R (2015): without shear reinforcement

$$v_c = \frac{4}{5}k\sqrt{f_c'} \quad (4.6a)$$

$$k = \sqrt{2\rho_f n_f + \left(\rho_f n_f\right)^2} - \rho_f n_f \quad (4.6b)$$

To date, CSA S806 (2012) and ACI 440.1R (2015) lack provisions for estimating the ultimate capacity of FRPRC two-way slabs with FRP shear reinforcement. The following section presents proposed design provisions as an extension to CSA S806 (2012) and ACI 440.1R (2015) to account for FRP stirrups as shear reinforcement and their properties affecting the ultimate capacity of FRP-RC slab column connections. It is worth mentioning that the same procedure in adapting the aforementioned code provisions was originally proposed by El-Gendy and El-Salakawy (2016) for GFRP-reinforced edge connections reinforced with GFRP ribbed shear studs.

4.6.2. Slabs with Shear Reinforcement

Regarding steel-reinforced two-way slabs with shear reinforcement, ACI 318 (2014) and CSA A23.3 (2014) require that the shear stresses be checked either inside or outside the shear-reinforced zone. The critical shear section inside the shear-reinforced zone is located at 0.5d from the column faces, while the critical section outside the shear reinforcement lies at 0.5d from the outermost shear reinforcement. Within the shear reinforced zone, the factored shear-stress resistance, computed as (v_c + v_s), where v_c and v_s are the summations of concrete and shear-reinforcement contributions to the shear strength inside the punching zone. Design codes calculated the concrete contribution inside and outside the region reinforced with shear stirrups as 50% of the punching-shear strength of slabs without shear reinforcement. Accordingly, in this paper, the concrete contribution inside and outside the shear-reinforced zone for FRP-reinforced two-way slabs is proposed to have a value equal to 50% of the least of Eqns. (4.3) to (4.5) according to CSA S806 (2012) or Eq. (4.6) according to ACI 440.1R (2015).

In order to calculate the FRP-stirrup contribution, Eqns. (4.8) and (4.10) for steel stirrups have been modified by replacing, f_y (yielding strength) with a specific stress (f_{fv}) at a limiting strain value (ε_{fv}) of 5000 or 4000 μs according to CSA S806 (2012) and ACI 440.1R (2015), respectively, where f_{fv} equals ε_{fv} multiplied by the FRP-stirrup modulus of elasticity (E_{fv}). It should be noted that the f_{fv} should be less than the stress corresponding to the failure of the stirrup corners or bends as determined with the appropriate procedure in accordance with ACI 440.1R (2015) and CSA S806 (2012). The proposed design equations can be summarized as follows.

Proposed design provisions for CSA S806 (2012) with the shear-reinforced zone

$$v_{c,inside} = v_{c,outside} = 0.028\lambda\phi_c \left(E_f \rho_f f_c^{'}\right)^{\frac{1}{3}} \tag{4.7}$$

$$v_{fv} = \frac{\phi_f A_{fv}\left(0.005E_{fv}\right)}{b_o S_{fv}} \tag{4.8}$$

Proposed design provisions for ACI440.1R (2015) with the shear-reinforced zone

$$v_{c,inside} = v_{c,outside} = \frac{2}{5} k\sqrt{f_c^{'}} \tag{4.9}$$

$$v_{fv} = \frac{\phi_f A_{fv}\left(0.004E_{fv}\right)}{b_o S_{fv}} \tag{4.10}$$

4.6.3. Ultimate-Capacity Predications

This section presents an assessment of the accuracy of the current and proposed design equations (Eqs. 4.2- 4.10) by comparing their predictions with the experimental results and the results available in the literature for shear-reinforced edge connections. All safety factors and partial material factors in the equations were taken to be equal to 1.0. Table 4.4 provides the punching-shear predictions for all tested specimens with and without FRP shear reinforcement. The ACI 440.1R (2015) predications using the current Eq. 4.6 and proposed Eqns. 4.9 and 4.10, as expected, were consistently very conservative for specimens with and without shear reinforcement, respectively. For the test specimen without shear reinforcement, the current ACI 440.1R (2015) equation showed an average V_{test}/V_{pred} of 2.15. On the other hand, the proposed ACI 440.1R (2015) equations gave an average V_{test}/V_{pred} of 1.87 ± 0.25 (a corresponding COV

of 24.6%) for test specimens with FRP shear stirrups as well as other shear-reinforced edge connections reported in the literature. The reason for this is that the concrete-contribution fraction (v_c) involved only the reinforcement ratio in predicting the neutral axis depth (contribution of the compression area). The Equation (Eq. 4.6) does not consider axial stiffness, which might make the overall predications excessively conservative. In contrast, CSA S806 (2012) accounts for FRP axial stiffness in the v_c. It therefore yielded better predictions.

As shown in Table 4, the current CSA S806 (2012) Eqns. (4.2) to (4.5) and proposed Eqns. (4.7) and (4.8) gave better predications for test specimens without and with FRP shear stirrups involving shear-reinforced edge connections reported in the literature. The current CSA S806 (2012) equations gave an average V_{test}/V_{pred} of 1.29 for the test specimen without FRP shear stirrups. In addition, the proposed CSA S806 (2012) equations showed average V_{test}/V_{pred} values of 1.28 ± 0.24 (COV of 18.58%) with respect to the test specimens with FRP shear stirrups and shear-reinforced GFRP-RC edge connections from literature. The proposed design provisions provide a step forward for engineers in designing two-way FRPRC slabs with FRP stirrups. More experimental results under eccentric punching shear for interior and edge slab–column connections are urgently required.

Table 4.4. Tested-to-predicted punching-shear capacity

Reference	Test Specimen	*c*, mm	M/V, m	RFT. Type	$d_{avg.}$, mm	t_s, mm	ρ, %	Shear RFT Type	V_u, kN	Proposed Equations for CSA S806 (2012)			Proposed Equations for ACI 440.1R (2015)		
										V_{pred}, kN		V_u/V_{pred}	V_{pred}, kN		V_u/V_{pred}
										Inside	Outside		Inside	Outside	
This study	G	S 300	0.31	SG	160	200	1.55	---	314	244[a]	---	1.29	146	---	2.15
	G-CS-	S 300	0.31				1.55	GFRP stirrups	370	386	303	1.22	282	180	2.06
	G-CS-	S 300	0.30				1.55		444	396	484	1.12	288	286	1.55
	G-SS-	S 300	0.30				1.55		486	397	488	1.22	289	287	1.69
Mostafa and El-Salakawy (2018)	N-0.9-S8	S 300	0.40				0.85	SG shear studs	294	352	321	0.92	260	178	1.65
	N-0.9-S6	S 300	0.40				0.85		298	286	335	1.04	207	186	1.60
	N-0.9-C6	S 300	0.40				0.85	SG C. bars	253	174	322	1.45	118	179	2.14
	N-0.9-C8	S 300	0.40				0.85		286	201	323	1.42	140	180	2.04
El-Gendy and El-Salakawy (2016)	RD-75-M	S 300	0.40	GRD			0.85	GRD shear	256	154	332	1.66	116	183	2.21
	RD-50M	S 300	0.40				0.85		273	186	323	1.47	148	179	1.84
											Mean[c]	1.28		Mean [c]	1.87
											SD[c]	0.24		SD [c]	0.25
											COV[c] %	18.58		COV [c] %	13.46

C = shape of column stub and corresponding width; S = square; ρ_{avg} = average flexural tensile reinforcement ratio in both directions; SG = sand-coated glass-fiber; GRD = ribbed glass-fiber; C = corrugated.

[a] Calculated using Eq. (4.5).

[b] Calculated using Eq. (4.6).

[c] Calculated using the least of V_{pred} for specimens with shear reinforcement only.

Note: 1 kN = 0.2248 kip, 1 kN.m = 8.86 kip.in., 1 mm = 0.0394 in

4.7. Conclusion

On the basis of the test results and discussion presented, the following conclusions were drawn:

- Using either closed or spiral stirrups as shear reinforcement improved the punching behavior of FRPRC edge slab–column connections. The cracks were more widely distributed compared to the specimen without shear reinforcement, which failed in a brittle punching-shear mode.
- The specimens with FRP shear reinforcement extended 4.25d demonstrated a substantial increase in shear-strength increase over 38%, enhancement of deformation capacity of over 104%, and deformability and energy absorption of over 185%, and 194% (on average) were observed. This increase might be of interest because it gives significant warning before punching-shear failure occurs. As a result, these connections fail in mixed flexure–punching-shear failure.
- The FRP stirrups offered sufficient resistance and confinement to control the development of large shear cracks and effectively distributed the shearing forces around the punching-shear zone so that failure occurred inside or outside the shear-reinforced zone.
- In comparison to closed stirrups, spiral stirrups provided better performance as well as fast and easy installation during construction of the tested specimens for the same amounts of flexural and shear reinforcement. Specimen G-SS-4.25d, with spiral stirrups, showed an increase in the punching-shear strength, deformation capacity, and energy absorption of over 9%, 33%, and 36% compared to G-CS-4.25d, respectively. Both systems, however, could be used to effectively reduce the brittleness of the tested specimens.
- The results indicate that the shear-stress resistance of the concrete contribution decreased outside the shear-reinforced zone. For instance, specimen G-CS-1.75d failed outside the shear-reinforced zone under an ultimate shear-stress resistance of 1.21 MPa (0.18 ksi), which is 52% lower than the normalized shear-stress resistance of 2.56 MPa (0.37 ksi) for specimen G. Thus, it is reasonable to assume the concrete contribution to shear resistance outside the shear-reinforced zone be reduced by 50% as recommended in ACI 318 (2014) and CSA A23.3 (2014). Further experimental tests are needed, however, to examine the effect of FRP shear reinforcement with different extensions around the column to quantify this effect on the concrete contribution to the shear resistance.

- FRP shear stirrups between 1.75d and 2.25d achieved relatively high strains of 4129 and 3748 με (on average in both directions) at 95% of ultimate load, which implies that the FRP stirrups were still active up to 2.25d, respectively. In addition, limiting the extension of the FRP stirrups beyond 1.75d showed only limited deformation capacity and brittle punching failure occurred. Therefore, more experimental work is needed to determine a minimum extension limit of FRP stirrups for FRP-reinforced slab–column connections to overcome brittle punching failure.
- On the basis of the test results, FRP shear reinforcement can be designed with a strain value of 4000 or 5000 microstrains, as recommended in ACI 440.1R (2015) or CSA S806 (2012), respectively.
- The simplified approach proposed to predict the ultimate shear capacity of FRP-reinforced edge slab–column connections with FRP shear reinforcement as an extension to those in CSA S806 (2012) gave better predications with respect to the experimental test results as well as the available results in the literature.
- The proposed ACI 440.1R (2015) simplified approach was consistently very conservative for test specimens with FRP shear stirrups reported in this study and other data available in the literature. The reason for this is the high level of conservatism of the concrete-contribution (v_c) in ACI 440.1R (2015) (Eq. 6).
- The proposed design provisions provide a step forward for engineers in designing two-way FRPRC slabs with FRP stirrups. Nevertheless, more experimental results under eccentric punching shear for interior and edge slab–column connections are urgently required.

4.8. Acknowledgments

The authors wish to acknowledge the financial support of the Tier 1 Canada Research Chair in Advanced Composite Materials for Civil Structures, Natural Sciences and Engineering Research Council of Canada (NSERC Industrial Research Chair in Innovative FRP Reinforcement for Sustainable Concrete Infrastructure), and the Fonds de recherché du Québec – Nature et Technologies – (FRQ-NT). The assistance of the technical staff of the Structural and Materials Laboratory in the Department of Civil Engineering at the University of Sherbrooke is also greatly appreciated.

4.9. List of Symbols

d = effective slab depth

d_b = bar diameter

$b_{o;0.5d}$ = critical perimeter at a distance of 0.5d from the column face

c = distance from the centroid of the critical section to the face of the critical section (mm)

E_f = modulus of elasticity of FRP bars

E_{fv} = modulus of elasticity of FRP stirrups, straight portion

E_s = modulus of elasticity of steel

f_t' = split-cylinder tensile strength of concrete

f_c' = concrete-cylinder compressive strength

f_{fu} = ultimate tensile strength of FRP bars

f_{fv} = ultimate tensile strength of the straight portion of FRP stirrups

f_{fvb} = ultimate tensile strength of FRP stirrups at bend location

J = deformability factor

J_c = polar moment of inertia of critical section

M_{cr} = cracking unbalanced moment at column centroid

M_u = ultimate unbalanced moment at column centroid

M_o = ultimate unbalanced moment at centroid of the critical shear section

n_f = modular ratio (E_f/E_c)

n_s = numbers of stirrups at a perimeter of 0.5d from the column face

r_b = radius of the bend

s_{fv} = stirrup spacing

V_{cr} = first radial cracking load

V_u = ultimate vertical shear force at column centroid

V_u = ultimate punching-shear load

$v_{u.}$ = ultimate shear stress at 0.5d from column face

β_c = ratio of long side to short side of column

γ_v = fraction of unbalanced moment transferred by eccentricity of shear at slab–column connection

Δ_{Vu} = ultimate deflection at peak load

ε_{fv} = limiting tensile strain in FRP stirrups

A_{fv} = cross-sectional area of the FRP shear reinforcement at a perimeter of 0.5d from column face

ρ_b = average bottom flexural-reinforcement ratio

ρ_t = average top flexural-reinforcement ratio

ρ_{fv} = shear-reinforcement ratio at a perimeter of 0.5d from column face = (n_s*A_{fv}/S_{fv} b_o)

CHAPTER 5

ARTICLE 2: BEHAVIOR OF CONCRETE EDGE COLUMN-SLAB CONNECTIONS REINFORCED WITH GFRP BARS SUBJECTED TO DIFFERENT MOMENT-TO-SHEAR FORCE RATIOS

Foreword

Authors and Affiliation

- Ahmed E. Salama: PhD Candidate, Department of Civil Engineering, University of Sherbrooke, Quebec, Canada J1K 2R1, E-mail: Ahmed.Salama@USherbrooke.ca

- Mohamed Hassan: Postdoctoral Fellow, Department of Civil Engineering, University of Sherbrooke, Quebec, Canada J1K 2R1, E-mail: Mohamed.Hassan@USherbrooke.ca.

- Brahim Benmokrane: Professor of Civil Engineering and NSERC and Tier-1 Canada Research Chair Professor, Department of Civil Engineering, University of Sherbrooke, Sherbrooke, Quebec, Canada, J1K 2R1, Tel.: 1-819-821-7758.
  Corresponding author, E-mail: Brahim.Benmokrane@USherbrooke.ca.

Paper submitted to Composite for Construction Journal, ASCE on January 27, 2019

Paper status: Reviewed and revised manuscript submitted on July 17, 2019

Reference: Salama , A. E. , Hassan, M., and Benmokrane, B., 2019, " Behavior of Concrete Edge Column-Slab Connections Reinforced with GFRP Bars Subjected to Different Moment-to-Shear Force Ratios," *Composite for Construction Journal, ASCE.*

Abstract

Applications of glass fiber-reinforced-polymer (GFRP) bars as reinforcement for concrete structures have been growing in recent years. This paper presents test results from an experimental program conducted to study the punching-shear response of normal-strength concrete (NSC) and high strength concrete (HSC) edge column-slab connections. Five full-scale reinforced concrete (RC) edge slab–column connections and tested under vertical shear force and unbalanced moment until failure. Four of the five connections were reinforced with GFRP bars as flexural reinforcement; one connection was reinforced with steel bars for comparison. All of the slabs had identical geometries of 2500 × 1350 × 200 mm with a 300 mm square column stub protruding 700 mm above and below the slab surfaces. The test parameters were: (1) flexural-reinforcement type (steel and GFRP bars); (2) concrete strength (NSC and HSC); and (3) moment-to-shear force ratio (M/V) (0.3 m or 0.6 m). The test results revealed that all the connections failed by punching shear with no signs of concrete crushing. The HSC directly enhanced the punching-shear capacity, load–deflection response, and initial stiffness of the connections. These connections also evidenced fewer and narrower cracks compared to their counterparts cast with NSC. Increasing the M/V ratio produced significant shear stresses, thereby reducing the vertical load capacity by 31% and 30% for the NSC and HSC connections, respectively. The measured punching shear capacities of the tested connections were compared with the predictions using the available design provisions in Canada, the United States, and Japan.

keywords: Punching shear; fiber-reinforced polymer; edge column-slab connections; high-strength concrete; two-way slabs; moment-to-shear force ratio; shear-strength prediction.

5.1. Introduction

Glass fiber-reinforced-polymer (GFRP) reinforcing bars have recently gained wide acceptance as a viable construction material for sustainable new construction. The corrosion resistance of GFRP bars is a significant benefit for structures in highly corrosive environments such as parking garages maintained with deicing salts. Steel-reinforced-concrete flat-plate parking structures in North America are susceptible to accelerated deterioration given the harsh exposure conditions to which they are subject, including freeze–thaw cycles, wet–dry cycles, and diffusion of deicing salts. The latter specifically increase the vulnerability of steel bars to electrochemical corrosion (El-Gendy et al. 2014 and El-gabbas et al. 2016). Moreover, the increased punching-shear stresses around the column resulting from vertical shear forces or vertical shear forces combined with unbalanced moments transferred between the slab and column cause a type of local brittle failure around the column known as punching-shear failure. This failure is exacerbated in the case of edge column-slab connections due to the unbalanced moment, which produces more shear stresses, minimizing connection strength and ductility. Replacing steel with FRP bars can eliminate the corrosion of steel reinforcement, reduce maintenance costs, and improve the life-cycle cost-effectiveness of structures (Benmokrane et al. 2012; Ahmed et al. 2017; Hassan et al. 2017).

Past research data has focused mostly on interior connections reinforced solely with FRP bars subjected to concentric loading alone or a combination of unbalanced moment and shear (El-Ghandour et al. 2003; Ospina et al. 2003; Lee et al. 2009; Nguyen-Minh and Rovank 2013; Dulude et al. 2013; Hassan et al. 2013 a,b ; Hassan et al. 2014 a, b, Gouda and El-Salakawy 2015, 2016; Hassan et al. 2017; Hussein and El-Salakawy 2018). Using HSC for interor connections increased the punching-shear capacity and the initial stiffness compared to NSC, however, it had little effect on the post-cracking stiffness (Zhang et al. 2005; Hassan et al. 2013; Gouda and El-Salakawy 2015; Hussein and El-Salakawy 2018). In contrast, increasing *M/V ratio* decreased the punching-shear capacity and increased the strains in the reinforcing bars (Zaghloul 2002; Gouda and El-Salakawy 2016). To date, very limited research has been conducted on edge slab-column connections reinforced with FRP bars/grids (Zaghloul 2007; El Gendy and El-Salakawy 2016 , 2018 ; Mostafa and El-Salakawy 2018). El-Gendy and El-Salakawy (2016) investigated the effect of different *M/V* ratios on the punching-shear behavior

of GFRP-reinforced edge column-slab connections with NSC. Three full-scale connections were tested with *M/V* ratios of 0.2, 0.4, and 0.6 m. They concluded that increasing the *M/V* ratio significantly decreased the deformability and shear-force capacity of the connections. Recently, El Gendy and El-Salakawy (2018) investigated the effect of flexural-reinforcement type (steel and sand coated) on punching shear capacity of edge column-slab connections having the same reinforcement ratios. The authors reported that the flexural-reinforcement type had a significant effect on the punching-shear capacity and post-cracking stiffness of the connections. The punching-shear capacity and the post-cracking stiffness of the steel connection were increased by 35% and 200% compared to its counterpart reinforced with same amount of GFRP bars due to the higher axial reinforcement stiffness of the steel bars.

The use of HSC for construction has been growing in recent years. HSC has higher compressive and tensile strengths and a higher modulus of elasticity than NSC. Consequently, HSC can improve punching capacity, allowing greater forces to be transferred through the slab–column connection. To the authors' best knowledge, no research has been conducted on the effect of different *M/V* ratios on GFRP-reinforced edge column-slab connections constructed with HSC. In addition, only three HSC edge connections reinforced with GFRP bars have been reported in the literature (Mostafa and El-Salakawy 2018).They concluded that the use of HSC enhanced the uncracked stiffness and punching-shear capacity. Doubling the concrete strength from 40 to 80 MPa resulted in an 83% and 10% increase in the uncracked stiffness and ultimate capacity, respectively, compared to their NSC counterparts. Moreover, ACI 440.1R-15 (ACI 2015) and CSA S806-12 (CSA 2012) have provided design provisions to calculate the punching-shear strength of FRP-RC column-slab connections regardless of the type of loading applied to the connections. These provisions have provided reasonable predictions for edge and interior slab–column connections subjected to combined vertical shear force and unbalanced moment (El-Gendy and El-Salakawy 2016, 2018; Gouda and El-Salakawy 2015, 2016; Hussein and El-Salakawy 2018; Mostafa and El-Salakawy 2018).

The work presented in this paper extends an extensive research project conducted at the University of Sherbrooke (Quebec, Canada) to develop and implement GFRP bars for two-way slabs for parking garages and buildings. The first phase of this research program has been completed (Dulude et al. 2013; Hassan et al. 2013 & 2014 a, b; Hassan et al. 2017). A total of

40 GFRPRC slabs were tested under concentric loading. The test results and findings contributed to the assessment of the first punching-shear equation in CSA S806-12 (CSA 2012). It also contributed to field implementation of GFRP bars in flat-slab parking structures in a demonstration area (350 m^2) at city-hall parking garage (Quebec, Canada, 2010) and helped in designing the world's first flat-slab parking garage totally reinforced with GFRP bars (La Chancelière parking garage, Quebec City, Canada, 2011) (Benmokrane et al. 2012 and Ahmed et al. 2017).

This paper presents experimental tests on GFRP-reinforced edge slab–column connections with the aim of investigating the influence of the reinforcement type, concrete strength, and *M/V* ratio on punching-shear strength. Detailed measurements of the deflections, slab–column rotation, concrete strains, and flexural-reinforcement strains facilitate a better understanding of the behavior of GFRP-reinforced edge slab–column connections. The punching-shear capacities of the test connections were predicted by ACI 440.1R-15 (ACI 2015), CSA S806-12 (CSA 2012) and JSCE-97 (JSCE 1997). The findings of this research will support the work of North American technical committees engaged in developing standards and design provisions for GFRP-RC edge slab–column connections made with normal- and high-strength concrete subjected to different *M/V* ratios.

5.2. Experimental Program

5.2.1. Material Properties

Reinforcing bars. Two types of reinforcing bars were used as flexural reinforcement in this study: sand-coated GFRP and deformed steel bars. Sand-coated Grade II and III GFRP bars compliant with CSA S807-15 (CSA 2015), were used in all the GFRP-reinforced connections. The GFRP straight bars were manufactured by combining the pultrusion process with an inline sand-coating process for the bar surface to improve bonding between the GFRP bars and surrounding concrete (Pultrall, 2016). It should be noted that the straight portions of the GFRP bent bars were manufactured by pultrusion, whereas the bent portions were manufactured with a unique fabrication method (Pultrall, 2016). The bottom flexural-reinforcement bars were bent and straight No. 20 GFRP bars in the direction perpendicular and parallel to the free edge, respectively. The bent GFRP bars were manufactured with bent ends to provide enough

anchorage close to the edges. Straight No. 15 GFRP bars were used as top flexural reinforcement in both orthogonal directions. The tensile properties of the straight and bent GFRP bars were determined by testing five representative specimens according to ASTM D7205-11 (ASTM 2011) and the B.5 test method in ACI 440.3R-12 (ACI 2012), respectively. Deformed 15M and 20M (Type 44W) steel bars were used as top and bottom reinforcement in the reference slab. The column stub was reinforced with 25M and 10M steel bars as longitudinal and transverse reinforcement, respectively. The steel-bar properties were provided by the manufacturer. Table 5.1 summarizes the mechanical properties of the reinforcing bars. Figure 5.1 shows a typical assembled slab cage, GFRP materials, and column reinforcement.

Concrete. All connections were cast with ready-mixed NSC and HSC with target compressive strengths of 35 and 70 MPa, respectively. The slab and column stub were cast monolithically to ensure the same material properties for the connection. The concrete compressive strength (f_c') and tensile splitting strength (f_t') for each connection were determined by testing three 100 x 200 mm concrete cylinders on the day of testing. Table 5.2 lists the average concrete compressive strength on the day of testing for each connection.

Table 5.1– Tensile Properties of the Reinforcing Bars

Bar Designation	Nominal Cross-Sectional Area [a] (mm^2)	Immersed Cross-Sectional Area, (mm^2)	Ultimate Tensile Strength [b] (MPa)	Tensile Modulus of Elasticity [c] (GPa)	Ultimate Tensile Strain (%)
Straight flexural GFRP bars					
No. 15 GFRP bar	199	240	1323 ±12	64.8±0.5	2.04 ±0.05
No. 20 GFRP bar	285	333	1334 ±85	64.9±0.6	2.06 ±0.13
Bent flexural GFRP bars					
No. 20 straight portion	285	331	1210±63	53.0±0.48	2.28±0.15
No. 20 bent portion			f_{fvb} = 490±44	------	------
Steel bars					
10M	100	------	f_y = 420	200	ε_y = 0.21
15M	200	------	f_y = 440	198	ε_y = 0.22
20M	300	------	f_y = 460	200	ε_y = 0.23
25M	500	------	f_y = 470	204	ε_y = 0.23

[a] according to CSA S807-15 (CSA 2015).

[b and c] calculated using nominal cross-sectional areas of the reinforcing bars.

f_{fvb} = ultimate tensile bend strength obtained from the B.5 test method according to ACI 440.3R-12 (ACI 2012)

f_y = steel yielding strength, ε_y = steel yielding strain.

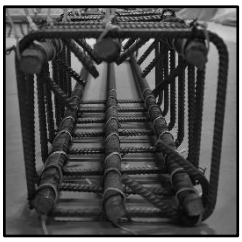

(a) Column reinforcement

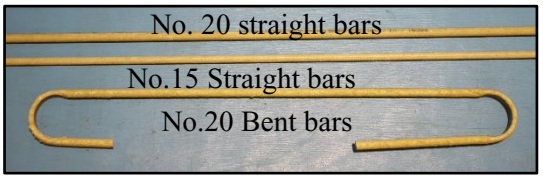

(b) GFRP bars

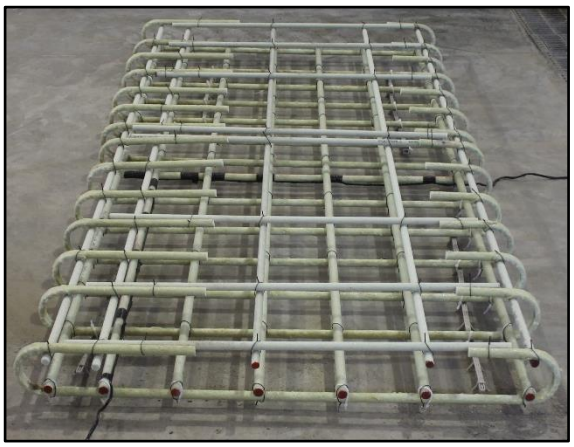

(c) Assembled slab cage

Figure 5.1– GFRP bars, connection reinforcement cage, and column-reinforcement details

5.2.2. Test Matrix and Parameters

A total of five full-scale edge slab–column connections were designed, constructed, and tested up to failure under combined monotonic static vertical load and unbalanced moment. Four connections (G-N-0.3, G-H-0.3, G-N-0.6, and G-H-0.6) were reinforced with GFRP bars and one connection was reinforced with steel bars (S-N-0.3) for comparison. The test specimens represented edge connections in a prototype of flat-plate parking structure with 5 × 5 m^2 panels. The building was assumed to have a live service load of 2.40 kN/m^2, a superimposed dead load of 1.0 kN/m^2, and a self-weight of 4.80 kN/m^2. The total ultimate factored loads on the floor, including the slab weight, were estimated according to the NBCC (2015). The GFRP-RC connections were designed in accordance with Canadian standards CSA S806-12 (CSA 2012) and CSA A23.3-14 (CSA 2014). The flexural reinforcement ratio of the steel-RC connection was, however, chosen to be similar to that of the GFRP-RC connections. Each connection was simply supported on three edges, simulating lines of contra flexure in the prototype floor and monolithic with a column at the middle of the fourth edge. The lines of contra flexure were assumed to be 0.2L from the column centerlines, where L is the span between column centerlines. All slabs had identical geometries of 2500 × 1350 × 200 mm with a 300 mm square column stub protruding 700 mm above and below the slab surfaces. The slabs were simply supported on a 2000 × 1150 mm perimeter on the bottom face of the slab. The nominal concrete

cover on both the top and bottom faces of the slabs was 21 mm. Figure 5.2 shows the typical geometry and reinforcement details of the test connections.

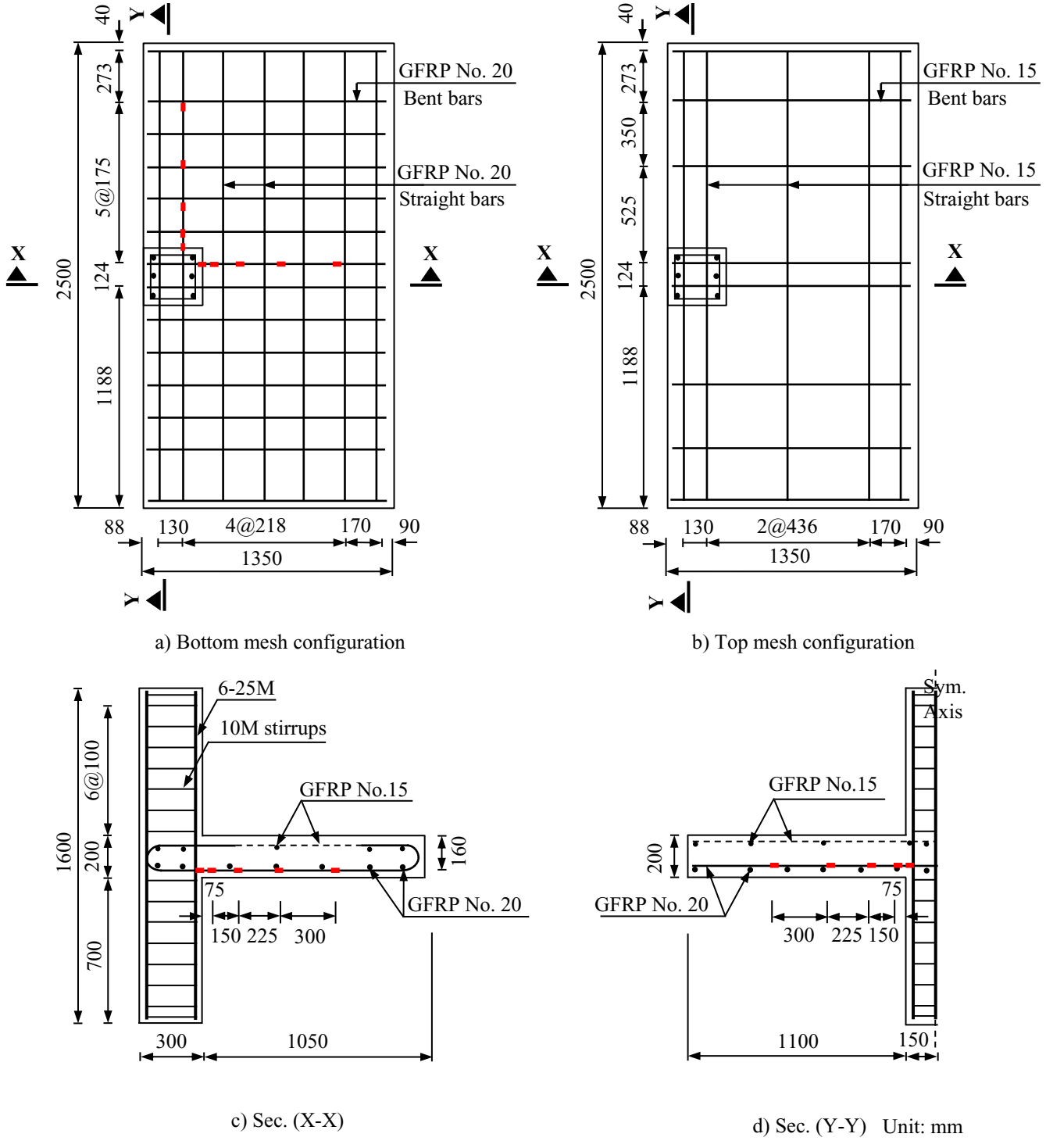

Figure 5.2 – Connections concrete dimensions and reinforcement configuration

Table 5.2 – Details of Test Connections

Connection	RFT Type	d_x, mm	d_y, mm	Flexural Reinforcement				M/V m	fc' MPa	ft' MPa
				Tension (bottom)	Compression (top)	Ratio,%				
						ρ_b	ρ_t			
S-N-0.3	Steel	169.0	149.0	7 -20M/14 -20M	5 -15M/ 8-15M	1.09	0.34	0.3	39.2	3.73
G-N-0.3	GFRP	169.5	150.5	7 No.20/14 No.20	5 No.15/ 8 No.15	1.04	0.34	0.3	37.1	3.73
G-H-0.3	GFRP	169.5	150.5	7 No.20/14 No.20	5 No.15/ 8 No.15	1.04	0.34	0.3	85.8	6.54
G-N-0.6	GFRP	169.5	150.5	7 No.20/14 No.20	5 No.15/ 8 No.15	1.04	0.34	0.6	38.8	3.56
G-H-0.6	GFRP	169.5	150.5	7 No.20/14 No.20	5 No.15/ 8 No.15	1.04	0.34	0.6	86.0	6.54

d_x, d_y = effective slab depths in the x and y directions; $d_x = t - 0.5d_b - 21$; $d_y = t - 1.5\ d_b - 21$; ρ_b, ρ_t = average tensile and compression flexural reinforcement ratios within effective widths, respectively; M/V= moment-to-shear force ratio; fc' = concrete compressive strength and f_t'= tensile splitting strength.

The test matrix was designed to investigate the effects of the reinforcement type (steel and GFRP), concrete strength (NSC and HSC); and varied *M/V* ratios (0.3 m and 0.6 m) on the punching behavior and strength of edge-slab connections. All of the slabs had an identical number of bars on the tension and compression sides (bottom and top). The bottom and top meshes consisted of 20M or No. 20 (#20) and 15M or No. 15 (#15) steel or GFRP bars, respectively. It should be mentioned that two bars were passing through the column core to satisfy the requirement for structural integrity reinforcement in CSA A23.3-14 (CSA 2014). The average bottom reinforcement ratios were 1.09% and 1.04% for the steel and GFRP connections, respectively. Table 2 presents the test matrix and characteristics for each connection. The test matrix consisted of five slabs, four GFRPRC connections (G-N-0.3, G-H-0.3, G-N-0.6, and G-H-0.6) were constructed using NSC and HSC and tested under M/V ratios of 0.30 m or 0.6 m, while the remaining slab (S-N-0.3) was reinforced with steel bars and served as a reference for comparison. The connections were labelled with letters denoting the reinforcement type (G or S for GFRP or steel bars) and concrete type (N for NSC and H for HSC), followed by the M/V value (0.3 or 0.6). The column stub was reinforced with six 25M steel bars as longitudinal reinforcement and 10M transverse steel stirrups spaced at 100 mm. The chosen configuration satisfactorily avoids the premature failure of the column stub in steel-RC edge connections during testing (Megally and Ghali 2000).

5.2.3 Test Setup and Procedure

All of the connections were tested in the structural laboratory at the University of Sherbrooke under combined vertical shear force (V) and unbalanced moment (M_{un}) until failure. Figure 5.3 shows the test setup and schematic. Vertical shear force was simulated by vertically applying a downward load through the column with a 1500 kN hydraulic jack, which was installed in the middle of a rigid steel I-beam supported on two steel portal frames. To facilitate free horizontal movement of the column during lateral loading, a steel pan with rollers was placed between the vertical jack and the top of the upper concrete column. Two 1000 kN horizontal hydraulic jacks were installed on two very rigid reaction frames firmly fastened to the laboratory strong floor to apply lateral loads. The vertical and lateral jacks were controlled with three manual hydraulic pumps. The loads were monitored with three load cells on each pump and connected to the data-acquisition system. The connections were simply supported on the bottom surface along three sides during testing with the fabricated supporting steel bed. The bottom supporting frame was braced with eight double angles back to back and prestressed to the laboratory floor with four 38 mm diameter steel tie rods to avoid any lateral movement. On the slab top face, three supported edges were restrained by steel reaction beams to prevent slab lifting. To simulate slab rotation at the lines of contra flexure during the entire test, neoprene bearing pads 20 mm thick and 100 mm wide were placed between the slab and supporting bed and between the slab and top restraining beams along the support lines.

The connections were tested under two different M/V ratios of 0.3 and 0.6 m. The unbalanced moments were calculated by multiplying the two lateral forces applied to each column by the distance from the application point to the center of the slab: 675 mm. The vertical load was applied monotonically at a load-controlled rate of 5 kN/min, whereas the horizontal forces were simultaneously applied with the vertical force in small increments to maintain a constant M/V ratio of 0.3 or 0.6 m throughout the test until failure.

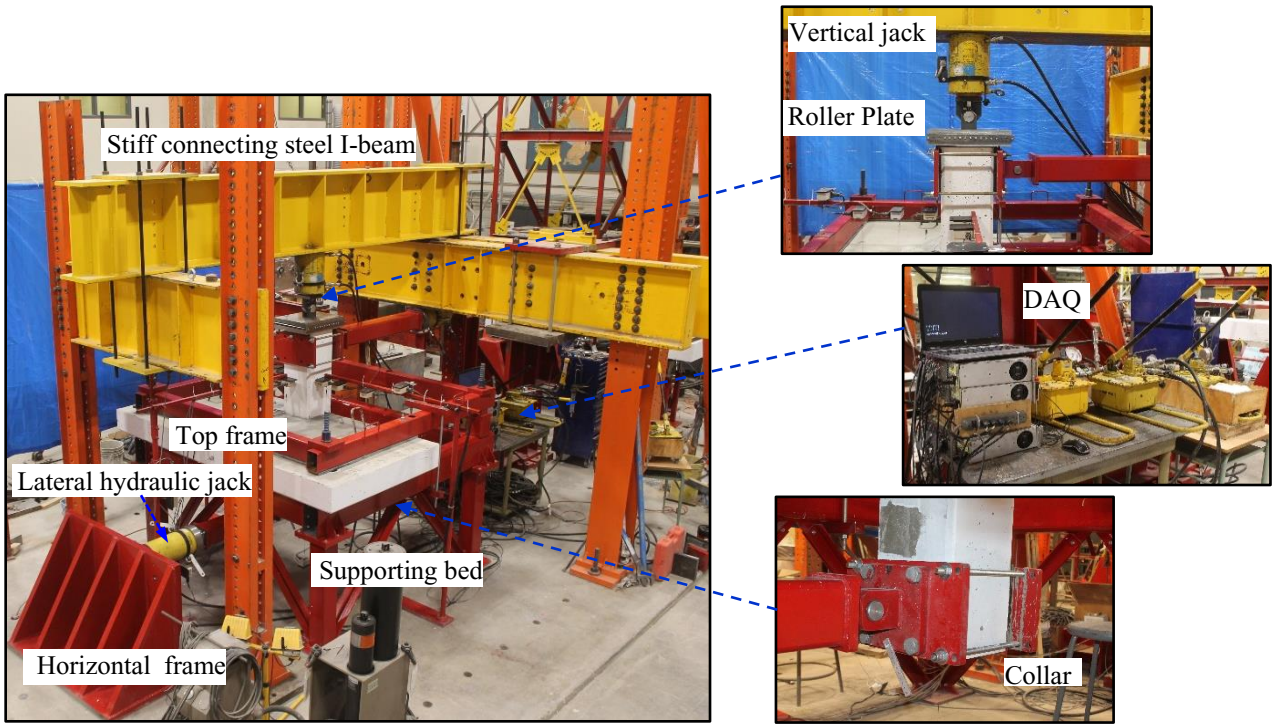

(a) Test setup photo

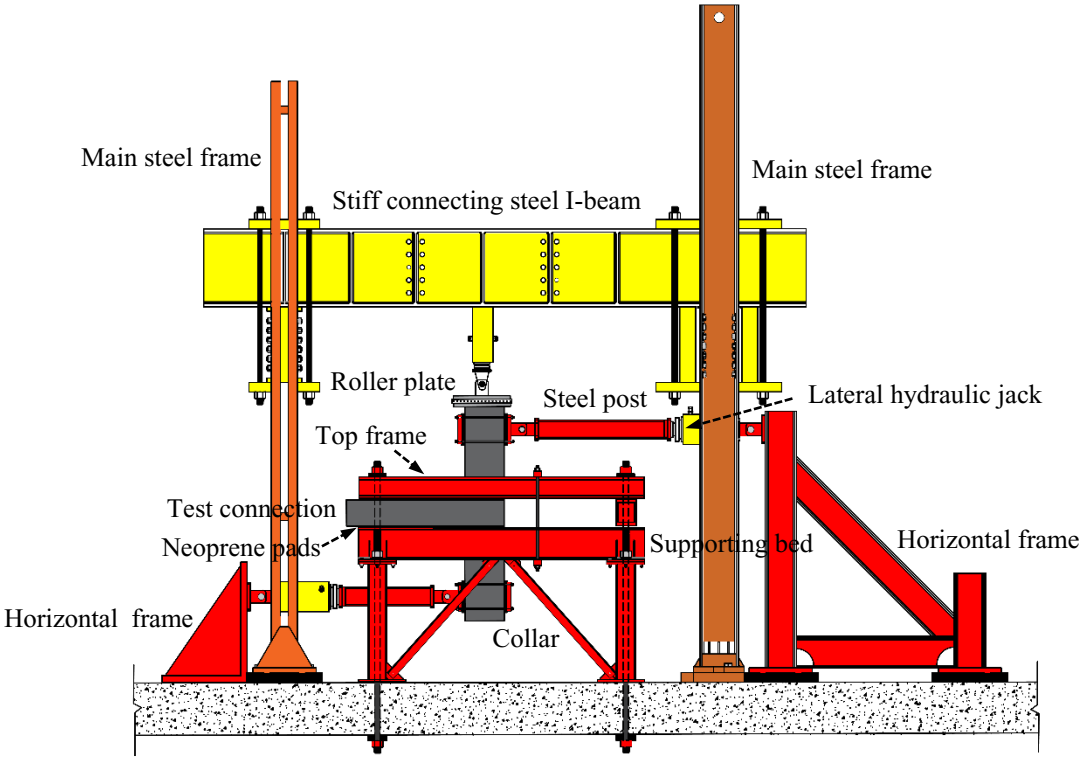

(b) Schematic drawing

Figure 5.3 –Test setup and schematic

5.2.4 Instrumentation

Extensive instrumentation was used to help understand connection behavior. A total of 11 electrical strain gauges were mounted on the bottom flexural-reinforcement bars in both orthogonal directions at different positions to monitor the strains during loading. Figure 5.1 shows the different locations of the attached strain gauges on the two selected tension bars from the column face in each direction. Moreover, five concrete electrical resistance strain gauges (C1 to C5) were mounted close to the column face to measure concrete strain on the slab compression side, as shown in Fig. 5.4. A series of linear potentiometers (LPOTs) were mounted to measure slab deflections and column lateral displacements. Slab deflections were monitored with 14 vertical LPOTs at different locations along the column centerlines in both orthogonal directions (Fig. 5.4). Two LPOTs were mounted horizontally at the tips of the upper and lower column stubs to measure the horizontal column displacement. To monitor any possible shifting of the connection or test setup, two LPOTs were installed in the horizontal-loading directions at the center of slab thickness and frame-test setup. All instruments were installed on rigid steel frames, separated from the testing frame and attached directly to the laboratory floor to prevent any frame deformations from affecting the measurements. The strain gauges and POTS were connected to a data-acquisition system to record the readings. During the test, crack propagation was marked, and the corresponding loads recorded. Figure 5.4 shows the different positions of the linear potentiometers.

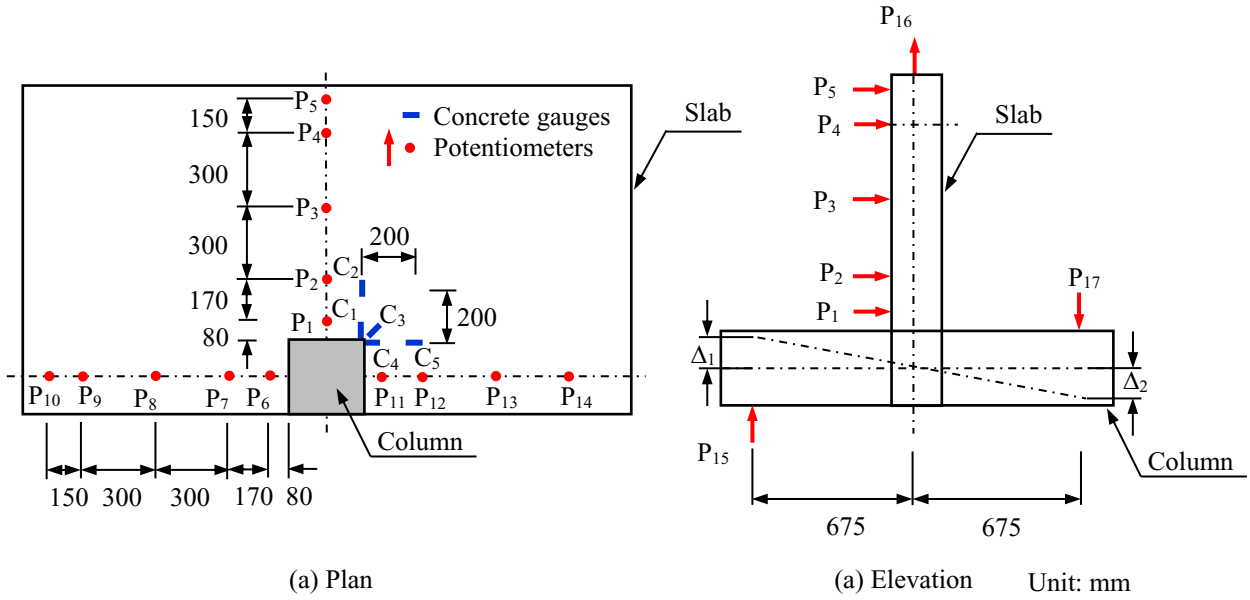

(a) Plan (a) Elevation Unit: mm

Figure 5.4 – Instrumentations (Note: All dimensions in mm)

5.3. Test Results and Observations

5.3.1. Cracking and Mode of Failure

During the test, flexural cracks appeared first on the slab tension side. The loads corresponding to the appearance of the first crack (cracking load V_{cr} and unbalanced moment M_{cr}) as well as the corresponding deflections (Δ_{cr}) were recorded in Table 5.3. The first flexural crack began to appear at vertical loads from 37.9 to 45.4 kN and from 65.9 to 73.5 kN for the NSC and HSC connections, respectively. These radial flexural cracks originated in the inner slab–column interface and propagated towards the supports. Inclined torsion cracks formed at the inner corners of the columns at about 35° from the slab edge. These cracks started to appear at about 25 % of the ultimate loads, then propagated upward the slab edge to half of the slab depth at approximately 50% of the ultimate loads. Thereafter, circumferential (tangential) cracks generated around the column and crossed over the radial cracks at higher loads, while the torsion cracks continued their way to the compression face of the slab. As the loads increased, the number of such cracks and their widths in the column vicinity increased. Shear cracks initiated on the slab tension side and propagated towards the compression side of the slab until failure occurred. All connections failed abruptly. At failure, a major tangential crack was intercepted by the flexural cracks in an approximately perpendicular manner, forming the punching cone.

In all of the slabs, some cracks developed on the compression faces at approximately 60% to 70% of the ultimate failure load. Figure 5.5 shows the typical cracks in the column vicinity on the tension and compression sides of some tested connections.

Regardless of the reinforcement type, the final mode of failure for all of the connections was punching shear without any signs of concrete crushing. This failure was characterized by an immediate drop in the ultimate load, accompanied by the appearance of a clear crack defining the failure surface. It should be noted that the punching-shear failure occurred in the steel connection initiated as yielding of steel bars. The induced yielding in the steel bars widened the shear cracks, which decreased the contribution of the aggregate interlock to the shear strength. All connections displayed similar crack patterns on the tension surface regardless reinforcement type and concrete strength on the tension side. Increasing the *M/V* ratio to 0.6, however, decreased the number of cracks at failure on the tension side of the GFRP connections, regardless of the concrete strength. That can be attributed to the increase in shear stresses applied to shear critical section, which accelerated the incidence of punching-shear failure before the formation of the significant flexural cracks. El-Gendy and El-Salakawy (2016) made the same observation based on testing NSC connections under different *M/V* ratios. On the other hand, The HSC connections evidenced narrower cracks as well as considerable splitting of the concrete cover, however, once punching failure occurred. This behavior is similar to that observed in steel- and FRP-reinforced-concrete connections (Marzouk et al. 1998 and Mostafa et al. 2018).

To examine the development of the inner diagonal cracks through the slab thickness, some tested connections were sawed through a line perpendicular to the free edge and adjacent to the column. Table 5.3 and Figure 5.6 illustrate the inclination angle of the punching cone of the tested connections. Figure 5.6 shows that the sawn connections had a main diagonal shear crack starting at the column face and extending to the slab tension side at different inclination angles (α_{cone}), where α_{cone} is the average angle for the critical shear crack with the slab tension side. The inclination angle of the critical shear crack (α_{cone}) was significantly affected by the *M/V* ratio rather than concrete compressive strength.

An increase in the *M/V* ratio from 0.3 to 0.6 for NSC and HSC connections resulted in a slightly steeper shear crack. It can be also observed that the direction of the cracks at the free edge was

consistent with the direction of the punching force, particularly when the *M/V* ratio was small (i.e. G-H-0.3). The inclined cracks at the free edge, however, ran in the direction opposite to the punching-shear force as a result of the high unbalanced moment, which produced reversed shear stresses in the direction opposite to that caused by the vertical shear force (Fig. 5.6b). This behavior is similar to that observed in steel-reinforced-concrete edge connections (El-Salakawy et al. 1998, 2000). On the other hand, the inclined shear crack at failure was not significantly influenced by the reinforcement type or concrete strength.

5.3.2. Vertical Load-Deflection Behavior

Figure 5.7 provides the applied vertical load versus deflection relationships for the tested connections at 80 mm from the column faces along column centerlines in the perpendicular direction to the free edge. All of the connections show a typical bilinear load–deflection response in both orthogonal directions. The first line represents the pre-cracking stiffness, k_i, calculated as the slope of the load–deflection curve before cracking, whereas the second line illustrates the post-cracking stiffness , k_p, calculated as the slope of the load–deflection curve after cracking. The sudden drop in the applied vertical load in all tested connections after reaching their maximum capacities confirmed the occurrence of punching-shear failure. As seen in Fig. 5.7, the load–deflection relationships and connection stiffness were significantly affected by the test parameters. GFRP-reinforced connection G-N-0.3 exhibited higher deflection values than of its steel-reinforced counterpart S-N-0.3 at the same load level. The ultimate deflection of connection G-N-0.3 was 79% higher than connection S-N-0.3. This can be attributed to the GFRP bars having a lower modulus of elasticity than the steel bars (approximately $E_f = 0.25\ E_s$).

Using HSC directly enhanced the uncracked stiffness, k_i, of the tested connections as evidenced in Fig. 5.7b. The pre-cracking stiffness , k_i , of G-H-0.3 and G-H-0.6 (HSC) was 103.7 and 101.3 kN/mm, compared to 80.9 and 78.5 kN/mm, respectively, for G-N-0.3 and G-N-0.6. The pre-cracking stiffness, k_i, increased by 29% (on average) in connections G-H-0.3 and G-H-0.6 compared to their counterparts G-N-0.3 and G-N-0.6. The post-cracking stiffness , k_p, of the NSC and HSC connections did not, however, change significantly after cracking. Furthermore, the ultimate deflection of the HSC connections was 15.5% (on average) higher than that of the

NSC connections. This indicates that using the HSC in the GFRP-reinforced slabs enhanced the overall response of the test connections and made it possible to achieve significantly higher deflections at failure (Hassan et al 2013). Increasing the *M/V* ratio from 0.3 to 0.6 had a significant impact on the overall performance as well as the ultimate deflection for all of the GFRP connections. The ultimate deflections for connections G-N-0.6 and G-H-0.6 were 47% and 46% lower than that of their counterparts G-N-0.3 and G-H-0.3, respectively.

5.3.3. Moment–Rotation Relationships

Figure 5.8 gives the applied unbalanced moment versus column rotation relationships for all tested connections. The column rotation was calculated as the ratio of the sum of measured displacements at the column ends by means of potentiometers P_{12} and P_{16} to the distance between the two loading rams (see Fig. 5.4). The ultimate rotations for connections S-N-0.3, G-N-0.3, G-H-0.3, G-N-0.6, and G-H-0.6 were 0.027, 0.0188, 0.0223, 0.0233, and 0.029 radians, respectively. As seen in Fig. 5.8, the measured rotations of the columns at failure increased with as the *M/V* ratio increased, regardless of the concrete strength. For instance, the rotation capacities increased by 19% and 25% for connections G-N-0.6 and G-H-0.6 compared to connections G-N-0.3 and G-H-0.3, respectively. The ultimate moment increased by 35% and 40 % for connections G-N-0.6 and G-H-0.6 compared to connections G-N-0.3 and G-H-0.3, respectively. On the other hand, using HSC significantly increased the rotation capacities in connections G-H-0.3 and G-H-0.6 by 24% and 30% compared to their NSC counterparts G-N-0.3 and G-N-0.6, respectively. It is the worth mentioning that the comparison with steel connection S-N-0.3 was not possible because the mounted lateral LPOTs stopped reading before failure.

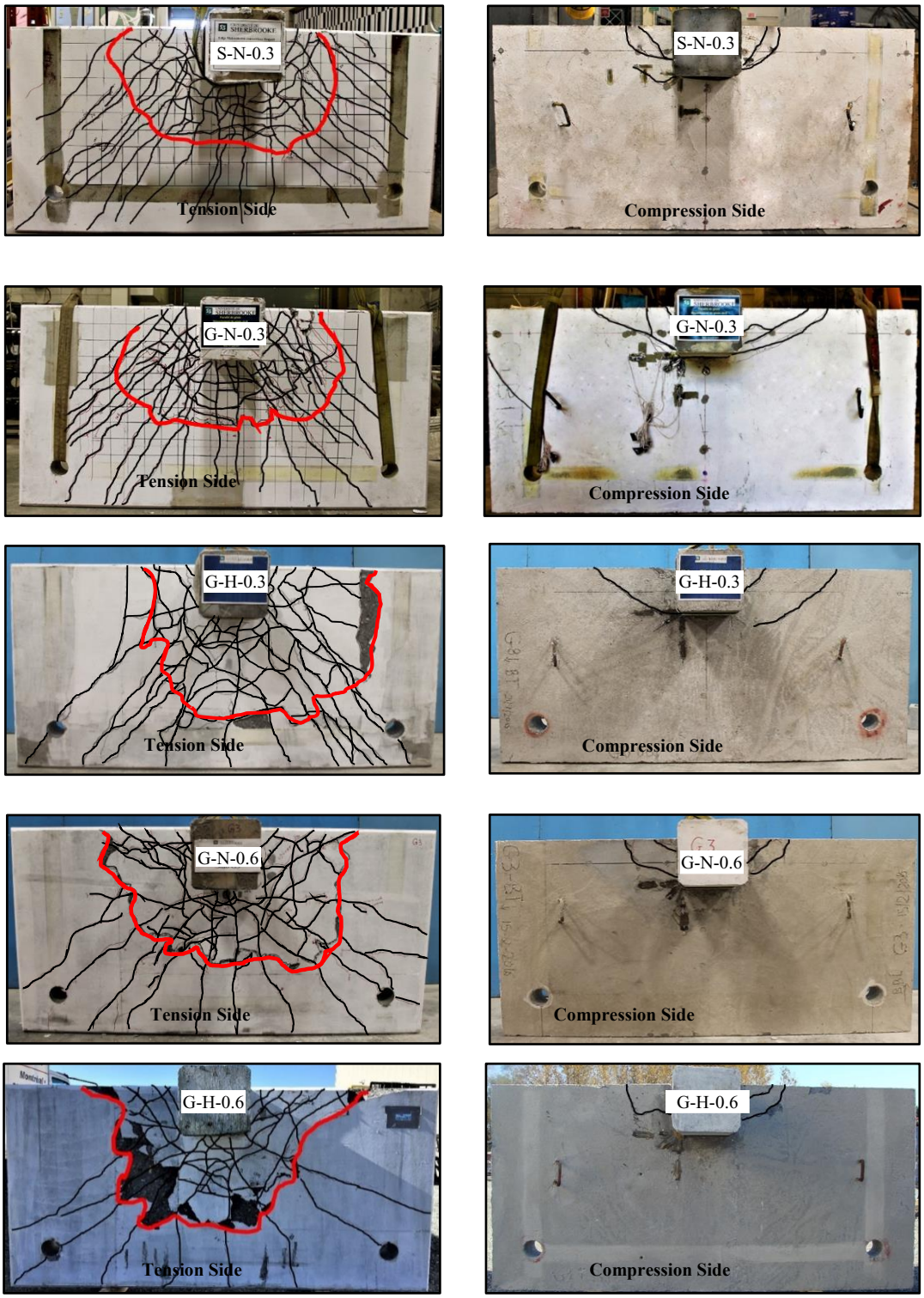

Figure 5.5 – Cracking patterns and punching-shear failure surface for the tested connections

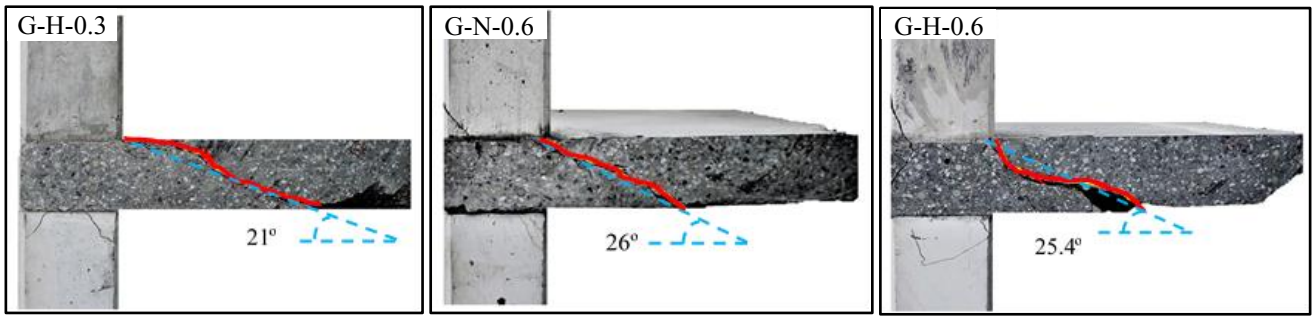

(a) Shear cracks and failure envelope of the sawed connections

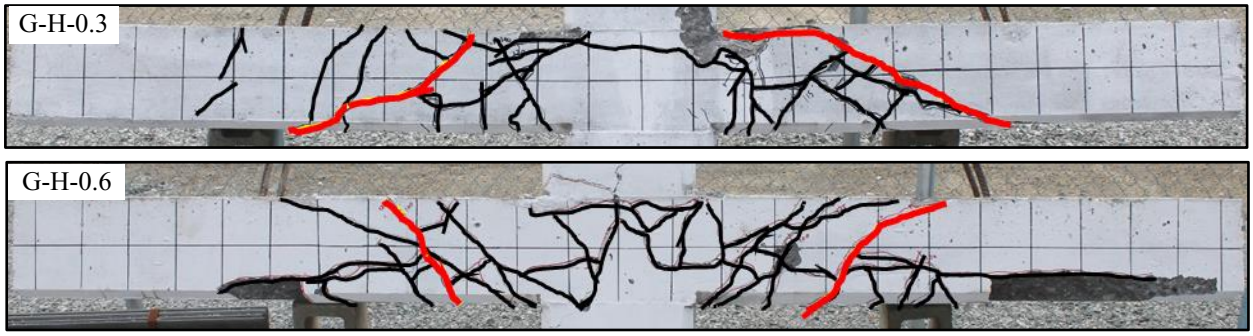

(b) Typical shear cracks along the free edge

Figure 5.6 – Shear cracks progression along the sawed sections and the free edge

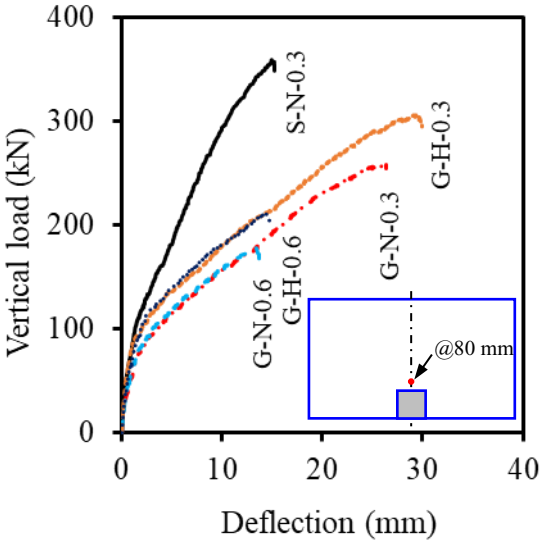

a) In the Perpendicular direction to the free edge

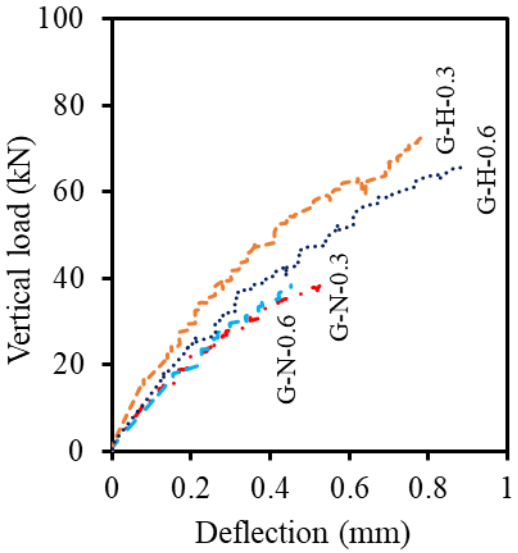

b) Pre-cracking stiffness for connections G-N-0.3, G-H-0.3, G-N-0.6,G-H-0.6

Figure 5.7 – Vertical load–deflection relationships

Table 5.3 – Summary of Test Results

Connection	V_{cr}, kN	M_{cr}, kN.m	Δ_{cr}, mm	$V_{u\ test}$, kN	$M_{u\ test}$, kN.m	Δ_{vu}, mm	$v_{u\ test}$, MPa	k_i, kN/mm	k_p, kN/mm	α_{cone} *degrees*	$\varepsilon_{r\ max,}$ ($\mu m/m$) ⊥ a	$\varepsilon_{r\ max,}$ ($\mu m/m$) // a	$\varepsilon_{c\ max}$ ($\mu m/m$)
S-N-0.3	45	12	0.36	359	106	15	2.7	112.4	20.6	–	3393	2683	-796
G-N-0.3	40	11	0.55	260	79	26	2.0	80.9	7.7	–	7570	5208	-1302
G-H-0.3	73	22	0.78	306	92	30	2.3	103.7	8.1	21.0	8381	6246	-775
G-N-0.6	38	24	0.44	178	107	13	2.1	78.5	7.9	26.0	8248	4267	-1133
G-H-0.6	66	40	0.89	213	129	15	2.5	101.3	8.0	25.4	8876	4678	-817

[a] Position perpendicular (⊥) or parallel (//) to the free edge

V_{cr} = cracking vertical shear force at column centroid; M_{cr} = cracking unbalanced moment at column centroid; Δ_{cr} = deflection corresponding to cracking load; $V_{u\ test}$ = ultimate vertical shear force at column centroid; $M_{u\ test}$ = ultimate unbalanced moment at the at column centroid; Δ_{vu} = deflection corresponding to ultimate loads; k_i = pre-cracking stiffness; k_p = post-cracking stiffness; α_{cone} = actual punching-shear-angle cone in the horizontal direction; $\varepsilon_{r\ max}$ = ultimate measured reinforcement strain; $\varepsilon_{c\ max}$ = ultimate measured concrete strain.

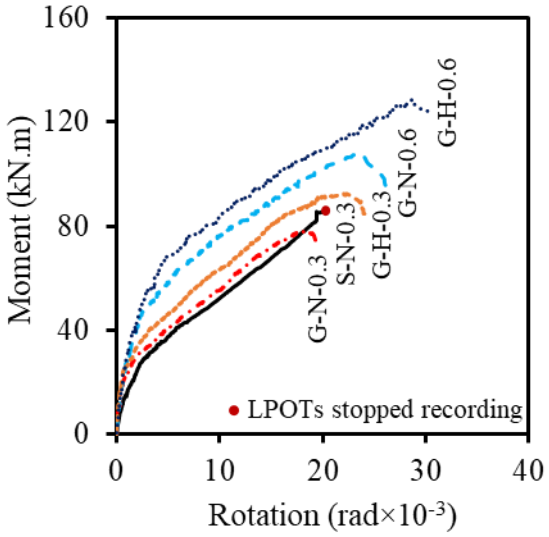

Figure 5.8 – Moment–rotation relationships

5.3.4. Strains in Flexural Reinforcement and Concrete

The applied vertical load versus the maximum flexural reinforcement and concrete strains for all of the connections have been graphed in Fig. 5.9. The reinforcement strains for each connection were recorded at 75 mm from the column faces perpendicular and parallel to the free edge, while the maximum concrete strain was measured at the column face by gauge C_1 (Fig. 5.4). Table 5.3 reports the maximum reinforcement and concrete strains. Connection S-N-0.3, reinforced with steel bars, exhibited no signs of yielding before the occurrence of punching-shear failure. On the other hand, the maximum reinforcement strain in the GFRP-reinforced connections were 7570, 8381, 8248, 8876 µm/m, representing 40%, 44, 43%, and 46% of the guaranteed ultimate tensile strength for connections G-N-0.3, G-N-0.6, G-H-0.3, and G-H-0.6, respectively. Furthermore, the maximum measured concrete strains at the column face were below the specified concrete crushing strains of 3500 and 3000 µm/m according to CSA S806-12 (CSA 2012) and ACI 440.1R-15 (ACI 2015), respectively. The attained reinforcement and concrete-strain values were consistent with the incidence of the punching failure, without concrete crushing, on the compression zone or GFRP-reinforcement rupture.

Figures 5.10 and 5.11 show the reinforcement-strain distribution along the selected tension reinforcing bars at different loading stages in the perpendicular and parallel directions to the free edge, respectively. As expected, the tension-reinforcement strains in the column vicinity

were high owing to the combined shear stresses resulting from the vertical shear force and the unbalanced moment. These strains were lower away from the column vicinity toward the supported slab edge until reaching very low strain values at 750 mm from the column face in both orthogonal directions. This implies that the sand-coated GFRP bars adequately transferred loads with no signs of bar slippage or bond failure during the tests. Apparently, due to the low axial stiffness of GFRP bars, the reinforcement strains in the GFRP-reinforced connection G-N-0.3 were higher than in its steel-reinforced counterpart S-N-0.3, although similar strain profiles were observed until failure. This is consistent with the same observations in many studies (Hussein et al. 2004; Hassan et al. 2013; El-Gendy and El-Salakawy 2016). On the other hand, increasing the *M/V* ratio yielded higher reinforcement strains in the GFRP bars along the perpendicular direction to the free edge than those measured strains in the GFRP bars in the parallel direction to the free edge. In contrast, the HSC connections revealed lower concrete strains than the NSC connections.

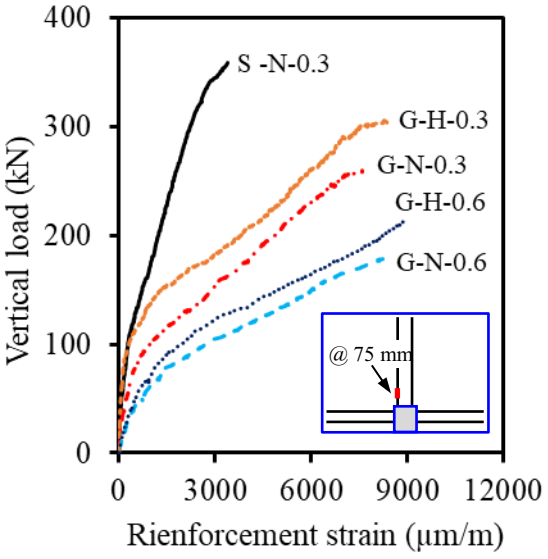

a) In the perpendicular direction to the free edge

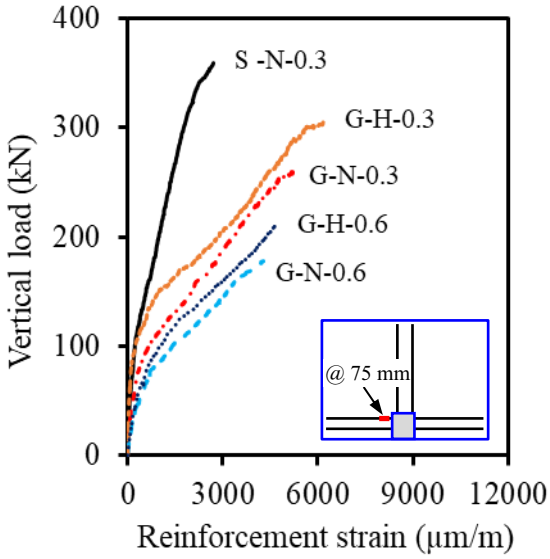

b) In the parallel direction to the free edge

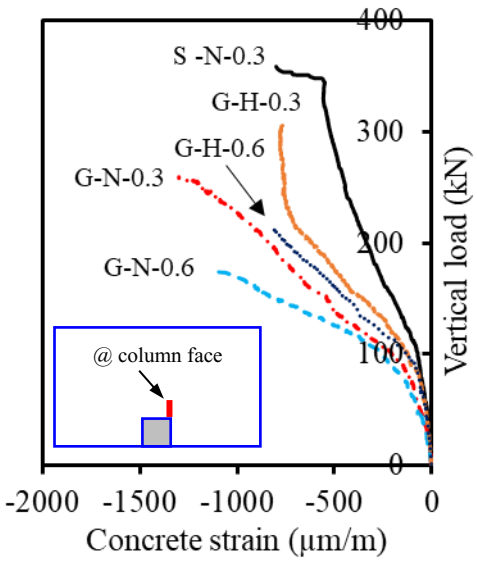

C) Maximum concrete strain around the column

Figure 5.9 – Vertical load-strain relationships

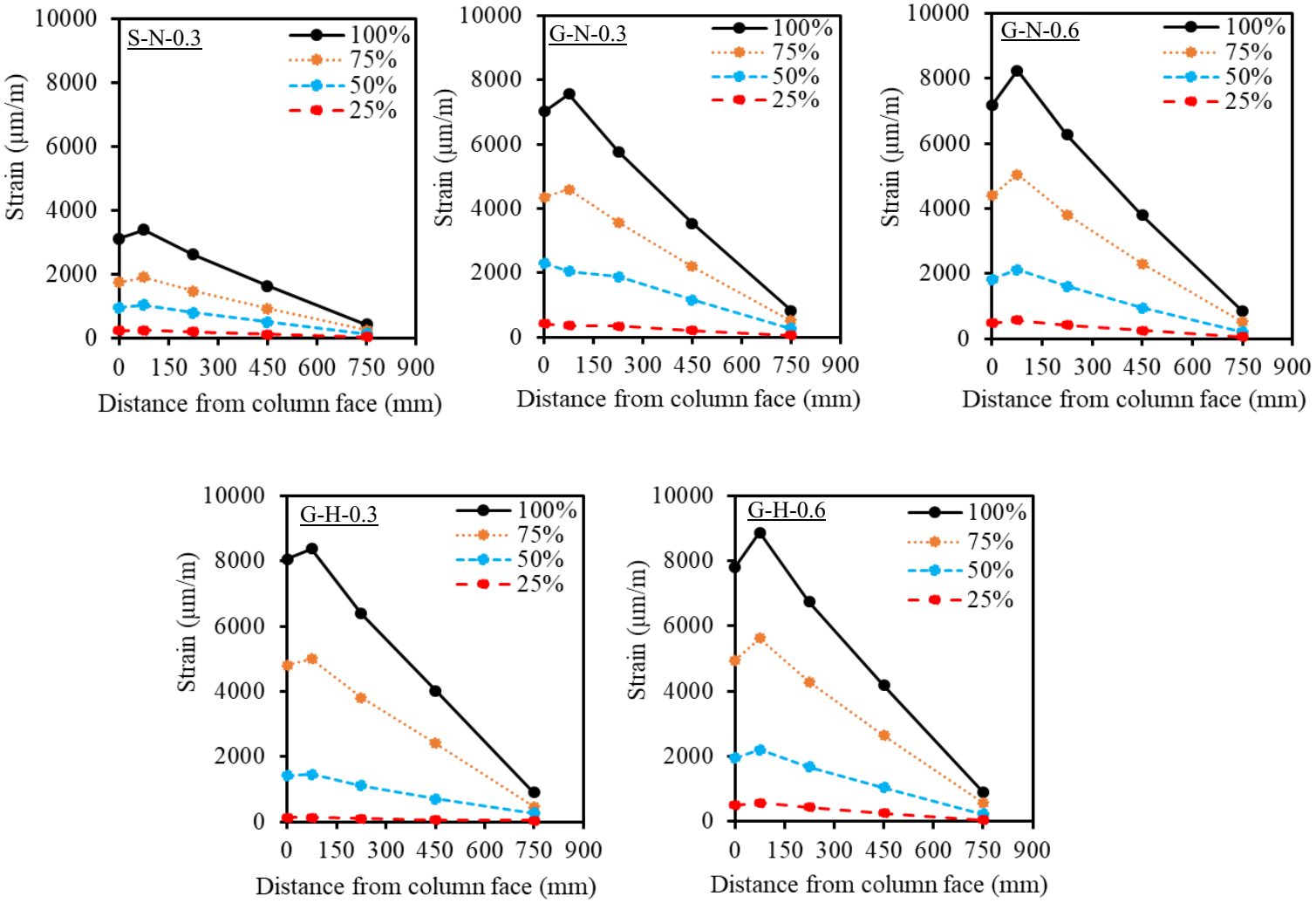

Figure 5.10 – Flexural reinforcement-strain distribution in the perpendicular direction to the free edge

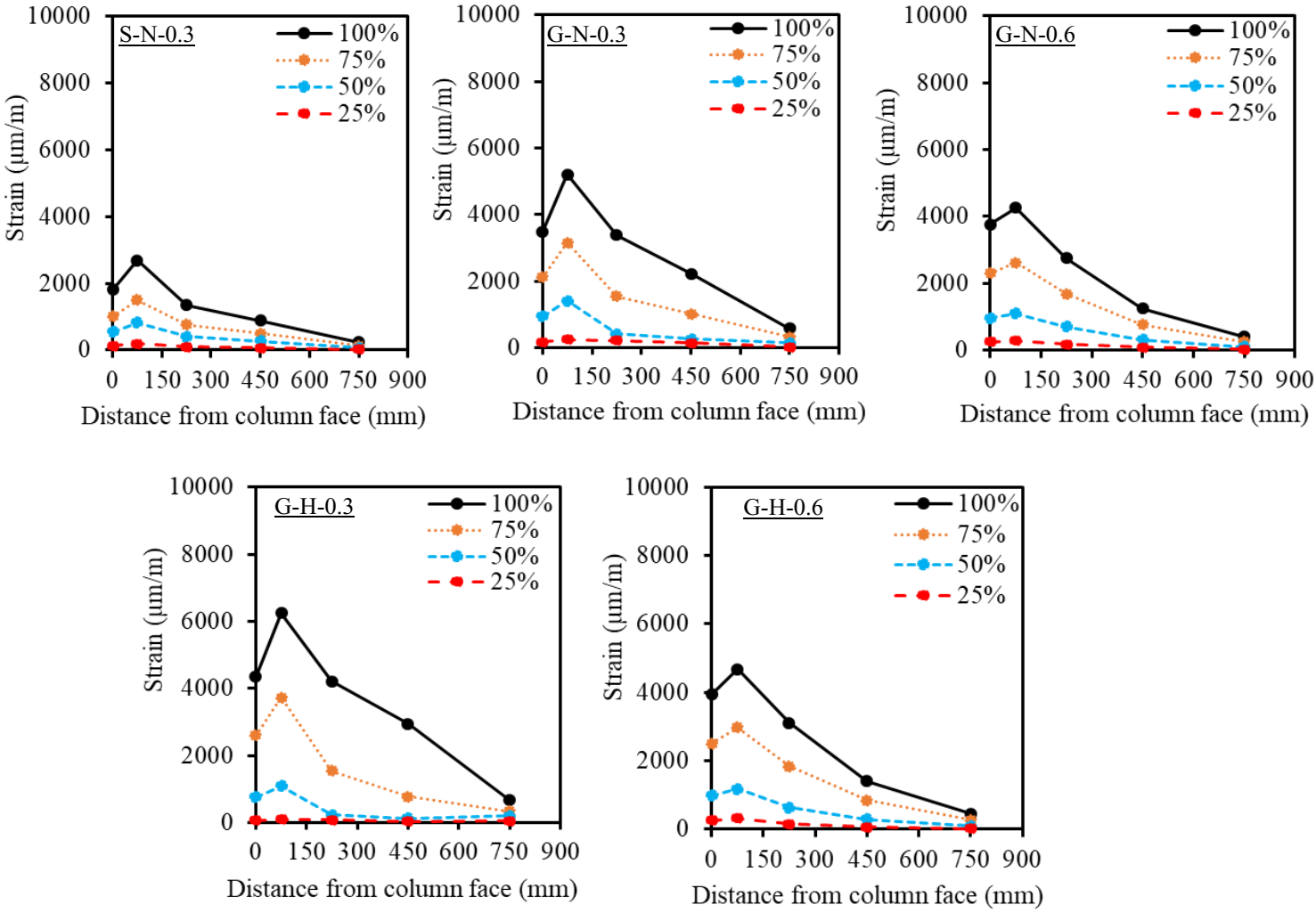

Figure 5.11 – Flexural reinforcement-strain distribution in the parallel direction to the free edge

5.4. Discussion

5.4.1. Influence of Reinforcement Type

The GFRP- and steel-reinforced connections with the same reinforcement ratio exhibited similar responses in terms of crack pattern, mode of failure, and punching-shear failure surface, regardless of reinforcement type. Table 3 reports the vertical shear force and bending moment at ultimate and the corresponding ultimate punching-shear stress calculated at 0.5d from the column face for the tested connection. The results in Table 3 show that the GFRP-reinforced connection with the same reinforcement ratio as its steel-reinforced counterpart evidenced 28% lower punching-shear stress at failure. This was related to the smaller dowel action and lower modulus of elasticity of the GFRP reinforcing bars compared to the steel bars. Using a GFRP-reinforcement ratio equal to the steel-reinforcement ratio yielded a smaller neutral-axis depth, higher strains, and deeper, wider cracks at the same load level. Thus, both the contributions of the uncracked concrete and aggregate interlock decreased, which, in turn, yielded lower punching-shear capacity.

5.4.2. Influence of Moment-to-Shear Force Ratio (M/V)

During a lateral-load exposure or slab discontinuity, the unbalanced moment transferred between the slabs and columns could produce significant shear stresses that increase the likelihood of brittle failure. Regardless of the concrete strength, increasing the M/V ratio significantly affected the slab punching-shear strength, deformation capacity, and energy absorption for all of the NSC and HSC connections. Increasing the *M/V* ratio from 0.3 to 0.6 (G-N-0.3 to G-N-0.6, fabricated with NSC) yielded a 31% decrease in the ultimate capacity. A similar was noted between the HSC connections, with G-H-0.6 showing a 30% decrease in ultimate capacity compared to G-H-0.3. This can be attributed to the higher shear stresses due to combined vertical shear force and high unbalanced moment. It is worth mentioning that the *M/V* ratio had a comparable effect on the GFRP connections constructed with NSC and HSC. Ozden et al. (2006) reported the same findings for interior steel-reinforced NSC and HSC connections tested under different M/V ratios.

5.4.3. Influence of Concrete Strength

Using HSC enhanced overall slab behavior and, consequently, increased the ultimate punching-shear capacity of the connection. The higher concrete strength helped enhance the contribution of the compressive block above the neutral axis after cracking, which yields higher punching-shear strength. The ultimate punching-shear strength of G-H-0.3 and G-H-0.6 was 17.6% and 19.3% higher than that of their counterparts G-N-0.3 and G-N-0.6, respectively. In comparison to the NSC connections, the HSC connections evidenced final punching failure associated with considerable spalling of the concrete cover in the failure area around the column. This can be attributed to the brittleness of the HSC, which allowed the cracks to propagate through the course aggregate particles (Gouda and El-Salakawy 2015). Furthermore, the HSC connections recorded lower concrete strains than the NSC connections. This relates to the high tensile strength, which delays slab cracking, and the higher modulus of elasticity helped reduce induced strains. On the other hand, the HSC connections yielded lower strains in the GFRP bars at early loading stages than their NSC counterparts. At higher loading stages, the induced strains were slightly higher than that of their NSC counterparts.

5.5. Punching Shear Design Equations

The design of edge slab–column connection always includes sustainable unbalanced moment due to the existence of gravity load, wind, earthquake, or other lateral forces in the structure. Consequently, the factored shear stress is a combination of a vertical shear force and an unbalanced moment transferred from the slab to the column**.** The maximum factored shear stress,v_u, is calculated at a distance $d/2$ from the column face according to the design provisions in ACI 318-14 (ACI 2014) and CSA A23.3-14 (CSA 2014) for slabs without shear reinforcement.

$$v_u = \frac{V_u}{b_{o;\,0.5d}\; d} + \frac{\gamma_v M_o}{J_c}\; c \tag{5.1}$$

where v_u = ultimate shear stress at $0.5d$ from the column face; $b_{o;0.5d}$ = critical shear perimeter at $0.5d$ from the column face; γ_v = fraction of unbalanced moment transferred by shear eccentricity; d = effective slab depth; M_o = ultimate unbalanced-moment centroid of the critical

shear section; c = distance from the centroid of the critical shear section to the face of shear critical section; and J_c = polar moment of inertia of the critical shear section as per Eq. (5.2).

$$J_c = \frac{2b_1^3 d}{3} + \frac{b_1 d^3}{6} - b_o\, d\, c^2 \tag{5.2}$$

where b_1 and b_2 = width of the critical section for the shear measured parallel and perpendicular to the direction of the unbalanced moment, respectively

The current design equations for FRP slabs without shear reinforcement are relatively similar to those for steel-reinforced slabs with some modifications accounting for the mechanical properties of FRP bars, especially the lower modulus of elasticity of FRP bars. In this section, the punching-shear capacities of the tested edge slab–column connections were predicted using the punching-shear equations in FRP design provisions, ACI 440.1R-15 (ACI 2015), CSA S806-12 (CSA 2012), and JSCE-97 (JSCE 1997), as listed in Table 5.4. In addition, a recent model proposed by Hassan et al. (2017) for estimating the punching-shear capacity of GFRP-RC interior connections (Table 5.4) was examined for the tested GFRP-RC edge connections. The predictions yielded by these equations were compared to the experimental results to evaluate their accuracy in predicting the punching-shear capacity of the tested connections.

Table 5.4 – Punching Shear Design Equations

Reference	Equation
JSCE-97 (JSCE 1997)	$v_c = \beta_d \beta_p \beta_r f_{pcd} \frac{1}{\gamma_b}$ (1a) $\beta_d = (1000/d)^{0.25} \leq 1.5$, (1b) $\beta_p = (100\rho_f E_f/E_S)^{\frac{1}{3}} \leq 1.5$, (1c) $\beta_r = 1 + \frac{1}{1+0.25\frac{u_o}{d}}$, (1d) $f_{pcd} = 0.2\sqrt{f_c'} \leq 1.2$ (1e) where β_d = coefficient to consider the effective depth; β_p = factor to consider difference in the modulus of elasticity between FRP and steel bars; E_s = modulus of elasticity of steel; E_s = modulus of elasticity of FRP bars; u_o = perimeter of reaction area of supporting column; γ_b = partial factor of safety equal to 1.3 or 1.5 for concrete strengths below and above 50 MPa, respectively, which was set to 1.0 to get an unfactored prediction of capacity; f_{pcd} = design compressive strength of concrete (MPa); f_c' = concrete compressive strength (MPa); and d = effective slab depth (mm).
CAN/CSA S806-12 (2012)	The least of the following equations: $v_c = 0.028\lambda \emptyset_c \left(1 + \frac{2}{\beta_c}\right)\left(E_f \rho_f f_c'\right)^{\frac{1}{3}}$ (2) $v_c = 0.147 \lambda \emptyset_c \left(0.19 + \frac{\alpha_s d}{b_{o;0.5d}}\right)\left(E_f \rho_f f_c'\right)^{\frac{1}{3}}$ (3) $v_c = 0.056 \lambda \emptyset_c \left(E_f \rho_f f_c'\right)^{\frac{1}{3}}$ (4) where βc = ratio of long side to short side of the column; ϕ_c = concrete resistance factor (0.65); λ = concrete density factor (1 for normal weight); ρf = reinforcement ratio of FRP bars; α_s = factor equals 4 for interior columns, 3 for edge columns, 2 for corner columns; $b_{o,0.5d}$ = perimeter of critical shear section located at $d/2$ from the column face (mm).
ACI 440.1R (2015)	$v_c = \frac{4}{5} k \sqrt{f_c'}$ (5) where $k = \sqrt{2\rho_f n_f + (\rho_f n_f)^2} - \rho_f n_f$; n_f = ratio of modulus of elasticity of FRP bars to modulus of elasticity of concrete (E_f / E_c); E_c = modulus of elasticity of concrete ($E_c = 4700\sqrt{f_c'}$).
Hassan et al. (2017)	$v_c = 0.065 \lambda \emptyset_c \left(0.65 + \frac{4d}{b_{o;0.5d}}\right)\left(E_f \rho_f f_c'\right)^{\frac{1}{3}} \left(\frac{125}{d}\right)^{\frac{1}{6}}$ where $\left(\frac{125}{d}\right)^{\frac{1}{6}}$ = size effect factor for column-slab connection with effective depth greater than 300 mm.

5.6. Comparison Between Predicted and Test Results

Table 5.5 presents the ratio between the tested and predicted punching-shear capacity. All safety factors and partial material factors in the equations were taken to be equal to 1.0. The punching-shear predictions listed in Table 5 show that the punching-shear equations of JSCE-97 (JSCE 1997) and CSA S806-12 (CSA 2012) equations reasonably predicted the punching-shear capacities of the tested connections with average of $V_{u\,test}/V_{JSCE} = 1.28 \pm 0.13$ and $V_{u\,test}/V_{CSA} = 1.27 \pm 0.04$, respectively. These equations include the effect of FRP axial stiffness by replacing the flexural-reinforcement ratio (ρ_s) with ($\rho_f E_f / E_s$), which gives good predications. However, the punching-shear design equation adopted in ACI 440.1R-15 (ACI 2015) underestimates the punching-shear capacity with average of $V_{u\,test}/V_{ACI} = 2.13 \pm 0.09$. The ACI 440.1R-15 (ACI 2015) equation has some shortcomings due to retaining the reinforcement ratio only in predicting the depth of the neutral axis and dropping the FRP axial stiffness. In contrast, the Hassan et al. equation (2017) overestimated the punching-shear capacity with average of $V_{u\,test}/V_{Hassan} = 0.88 \pm 0.06$. This can be attributed to the type of loading and connection, as the Hassan et al. equation was based primarily on concentric punching-shear tests that were conducted on interor slab–column connections.

CSA S806-12 (CSA 2012) limits the applicability of its equation to a maximum concrete strength of 60 MPa. However, using the CSA S806-12 (CSA 2012) equations for the HSC, G-H-0.3 and G-H-0.6 with a concrete compressive strength of 85.83 and 86 MPa, respectively, yielded average of $V_{u\,test}/V_{\mathrm{CSA}} = 1.19 \pm 0.08$. Thus, the CSA S806-12 (CSA 2012) punching-shear equation proved to be more effective for concrete strengths higher than 60 MPa. Further investigations are needed, however, to quantify the concrete compressive-strength limit in the CSA S806-12 (CSA 2012) equation.

Table 5.5 – Punching Shear Capacity Prediction

Connection	V_u (kN)	CSA S806-12 (CSA2012)		ACI 440-15 (ACI 2015)		JSCE-97 (JSCE 1997)		Hassan et al. (2017)	
		V_{CSA} (kN)	$V_{u\,test}/V_{CSA}$	V_{ACI} (kN)	$V_{u\,test}/V_{ACI}$	V_{JSCE} (kN)	$V_{u\,test}/V_{JSCE}$	V_{Hassan} (kN)	$V_{u\,test}/V_{Hassan}$
G-N-0.3	260	210	1.24	121	2.15	228	1.14	286	0.91
G-H-0.3	306	245	1.24	152	2.01	228	1.34	379	0.81
G-N-0.6	178	140	1.27	80	2.22	150	1.19	191	0.93
G-H-0.6	213	162	1.31	100	2.13	150	1.42	249	0.85
Average			1.27		2.13		1.28		0.88
SD			0.04		0.09		0.13		0.06

5.7. Summary and Conclusion

This study assessed the performance and punching-shear strength of NSC and HSC edge slab–column connections reinforced with GFRP bars subjected to low and high *M/V* ratios. Based on the experimental results and discussion, the following conclusions were drawn:

- The tested connections experienced punching-shear failure as the final mode without any signs of concrete crushing. This failure was characterized by an immediate drop in the ultimate load, accompanied by the appearance of a clear crack defining the failure surface.
- Using HSC significantly enhanced the punching-shear capacity, deflection, and initial stiffness of the GFRP-reinforced connections. The punching-shear capacity, deflection, and initial stiffness of the HSC connections were 18.5%, 15.5%, and 29% (on average) higher than that of the GFRP-reinforced connections constructed with NSC, respectively. The post-cracking stiffness, however, was similar to the NSC GFRP-reinforced connections.
- Increasing the *M/V* ratio from 0.3 m to 0.6 m for the NSC and HSC connections resulted in slightly steeper shear cracks. The inclined cracks at the free edge ran in opposite direction to the punching-shear force as a result of the reversed shear stresses caused by highly unbalanced moment.
- Increasing the *M/V* ratio transferred between the slabs and columns produced significant shear stresses that increased the likelihood of brittle failure and resulted in a reduction in the vertical-load capacity by approximately 31% and 30% for the NSC and HSC connections, respectively.
- The JSCE-97 (JSCE 1997) and CSA S806-12 (CSA 2012) reasonably predicted the punching capacities of the tested connections with average of $V_{u\,test}/V_{\mathrm{JSCE}} = 1.28 \pm 0.13$ and

$V_{u\ test}/V_{CSA}$ = 1.27 ± 0.04, respectively. The ACI 440.1R-15 (ACI 2015) equation, however, underestimated, giving average of $V_{u\ test}/V_{ACI}$ = 2.13 ± 0.09. In contrast, the Hassan et al. equation (2017) overestimated the capacity of the tested connections with an average of $V_{u\ test}/V_{Hassan}$ = 0.88 ± 0.06.

- Using the actual concrete strengths of 85 and 86 MPa for the HSC connections (G-H-0.3 and G-H-0.6) in the CSA S806-12 (CSA 2012) equation better estimated the ultimate capacity ($V_{u\ test}/V_{CSA}$ = 1.19 ± 0.08) than using the 60 MPa concrete-strength limit as per CSA S806-12 (CSA 2012). Further research, however, is needed with a wide range of concrete strengths.

5.8. Acknowledgments

The authors would like to express their special thanks and gratitude to the Natural Science and Engineering Research Council of Canada (NSERC), the NSERC Research Chair in Innovative FRP Reinforcement for Concrete Structures, the Tier-1 Canada Research Chair in Advanced Composite Materials for Civil Structures, the Fonds Québécois de la Recherche sur la Nature et les Technologies (FQRNT), the Canadian Foundation for Innovation (FCI), and the technical staff of the structural laboratory in the Department of Civil Engineering at the University of Sherbrooke.

CHAPTER 6

ARTICLE 3: EFFECT OF GFRP SHEAR STIRRUPS ON THE STRENGTH OF TWO-WAY GFRPRC EDGE SLABS: EXPERIMENTAL AND FINITE-ELEMENT INVESTIGATIONS

Foreword

Authors and Affiliation

- Ahmed E. Salama: PhD Candidate, Department of Civil Engineering, University of Sherbrooke, Quebec, Canada J1K 2R1, E-mail: Ahmed.Salama@USherbrooke.ca

- Mohamed Hassan: Postdoctoral Fellow, Department of Civil Engineering, University of Sherbrooke, Quebec, Canada J1K 2R1, E-mail: Mohamed.Hassan@USherbrooke.ca.

- Brahim Benmokrane: Professor of Civil Engineering and NSERC and Tier-1 Canada Research Chair Professor, Department of Civil Engineering, University of Sherbrooke, Sherbrooke, Quebec, Canada, J1K 2R1, Tel.: 1-819-821-7758.
  Corresponding author, E-mail: Brahim.Benmokrane@USherbrooke.ca.

Paper submitted to Structural Engineering Journal, ASCE on February 11, 2019

Paper status: Accepted on October 2, 2019

Reference: Salama , A. E. , Hassan, M., and Benmokrane, B., 2019, "Effect of GFRP Shear Stirrups on the Strength of Two-Way GFRPRC Edge Slabs: Experimental and Finite-Element Investigations," *Structural Engineering Journal, ASCE.*

Abstract

Glass-fiber-reinforced-polymer (GFRP) reinforcing bars have recently gained wide acceptance as a viable construction material for sustainable new constructions. Yet current codes and guidelines have not addressed the design of GFRP-reinforced-concrete edge-slab–column connections with FRP stirrups as shear reinforcement. This paper summarizes the experimental results for full-sized edge-slab–column connections reinforced with GFRP bars and stirrups. The effectiveness of the GFRP stirrups and their extension from the column face on the performance of the tested connections are examined. In addition, a nonlinear 3D finite-element analysis (FEA) is used to perform an in-depth investigation. Then, a comprehensive parametric investigation is presented on edge connections with different stirrup sizes, extensions located at different distances from the column, and different spacings. The test results reveal that the presence of GFRP stirrups as shear reinforcement in the slab around the column perimeter improved the punching-shear response. In addition, the FEA results are in good agreement with the experimental results in terms of ultimate load, cracking patterns, strains in the reinforcement and concrete, and load–deflection relationships, thereby confirming the accuracy of the finite-element model. The results confirm that the punching-shear resistance decreased with increasing stirrup spacing and increased with increasing stirrup size and extension from the column. Based on the numerical-simulation results, a simple design approach to predicate the ultimate capacity of the tested connections is proposed. The model yielded good yet conservative predictions with respect to the experimental results as well as the available results in the literature.

Keywords: Punching shear, two-way flat slabs; edge connections; GFRP reinforcement; stirrups; finite-element analysis (FEA); shear reinforcement; strength, design codes.

6.1. Introduction

Two-way reinforced-concrete (RC) flat-slab systems are very popular in construction because of their functional and economic advantages. This structural system is vulnerable to a type of brittle failure known as punching-shear failure. One essential consideration when designing edge-slab–column connections is the lack of symmetry of the slab portion resisting the punching action combined with a large unbalanced moment at the free edge. Unbalanced bending moments transferred between the slab and column might produce significant shear stresses that increase the possibility of brittle failure. Avoiding such a failure is of paramount importance. Various solutions have been implemented to mitigate punching-shear failure at slab–column connections. Examples are simply (1) increasing the slab thickness, adding a drop panel or capital, or increasing the column dimensions; (2) using higher-strength concrete; or (3) providing additional shear strength through shear reinforcement in the form of stirrups, shear studs, shear heads, or corrugated bars in the slab around the column perimeter. The latter solution is more effective and practical than the other two methods to increase the punching-shear strength and deformation capacity of slab–column connections (Megally and Ghali 2000; Lips et al. 2012) which is one of the primary motivations of this research.

Glass-fiber-reinforced-polymer (GFRP) reinforcing bars have recently gained wide acceptance as a viable construction material for sustainable new constructions. The noncorrodible nature of GFRP bars is a significant benefit for reinforced-concrete elements in harsh environments such as parking garages treated with de-icing salts. Past research data has mostly focused on interior connections entirely reinforced with GFRP bars under the transfer of shear or combined shear and unbalanced moments (Lee et al. 2009; Dulude et al. 2013; Hassan et al. 2013a, b; Hassan et al. 2014a, b; Gouda and El-Salakawy 2016; Hassan et al. 2017). There is, however, very limited research on FRP edge-slab–column connections reinforced with shear reinforcement (Zaghloul 2007, El Gendy et al. 2016, Mostafa et al. 2018). GFRP shear reinforcement as stirrups, shear studs, and corrugated bars have proved effective in enhancing slab strength and deformation in tests on interior GFRPRC and edge-slab–column connections subjected to concentric loading alone or shear–moment transfer (Lee et al. 2009; Dulude et al. 2013; Hassan et al. 2013a, b; Hassan et al. 2014a, b; El-Gendy and El-Salakawy 2015; Mostafa and El-Salakawy 2018).

Hassan et al (2013a) tested new types of discrete closed and spiral FRP shear stirrups in interior connections. Their use of FRP shear stirrups significantly increased the punching-shear strength and deflection, on average, by 27% and 107%, respectively. Their findings also revealed that FRP shear stirrups controlled the propagation of shear cracks and that the full flexural mechanism could be attained. El-Gendy and El-Salakawy (2015) tested another type of FRP shear reinforcement called headed studs. The average increases in punching-shear strength and deformation capacity for edge connections were 40% and 98%, respectively. Mostafa and El-Salakawy (2018) examined the effects of sand-coated double-headed GFRP studs and GFRP corrugated bars in tests on edge connections reinforced with GFRP bars. The test results indicate that both types of shear reinforcement were highly satisfactory in preventing brittle punching-shear failure in the column vicinity. The ultimate shear strength and deformation capacity increased by 27% and 16% and by 64% and 46%, respectively, (on average) for the connections with shear studs and corrugated bars, compared to their counterparts with no shear reinforcement.

The punching-shear behavior of two-way slabs is complex with a large number of parameters that cannot be fully covered solely with an extensive experimental investigation. Therefore, in addition to experimental investigations, finite-element analysis (FEA) is important in simulating structural elements and providing insight into their behavior. Furthermore, FEA can depict crack progression, deflections, and failure mechanisms as well as record more information for unknown test measurements. To the authors' best knowledge, no tests have yet been done on GFRP edge-slab connections with GFRP stirrups as shear reinforcement. In addition, neither ACI 440.1R (2015) nor CAN/CSA S806 (2012) address the design of GFRP-slab–column connections with FRP shear reinforcement due to the limited research on such connections.

The experimental work presented in this paper extends an extensive research program carried out at the University of Sherbrooke to design and implement GFRP bars in parking structures. The first phase of this project has been completed (Dulude et al. 2013; Hassan et al. 2013a, b; Hassan et al. 2014a, b; Hassan et al. 2017). A total of 30 GFRP-RC slabs were tested under concentric loading. The test results and findings contributed to the assessment of the first punching-shear equation in CAN/CSA S806 (2012). They also contributed to field applications for implementing GFRP bars in flat-slab parking structures (Hôtel de Ville parking garage, QC,

Canada) and helped in designing the world's first flat-slab parking garage (La Chancelière parking garage, Qc, Canada) entirely reinforced with GFRP bars (Ahmed et al. 2016). This paper summarizes the experimental results on GFRP-reinforced edge-slab–column connections with discrete closed GFRP stirrups. The presence of GFRP shear stirrups in the column periphery and their extension from the column face are examined. A nonlinear 3D finite-element modeling was constructed using the ANSYS commercial FEA program (ANSYS User's Manual 2018) to simulate the behavior of the tested connections. The model developed was validated against the experimental results and an extensive parametric study was conducted to investigate the critical parameters influencing the shear capacity of such connections, i.e., FRP-stirrup extension, stirrup size, and spacing between stirrups. Lastly, a simplified design approach is proposed to estimate the punching capacity of edge connections reinforced with shear stirrups based on the FE results. The proposed approach was verified against the experimental results and those available in the literature.

6.2. Research Significance

Field applications in recent years have demonstrated the excellent performance and durability of GFRP-reinforced structures. Code-writing bodies in the US and Canada have tasked several technical committees with producing standards and guidelines for elements reinforced with GFRP. ACI 440.1R (2015) and CAN/CSA S806 (2012) do not address the design of such GFRP-reinforced slab–column connections with FRP shear reinforcement due to very limited research. This paper presents pioneering test results from full-sized GFRPRC edge-slab–column connections with GFRP stirrups tested under combined vertical shear and unbalanced moment. The purpose was to assess the effectiveness of the GFRP stirrups, taking into account the effect of the GFRP-stirrup extension within the slab in a cruciform layout around the column faces. A nonlinear FEA was used as a powerful tool to capture slab responses, followed by a comprehensive parametric study to investigate the key parameters influencing the shear capacity of such connections. The paper also establishes design provisions and recommendations for engineers in designing FRP-RC slab–column connections with GFRP shear stirrups.

6.3. Summary of Experimental Program

6.3.1. Test Connections and Procedure

Three full-scale edge-slab-column connections were constructed and tested to failure under eccentric shear stresses. The test connections represented edge connections from a prototype of GFRP-RC flat-plate parking structure with 5 × 5 m^2 square panels. This prototype was designed for flexure in accordance with Canadian standards CAN/CSA S806 (2012) and CAN/CSA A23.3 (2014). The total ultimate factored loads on the floor, including the slab weight, were estimated in accordance with National Building Code of Canada (NBCC 2015). All slabs had identical geometries of 2500 × 1350 × 200 mm with a 300-mm square column stub protruding 700 mm above and below the slab surfaces. Each connection was simply supported on three edges and monolithic with a column at the middle of the fourth edge. Figure 6.1 shows the overall slab geometry. The lines of contra flexure were assumed to be 20% from the span between the column centerlines. All test connections were reinforced with sand-coated GFRP bars as flexural reinforcement. Two of the connections were reinforced with GFRP shear stirrups around the punching-shear zone; one had no shear reinforcement for comparison purposes. Table 6.1 provides the characteristics of each connection . The stirrups were arranged in a cruciform pattern with a constant spacing of *d*/2, where *d* is the slab effective depth equal to 160 mm. The first line of stirrups was located at *d*/4 from the column face for all connections with shear reinforcement. Two connections (G-CS-1.75d and G-CS-4.25d) were reinforced in shear with closed GFRP stirrups (No. 10) extending 1.75d and 4.25d away from the column face to evaluate the effect of stirrup extension on the punching strength and behavior and to compare its behavior in the control slab (G). It is worth mentioning that none of the current FRP design codes and guidelines (CAN/CSA S806 2012 and ACI 440.1R 2015) have addressed the design of slab–column connections with FRP shear reinforcement. A preliminary design for the amount of shear stirrups in connections—G-CS-1.75d and G-CS-4.25d—was determined using a proposed model for interor connections reinforced with FRP stirrups (Hassan et al. 2014). Figure 6.2 shows the shear-stirrup layout and arrangement. All connections were tested under a vertical shear force (V) applied to the face of the upper column stub and an unbalanced moment (M_{un}) through two opposite horizontal loads (P) applied at the tips of the column ends. The moment-to-shear ratio, M_{un}/V, was 0.3 m based on analysis of the prototype flat-plate structure

using the equivalent frame method according to CAN/CSA A23.3 (2014). The vertical load was applied monotonically at a load-controlled rate of 5 kN/min, whereas the horizontal loads were simultaneously applied with the vertical force in small increments to maintain a constant M_{un}/V of 0.3 m throughout the test until failure.

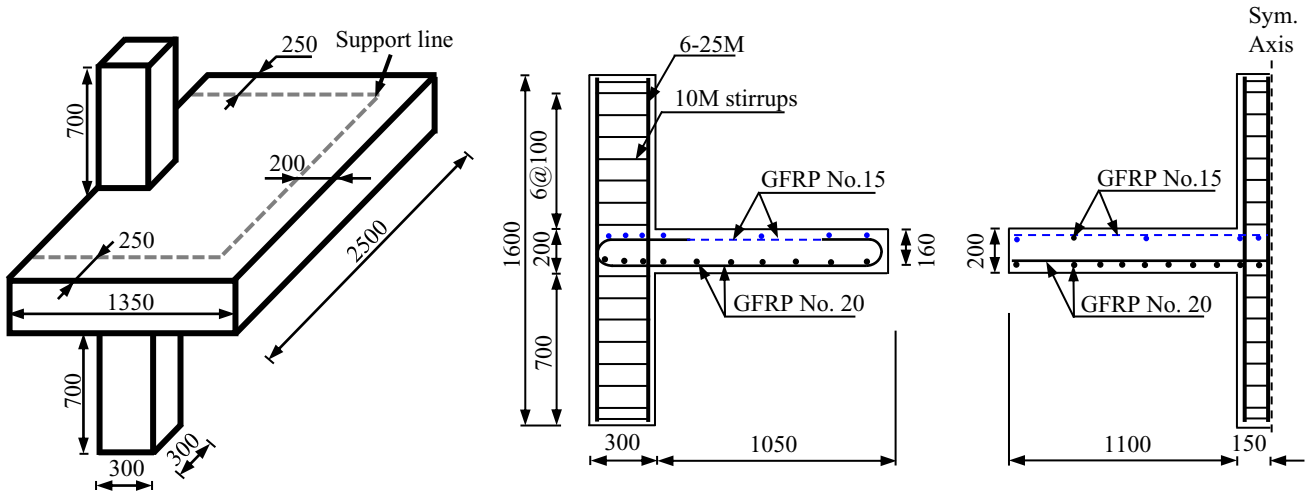

(a) Concrete dimension (b) Section (X-X) (c) Section (Y-Y)

Figure 6.1– Slab geometry and concrete dimensions

Table 6.1 – Details of test connections

Slab[a]	f'_c[b], MPa	Bottom Tensile Reinforcement			Top Compression Reinforcement			Shear Reinforcement Stirrup					
		⊥[c]	//[c]	ρ_b, (%)	⊥[c]	//[c]	ρ_t, (%)	d_b, mm	A_{fv}	r_b, mm	S_o; mm	S_{fv}; mm	Extent
G	41.4	20 No. 20	10 No. 20	1.55	10 No. 15	7 No. 15	0.65	-----	---	-----	------	----	----
G-CS-1.75d	47.6	20 No. 20	10 No. 20	1.55	10 No. 15	7 No. 15	0.65	9.5	71	38.1	0.25d	0.5d	1.75d
G-CS-4.25d	51.3	20 No. 20	10 No. 20	1.55	10 No. 15	7 No. 15	0.65	9.5	71	38.1	0.25d	0.5d	4.25d

[a] G-aa-xd: G for GFRP tension reinforcement, aa for stirrup configuration (CS for closed stirrups); and x*d* for stirrup distance from the column faces relative to the average effective depth, if any.
[b] Cylinder strength on the day of testing (100×200mm cylinders).
[c] Position perpendicular (⊥) or parallel (//) to the free edge.
S_o = distance between column face and first line of shear stirrups and S_{fv} = spacing between consecutive lines of shear stirrup.

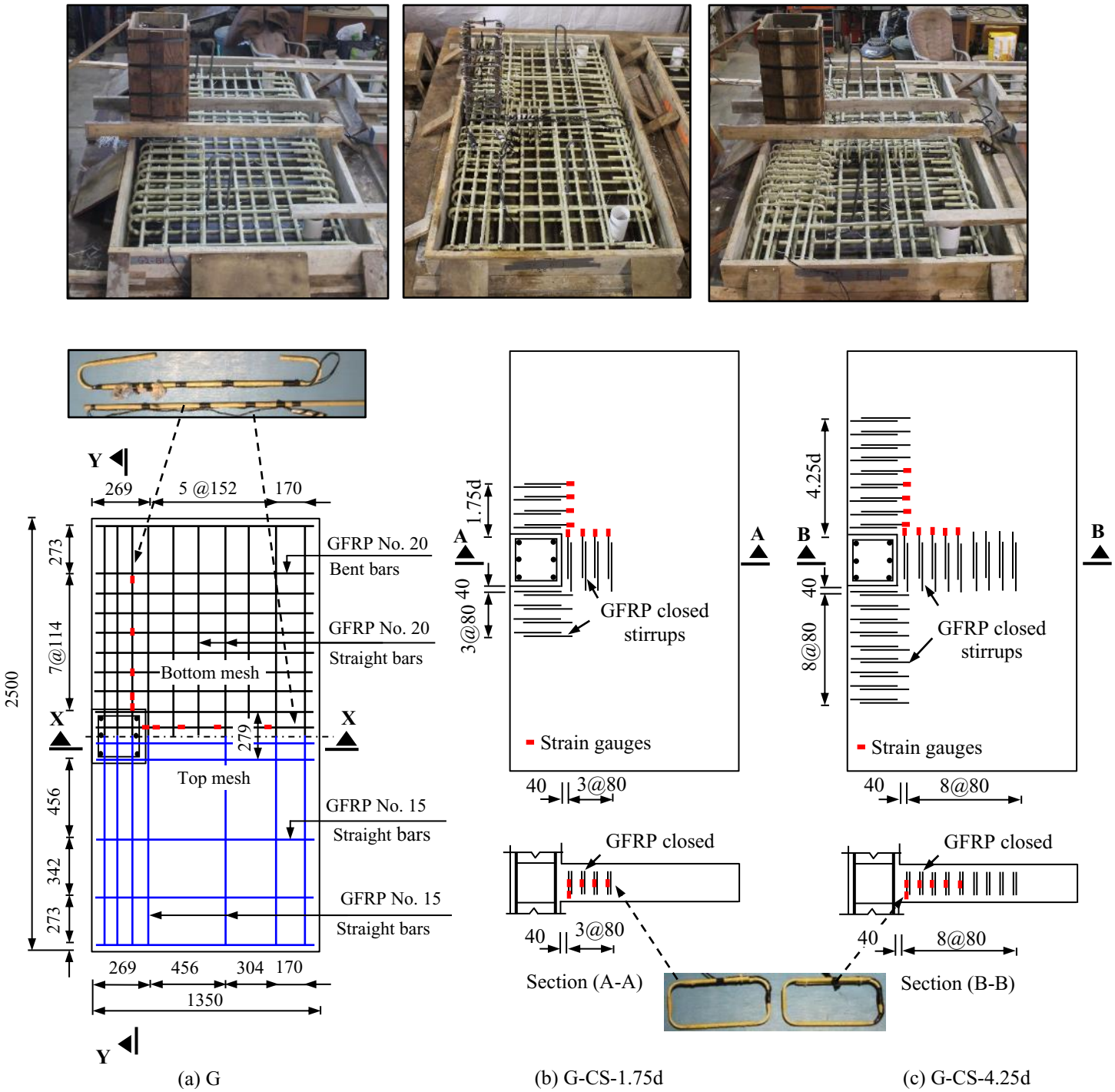

(a) G (b) G-CS-1.75d (c) G-CS-4.25d

Figure 6.2 – Typical reinforcement details and stirrup layout for slabs with and without shear reinforcement

6.3.2. Material Properties

The test connections were cast with a ready-mixed normal-weight concrete with a targeted 28-day compressive strength of 35 MPa. The concrete compressive of each connection was determined on the day of testing with three 100 × 200 mm concrete cylinders. The concrete compressive strength (f_c') ranged from 41.4 to 52.5 MPa. Table 6.1 presents the concrete strengths of the test connections. The sand-coated GFRP bars and stirrups were manufactured with the pultrusion process (Pultrall Inc. 2018). Sand-coated Grade II and III GFRP bars as classified in CSA S807 (CSA2015) as sizes No. 15 and No. 20, respectively, were used as flexural reinforcement in all tested connections. Each connection was reinforced with straight GFRP bars, except for the tension reinforcement (bottom) in the short direction, which had double bent ends to provide adequate anchorage and avoid any unexpected slippage mode of failure. Each slab was monolithic with a square column stub, which was designed to transfer shear force and lateral moment to the slab without any premature column failure. The column reinforcement consisted of six 25M deformed steel bars (three bars on each face) with 10M deformed closed steel ties at 100 mm. The tensile properties of the GFRP bars were determined by testing five samples according to ASTM D7205M (2011). Table 6.2 presents the tensile properties of the flexural bars, which were calculated based on nominal cross-sectional areas. Sand-coated discrete closed GFRP stirrups (No. 10) were used as shear reinforcement. The stirrups had an overall depth of 145 mm, width of 290 mm, and bent radius (r_b) of 38.1 mm. The tensile properties of the straight portions of the GFRP stirrups were determined according to ASTM D7205M (ASTM 2011). The bent strength of the FRP stirrups and bent bars were determined with the B.5 test method in accordance with ACI 440.3R-04 (2004). Table 6.1 presents the bent strength of the GFRP stirrups and bent bars.

Table 6.2 – Tensile properties of the reinforcing bars and shear reinforcement

Bar Designation	Nominal Cross-Sectional Area[a] (mm^2)	Immersed Cross-Sectional Area, (mm^2)	Ultimate Tensile Strength [b] (MPa)	Tensile Modulus of Elasticity [c] (GPa)	Ultimate Tensile Strain (%)
Straight flexural GFRP bars					
No. 15 GFRP bar	199	240	1323 ±12	64.8±0.5	2.04 ±0.05
No. 20 GFRP bar	285	333	1334 ±85	64.9±0.6	2.06 ±0.13
Bent flexural GFRP bars					
No. 20 straight portion	285	331	1210±63	53.0±0.48	2.28±0.15
No. 20 bent portion			f_{fvb} = 490±44	------	------
Steel bars					
10M	100	------	f_y = 420	200	ε_y = 0.21
25M	500	------	f_y = 470	204	ε_y = 0.23

[a] according to CSA S807-15 (CSA 2015).

[b and c] calculated using nominal cross-sectional areas of the reinforcing bars.

f_{fvb} = ultimate tensile bend strength obtained from the B.5 test method according to ACI 440.3R-12 (ACI 2012)

f_y = steel yielding strength, ε_y = steel yielding strain.

6.3.3. Experimental Setup and Instrumentation

All test connections were tested under combined vertical shear force (V) and unbalanced moment (M_{un}) until failure. The vertical shear force was applied using a 1500 kN hydraulic jack while two 1000 kN horizontal hydraulic jacks were installed on two rigid reaction frames to apply the lateral loads. To free horizontal movement of the column during application of the lateral loads, a steel pan with rollers was placed between the vertical jack and the top of the upper concrete column. Figure 6.3 shows the test setup. All test connections were simply supported on the bottom surface along three sides during testing with a new fabricated supporting steel bed. This supporting bed was prestressed directly on the laboratory strong floor with four 38 mm diameter steel tie rods before placing the test connection to avoid any lateral movement that might be expected. On the slab top face, steel reaction beams restrained the three supported edges to prevent slab lifting. To allow for slab rotation at the lines of contra flexure during the entire test, 20 mm thick neoprene pads were placed between the slab and supporting bed and between the slab and top restraining beams along the support lines. The test connections were equipped with extensive external and internal instrumentation to aid in understanding connection behavior. The flexural-reinforcement strains in both orthogonal directions were measured with 11 electrical resistance strain gauges (see Fig. 6.2). The strains in the GFRP

stirrups were monitored with 6 mm electrical strain gauges mounted at mid-height of the vertical legs of the GFRP stirrups and bend location in each orthogonal direction (see Fig. 6.2). The concrete strains induced on the compression side were measured with five concrete strain gauges mounted in the column vicinity. The connection deflection at the different locations along the column centerlines in both orthogonal directions was captured with 14 string potentiometers (pots). Figure 6.3 shows the different positions of linear potentiometers and the concrete gauges. All the instruments were connected to a data-acquisition system (DAQ) to record the applied loads, deflections, strains in GFRP bars and shear stirrups, and concrete strains. During testing, the progression of cracks was marked, and the corresponding loads were recorded.

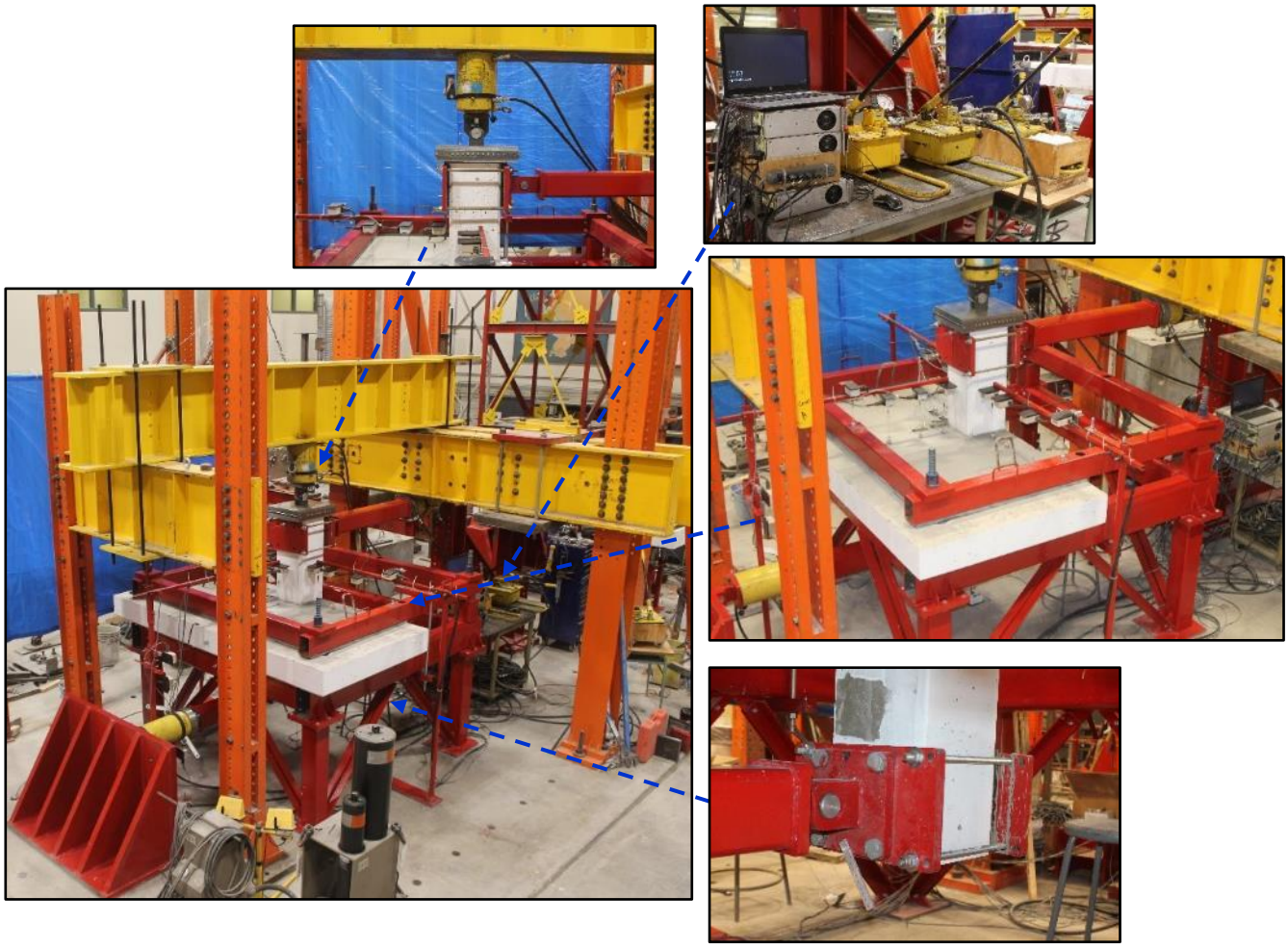

Figure 6.3 – Test setup and instrumentation

6.4. Test Results and Discussion

6.4.1. General Cracking Pattern and Failure Mode

The test connections displayed similar crack propagation on the tension side of the slab (bottom surface). The connections with shear reinforcement, however, evidenced more intensive cracks with larger punching-shear-failure surfaces compared to their counterpart without shear reinforcement. During the test, flexural cracks appeared first on the slab tension side. The first flexural crack began to appear at about 15% to 16% of the ultimate vertical load. These radial flexural cracks originated from the inner slab–column interface and propagated towards the supports. Inclined torsion cracks formed at the inner corners of the columns. These cracks started to appear at about 25% of the ultimate load, then propagated upward the slab edge to half of the slab depth at around 50% of the ultimate load. Thereafter, tangential cracks generated around the column and crossed over the radial cracks at higher loads. As the load increased, the number of such cracks and their widths in the column vicinity increased. Shear cracks initiated from the slab tension side and propagated towards the slab compression side until failure occurred. At failure, a major tangential crack was intercepted by the flexural cracks in approximately perpendicular manner, forming the punching cone. Fig. 6.4 presents an overview of the cracking pattern for all the test connections in tension and free edge sides and along the sawed sections.

The control connection G, without shear reinforcement, experienced a typical brittle punching-shear failure without much warning. The failure mode for connection G-CS-1.75d, with stirrups extending 1.75d, was punching-shear failure outside the shear-reinforced zone. Some deformability was, however, achieved before failure compared to its counterpart G, without shear reinforcement. On the other hand, the 4.25d extension of the FRP stirrups in connection G-CS-4.25d offered sufficient resistance, larger deformations, and concrete crushing at the column vicinity on the compression side of the slabs, which gave early warning signs before the punching-shear failure. The final failure mode was mixed flexural/punching-shear failure inside the shear-reinforced zone. Figure 6.4 shows the sawn sections of the connections with and without GFRP shear stirrups. Connection G evidenced a single diagonal shear crack, while connection G-CS-1.75d had a horizontal splitting crack over the top of the stirrups. This splitting crack became an inclined shear crack beyond the outermost set of shear stirrups. Connection G-CS-4.25d had several inclined shear cracks within the regions reinforced with the shear stirrups

as well as horizontal splitting cracks located above the stirrups. The formation of the horizontal splitting cracks near the columns is assumed to have caused the slight gradual drops in load capacity. Lastly, these inclined and splitting cracks created the failure surfaces.

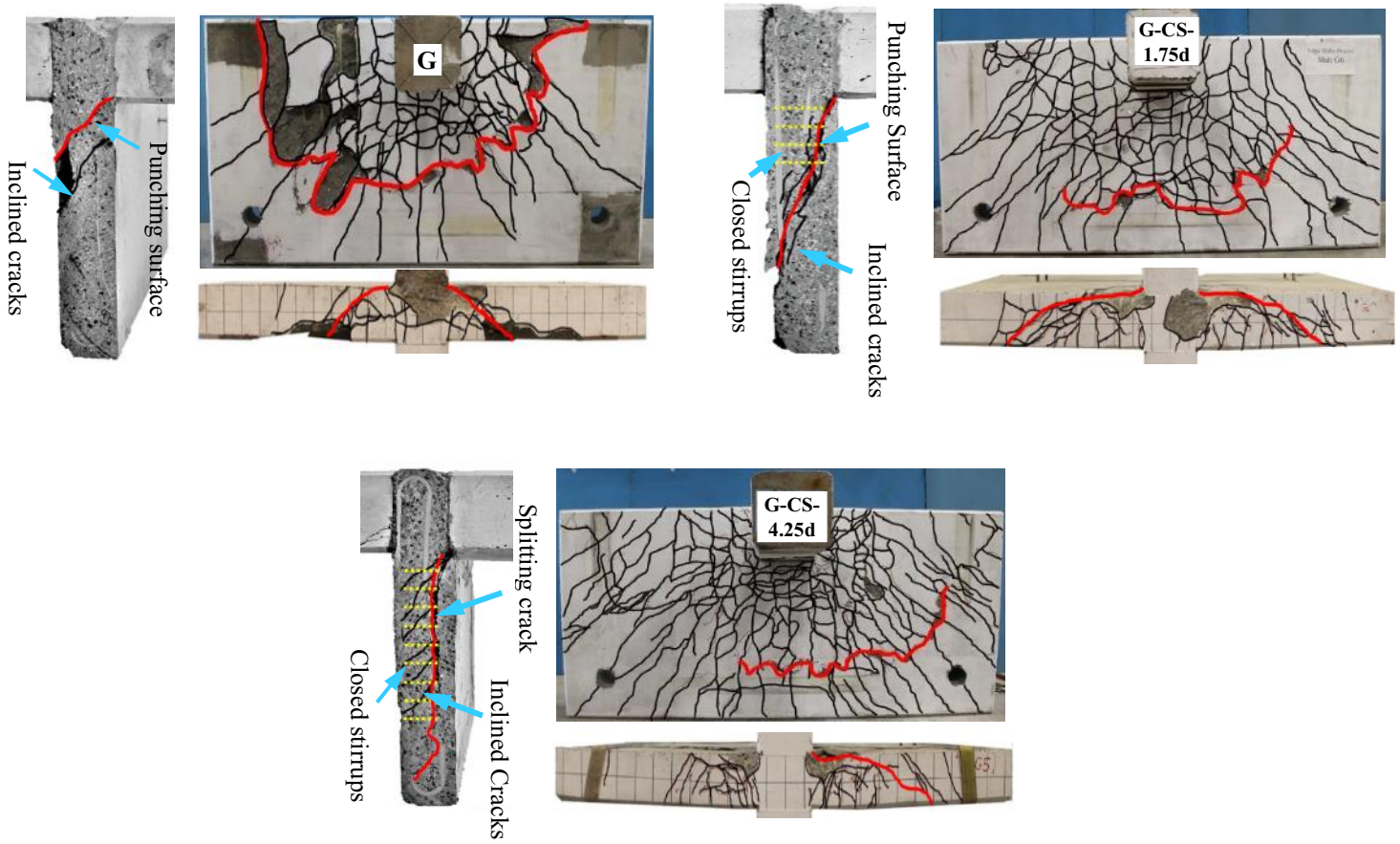

Figure 6.4 – Final punching-shear failure surface (in bold) on slab tension side and free edge and saw-cut section

6.4.2. Ultimate Capacity and Load–Deflection Characteristics

In general, the presence of GFRP shear stirrups inside the punching-shear zone significantly improved slab behavior and the punching mechanism. The strength and deformation capacity of the shear-reinforced slabs were, however, strongly influenced by the characteristics of the shear reinforcing system (i.e., extension, amount, type, etc.). Figure 6.5 plots the applied vertical load versus the deflection relationships at 80 mm from the column face. In general, the initial uncracked stiffness for all connections was similar, with or without shear reinforcement. The slabs with shear reinforcement, however, exhibited slightly higher post-cracking stiffness than

their counterpart without shear reinforcement. Control connection G and connection G-CS-1.75d, which had limited stirrups around the column, produced similar bilinear load–deflection responses until punching failure occurred. These two connections failed at ultimate loads of 314 and 370 kN and at 21 and 28 mm, respectively. Compared to connection G, connection G-CS-1.75d had failure load and deflection that were 18% and 34% higher, respectively. Connection G-CS-4.25d, with shear reinforcement extending 4.25d, experienced gradual failure with considerable post-peak deformations. The GFRP stirrups offered sufficient resistance and confinement to control the development of large shear cracks and effectively distributed the shearing forces around the punching-shear zone. The more significant increase in deformability in connection G-CS-4.25d could be attributed to the flexure mechanism due to the mobilization of the shear stirrups before punching-shear failure occurred. Connection G-CS-4.25d failed at an ultimate load of 444 kN, with a corresponding ultimate deflection of 36 mm. The resulting ultimate load and maximum deformation of G-CS-4.25d at failure were 1.41 and 1.8 times, respectively, that of connection G. This confirms the effectiveness of closed stirrups in achieving substantial deformations before slab collapse. Table 6.3 shows a summary of the test results for all connections. These results indicate the effect of the GFRP shear stirrups in increasing the punching-shear strength and the deformation capacity of the tested connections, even with the limited stirrup extension around the column. Moreover, increasing the stirrup extension around the column from 1.75d to 4.25d increased the vertical-shear force by 20%.

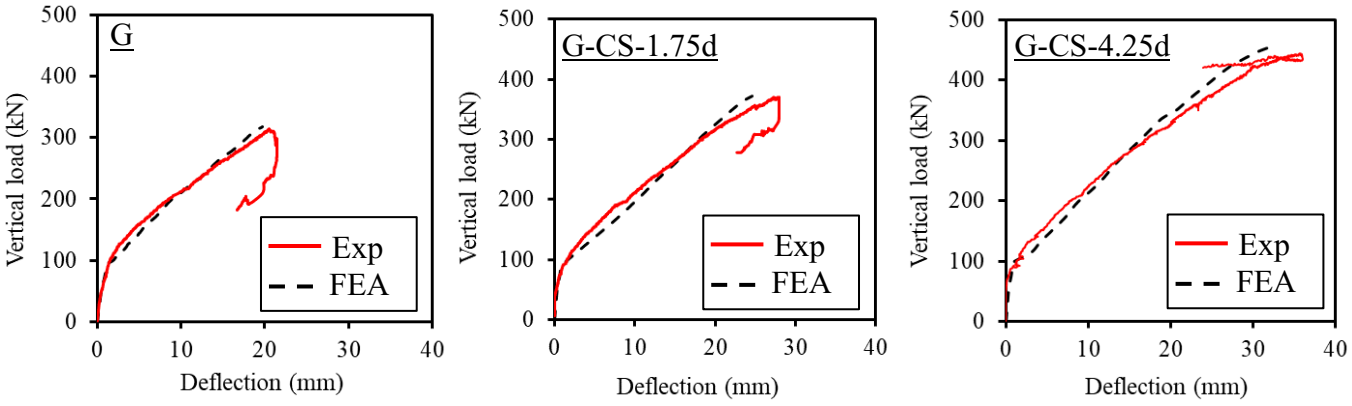

Figure 6.5 – Comparison between FEA and test results in terms of vertical-load deflection

Table 6.3 – Summary of the test and FEA results

Slab	Ultimate Load			M_u/V_u, (m)	Δ_{vu}, (mm)	$\Delta_{FE.}$, (mm)	Strains at Ultimate Load (με)						Average Stirrup Strain (με)		Maximum Stirrup Strain (με)	
	V_u, (kN)	$V_{FE.}$, (kN)	M_u, (kN.m)				Concrete, (με)		Flexural reinforcement		FRP stirrups @ 0.25 d					
							Exp.	FE.	Exp. [a]	FE.	Exp. [a]	FE.	⊥ [a]	// [a]	⊥ [a]	// [a]
G	314	318	98	0.31	20.55	19.72	784	820	6432	6708	-----	-----	-----	-----	-----	-----
G-CS-1.75d	370	372	115	0.31	28.08	24.2	979	930	8661	8610	2579	2589	3215	2519	3918	3402
G-CS-4.25d	444	456	133	0.30	35.82	32.5	2444	2430	13226	11845	5789	5622	5417	5193	6412	5899

[a] Position perpendicular (⊥) or parallel (//) to the free edge

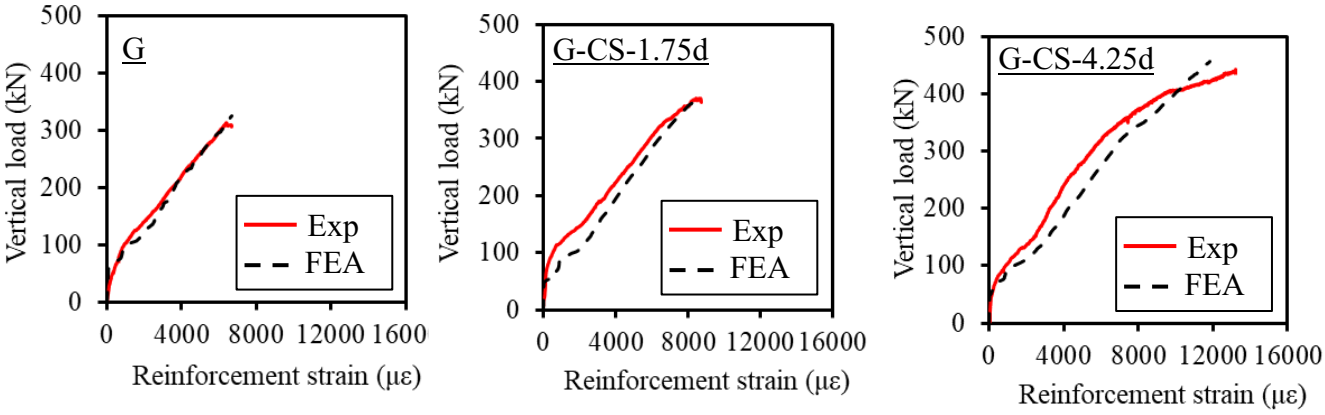

(a) Flexural reinforcement strains

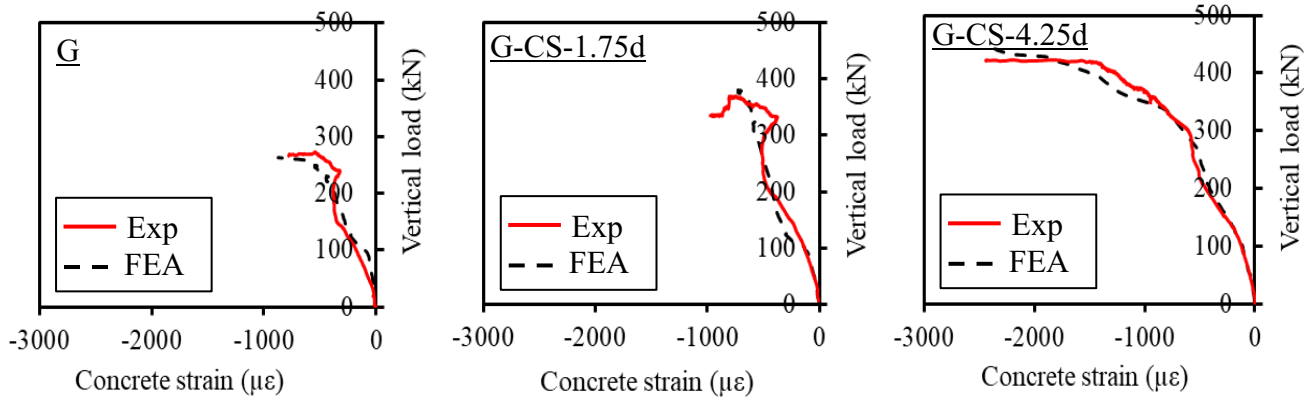

(b) Concrete strains

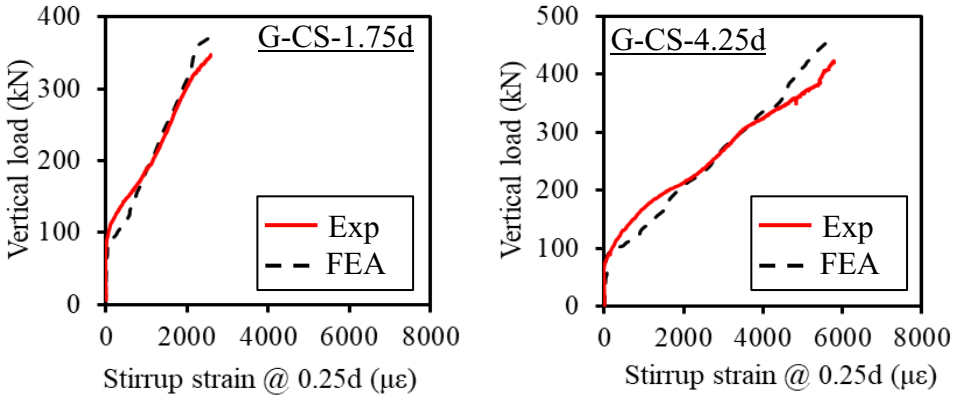

(c) Stirrup strains

Figure 6.6 – Comparison between FEA and test results in terms of vertical-load reinforcement bars, concrete, and stirrup strains perpendicular to the free edge

6.4.3. Flexural Reinforcement and Concrete Strains

Figure 6.6 plots the applied vertical load versus the flexural tension reinforcement and concrete strains for all the tested connections. The flexural-reinforcement strains were measured at 75 mm from the column face perpendicular to the free edge, whereas the concrete strains were recorded at the column face. Table 3 reports the maximum reinforcement and concrete strains. Connection G, without shear reinforcement, had lower tensile strain than its counterparts with GFRP shear stirrups. The maximum recorded strain in flexural bars was 6430 με, which represents 35% of the ultimate tensile strength. Moreover, the maximum concrete strains around the column vicinity were low and below the concrete crushing strain of 3500 and 3000 με, as per CAN/CSA S806 (2012) and ACI 440.1R (2015), respectively. Connections G-CS-1.75d and G-CS-4.25d, with shear reinforcement, exhibited higher strains in the GFRP flexural bars and higher concrete strains values than control connection G at ultimate. The GFRP stirrups offered sufficient resistance and confinement to control the development of large shear cracks and effectively distributed the shearing forces in the punching-shear zone, which mobilized the flexural reinforcement to achieve higher strains. This observation coincides with past findings for interior GFRP-reinforced slab–column connections with FRP stirrups (Hassan et al. 2014a). The maximum reinforcement strains were 8700 and 13200 με, respectively, representing 47% and 71%, of the ultimate tensile strength, respectively. The maximum recorded concrete strains were 979 and 2444 με (< 3000 or 3500) for G-CS-1.75d and G-CS-4.25d, respectively. No signs of concrete crushing in the compression zone for connection G-CS-1.75d, where the mode of failure was triggered by brittle punching-shear failure occurring outside the shear-reinforced zone. In contrast, for connection G-CS-4.25d, the achieved higher concrete strains indicated the concrete crushing at the column vicinity on the compression side of the slabs which evidenced the occurrence of the mixed flexure-punching shear failure.

6.4.4. Shear-Reinforcement Strains

Figure 6.6 shows the stirrup strain in the vertical portion of the FRP stirrup at 0.25d from the column face, while Fig. 6.7 plots the applied vertical load versus the measured average strains located between 0.25d to 1.25d from the column face in both orthogonal directions. As shown in Figs. 6.6 and 6.7, the contribution of the GFRP stirrups to the punching-shear strength was insignificant before cracking, however, the stirrup contribution began to appear after the progression of shear cracks. Thereafter, the stirrups transferred most of the forces across these

shear cracks and controlled their further widening. In addition, the average strains at the mid-height of the vertical portions of the FRP stirrups in both directions were 2867 and 5305 μs for connections G-CS-1.75d and G-CS-4.25d, respectively. These values are close to the strain limits of 4000 or 5000 μs specified in ACI 440.1R (2015) and CAN/CSA S806 (2012) for shear design of FRP stirrups. Thus, the FRP shear reinforcement might be designed with a strain value of 4000 or 5000 μs, as recommended in ACI 440.1R (2015) and CAN/CSA S806 (2012). Table 6.3 lists the maximum and average recorded strains in the FRP stirrups in both directions. Figure 6.8 depicts the vertical-strain distributions in the GFRP stirrups at 95% of the ultimate load along both orthogonal directions. The maximum measured strains were monitored up to a distance of 0.25d to 1.25d from the column faces without any apparent signs of tensile rupture in the vertical or bent portions of the stirrups. The FRP shear stirrups between 1.75d and 2.25d achieved relatively high strains at 95% of the ultimate load. This implies that the FRP stirrups were still active up to 2.25d. In addition, limiting the extension of the FRP stirrups in connection G-CS-1.75d beyond a distance of 1.75d exhibited limited deformation capacity. Further research, however, is needed to determine the corresponding distance for FRP stirrups.

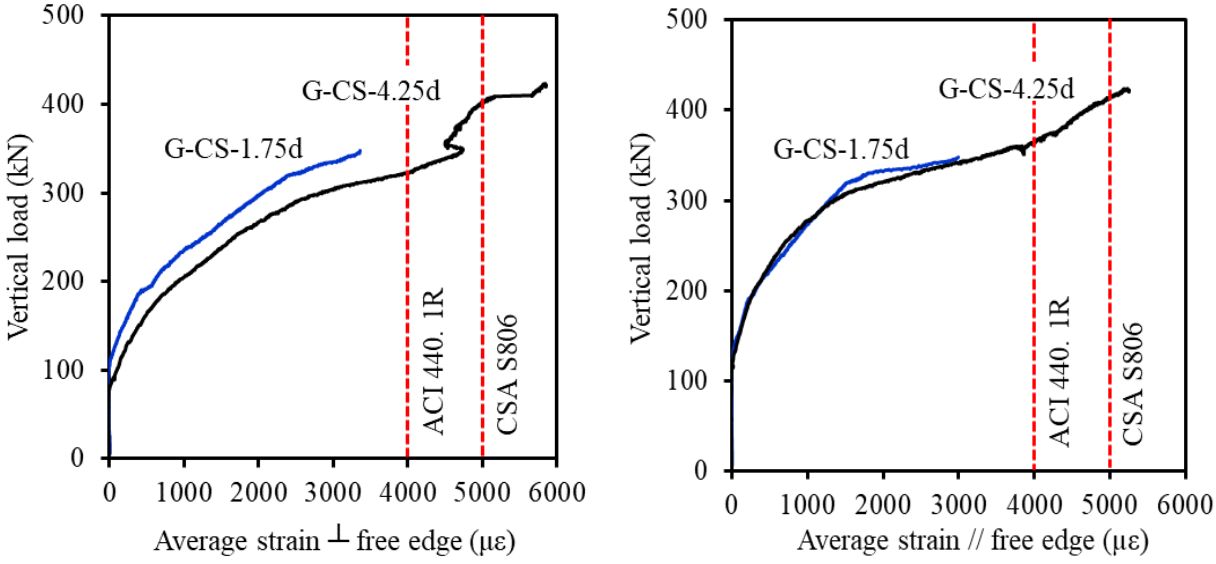

(a) Perpendicular direction to the free edge

(b) Parallel direction to the free edge

Figure 6.7 – Average stirrup strain in vertical legs from 0.25d to 1.25d

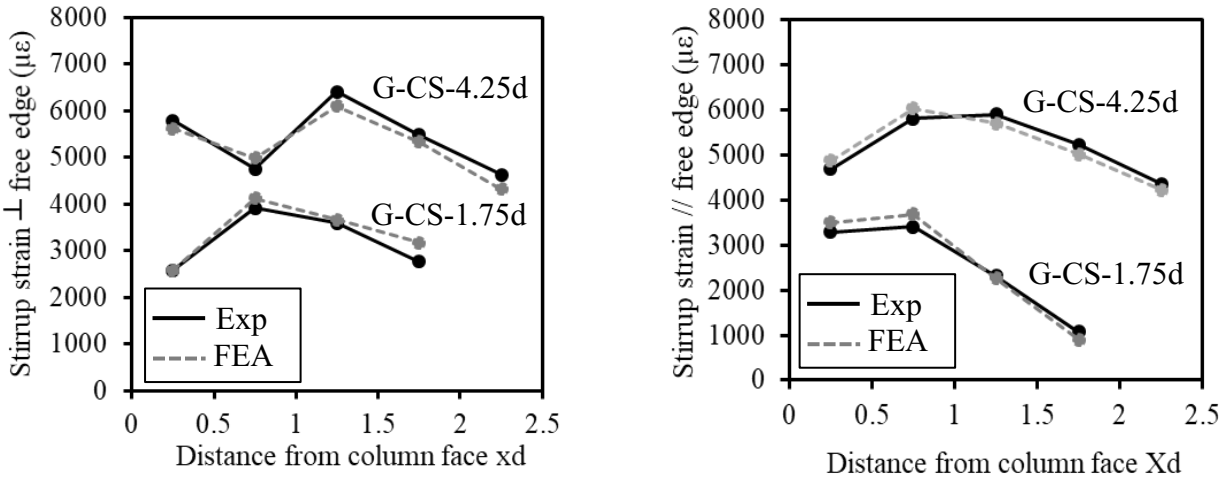

(a) Perpendicular direction to the free edge

(b) Parallel direction to the free edge

Figure 6.8 – Strain profile of the vertical legs of the stirrups for slabs with shear reinforcement

6.5. Finite-Element Simulations

The FEA was carried out using a finite-element software package: ANSYS (ANSYS User's Manual 2018). An FEA simulation was developed to investigate the punching-shear response and strength of connections tested. The models were validated with the authors' experimental data presented herein, and then an extensive parametric study was conducted to investigate the critical parameters influencing the shear capacity of such connections. The following section describes the element types used to model the different materials; constitutive models for concrete, steel, and FRP; meshing; and boundary conditions.

6.5.1 Material Properties

An eight-node 3-D solid element, SOLID 65, was used to model the concrete. This element is capable of considering cracking in three orthogonal directions: crushing, plastic deformation, and creep. To properly model the concrete, the considered model for concrete comprises linear and multi-linear isotropic material properties in addition to the concrete model defined in ANSYS (Wolanski 2004, Chansawat et al. 2006, Özcan et al. 2009).

The linear isotopic material properties include the elastic modulus of concrete and Poisson's ratio. The elastic modulus was calculated using Eq. (6.1) and Poisson's ratio was assumed to be 0.2 whereas the uniaxial cracking stress was computed with Eq. (6.2). Figure 6.9a plots the

multilinear isotropic stress–strain curve of the concrete with ignoring the descending branch, as recommended in past studies (Gorji 2009; Wolanski 2004; and Büyükkaragöz 2010). The first point on the curve represents the linear behavior of the concrete up to 30% of the ultimate compressive strength whereas the ascending branch of the curve was obtained using the Desayi model (Desayi and Krishnan 1964), as given by Eq. (6.3) and (6.4), up to the uniaxial crushing stress (f_c'). The ascending branch of the curve represents the stage after cracking where the uniaxial cracking stress of the concrete element is set to zero in the direction normal to the crack plane. The shear transfer coefficient for open cracks β_t and β_c for closed cracks quantifies the ratio of shear transferred across the cracks. The shear-transfer coefficient ranged from 0.0 to 1.0, with 0.0 representing a complete loss of shear transfer and 1.0 representing no loss of shear transfer (ANSYS, Release 19.1 2018). β_t and β_c have been used in past studies with different ranges (Kachlakev et al. 2001, Wolanski 2004, Mostofinejad et al. 2006, Qi Zhang 2004). The values of β_c and β_t were determined after preliminary analysis of the tested connections to capture the load–deflection behavior at cracking and ultimate load. In this study, β_t was assumed to be within 0.25 to 0.5, while β_c was assumed to be within 0.5 to 0.95. Figure 6.10 depicts the load–deflection response of connection G-CS-4.25d with different shear-transfer coefficients. As shown in Fig. 6.10, β_t of 0.3 and β_c of 0.8—indicating good agreement with the stiffness change and the ultimate loading of connection G-S-4.25d—were adapted in this work.

$$E_C = 4500\sqrt{f_c'} \tag{6.1}$$

$$f_r = 0.6\sqrt{f_c'} \tag{6.2}$$

$$\varepsilon_o = \frac{2\,f_c'}{E_c} \tag{6.3}$$

$$f = \frac{E_c\,\varepsilon}{1+\left(\varepsilon/\varepsilon_o\right)^2} \tag{6.4}$$

A 3-D spar element, LINK 180, was used to the model steel and FRP reinforcement. A LINK 180 element is a uniaxial tension–compression element with two nodes and three degrees of freedom translations in the nodal x, y, and z directions. This element is also capable of simulating nonlinearity and plastic deformations. A LINK180 element is defined by linear and bilinear isotropic material properties to model steel reinforcement. GFRP reinforcement, however, is defined by linear-elastic material properties. Poisson's ratios of 0.3 and 0.25 were

assumed for the steel and GFRP bars, respectively. The elastic modulus of the GFRP flexural bars and shear stirrups were determined experimentally, as listed in Table 6.2. Figure 6.9b provides the stress–strain relationships for the GFRP and steel bars used in this study (note that the steel bars were only used in the columns). A discrete model concept was used to model reinforced-concrete elements. Both the concrete and reinforcement mesh shared the same nodes (location and numbering). As the GFRP reinforcement did not experience any bar slippage or bond failure during the tests, a perfect bond was assumed in order to simulate the bond between the reinforcement and concrete. The steel loading plates were modeled as an eight-node solid element, SOLID45, with three degrees of freedom translations in the nodal x, y, and z directions at each node. This element is capable of plasticity, creep, swelling, stress stiffening, large deflection, and large strain. A SOLID45 element is defined by linear isotropic properties and ignoring strain hardening. The modulus of elasticity and Poisson's ratio used for the steel loading plates were 200 GPa and 0.3, respectively.

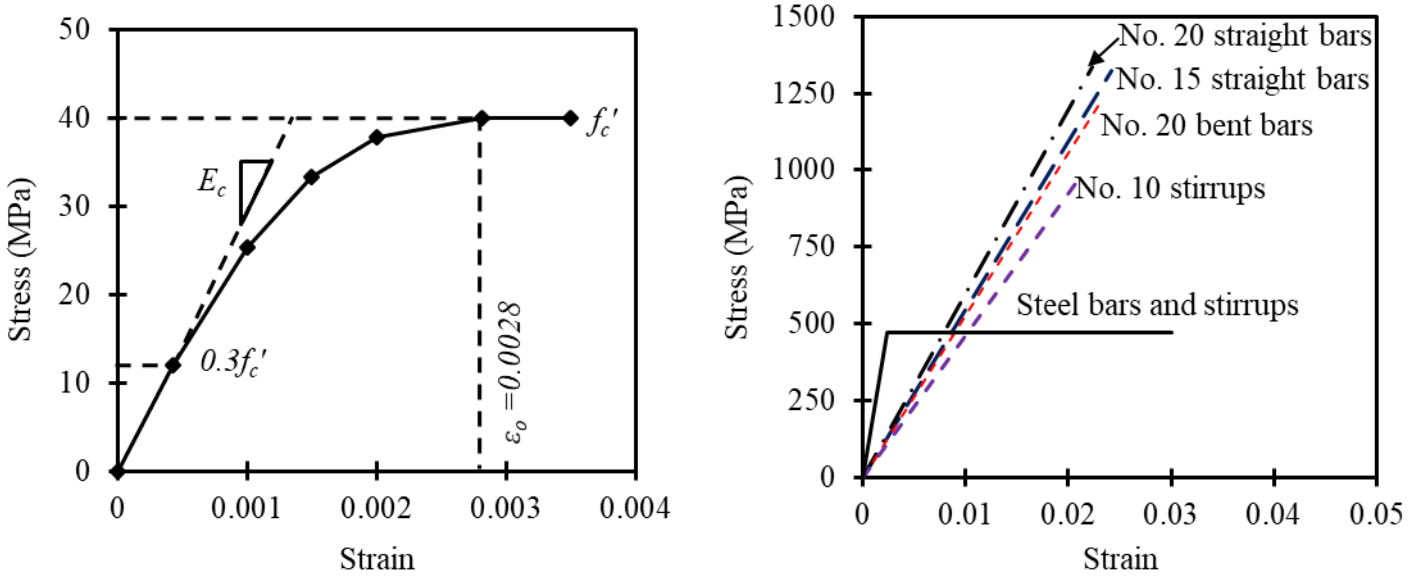

(a) concrete (b) GFRP and steel bars

Figure 6.9 – Stress–strain relationships used in the FE model

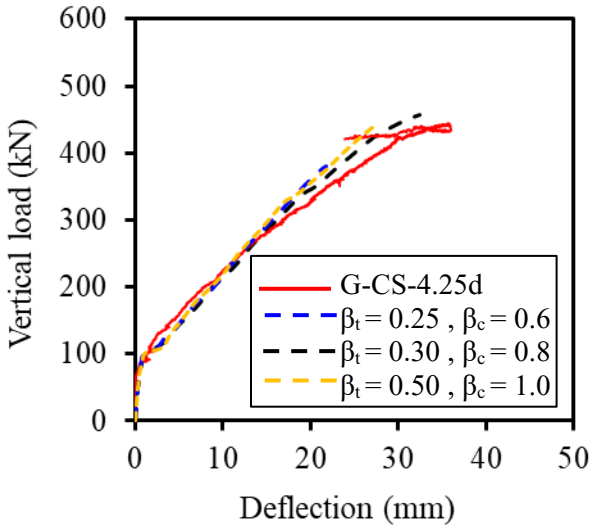

Fig. 6.10 – Load-deflection response with different shear transfer coefficients

6.5.2. Model Geometry, Loading and Boundary Conditions

Figure 6.11 gives a complete view of the overall mesh of the concrete, reinforcement configuration, loading plates, and boundary conditions of the FE model. Only the half model of the tested connection was simulated, taking advantage of slab symmetry about the axis of symmetry perpendicular to the free edge. The boundary conditions at this axis of symmetry were set to represent the effect of continuity. To simulate the test boundary conditions, the slab was restrained against vertical movement in the y direction along the three simply supported edges, while the slab corners were restrained against movement in the three directions. The loads were applied through the nodes over the top and side steel plates to simulate vertical shear (V) and unbalanced moment (Mun). Moreover, a convergence study was carried out on the simulated test connections with different mesh sizes in order to determine an appropriate mesh density. The selected mesh sizes ranged from 20 to 80 mm in increments of 10 mm. Figure 6.12 shows the results of the convergence study for G-CS-4.25d. Based on this study, a uniform mesh size of 40 mm was chosen for the concrete and reinforcement elements of the simulated connections. It should be mentioned that decreasing mesh size beyond 40 mm increased the computational time without any significant change in the numerical results.

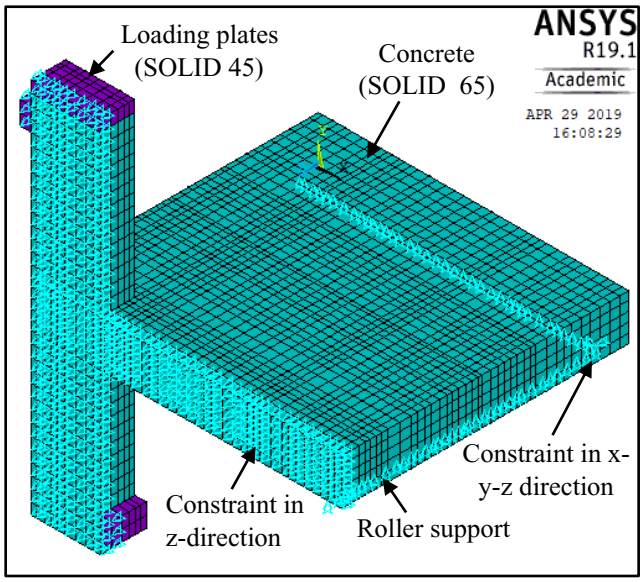

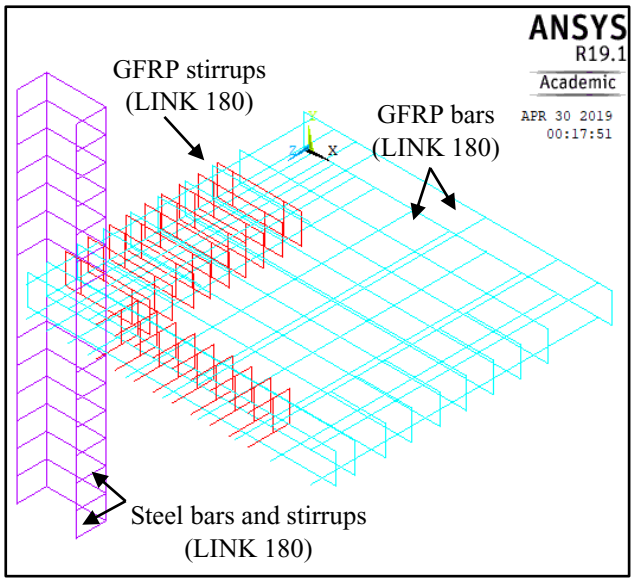

(a) Element types and boundary conditions

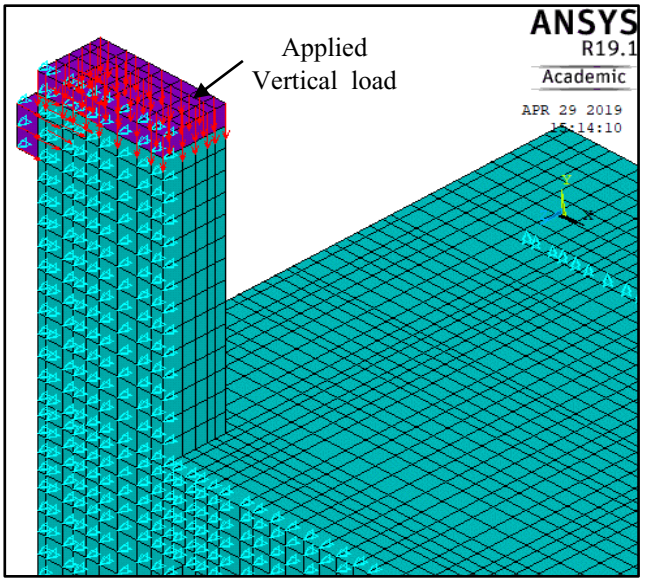

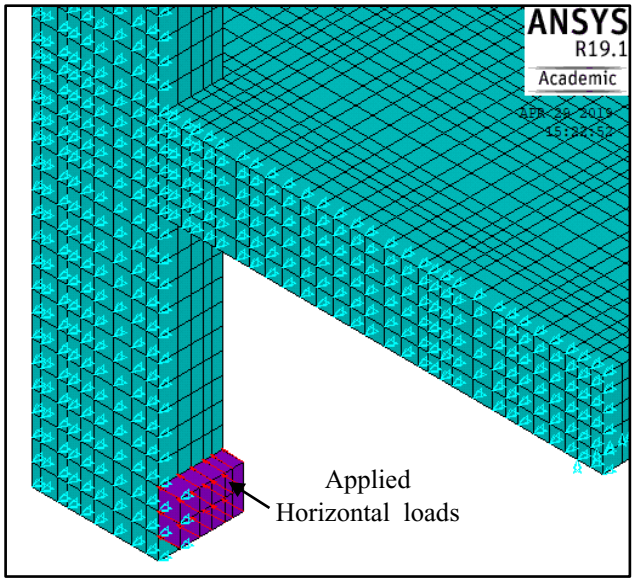

(b) Applied vertical and horizontal loads

Figure 6.11 – Geometry and reinforcement details of ANSYS model

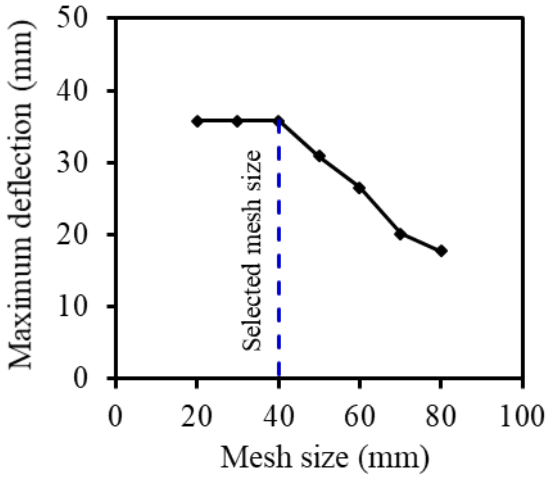

Fig. 6.12 – Mesh convergence study for G-CS-4.25d

6.5.3. Model Verification

The results of the finite-element analysis (FEA) were verified against the experimental results of the tested connections to examine the validity of the FE model in describing slab behavior. The comparison was performed with respect to the load–deflection responses; ultimate capacity; and ultimate strains in the concrete, flexural bars, and shear stirrups; strain distributions in the shear stirrups; and cracking propagation. Figure 6.5 depicts the experimental and predicted vertical load–deflection curves for the tested connections. The results obtained from the nonlinear FEA accurately describe the response of the tested slabs and the reduction in stiffness after cracking. The FEA of the slabs predicted a punching-shear capacity almost 1% higher than the test results, but the differences are not significant. As for the deflection values at ultimate load, the predicted values ($\Delta_{FE.}$) were mostly safer than those obtained experimentally ($\Delta_{exp.}$). Table 6.3 presents the numerical and experimental deflections at failure. The average numerical-to-experimental deflection at ultimate load was 91% with a standard deviation of 5%. This indicates a good prediction by the FEA. Figure 6.13 gives the deformed shapes at ultimate load for all slabs produced by FEA. Figure 6.6 plots the applied vertical load versus the maximum recorded strains in the concrete, flexural bars, and FRP stirrups located at 0.25d from the column face. As the figure shows, the analytically predicted and experimentally measured strains are in good agreement. The average numerical-to-experimental strains at ultimate load in the concrete, reinforcement, and stirrups were 99%, 98%, and 99% with standard deviations of 5%, 7%, and 2%, respectively. Figure 6.8 compares the measured and predicted vertical strain distributions

in the GFRP stirrups at 95% of the ultimate load along both orthogonal directions. The FEA properly reproduces the experimentally measured stains, as shown in Fig. 6.8. The average numerical-to-experimental vertical strains at 95% of the ultimate load in the FRP stirrups was 98%, with a standard deviation of 6%. Furthermore, cracking propagation in both the tests and FEA started on the tension side of the slabs. The cracking started at a vertical load of approximately 49 kN to 59 kN. Cracking initiated from the inner corners of the columns and developed toward the slab edges. Cracks on the compressive side of the slabs also developed at approximately 75% of the ultimate load. Cracking propagation yielded by the finite-element simulations was in good agreement with the experimentally observed cracks. Figure 6.14 shows the typical crack progression on the tension side of connection G-CS-1.75d at different loading stages, as determined by the FE modeling. In short, the model was able to predict, with reasonable accuracy, the load–deflection behavior; experimentally monitored strains in the flexural bars, concrete, and stirrups; strain distributions in the shear stirrups; and the cracking pattern.

6.6. Parametric Study

The calibrated FEA model presented herein was used to develop an extended parametric study, pertaining, in particular, to GFRP edge slabs with FRP stirrups. The influence of stirrup extension, diameter, and stirrup-to-stirrup spacing in the punching-shear zone were investigated.

6.6.1. Effect of Stirrup Extension from the Column Face

The effectiveness of shear reinforcement to increase the punching-shear capacity of a slab–column connection depends on the extension of the shear reinforcement around the column. Figure 6.15a depicts the vertical load–deflection relationships with different stirrup extensions, ranging from 1.75d to 4.25d in increments of 0.5d from the column face. As expected, the slab with the lowest stirrup extension around the column, 1.75d, experienced the lowest stiffness and punching capacity. Increasing the GFRP-stirrup extension from 1.75d to 4.25d significantly improved the punching-shear and deformation capacities, which is in good agreement with the experimental results. The GFRP stirrups provided sufficient resistance and confinement, which, in turn, controlled the progression of shear cracks and effectively distributed the shearing forces in the punching-shear zone. The stirrup extension, however, had less impact on the post-

cracking stiffness. According to the FEA predictions of the slabs, the vertical shear force increased significantly (18%) by increasing the stirrup extension from 1.75d to 4.25d. This is almost 2% lower than the experimental results of connections G-CS-1.75d and G-CS-4.25d.increasing the stirrup extension from 1.75d to 4.25d.

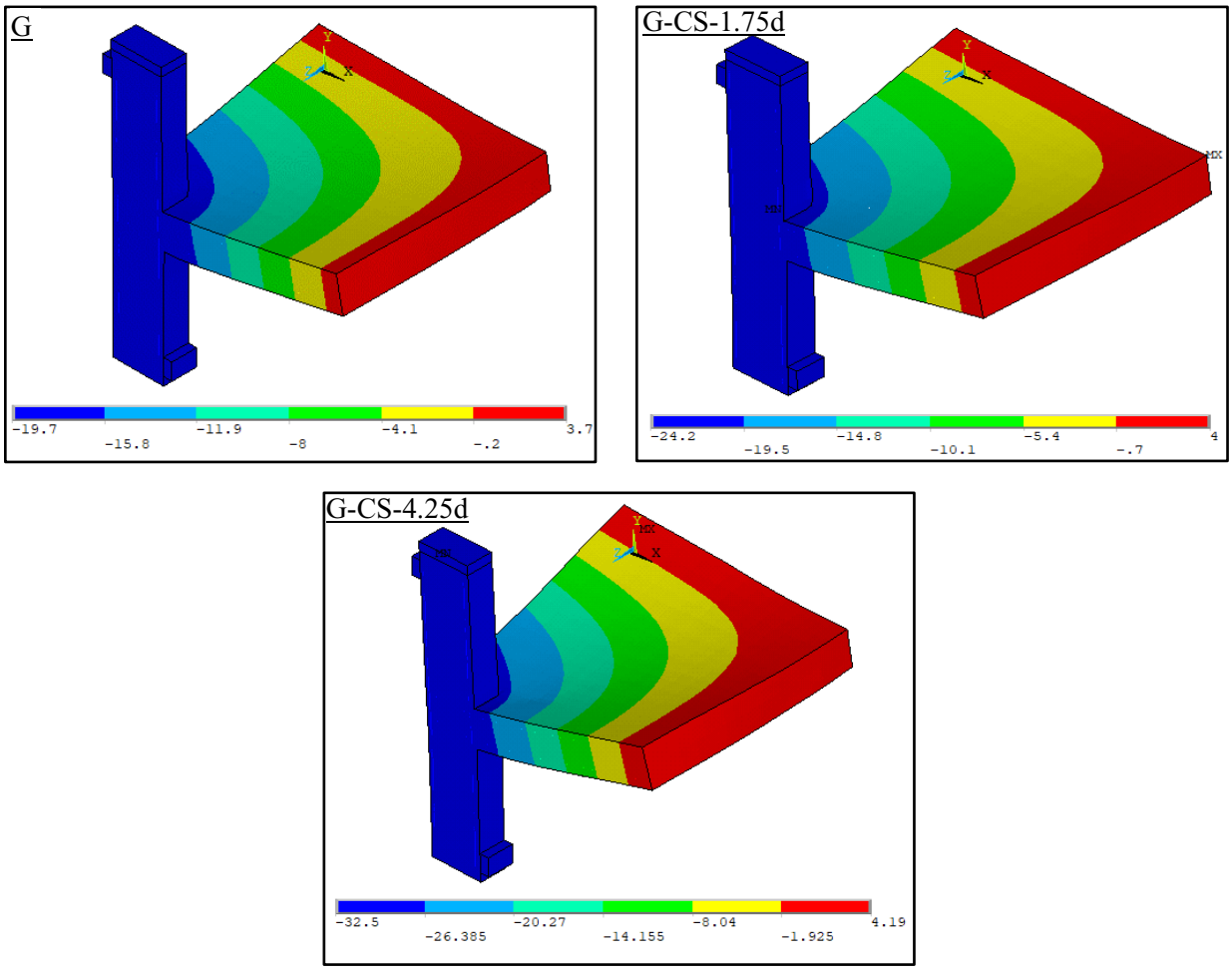

Figure 6.13 – Deformed shapes of simulated connections

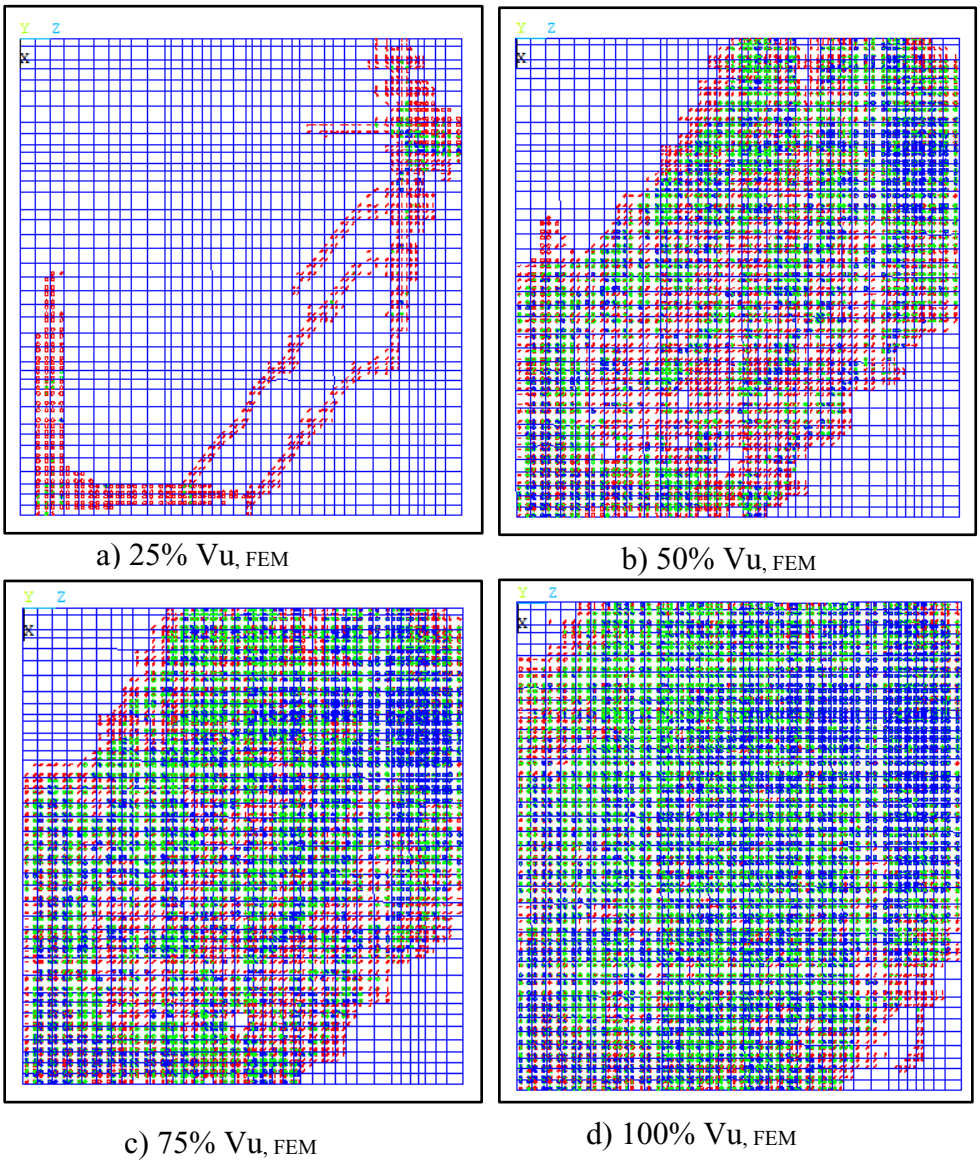

a) 25% Vu, FEM

b) 50% Vu, FEM

c) 75% Vu, FEM

d) 100% Vu, FEM

Figure 6.14 – Cracking progression at different loading levels for connection G-CS-1.75d

6.6.2. Effect of Stirrup Diameter

The numerical modeling of G-CS-1.75d was considered in order to address the effect of using different stirrup diameters (8, 10, and 12 mm). Figure 6.15 b depicts the effect of stirrup diameter on ultimate capacity. Increasing stirrup diameter has a direct contribution to the ultimate capacity, whereas the shear-reinforcement area at the critical section of the punching shear is increased. Increasing the stirrup diameter from 8 mm to 12 mm increased the punching capacity and deflection by approximately 23% and 14%, respectively. Note that the numerical results are

limited to stirrups with 12 mm diameter because the stirrup diameter is restricted by the slab's effective depth. From the practical point of view, the ratio between the bent radius and stirrup diameter should not less than 4 (ACI 440.1R 2015). Therefore, more experimental testing is needed to accurately investigate the effect of stirrup diameter with greater slab thicknesses.

6.6.3. Effect of Spacing Between Stirrups

The spacing between stirrups is one of the most significant parameters affecting the punching shear strength, slab deformation, failure mechanism, and development of the internal diagonal shear cracks. After the development of shear cracks, the shear stirrups transferred most of the forces across the developed shear cracks and delayed further widening, particularly when the stirrup spacing was reduced. This, in turn, increased the punching-shear and deformation capacities of the tested connections. Figure 6.15 c compares the numerical results at different stirrup spacings between 0.25d (40 mm) and 0.75d (120 mm). As seen in Fig. 6.13 c, the post-cracking stiffness, punching strength, and deformation capacity decreased when the spacing between stirrups was increased from 40 mm to 120 mm. According to the FEA results, the predicated ultimate strength and deformation capacity decreased by 18% and 13%, respectively. Based on the numerical results, the spacing between FRP stirrups should not exceed 0.5d, as per CAN/CSA A23.3 (2014) for steel-reinforced slabs. Further experimental testing on such connections reinforced with FRP is, however, needed.

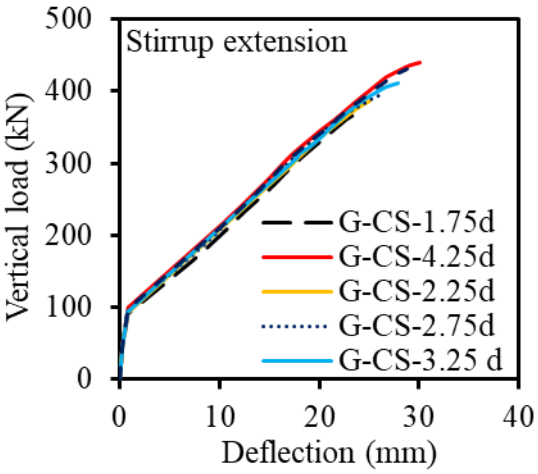

(a) Effect of GFRP-stirrup extension

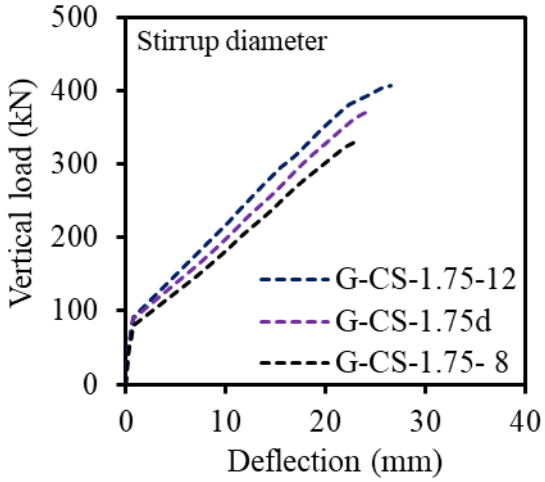

(b) Effect of GFRP-stirrup diameter

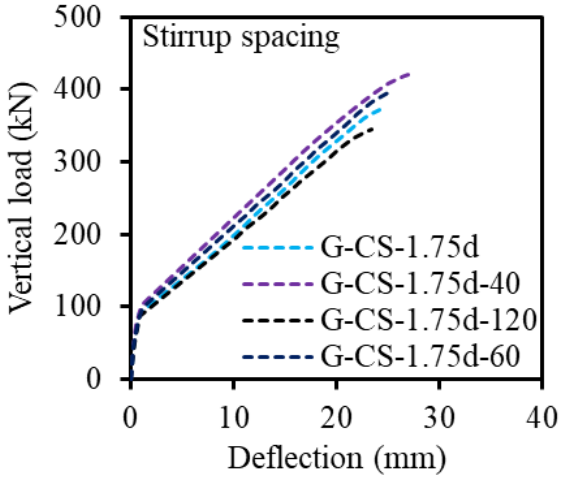

(c) Effect of GFRP stirrup spacing

Figure 6.15 – Parametric study vertical load–deflection results

6.7. Proposed Approach

So far, CAN/CSA S806 (2012) and ACI 440.1R (2015) lack provisions for estimating the ultimate capacity of two-way FRPRC slabs with FRP shear reinforcement, due to the distinct lack of experimental work. This section proposed a simple design approach to predict the punching-shear capacity of FRP-RC edge slab column connections reinforced with FRP shear stirrups. The CAN/CSA S806 concrete shear-strength equation for slabs without shear reinforcement was adapted by introducing a new parameter β to consider the contribution of FRP shear stirrups, based on the finite-element parametric study. The approach also modified

the equation for the stirrup-contribution equation in CAN/CSA A23.3 to consider the difference between the mechanical characteristics of FRP and steel reinforcement. The nominal punching-shear capacity, V_f, of two-way slabs due to moment transfer by eccentricity of shear is calculated with Eq. (6.5) according to ACI 318 (2014) and CAN/CSA A23.3 (2014).

$$V_f = v_u / \left(\frac{1}{b_{o;\,0.5d}\ d} + \frac{\gamma_v\, c}{J_c} e \right) \tag{6.5}$$

where v_u = ultimate shear stress at $0.5d$ from column face; $b_{o;0.5d}$ = critical shear perimeter at $0.5d$ from the column face; γ_v = fraction of unbalanced moment transferred by shear eccentricity; d = effective slab depth; c = distance from the centroid of the critical shear section to the face of shear critical section; e = eccentricity of the shear force from the centroid of the critical shear section; and J_c = polar moment of inertia of critical shear section.

The factored shear–stress resistance, computed as v_c+v_f, where v_c and v_f are the concrete and shear-reinforcement contributions to the shear strength inside the punching zone, respectively. Equation (6.6) is proposed to calculate the FRP-stirrup contribution (v_f). This equation is a modified version of the equation for steel stirrups in CAN/CSA A23.3 (2014), replacing f_y (yielding strength) with a specific stress (f_{fv}) at a limiting strain value (ε_{fv}) of 4000 με, as per ACI 440.1R (2015). This is close to the average strain of the FRP stirrups in both orthogonal directions based on the numerical (3920 με) and experimental results (4086 με). In addition, the average strain of the FRP stirrups in both orthogonal directions was 3718 με for the simulated GFRP-reinforced edge slab-column connections in the parametric study as listed in Table 6.4.

$$v_f = \frac{A_{fv}\, f_{fv}}{b_o\ s_{fv}} \tag{6.6 a}$$

$$f_{fv} = 0.004\, E_{fv} \tag{6.6 b}$$

where A_{fv} = cross-sectional area of the FRP shear reinforcement at a perimeter of $0.5d$ from the column face; d_b = stirrup diameter; r_b = bend radius of stirrup; f_{fv} = tensile strength in the straight portion of the FRP stirrups; $b_{o,0.5d}$ = perimeter of shear critical section at a distance of $0.5d$ from the column face; and s_{fv} = stirrup spacing measured perpendicular to $b_{o;0.5d}$.

The concrete shear strength inside the shear reinforced zone was quantified from the relation $v_{c\ inside} = v_{FE} - v_f$, where v_{FE} is the ultimate shear stress from FE results and v_f is the FRP-stirrup

contribution computed from Eq. 6.6 and listed in Table 6.4. $v_{c\ inside}$ was expressed as a ratio of the CAN/CSA S806 (2012) concrete shear-strength equation for two-way slabs without shear reinforcement ($v_{c\ CSA}$), as shown in Eq. (6.7). $v_{c\ CSA}$ was modified with a multiplier factor β to consider a reduction in concrete strength due to the contribution of FRP shear stirrups, as shown in Eq. (6.8). β was calculated based on the FE parametric study. A regression analysis was performed to quantify the best fit for $v_{c\ inside}$. This factor was found to be 0.64 (on average) using a stirrup strain of 4000 με (as per ACI440.1R 2015). It is worth mentioning that, a close value was achieved for β using the FE stirrup-strain results. The final form of $v_{c\ inside}$ is presented in Eq. (6.9).

$$v_{c\ CSA} = 0.056\ \lambda\ \emptyset_c \left(E_f\ \rho_f\ f_c'\right)^{\frac{1}{3}} \tag{6.7}$$

$$v_{c\ inside} = \beta \times 0.056\ \lambda\ \emptyset_c \left(E_f\ \rho_f\ f_c'\right)^{\frac{1}{3}} \tag{6.8}$$

$$v_{c\ inside} = 0.036\ \lambda\ \emptyset_c \left(E_f\ \rho_f\ f_c'\right)^{\frac{1}{3}} \tag{6.9}$$

where λ = concrete density factor (1 for normal weight); ϕ_c = concrete resistance factor (0.65); E_f = elastic modulus of the FRP bars; and ρ_f = FRP-reinforcement ratio.

As shown in Table 6.5, the proposed approach gave reasonable predications with respect to the experimental results as well as against the results reported in the literature for connections reinforced with different types of FRP shear reinforcement such as corrugated bars, shear studs, and grids (El-Gendy and El-Salakawy 2015; Mostafa and El-Salakawy 2018; Zaghloul 2007): an average V_{test}/V_{pred} of 1.08 ± 0.22 and a corresponding COV of 20.40%. Further research, however, is required to assess the accuracy of the proposed approach that takes into consideration a large number of different variables influencing the behavior and strength of such FRP-reinforced slab–column connections.

Table 6.4 – Results of finite element parametric study

Connection	Parameter	Ultimate Load			Average Stirrup Strains (με)		Using Average Stirrup Strains			Using ACI 440.1R Strain Limit (4000 με)		
		$V_{FE.}$, (kN)	$\Delta_{FE.}$, (mm)	v_{FE} (MPa)	⊥ [a]	// [a]	v_f (Eq.6) (MPa)	$v_{c\ inside} = v_{FE} - v_f$ (MPa)	$v_{c\ inside}/v_{c\ CSA}$	v_f (MPa)	$v_{c\ inside} = v_{FE} - v_f$ (MPa)	$v_{c\ inside}/v_{c\ CSA}$
G-CS-1.75d	Stirrup extension	372	24.2	2.83	3390	3174	1.31	1.52	0.77	1.60	1.24	0.62
G-CS-2.25d		387	25	2.95	3743	3402	1.43	1.52	0.76	1.60	1.35	0.68
G-CS-2.75d		397	26.5	3.02	3918	3687	1.52	1.51	0.76	1.60	1.43	0.72
G-CS-3.25d		411	28	3.13	4124	3965	1.61	1.52	0.76	1.60	1.53	0.77
G-CS-3.75d		430	28.92	3.27	4529	4300	1.76	1.51	0.76	1.60	1.68	0.84
G-CS-4.25d		439	31	3.34	4857	4756	1.92	1.42	0.72	1.60	1.75	0.88
G-CS-1.75d-8	Stirrup diameter	332	23.13	2.53	3125	2832	0.84	1.69	0.85	1.12	1.40	0.71
G-CS-1.75d-12		407	26.4	3.10	3809	3578	2.35	0.75	0.38	2.54	0.56	0.28
G-CS-1.75d-40	Stirrups spacing	420	27	3.20	3827	3583	2.36	0.83	0.42	2.55	0.64	0.32
G-CS-1.75d-60		400	25.6	3.05	3645	3412	1.88	1.17	0.59	2.13	0.92	0.46
G-CS-1.75d-120		344	23.5	2.62	3265	2875	0.82	1.80	0.91	1.06	1.56	0.78
Average					3839	3597			0.70			0.64

[a] Position perpendicular (⊥) or parallel (//) to the free edge; $v_{c\ CSA}$ = concrete contribution determined from CAN/CSA S806 (2012) (Eq.7); v_f = ultimate punching-stress provided by the FRP shear stirrups (Eq. 6)

Table 6.5 –Tested-to-predicted punching shear capacities using the simplified proposed equation

Reference	Slab	C_1 x C_2, (mm x mm)	t, (mm)	d, (mm)	ρ_l, (%)	RFT. Type	Shear RFT Type	M/V (m)	$V_{u\ test}$, (kN)	Proposed Simplified Equation		
										$V_{in,\ pred,}$ kN	$v_{in,\ pred,}$ [a] (MPa)	V_u/V_{pred}
This study	G-CS-1.75d	300 x 300	200	160	1.55	SG	SG stirrups	0.31	370	371	2.87	1.00
	G-CS-4.25d	300 x 300			1.55	SG	SG stirrups	0.30	444	381	2.90	1.16
Mostafa et al. (2018)	N-0.9-C8	300 x 300			0.85	SG	SG C. bars	0.40	286	204	1.82	1.40
	N-0.9-C6	300 x 300			0.85	SG	SG C. bars	0.40	253	183	1.64	1.38
	N-0.9-S8	300 x 300			0.85	SG	SG studs	0.40	294	324	2.90	0.91
	N-0.9-S6	300 x 300			0.85	SG	SG studs	0.40	298	272	2.43	1.09
El-Gendy et al. (2015)	RD-75-M	300 x 300			0.85	GRD	GRD studs	0.40	256	236	2.11	1.09
	RD-50M	300 x 300			0.85	GRD	GRD studs	0.40	273	295	2.64	0.92
Zaghloul (2007)	ZJEFCS	250 x 250	150	120	0.85	NEF	NEF studs	0.42	230	314	5.43	0.73
Average [c]												1.08
SD [c]												0.22
COV% [c]												20.40

C_1 = shorter side of the column; C_2 = longer side of the column; ρ_l is the average flexural tensile-reinforcement ratio; SG = sand-coated glass-fiber bars; GRD = ribbed glass-fiber bars; NEF= NEFMAC 2-D carbon-fiber grids, C. bars =corrugated bars.

6.8. Summary and Conclusions

This paper reported the test results of full-scale RC edge slab–column connections reinforced with GFRP bars and shear stirrups. Finite-element models were also created in this study. The simulation was verified against the experimental results presented herein and used to develop an extended parametric study to investigate the behavior and critical parameters influencing the shear strength of GFRP edge connections reinforced with shear stirrups. Based on the work presented in this paper, the following conclusions can be drawn:

- Using closed shear stirrups improved the punching behavior of GFRP-reinforced-concrete edge-slab–column connections. The crack widths were effectively reduced, and the cracks were more widely distributed compared to the connection without shear reinforcement, which failed in a brittle punching-shear mode.
- The connections reinforced with GFRP shear stirrups achieved higher strains in the flexural-reinforcement bars than their counterpart with no shear reinforcement. The GFRP stirrups offered sufficient resistance and confinement to control the development of large shear cracks and effectively distributed the shearing forces in the punching-shear zone, which mobilized the flexural bars to achieve higher strains.
- The FRP shear stirrups between 1.75d and 2.25d achieved relatively high strains at 95% of ultimate load, respectively, which implies that the FRP stirrups were still active up to 2.25d. Further investigation, however, is needed to determine the minimum extension limit for FRP stirrups.
- The FEA adequately predicted the experimental response of the tested GFRP-reinforced edge-slab–column connections. The numerical results were in good agreement compared to the experimental ones. The FE model can be an effective tool for providing insight into behavior and the various aspects affecting punching shear in edge connections.
- The proposed design approach gave good yet conservative predications for the punching-shear strength of GFRP-RC edge connections with different types of FRP shear reinforcement as stirrups, studs, and corrugated bars. The proposed approach showed an average V_{test}/V_{pred} of 1.08 ± 0.22 with a COV of 20.40%. This approach signals an innovation for using FRP shear stirrups in FRP-RC edge-slab–column connections. More investigations are, however, needed to refine this proposed approach.

6.9. Acknowledgements

The authors wish to express their sincere gratitude to the Canada Research Chair in Advanced Composite Materials for Civil Structures, the Natural Sciences and Engineering Research Council of Canada (NSERC), the Fonds de recherché du Québec en Nature et technologies (FRQ-NT) and technical staff of the structural and materials laboratory in the Department of Civil Engineering at the University of Sherbrooke.

CHAPTER 7
CONCLUSIONS AND RECOMMENDATIONS

7.1. Summary

The main objective of the current research was to examine the punching-shear strength and behavior of reinforced concrete GFRP-RC edge slab-column connections with and without GFRP stirrups shear reinforcement. Nine full-scale connections—one reinforced with steel bars, five reinforced with GFRP bars, and three reinforced with GFRP bars and stirrups as shear reinforcement, were presented. The test variables were chosen to examine the effect of GFRP stirrups type and extension, flexural reinforcement ratio and type, concrete strength, and moment-to-shear ratios. Strength, deformation, energy absorption and failure mode of the tested connections were investigated. Evaluation of the ultimate punching shear capacity using current FRP codes was introduced. This was followed by a finite element parametric study using ANSYS software to investigate the key parameters influencing the shear capacity of such connections with FRP stirrups. Finally, a simplified design approach for edge connections with FRP stirrups was also proposed based on the finite element parametric study. The proposed approach was evaluated against the experimental results for the tested connections and other specimens in the literature. based on the conducted experimental and analytical investigations, the following concluding remarks can be drawn as follows.

7.2. Conclusions

7.2.1. GFRP–RC Edge Slab-column Connections with GFRP Stirrups Shear Reinforcement

- Using either closed or spiral stirrups as shear reinforcement improved the punching behavior of FRPRC edge slab–column connections. The cracks were more widely distributed compared to the specimen without shear reinforcement, which failed in a brittle punching-shear mode.

- The specimens with FRP shear reinforcement extended 4.25d demonstrated a substantial increase in shear-strength increase over 38%, enhancement of deformation capacity of over 104%, and deformability and energy absorption of over 185%, and 194% (on average) were observed. This increase might be of interest because it gives significant warning before punching-shear failure occurs. As a result, these connections fail in mixed flexure–punching-shear failure.
- The FRP stirrups offered sufficient resistance and confinement to control the development of large shear cracks and effectively distributed the shearing forces around the punching-shear zone so that failure occurred inside or outside the shear-reinforced zone.
- In comparison to closed stirrups, spiral stirrups provided better performance as well as fast and easy installation during construction of the tested specimens for the same amounts of flexural and shear reinforcement. Specimen G-SS-4.25d, with spiral stirrups, showed an increase in the punching-shear strength, deformation capacity, and energy absorption of over 9%, 33%, and 36% compared to G-CS-4.25d, respectively. Both systems, however, could be used to effectively reduce the brittleness of the tested specimens.
- The results indicate that the shear-stress resistance of the concrete contribution decreased outside the shear-reinforced zone. For instance, specimen G-CS-1.75d failed outside the shear-reinforced zone under an ultimate shear-stress resistance of 1.21 MPa (0.18 ksi), which is 52% lower than the normalized shear-stress resistance of 2.56 MPa (0.37 ksi) for specimen G. Thus, it is reasonable to assume the concrete contribution to shear resistance outside the shear-reinforced zone be reduced by 50% as recommended in ACI 318 (2014) and CSA A23.3 (2014). Further experimental tests are needed, however, to examine the effect of FRP shear reinforcement with different extensions around the column to quantify this effect on the concrete contribution to the shear resistance.
- FRP shear stirrups between 1.75d and 2.25d achieved relatively high strains of 4129 and 3748 μs (on average in both directions) at 95% of ultimate load, which implies that the FRP stirrups were still active up to 2.25d, respectively. In addition, limiting the extension of the FRP stirrups beyond 1.75d showed only limited deformation capacity and brittle punching failure occurred. Therefore, more experimental work is needed to determine a minimum extension limit of FRP stirrups for FRP-reinforced slab–column connections to overcome brittle punching failure.

- On the basis of the test results, FRP shear reinforcement can be designed with a strain value of 4000 or 5000 microstrains, as recommended in ACI 440.1R (2015) or CSA S806 (2012), respectively.
- The simplified approach proposed to predict the ultimate shear capacity of FRP-reinforced edge slab–column connections with FRP shear reinforcement as an extension to those in CSA S806 (2012) gave better predications with respect to the experimental test results as well as the available results in the literature.
- The proposed ACI 440.1R (2015) simplified approach was consistently very conservative for test specimens with FRP shear stirrups reported in this study and other data available in the literature. The reason for this is the high level of conservatism of the concrete-contribution (v_c) in ACI 440.1R (2015) (Eq. 6).
- The proposed design provisions provide a step forward for engineers in designing two-way FRPRC slabs with FRP stirrups. Nevertheless, more experimental results under eccentric punching shear for interior and edge slab–column connections are urgently required.
- The FEA adequately predicted the experimental response of the tested GFRP-reinforced edge-slab–column connections. The numerical results were in good agreement compared to the experimental ones. The FE model can be an effective tool for providing insight into behavior and the various aspects affecting punching shear in edge connections.
- The proposed design approach based on the results on the FEA analysis gave good yet conservative predications for the punching-shear strength of GFRP-RC edge connections with different types of FRP shear reinforcement as stirrups, studs, and corrugated bars. The proposed approach showed an average V_{test}/V_{pred} of 1.08 ± 0.22 with a COV of 20.40%. This approach signals an innovation for using FRP shear stirrups in FRP-RC edge-slab–column connections. More investigations are, however, needed to refine this proposed approach.

7.2.2. GFRP–RC Edge Slab-Column Connections without Shear Reinforcement

- The tested connections without shear reinforcement experienced punching-shear failure as the final mode without any signs of concrete crushing. This failure was characterized by an

immediate drop in the ultimate load, accompanied by the appearance of a clear crack defining the failure surface.

- Using HSC significantly enhanced the punching-shear capacity, deflection, and initial stiffness of the GFRP-reinforced connections. The punching-shear capacity, deflection, and initial stiffness of the HSC connections were 18.5%, 15.5%, and 29% (on average) higher than that of the GFRP-reinforced connections constructed with NSC, respectively. The post-cracking stiffness, however, was similar to the NSC GFRP-reinforced connections.
- Increasing the *M/V* ratio from 0.3 m to 0.6 m for the NSC and HSC connections resulted in slightly steeper shear cracks. The inclined cracks at the free edge ran in opposite direction to the punching-shear force as a result of the reversed shear stresses caused by highly unbalanced moment.
- Increasing the *M/V* ratio transferred between the slabs and columns produced significant shear stresses that increased the likelihood of brittle failure and resulted in a reduction in the vertical-load capacity by approximately 31% and 30% for the NSC and HSC connections, respectively.
- The JSCE-97 (JSCE 1997) and CSA S806-12 (CSA 2012) reasonably predicted the punching capacities of the tested connections with average of $V_{u\ test}/V_{\mathrm{JSCE}} = 1.28 \pm 0.13$ and $V_{u\ test}/V_{\mathrm{CSA}} = 1.27 \pm 0.04$, respectively. The ACI 440.1R-15 (ACI 2015) equation, however, underestimated, giving average of $V_{u\ test}/V_{ACI} = 2.13 \pm 0.09$. In contrast, the Hassan et al. equation (2017) overestimated the capacity of the tested connections with an average of $V_{u\ test}/V_{Hassan} = 0.88 \pm 0.06$.
- Using the actual concrete strengths of 85 and 86 MPa for the HSC connections (G-H-0.3 and G-H-0.6) in the CSA S806-12 (CSA 2012) equation better estimated the ultimate capacity ($V_{u\ test}/V_{\mathrm{CSA}} = 1.19 \pm 0.08$) than using the 60 MPa concrete-strength limit as per CSA S806-12 (CSA 2012). Further research, however, is needed with a wide range of concrete strengths.

7.3. Recommendations for Future Work

Results of the current study represent a promising step toward implementing GFRP bars and shear stirrups shear reinforcement in edge slab column connections. Based on the findings of the current study, additional researches are recommended to cover the following points:

1. Elaborating more experimental works is highly needed to generate data with emphasis on the following points;
   - Different shapes of shear reinforcement including, different layout and arrangement in FRP edge connections with high flexural reinforcement ratios;
   - Different anchorage types in flexural bars normal to the free edge;
   - Effect of column aspect ratio and shear perimeter-to- slab depth ratio;
   - Effect of openings in the column vicinity;
   - Effect of different slab thicknesses;
   - Edge connections with different column sizes;
   - Existence of marginal beam at the free edge of the connection; and
   - Effect of different sizes of drop panels.
2. Development an alternative design equation for the current punching shear equations in ACI 440.1R-15 and CSA S806-12 design codes including the most affecting paraments.
3. Development of mechanical model that can reasonably predict the punching shear capacity of FRP edge connections with shear reinforcement based on the interaction between shear and unbalanced moment.
4. Study the effect of reversed cyclic unbalanced moment on the behavior edge slab column connections reinforced with and without FRP shear reinforcement.
5. One further step is to study the punching shear strength and performance of GFRP corner slab-column connections.

7.4. Résumé

L’objectif principal du présent projet de recherche était d’examiner la résistance au poinçonnement et le comportement des jonctions dalle-poteau en béton armé de PRFV avec et sans armatures de cisaillement constituées d’étriers en PRFV. Neuf (9) jonctions pleine grandeur

(une jonction avec des barres d'armature en acier à des fins de comparaison, cinq jonctions avec uniquement des barres d'armature en flexion en PRFV et trois jonctions avec des barres et des étriers en PRFV comme armatures de cisaillement) ont été étudiées. Les paramètres d'essais ont été choisis pour examiner l'effet du type d'étrier en PRFV et leur prolongement, l'effet du type et du taux d'armature en flexion, l'effet de la résistance en compression du béton, et l'effet des rapports moment/cisaillement. La résistance, la déformation, l'absorption d'énergie et les modes de rupture des jonctions testées ont été étudiés. L'évaluation de la résistance ultime de poinçonnement à l'aide des codes de conception actuels sur les PRF a été présentée. Ensuite, une étude paramétrique par éléments finis à l'aide du logiciel ANSYS a été réalisée pour étudier les principaux paramètres influençant la résistance au cisaillement de telles jonctions. Enfin, deux méthodes simplifiées de calcul pour les jonctions de rive sans et avec étriers en PRF ont également été proposées sur la base de l'étude paramétrique par éléments finis. Les méthodes proposées ont été évaluées à l'aide des résultats expérimentaux obtenus des essais sur les jonctions et d'autres spécimens dans la littérature. Sur la base des études expérimentales et analytiques menées, les conclusions finales suivantes peuvent être tirées ci-après.

7.5. Conclusions

7.5.1. Jonctions PRV–RC Bord Dalle-Colonne avec Étriers PRV Renfort de Cisaillement

- L'utilisation d'étriers fermés ou à spirale comme renfort de cisaillement a amélioré le comportement de poinçonnage des raccords de la dalle et de la colonne du bord du FRPRC. Les fissures étaient plus largement réparties que l'éprouvette sans renfort de cisaillement, qui s'est rompue en mode de cisaillement fragile.
- Les éprouvettes avec renfort en cisaillement FRP prolongé 4.25d ont montré une augmentation substantielle de la résistance au cisaillement de plus de 38%, une augmentation de la capacité de déformation de plus de 104%, et une déformabilité et une absorption d'énergie de plus de 185%, et 194% (en moyenne) ont été observés. Cette augmentation pourrait être intéressante parce qu'elle donne un avertissement important

avant qu'une rupture de poinçonnage-cisaillement ne se produise. Par conséquent, ces raccords se rompent en cas de rupture mixte flexion-poinçonnage-cisaillement.

- Les étriers FRP offraient une résistance et un confinement suffisants pour contrôler le développement de grandes fissures de cisaillement et répartissaient efficacement les forces de cisaillement autour de la zone de cisaillement de façon à ce que la rupture se produise à l'intérieur ou à l'extérieur de la zone de cisaillementzone renforcée.
- Par rapport aux étriers fermés, les étriers hélicoïdaux ont fourni de meilleures performances ainsi qu'une installation rapide et facile pendant la construction des éprouvettes testées pour les mêmes quantités de renfort de flexion et de cisaillement. L'éprouvette G-SS-4.25d, avec étriers hélicoïdaux, a montré une augmentation de la résistance au cisaillement, de la capacité de déformation et de l'absorption d'énergie de plus de 9 %, 33 % et 36 % par rapport à G-CS-4.25d, respectivement. Cependant, les deux systèmes pourraient être utilisés pour réduire efficacement la fragilité des éprouvettes testées.
- Les résultats indiquent que la résistance au cisaillement de l'apport de béton a diminué en dehors de la zone de cisaillement. Par exemple, l'éprouvette G-CS-1.75d s'est rompue à l'extérieur de la zone renforcée de cisaillement sous une résistance ultime à la contrainte de cisaillement de 1.21 MPa (0.18 ksi), ce qui est inférieur de 52 % à la résistance normalisée à la contrainte de cisaillement de 2.56 MPa (0.37 ksi) pour l'éprouvette G. Ainsi, il est raisonnable de supposer que la contribution du béton à la résistance au cisaillement à l'extérieur de la zone renforcée par cisaillement soit réduite de 50 %, comme le recommandent l'ACI 318 (2014) et la norme CSA A23.3 (2014). D'autres essais expérimentaux sont cependant nécessaires pour examiner l'effet du renforcement en cisaillement FRP avec différentes extensions autour de la colonne afin de quantifier cet effet sur la contribution du béton à la résistance au cisaillement.
- Les étriers de cisaillement FRP entre 1.75d et 2.25d ont obtenu des déformations relativement élevées de 4129 et 3748 μs (en moyenne dans les deux sens) à 95% de la charge ultime, ce qui signifie que les étriers FRP étaient encore actifs jusqu'à 2.25d, respectivement. De plus, le fait de limiter le prolongement des étriers en PRF au-delà de 1.75d n'a montré qu'une capacité de déformation limitée et une rupture de poinçonnage fragile s'est produite. Par conséquent, des travaux plus expérimentaux sont nécessaires pour déterminer une limite

d'extension minimale des étriers en PRF pour les raccordements PRF renforcés de la dalle et de la colonne afin de surmonter la rupture de poinçonnage fragile.

- Sur la base des résultats des essais, le renforcement en cisaillement FRP peut être conçu avec une valeur de déformation de 4000 ou 5000 microstrains, comme le recommande l'ACI 440.1R (2015) ou la norme CSA S806 (2012), respectivement.
- L'approche simplifiée proposée pour prévoir la capacité de cisaillement ultime des raccords de dalle-colonne renforcés en PRF avec renfort de cisaillement en PRF comme prolongement de ceux de la norme CSA S806 (2012) a donné de meilleures prédications en ce qui concerne les résultats des tests expérimentaux ainsi que les résultats disponibles dans la littérature.
- L'approche simplifiée proposée dans l'ACI 440.1R (2015) était toujours très prudente pour les spécimens d'essai avec étriers de cisaillement en PRF signalés dans cette étude et d'autres données disponibles dans la littérature. La raison en est le haut niveau de conservatisme de la contribution concrète (v_c) dans l'ACI 440.1R (2015) (Eq. 6).
- Les dispositions de conception proposées représentent un pas en avant pour les ingénieurs dans la conception de plaques FRPRC bidirectionnelles avec étriers FRP. Néanmoins, des résultats plus expérimentaux sous cisaillement excentrique de poinçonnage pour les raccordements intérieurs et de bord dalle-colonne sont urgents.
- La FEA a adéquatement prédit la réponse expérimentale des raccords GFRP-dalle-bord-colonne renforcés testés. Les résultats numériques concordent bien avec les résultats expérimentaux. Le modèle FE peut être un outil efficace pour fournir des informations sur le comportement et les différents aspects affectant le cisaillement de poinçonnage dans les raccords de bord.
- L'approche de conception proposée basée sur les résultats de l'analyse de la FEA a donné de bonnes bases, mais prudentes, pour la résistance au poinçonnage-cisaillement des raccords de bord de la GFRP-RC avec différents types de renfort de cisaillement en FRP comme étriers, goujons et barres ondulées. L'approche proposée montrait un V_{test}/V_{pred} moyen de 1,08±0.22 avec un COV de 20.40 %. Cette approche signale une innovation pour l'utilisation des étriers de cisaillement FRP dans les raccordements FRP-RC bord-dalle-colonne. D'autres enquêtes sont toutefois nécessaires pour peaufiner cette approche proposée.

7.5.2. Jonctions PRV–RC Bord Dalle-Colonne sans Armatures de Cisaillement

- Les raccords testés sans renfort de cisaillement ont subi une rupture de cisaillement comme mode final sans aucun signe de concassage du béton. Cette rupture a été caractérisée par une chute immédiate de la charge ultime, accompagnée de l'apparence d'une fissure claire définissant la surface de rupture.
- L'utilisation du HSC a considérablement amélioré la capacité de poinçonnage-cisaillement, la déflexion et la rigidité initiale des raccords renforcés par la PRV. La capacité de poinçonnage-cisaillement, la déflexion et la rigidité initiale des raccords HSC étaient de 18.5 %, 15.5 % et 29 % (en moyenne) supérieures à celles des raccords renforcés PRV construits avec du NSC, respectivement. La rigidité postérieure à la fissuration était toutefois semblable aux raccords renforcés NSC GFRP.
- L'augmentation du rapport M/V de 0.3 m à 0.6 m pour les raccords NSC et HSC a entraîné des fissures de cisaillement légèrement plus prononcées. Les fissures inclinées au bord libre allaient dans une direction opposée à la force de poinçonnage-cisaillement en raison des contraintes de cisaillement inversées causées par un moment très déséquilibré.
- Le JSCE-97 (JSCE 1997) et le CSA S806-12 (CSA 2012) ont raisonnablement prédit les capacités de poinçonnage des raccords testés avec une moyenne de $V_{u\,test}/V_{JSCE}$ = 1.28±0.13 et $V_{u\,test}/V_{CSA}$ = 1.27±0.04, respectivement. L'équation de l'ACI 440.1R-15 (IPEC 2015) a toutefois été sous-estimée, ce qui donne une moyenne de l'essai de l'ACI $V_{u\,test}/V_{ACI}$ = 2.13±0.09. En revanche, l'équation de Hassan et al. (2017) a surestimé la capacité des connexions testées avec une moyenne de $V_{u\,test}/V_{Hassan}$ = 0.88±0.06.
- En utilisant la résistance réelle du béton de 85 et 86 MPa pour les raccords HSC (G-H-0.3 et G-H-0.6) dans l'équation de la norme CSA S806-12 (CSA 2012), on estime mieux la capacité ultime ($V_{u\,test}/V_{CSA}$ = 1.19±0.08) qu'en utilisant le béton de 60 MPa-limite de résistance conformément à la norme CSA S806-12 (CSA 2012). Des recherches plus poussées sont toutefois nécessaires avec un large éventail de points forts concrets.

7.6. Recommandations pour des Travaux Futurs

Les résultats de la présente étude représentent une étape prometteuse dans l'application de barres d'armature et des étriers de cisaillement en PRFV dans les jonctions de dalle-poteau de rive. Sur la base des conclusions de l'étude actuelle, il est recommandé d'effectuer des recherches supplémentaires pour couvrir les points suivants :

1. Il est indispensable de développer davantage de travaux expérimentaux pour générer des données tout en mettant l'accent sur les points suivants :

    - Différentes formes d'armatures de cisaillement, y compris différentes dispositions et agencements dans les jonctions de rive en PRF avec des taux d'armature en flexion élevés ;
    - Différents types d'ancrages pour les armatures de flexion perpendiculaires au côté libre ;
    - Effet des sections du poteau et du rapport profondeur du périmètre de cisaillement/épaisseur de la dalle ;
    - Effet des ouvertures au voisinage du poteau ;
    - Effet de différentes épaisseurs de dalle ;
    - Jonctions de rive avec différentes dimensions de poteau ; et
    - Présence de poutre périphérique sur le bord libre de la jonction.
    - Effet de différentes dimensions de panneaux de retombée.
2. Élaborer une équation alternative à l'équation de calcul du poinçonnement des guides et normes de conception de l'ACI 440.1R-15 et de la CSA S806-12, en tenant compte des paramètres les plus importants.
3. Développement d'un modèle mécanique permettant de prédire de manière raisonnable la résistance au cisaillement des jonctions de rive en PRF en se basant sur l'interaction entre le cisaillement et le moment non équilibré.
4. Étudier l'effet du moment cyclique inversé non équilibré sur le comportement des jonctions dalle-poteau de rive avec et sans armatures de cisaillement en PRF.
5. Une autre étape consiste à étudier la résistance au cisaillement et les performances des jonctions dalle-poteau de coin en béton armé de PRFV

BIBLIOGRAPHY

AASHTO (American Association of State Highway and Transportation Officials). (2009). "AASHTO LRFD bridge design guide specifications for GFRP–reinforced concrete bridge decks and traffic railings." *Washington, D.C.*

ACI (American Concrete Institute). (2012). "Guide Test Methods for Fiber-Reinforced Polymers (FRPs) for Reinforcing or Strengthening Concrete Structures." *ACI 440.3R-12, Farmington Hills, MI.*

ACI (American Concrete Institute). (2014). "Building code requirements for structural concrete and commentary." *ACI 318-14, Farmington Hills, MI.*

ACI (American Concrete Institute). (2015). "Guide for the design and construction of structural concrete reinforced with fiber-reinforced polymer bars." *ACI 440.1R-15, Farmington Hills, MI.*

ACI-ASCE Committee 445 on Shear Torsion. (1998). "Recent approaches to shear design of

Ahmed, E. A., Settecasi, F., and Benmokrane, B., (2014). "Construction and testing of steel-GFRP hybrid-reinforced-concrete bridge-deck slabs of the Ste-Catherine overpass bridges." *J. Bridge Eng., 10.1061/(ASCE) BE.1943-5592.0000581, 04014011.*

Ahmed, E.; Benmokrane, B.; and Sansfaçon, M. (2017). "Case Study: Design, Construction, and Performance of the La Chancelière Parking Garage's Concrete Flat Slabs Reinforced with GFRP Bars," *J. Comp. Constr., 21(1), 10.1061/(ASCE)CC.1943-5614.0000656.*

Arafa, A., (2017). "Assessment of strength, stiffness, and deformation capacity of concrete squat walls reinforced with GFRP bars." *Ph.D. Thesis, Sherbrooke Univ., Canada.*

ASTM. (2011). "Standard test method for tensile properties of fiber reinforced polymer matrix composite bars." *ASTM D7205/D7205M, West Conshohocken, PA.*

Bedard, C. (1992). "Composite reinforcing bars: assessing their use in construction." *Conc. Inter., 14(1), 55-59.*

Benmokrane, B., Ahmed, E., Dulude, C., and Boucher, E. (2012). "Design, construction, and monitoring of the first worldwide two-way flat slab parking garage reinforced with GFRP bars." *Proc., 6th Int. Conf. on FRP Comp. Civ. Eng., Università di Roma.*

Benmokrane, B., El-Salakawy, E., El-Gamal, S., and Goulet, S, (2007). "Construction and testing of an innovative concrete bridge deck totally reinforced with glass FRP bars: Val-Alain Bridge on Highway 20 East." J. Bridge Eng., 10.1061/(ASCE)1084-0702(2007)12:5(632), 632–645.

Broms, C.E., (1990). "Punching of Flat Plates - A Question of Concrete Properties in Biaxial Compression and Size Effect." *ACI Str. J., 87, 292-304*

Büyükkaragöz, A. (2010). "Finite element analysis of the beam strengthened with prefabricated reinforced concrete plate." *Scientific Research and Essays, 5(6), 533–544.*

Chaallal, O., and Benmokrane, B. (1993). "Physical and Mechanical Performance of an Innovative Glass-Fiber-Reinforced Plastic Rod." *Can. J. Civ. Eng., 20(2), 254-268.*

Chansawat, K., Yim, S., Miller, TH. (2011) "Nonlinear finite element analysis of a FRP strengthened reinforced concrete bridge." J Bridge Eng., 11(1), 21–32.

CSA (Canadian Standard Association). (2014). "Design of concrete structures." *CAN/CSA-A23.3-14, Rexdale, Ontario, Canada.*

CSA (Canadian Standards Association). (2012). "Design and construction of building structures with fiber reinforced polymers," *CAN/CSA S806-12, Rexdale, Ontario, Canada.*

CSA (Canadian Standards Association). (2014). "Canadian highway bridge design code." *CAN/CSA S6-14, Rexdale, Ontario, Canada.*

CSA (Canadian Standards Association). (2015). “Specification for fiber reinforced polymers,” *CAN/CSA S807-15, Rexdale, Ontario, Canada.*

Dam, Thai X., Wight, James K., and Parra-Montesinos, Gustavo J., (2017). “Behavior of Monotonically Loaded Slab-Column Connections Reinforced with Shear Studs.” *ACI Str. J., 114(1), 221-232.*

De Luca, A., Matta, F., and Nanni, A. (2009). “Behavior of full-scale concrete columns internally reinforced with glass FRP bars under pure axial load.” *COMP. & POLY. 2009, Amer. Comp. Manuf. Asso., Tampa, FL USA, 1-10*.

Deiveegan, A., and Kumaran, G. (2009). “Reliability analysis of concrete columns reinforced internally with glass fiber reinforced polymer reinforcement.” *ICFAI Univ. J. Struct. Eng., 2(2), 49–59.*

Desayi, P., Krishnan, S. (1964) “Equation for stress–strain curve of the concrete.” *ACI str. J. 61(3), 345–50.*

Design Manual No.3, (2007). “Reinforcing concrete structures with fiber reinforced polymers.” *Int. Sen. Innov. Str. Canada, Winnipeg, MB, Canada.*

Dulude, C., Hassan, M., Ahmed, E., and Benmokrane, B. (2013). “Punching shear behavior of flat slabs reinforced with glass fiber-reinforced polymer bars.” *ACI Struct. J., 110(5), 723–734*.

Elgabbas, F., Ahmed, E. and Benmokrane, B., (2016). “Experimental Testing of Concrete Bridge Deck Slabs Reinforced with Basalt-FRP Reinforcing Bars under Concentrated Loads.” *J. Brid. Eng., 10.1061/(ASCE)BE.1943-5592.0000892.*

Elgabry, A. and Ghali, A., (1996). “ Transfer of moments between columns and slabs.” ACI Str. J. 93, 56 61.

Elgabry, A.,(1991)."Shear and Moment Transfer of Concrete Flat Plates” Ph.D. Thesis, Univ. of Calgary.

Elgabry, Adel A. and Ghali, Amin, (1987). "Design of stud-shear reinforcement for slabs." ACI Str.J.,87(3), 350-361

El-Gendy, M., and El-Salakawy, E. (2016). "Effect of shear studs and high moments on punching behavior of GFRP-RC slab-column edge connections." *J. Compos. Constr., 10.1061/(ASCE)CC.1943-5614.0000668, 04016007.*

El-Gendy, M., and El-Salakawy, E., (2018). "Punching Shear Behavior of GFRP-RC Slab-Column Edge Connections." *ACI SP, SP-322, 5.1-5.20.*

El-Ghandour, A. W., Pilakoutas, K., and Waldron, P. (2003). "Punching shear behavior of fiber reinforced polymers reinforced concrete flat slabs: Experimental study." *J. Compos. Constr., 10.1061/(ASCE)1090-0268(2003)7:3(258).*

El-Mogy, M., El-Ragaby, A., and El-Salakawy, E. (2010). "Experimental testing and finite element modeling on continuous concrete beams reinforced with fiber reinforced polymer bars and stirrups." *Can. J. Civ. Eng., 40 (11), 1091–1102.*

El-Salakawy, E., Polak, M., and Soliman, M. (1998). "Slab-column edge connections subjected to high moments." *Can. J. Civ. Eng., 25(3), 526–538.*

El-Salakawy, E., Polak, M., and Soliman, M. (2000). "Reinforced concrete slab-column edge connections with shear studs." *Can. J. Civ. Eng., 27(2), 338–348.*

El-Salakawy, E.F., Polak, M.A., and Soliman, M.H. (1998). "Slab-column edge connections subjected to high moments." Can. J. of Civ. Eng., 25(3), 526–538.

El-Salakawy, E.F., Polak, M.A., and Soliman, M.H. (2000). " Reinforced concrete slab – column edge connections with shear studs." Can. J. Civ. Eng., 27(2),338–348.

Gardner, N.J., (1990). "Relationship of the punching shear capacity of reinforced concrete slabs with concrete strength." ACI Str. J.,87,66-71.

Gorji, M.S. (2009). "Analysis of FRP strengthened reinforced concrete beams using energy variation method." *World App. Sci. J. 6 (1), 105–111.*

Gouda, A., and El-Salakawy, E. (2015). "Punching shear strength of GFRPRC interior slab-column connections subjected to moment transfer." *J. Compos. Constr., 10.1061/(ASCE)CC.1943-5614.0000597, 04015037.*

Gouda, A., and El-Salakawy, E. (2016). "Behavior of GFRP-RC interior slab-column connections with shear studs and high-moment transfer," *J. Compos. Constr., 10.1061/(ASCE)CC.1943-5614.0000663.*

Hassan, M., Ahmed, E. A., and Benmokrane, B. (2013a). "Punching-shear strength of GFRP-reinforced concrete flat slabs," *Can. J. of Civ. Eng., 40(10), 951-960.*

Hassan, M., Ahmed, E. and Benmokrane, B, (2014 a), "Punching shear behavior of two-way slabs reinforced with FRP shear reinforcement." *J. Compos. Constr., 10.1061/(ASCE)CC.1943-5614.0000493.10.1061/(ASCE).*

Hassan, M., Ahmed, E., and Benmokrane, B. (2013 b). "Punching-shear strength of normal and high-strength two-way concrete slabs reinforced with GFRP bars." *J. Compos. Constr., 10.1061/(ASCE)CC.1943-5614.0000424, 04013003.*

Hassan, M.; Ahmed, E.; and Benmokrane, B, (2014 b), "Punching-shear design equation for two-way concrete slabs reinforced with FRP bars and stirrups." *Constr. and Build. Mat., 66, pp. 522-532.*

Hassan, M.; Fam, A., Benmokrane, B., and Ferrier, E. (2017). "Effect of column size and reinforcement ratio on shear strength of glass fiber-reinforced polymer reinforced concrete two-way slabs." *ACI Struct. J., 114(4), 937-950.*

Hussein, A. H., and El-Salakawy, E. (2018). "Punching Shear Behavior of Glass Fiber-Reinforced Polymer-Reinforced Concrete Slab-Column Interior Connections." *ACI Struct. J., 115(4),1075-1088.*

Issa, M. S., Metwally, I. M., and Elzeiny, S. M. (2011). "Structural performance of eccentrically loaded GFRP reinforced concrete columns." *Int. J. Civ. Struct. Eng., 2(1), 395–404.*

Jaeger, L. G., Mufti, A., and Tadros, G. (1997). "The concept of the overall performance factor in rectangular- section reinforced concrete beams." *Proce., the Third Int. Symp. Nonmetallic (FRP) Reinf. for Conc. Str. (FRPRCS-3), Japan Con. Inst., Sapporo, Japan, 2, 551-558.*

JSCE (Japan Society of Civil Engineers). (1997). "Recommendation for design and construction of concrete structures using continuous fiber reinforcing materials." *Concrete engineering, A. Machida, ed., Tokyo.*

Kachlakev, D., Miller, T., Yim, S., Chansawat, K., and Potisuk, T. (2001)."Finite Element Modeling of Reinforced Concrete Structures strengthened with FRP Laminates." *Final Report SPR-316, Oregon Dept. of Trans., Salem, Oregon*.

Kinnunen S., Nylander H., (1960). "Punching of Concrete Slabs without Shear Reinforcement." Royal Institute of Technology Stockholm, Sweden.

Lee, J.H., Yoon, Y.S., and Mitchell, D. (2009). "Improving Punching Shear Behavior of Glass Fiber-Reinforced Polymer Reinforced Slabs." *ACI Structural Journal, 106 (4), 427– 434.*

Lips, S.; Ruiz, M.; and Muttoni A. (2012). "Experimental Investigation on Punching Strength and Deformation Capacity of Shear-Reinforced Slabs." *ACI Structural Journal, 109 (6), 889-900.*

Marzouk, H., Emam, M., and Hilal, S, (1996). "Effect of High-Strength Concrete Columns on the Behavior of Slab-Column Connections." ACI Struct. J., 93(5), 545–555.

Marzouk, H., Imam, M., and Hilal, M. (1998). "Effect of High-Strength Concrete Slab on the Behavior of Slab-Column Connections." *ACI Struct. J., 95(3), 227-236.*

Megally, S., and Ghali, A. (2000) "Seismic behavior of slab-column connections." *Can. J. Civ. Eng.*, 27(1), 84-100.

Mokhtar, A., Ghali, A., and Dilger, W., (1985). "Stud shear reinforcement for flat concrete plates." ACI J. Pro. 82(5),676-683.

Morphy, R., Shehata, E., and Rizkalla, S. (1997). "Bent Effect on Strength of CFRP Stirrups." Proce., the Third International Symposium on Nonmetallic (FRP) Reinforcement for Concrete Structures (FRPRCS-3)." *Sapporo, Japan, 2, 19-26.*

Mortin, D., and Ghali, A., (1991). "Connection of flat plates to edge columns" ACI Str. J., 88(2).

Mostafa, A., and El-Salakawy, E. (2018). "Behavior of GFRP-RC Slab–Column Edge Connections with High-Strength Concrete and Shear Reinforcement." *J. of Compos. Constr., 10.1061/(ASCE)CC.1943-5614.0000831.*

Mostofinejad, D., and Talaeitaba, S.B. (2006). "Finite element modeling of RC connections strengthened with FRP laminates." *Ira. J. Sci. Tec., 30, 21–30.*

Nanni, A. (1993). "Flexural behavior and design of reinforced concrete using FRP rods." *J. Str. Eng., 119 (11), 3344 – 3359.*

National Research Council of Canada. (2015). "National building code of Canada." *NBCC 2015, Ottawa.*

Nguyen-Minh, L., and Rovnak, M. (2013). "Punching-shear resistance of interior GFRP reinforced slab-column connection." *J. Compos. Constr., 10.1061/(ASCE)CC.1943-5614.0000324, 2–13.*

Ospina, C. E., Alexander, S. D. B. and Cheng, J. J. R. (2003). "Punching of Two-Way Concrete Slabs with Fiber- Reinforced Polymer Reinforcing Bars or Grids." *ACI Struct. J., 100 (5), 589-598.*

Özcan DM, Bayraktar A, Sahin A, Haktanir T, Türker T. (2009). "Experimental and finite element analysis on the steel fiber-reinforced concrete (SFRC) beams ultimate behavior." *Const. Build. Mat. , 23 (2), 1064 –1077.*

Ozden, S., Ersoy, U., and Ozturan, T., (2006). "Punching Shear tests of normal- and high-strength concrete flat plates," *Can. J. Civ. Eng., 33(11), 1389-1400.*

Park, R., and Gamble, W. (1980). "Reinforced concrete slabs." Wiley, New York.

Perera, U. (2005). "Seismic Performance of Concrete Beam-Slab-Column Systems Constructed with a Re-Useable Sheet Metal Formwork System." *M.Sc. Thesis, Univ. of Melbourne, Victoria, Australia.*

Phillips, L.N. (1989). "Design with Advanced Composite Materials." Springer- Verlag.

Pultrall, (2016). "Technical Data Sheet." *www.pultrall.com.*

Razaqpur, A. G., Isgor, O. B., Cheung, M. S., and Wiseman, A. (2001). "Background to shear design provisions of the proposed Canadian standard for FRP reinforced concrete structures." *Proc., Int. Conf. Comp. Const., Porto, Portugal, 403 – 408.*

Razaqpur, A. G., Isgor, O. B., Greenaway, S., and Selley, A. (2004). "Concrete contribution to the shear resistance of FRP reinforced concrete members." *J. Comp. Const., ASCE, 8(5), 452-460.*

Reilly, J. L., Cook W., Bastien J., and Mitchell D., (2014). "Effects of delamination on the performance of two-way reinforced concrete slabs." J. of Compos. Constr., 10.1061/(ASCE)CF.1943-5509.0000457.

Rosenthal, I., (1959). "Experimental investigation of flat plate floors." ACI J. pro., 56, 153-166.

Salama, A., (2016) "punching shear behaviour of concrete edge slab–column connection reinforced with glass fiber reinforced polymer (GFRP) bars" Définition du Projet de Recherche au Doctorat, Sherbrooke university, QC, Canada.

Seible, F., Ghali, A., and Dilger, W., (1980). "Preassembled shear reinforcing units for flat plates." ACI J. Pro.,77(l), 28-35.

Shehata, E., Morphy, R. and Rizkalla, S. (2000). "Fiber Reinforced Polymer shear reinforcement for concrete members: behavior and design guidelines." *Can. J. Civ. Eng., 27, 859-872.*

Shehata, I.AE.M. and Regan, P.E., (1989). "Punching in R.C. Slabs." ASCE J. Str. Eng., 115 (7), 1726-1740

Sherif, A.G., (1996). "Behaviour of reinforced concrete flat slabs." *Ph.D. Thesis, , Univ. of Calgary, Alta.*

Stamenkovic, A., and Chapman, J.C. (1972). "Local strength of flat slabs at column heads." *Report 39, Constr. Indust. Res. and Info. Asso., London, U.K., 205–232.*

structural concrete." *J. Str. Eng., 124 (12), 1375–1417.*

Tavassoli, A., Liu, J., and Sheikh, S. (2015). "Glass fiber-reinforced polymer-reinforced circular columns under simulated seismic loads" *ACI Str. J., 112(10), 103–114.*

Wolanski, A.J. (2004). "Flexural behavior of reinforced and prestressed concrete beams using finite element analysis." *M.Sc. Thesis, Marquette University, Milwaukee, Wisconsin.*

Wu, W. P. (1990). "Thermomechanical Properties of Fiber Reinforced Plastic (FRP) Bars." *Ph.D. Thesis, West Virginia University, Morgantown, W.Va., 292 pp.*

Zaghlool, E.R.F. (1971). "Strength and behavior of corner and edge column–slab connections in reinforced concrete flat plates." *Ph.D. thesis, Department of Civil Engineering, The University of Calgary, Calgary, Alta.*

Zaghlool, E.R.F., de Paiva H.A.R., (1973-a). "Strength analysis of comer column-slab connection" J. Str. Div., ASCE, 99(ST1), Proc., 53-70.

Zaghlool, E.R.F., de Paiva H.A.R., (1973-b). " Tests of flat plate comer column- slab connection" J. Str Div., ASCE Pro., 99(ST3), 551-572.

Zaghloul, A. (2002). “Behaviour and Strength of CFRP-Reinforced Flat Plate Interior Column Connections Subjected to Shear and Unbalanced Moments.” *M.Sc. Thesis, Carleton Univ., Ottawa, ON, Canada.*

Zaghloul, A. E., Razaqpur, A. G., and Zaghloul, E.R. (2004). “Refined Prediction of Punching Shear Strength of Slab-Column Connections: Applications to Slab Reinforced with Steel or FRP.” *4th Inter. Conf. on Adv. Compos. Mat. in Brid. and Struct., Calagary, Alberta, 20-23.*

Zaghloul, A., (2007). “Punching shear strength of interior and edge column-slab connections in CFRP reinforced flat plate structures transferring shear and moment.” *Ph.D. Thesis, Carleton univ., Ottawa, ON, Canada.*

Zhang, Q. (2004). “Finite element application to slab-column connections reinforced with glass fiber-reinforced polymers.” *M.Sc. thesis, Memorial Univ., Newfoundland, St. John's, Canada.*

Zhang, Q., Marzouk, H., and Hussein, A., (2005). “A Preliminary Study of High Strength Concrete Two-Way Slabs Reinforced with GFRP Bars.” *Proceedings, 33rd CSCE Ann. Conf., Can. Soc. Civ. Eng., Toronto, ON, Canada.*

APPENDIX

1.1. Introduction

This chapter represents the calculations of flexure design and punching shear capacity predictions of the test connections that were reported and discussed in chapter 4 and 5. The flexural design of the connections for flexure is completed in accordance with the Canadian codes CSA A23.3-14 and CSA S806-12. However, the punching-shear capacity of the connections with and without shear reinforcement were predicted using new proposed equations and available equations in FRP codes and guides, CSA S806-12, ACI 440.1R-15 and JSCE-97, respectively.

1.2. Analysis of Prototype Structure

The prototype structure is a parking garage flat-plate structure with 5 × 5 m^2 square panels as shown in Fig A.1. The edge slab-column connection is bounded by the lines of contra flexure in the prototype floor, and monolithic with a column at the middle of the free edge. The parking garage flat plate structure is analysed using Equivalent Frame Method in CSA A23.3-14. In the equivalent frame method, the 3D flat-plate structure is idealized into 2D frames along column centre lines in both longitudinal and transverse directions, X and Y frames as shown in Figure A.1. Each equivalent frame shall consist of a row of columns and slab-beam strips bounded laterally by the panel centreline on each side of the centreline of columns. for analysis of each equivalent frame, a separate analysis can be carried for each floor with the fixed far ends of columns under gravity loading. The selected X and Y frames were analysed to determine their straining actions, bending moment and shear. Consequently, the applied *M/V* ratio and amount of flexural reinforcement can be estimated for the selected connection. The selected connection is located at the interstation between the centrelines A and 3.

1.2.1. Concrete Dimensions and Loads

- Concrete Dimensions
  - Slab Thickness (t_s) = 200 mm
  - Column Dimensions ($c_1 \times c_2$) =300 × 300 mm

- Service and Ultimate Loads

The loads were specified according to the National Building Code of Canada (NBCC 2015)

$$w_{D.L} = \gamma_c t_s + \text{Partations} = 24 \times 0.2 + 1.0 = 5.8 \text{ KN/m}^2,\ W_{L.L} = 2.4 \text{ KN/m}^2$$

$$w_s = w_{D.L} + w_{L.L} = 5.8 + 2.4 = 8.2 \text{ KN/m}^2$$

$$w_f = \max \begin{cases} 1.4 w_{D.L} = 1.4 \times 5.8 = 8.12 kN/\text{m}^2 \\ 1.25 W_{D.L} + 1.5 W_{L.L} = 1.25 \times 5.8 + 1.5 \times 2.4 = 10.85 kN/\text{m}^2 \end{cases}$$

1.2.2. Analysis of the Equivalent 2D Frame in X-direction

- Slab-Beam Stiffness and Fixed End Moment

For span A3−B3 at end A

- $\frac{C_1}{l_1} = \frac{300}{5000} = 0.06,\ \frac{C_2}{l_2} = \frac{300}{5000} = 0.06 \rightarrow k = 4.067, COF = 0.505$ (Table A. 1)
- $I_s = \frac{l_2 t_s^3}{12} = \frac{5000 \times 200^3}{12} = 3333 \times 10^6 \text{ mm}^4$
- $K_{A3-B3} = \frac{k E_c I_s}{l_1} = \frac{4.067 \times 3333 \times 10^6 \times E_c}{5000} = 2711062\ E_c$

$(M_{F.E.M})_f = 0.084\ w_f\ l_2\ l_1^2 = 0.084 \times 10.85 \times 5 \times 5^2 = 113.93$ kN.m

Note: The remaining spans will have the same values because they have the same geometry as well as the fixed end moment is constant of each span.

- **Equivalent Column Stiffness (K_{ec})**

The equivalent column stiffness (K_{ec}) represents the combined stiffens of the column (K_c) and attached torsional members (K_t), where the column is assumed to be attached to the slab by the transverse torsional members.

$$\frac{1}{K_{ec}} = \frac{1}{\Sigma K_c} + \frac{1}{K_t}$$

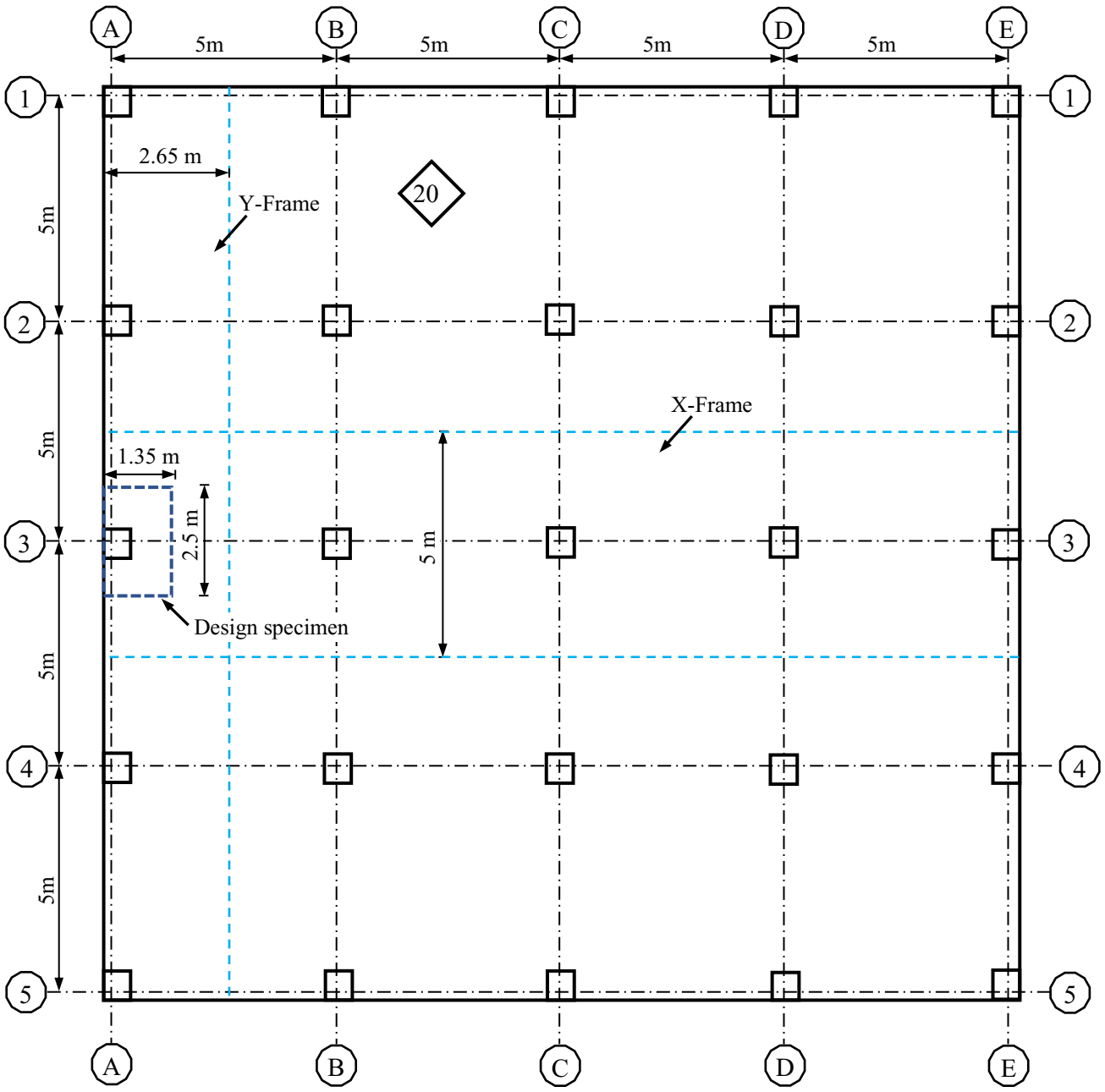

Figure A.1 – Plan of flat plate prototype

For column A3, the equivalent column stiffness was calculated as follows

Torsional member stiffness (K_t)

The factor (C) in the torsional member stiffness equation defines the cross section of the torsional members. The attached torsional members at the exterior column is a portion of the slab having width equal to column width y and depth equals slab thickness x (refer to Fig A.2a).

The Torsional member stiffness (K_t) was multiplied by 2 because two similar torsional members meet at column A3. The values of K_t for all other columns will be the same as column A3 because of similar column dimensions.

$$C = \Sigma \left(1 - 0.63 \frac{x}{y}\right) \frac{x^3 y}{3} = \left(1 - 0.63 \frac{200}{300}\right) \frac{200^3 \times 300}{3} = 464 \times 10^6 \text{ mm}^4$$

$$k_t = \Sigma \frac{9 E_c C}{l_2 \left(1 - \frac{c_2}{l_2}\right)^3} = 2 \times \frac{9 \times E_c \times 464 \times 10^6}{5000 \left(1 - \frac{300}{5000}\right)^3} = 2011115 E_c$$

Column stiffness (K_c)

The column stiffness (K_c) was multiplied by 2 for interior story with similar columns above and below

$$\frac{l_c}{l_u} = \frac{3200}{3000} = 1.07, \frac{t_a}{t_b} = 1 \rightarrow k_{AB} = 4.748, C_{AB} = 0.55 \text{ (Table A. 2)}$$

$$\Sigma K_c = \frac{k E_c I_C}{l_c} = 2 \times \frac{4.748 \times E_c \times (\frac{300^4}{12})}{3200} = 2003063 E_c$$

Table A.1 – Moment-Distribution Factors for flat plates (Wight and MacGregor 2011)

Carryover factor = COF							
c_2/l_2							
c_1/l_1		0.00	0.05	0.10	0.15	0.20	0.25
0.00	*M*	0.083	0.083	0.083	0.083	0.083	0.083
	k	4.000	4.000	4.000	4.000	4.000	4.000
	COF	0.500	0.500	0.500	0.500	0.500	0.500
0.05	*M*	0.083	0.084	0.084	0.084	0.085	0.085
	k	4.000	4.047	4.093	4.138	4.181	4.222
	COF	0.500	0.503	0.507	0.510	0.513	0.516
0.10	*M*	0.083	0.084	0.085	0.085	0.086	0.087
	k	4.000	4.091	4.182	4.272	4.362	4.449
	COF	0.500	0.506	0.513	0.519	0.524	0.530
0.15	*M*	0.083	0.084	0.085	0.086	0.087	0.088
	k	4.000	4.132	4.267	4.403	4.541	4.680
	COF	0.500	0.509	0.517	0.526	0.534	0.543
0.20	*M*	0.083	0.085	0.086	0.087	0.088	0.089
	k	4.000	4.170	4.346	4.529	4.717	4.910
	COF	0.500	0.511	0.522	0.532	0.543	0.554
0.25	*M*	0.083	0.085	0.086	0.087	0.089	0.090
	k	4.000	4.204	4.420	4.648	4.887	5.138
	COF	0.500	0.512	0.525	0.538	0.550	0.563

Equivalent column stiffness (K_c)

All columns have same dimensions and geometry, hence the K_{ec} value for all columns will be the same.

$$\frac{1}{K_{ec}} = \frac{1}{\Sigma K_c} + \frac{1}{K_t} = \frac{1}{2003062\ \mathrm{E_c}} + \frac{1}{2011115\ \mathrm{E_c}} \rightarrow K_{ec} = 1003540\ E_c$$

- **Moment-Distribution Coefficients for Slabs and Columns**

The stiffness, carry over, and distribution factors for slabs and columns are shown in Figure A.2b.

$$DF_{A3-B3} = \frac{K_{sb_{A3-B3}}}{K_{sb_{A3-B3}} + K_{ec_{A3}}} = \frac{2711062\ E_c}{2711062\ E_c + 1003540\ \mathrm{E_C}} = 0.73$$

$$DF_{K_{ec}\ Column\ A3} = \frac{K_{ec_{A3}}}{K_{sb_{A3-B3}} + K_{ec_{A3}}} = \frac{1003540\ E_c}{2711062\ E_c + 1003540\ \mathrm{E_C}} = 0.27$$

$$DF_{B3-A3} = \frac{K_{sb_{B3-A3}}}{K_{sb_{B3-A3}} + K_{sb_{B3-C3}} + K_{ec_{B3}}} = \frac{2711062\ E_c}{E_c(2711062 + 2711062 + 1003540)} = 0.422$$

$$DF_{K_{ec}\ Column\ B3} = 1 - 2(0.422) = 0.156$$

Table A.2 – Stiffness and carryover factors for columns (Wight and MacGregor 2011)

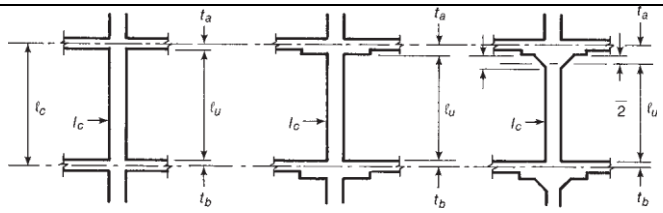

		l_c/l_u								
$t_a>t_b$		1.05	1.10	1.15	1.20	1.25	1.30	1.35	1.40	1.45
0.00	k_{AB}	4.20	4.40	4.60	4.80	5.00	5.20	5.40	5.60	5.80
	C_{AB}	0.57	0.65	0.73	0.80	0.87	0.95	1.03	1.10	1.17
0.2	k_{AB}	4.31	4.62	4.95	5.30	5.65	6.02	6.40	6.79	7.20
	C_{AB}	0.56	0.62	0.68	0.74	0.80	0.85	0.91	0.96	1.01
0.4	k_{AB}	4.38	4.79	5.22	5.67	6.15	6.65	7.18	7.74	8.32
	C_{AB}	0.55	0.60	0.65	0.70	0.74	0.79	0.83	0.87	0.91
0.6	k_{AB}	4.44	4.91	5.42	5.96	6.54	7.15	7.81	8.50	9.23
	C_{AB}	0.55	0.59	0.63	0.67	0.70	0.74	0.77	0.80	0.83
0.8	k_{AB}	4.49	5.01	5.58	6.19	6.85	7.56	8.31	9.12	9.98
	C_{AB}	0.54	0.58	0.61	0.64	0.67	0.70	0.72	0.75	0.77
1.0	k_{AB}	4.52	5.09	5.71	6.38	7.11	7.89	8.73	9.63	10.60
	C_{AB}	0.54	0.57	0.60	0.62	0.65	0.67	0.69	0.71	0.73
1.2	k_{AB}	4.55	5.16	5.82	6.54	7.32	8.17	9.08	10.07	11.12
	C_{AB}	0.53	0.56	0.59	0.61	0.63	0.65	0.66	0.68	0.69

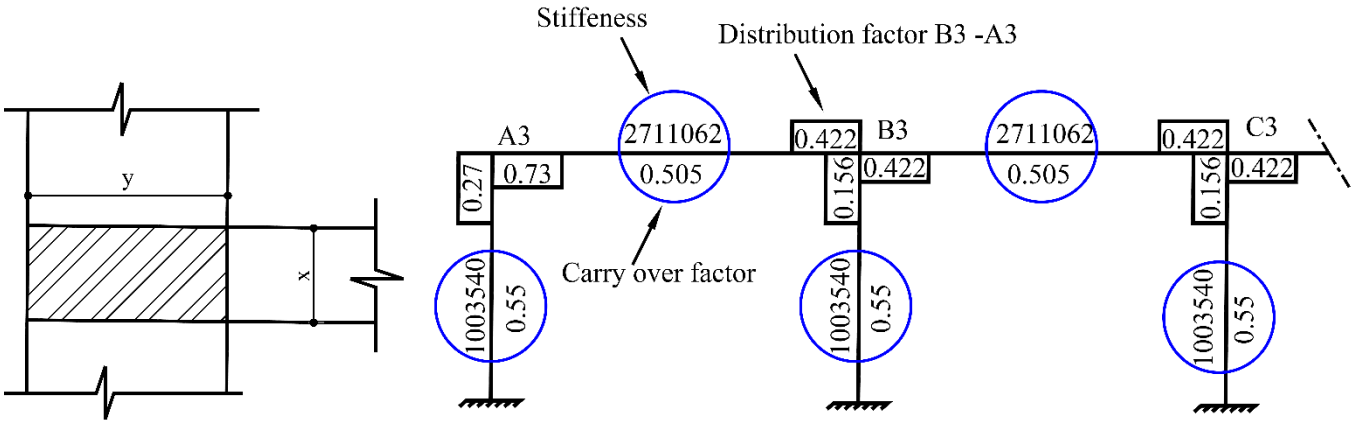

(a) (b)

Figure A.2 – (a) Column *A3* with attached torsional member; and (b) Stiffness, carry over, and distribution factors

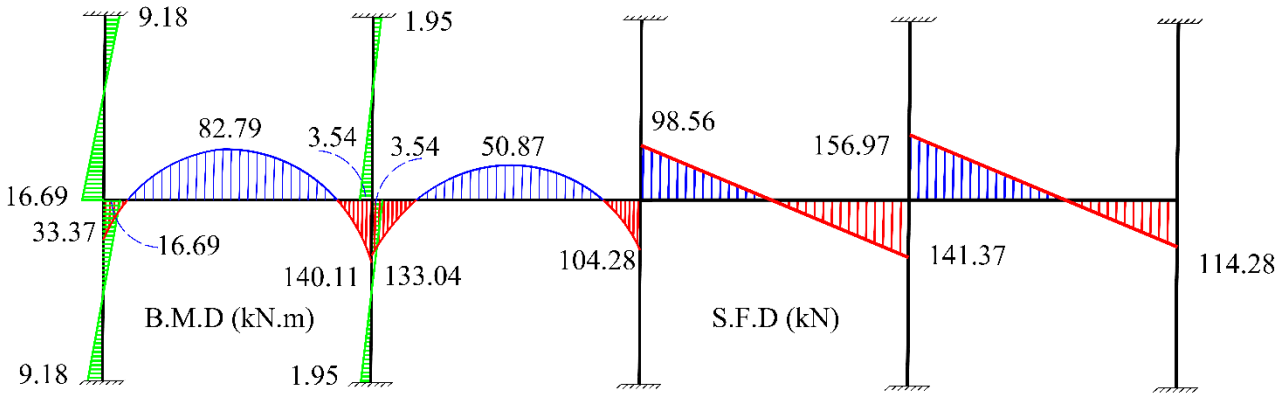

Figure A.3 – Moment and shear diagrams from equivalent frame analysis along line 3

- **Moment Distribution Analysis**

The moment distribution method is a convenient hand calculation method for analyzing partial frames in the Equivalent Frame Method. The moment-distribution analysis is carried out in Table A.3. The moment and shear force diagrams are plotted as shown in Figure A.3.

Table A.3– Moment distribution analysis in the X- frame

Joint	A		B			C
Member	Col.	Slab	Slab	Col.	slab	Slab
C.O. F		0.505			0.505	
D.F	0.27	0.73	0.422	0.156	0.422	0.422
FEM	0	113.93	-	0	113.93	-
BM	-30.76	-83.17	0	0	0	0
COM		0.	- 42	0	0	0
BM		0	17.72	6.56	17.72	0
COM		8.95	0		0	8.95
BM	- 2.42	- 6.53	0			
COM		0	- 3.29			
BM		0	1.39	0.51	1.39	0
COM		0.70	0		0	0.70
BM	- 0.19	- 0.51	0			
M_{final}	- 33.37	33.37	-	7.07	133.04	-

- **Distribution of Frame Moments**

Once the negative and positive moments have been determined for each equivalent frame, these are distributed to column and middle strips in the same way as in the direct-design method. The moment distribution for column and field strips in the longitudinal direction are listed in Table A.4.

Table A.4 – Distribution of frame moments

Joint	A	B		C		
Moment	33.37	82.79	140.11	133.04	50.87	104.28
Moment in column strip						
Percentage (%)	100	60	70-90	70-90	55-65	70-90
Moment (kN.m)	33.37	49.67	98 -126	93.13-119.74	27.98 - 33.07	73 – 93.87
Moments in field strip 2 half middle strips						
Percentage (%)	0	40	30-10	30-10	45-35	30-10
Moment (kN.m)	0	33.12	42.11 - 14.11	39.91 - 13.30	22.89 – 17.80	31.31 - 10.43

- **Moment-to-Shear Ratio at Column Centroid** (M/V)

  $M/V = 33.37/114.28 = 0.292 \rightarrow take\ M/V = 0.3$

1.2.3 Analysis of the Equivalent 2D frame in the Y-direction

- Slab-beam Stiffness and Fixed end moment

  For span 5A−4A at end 5

  - $\frac{C_1}{l_1} = \frac{300}{5000} = 0.06,\ \frac{C_2}{l_2} = \frac{300}{2650} = 0.11 \rightarrow k = 4.122, COF = 0.509$ (Table A. 1)
  - $I_s = \frac{l_2\, t_s^3}{12} = \frac{2650 \times 200^3}{12} = 1767 \times 10^6$
  - $K_{A3-B3} = \frac{k\, E_c I_s}{l_1} = \frac{4.122 \times 1767 \times 10^6 \times E_c}{5000} = 1456715\ E_c$

  $(M_{F.E.M})_f$ = 0.0842 w_f l_2 l_1^2 = 0.0842 × 10.85 × 2.65 × 5^2 = 60.52 kN.m

- **Equivalent column stiffness (K_{ec})**

For column 5A, the equivalent column stiffness was calculated as follows

Torsional member stiffness (K_t)

There is only one torsional member meet at column 5A. The value of K_t for all other columns will be the same as column 5A because of similar column dimensions.

$$C = \Sigma \left(1 - 0.63 \frac{x}{y}\right) \frac{x^3 y}{3} = \left(1 - 0.63 \frac{200}{300}\right) \frac{200^3 \times 300}{3} = 464 \times 10^6 \text{ mm}^4$$

$$k_t = \Sigma \frac{9 E_c C}{l_2 \left(1 - \frac{c_2}{l_2}\right)^3} = \frac{9 \times E_c \times 464 \times 10^6}{2650 \left(1 - \frac{300}{2650}\right)^3} = 2259689 E_c$$

Column stiffness (K_c)

$$\frac{l_c}{l_u} = \frac{3200}{3000} = 1.07, \frac{t_a}{t_b} = 1 \rightarrow k_{AB} = 4.748, C_{AB} = 0.55 \text{ (Table A. 2)}$$

$$\Sigma K_c = \frac{k E_c I_C}{l_c} = 2 \times \frac{4.748 \times E_c \times (\frac{300^4}{12})}{3200} = 2003063 E_c$$

Equivalent column stiffness (K_c)

$$\frac{1}{K_{ec}} = \frac{1}{\Sigma K_c} + \frac{1}{K_t} = \frac{1}{2003062 E_c} + \frac{1}{2259689 E_c} \rightarrow K_{ec} = 1061825 E_c$$

- **The Moment-Distribution Coefficients for Slabs and Columns**

The Stiffness, carry over, and distribution factors for slabs and columns are shown in Figure A.4.

$$DF_{5A-4A} = \frac{K_{sb_{A3-B3}}}{K_{sb_{A3-B3}} + K_{ec_{A3}}} = \frac{1456715 E_c}{1456715 E_c + 1061825 E_C} = 0.58$$

$$DF_{K_{ec}\ Column\ 5A} = \frac{K_{ec_{A3}}}{K_{sb_{A3-B3}} + K_{ec_{A3}}} = \frac{1061825 E_c}{1456715 E_c + 1061825 E_C} = 0.42$$

$$DF_{4A-5A} = \frac{K_{sb_{B3-A3}}}{K_{sb_{B3-A3}} + K_{sb_{B3-C3}} + K_{ec_{B3}}} = \frac{1456715 E_c}{E_c(1456715 + 1456715 + 1061825)} = 0.37$$

$$DF_{K_{ec}\ Column\ 4A} = 1 - 2(0.37) = 0.26$$

Table A.5 – Moment distribution analysis in the Y- frame

Joint	5		4			3
Member	Col.	Slab	Slab	Col.	slab	Slab
C.O. F		0.509			0.509	
D.F	0.42	0.58	0.37	0.26	0.37	0.37
F.E.M.	0	60.52	- 60.52	0	60.52	- 60.52
B.M.	-25.42	- 35.1	0	0	0	0
C.O.M		0	- 17.87	0	0	0
B.M		0	6.61	4.65	6.61	0
C.O.M		3.36	0		0	3.36
B.M	- 1.41	- 1.95	0			
C.O.M		0	- 0.99			
B.M		0	0.37	0.25	0.37	0
C.O.M		0.19	0		0	0.19
B.M	- 0.08	- 0.11	0			
M_{final}	- 26.91	26.91	-72.4	4.9	67.5	-56.97

- **Moment Distribution Analysis**

The moment-distribution analysis is carried out in Table A.5. The moment and shear force diagrams are plotted as shown in Figure A.5.

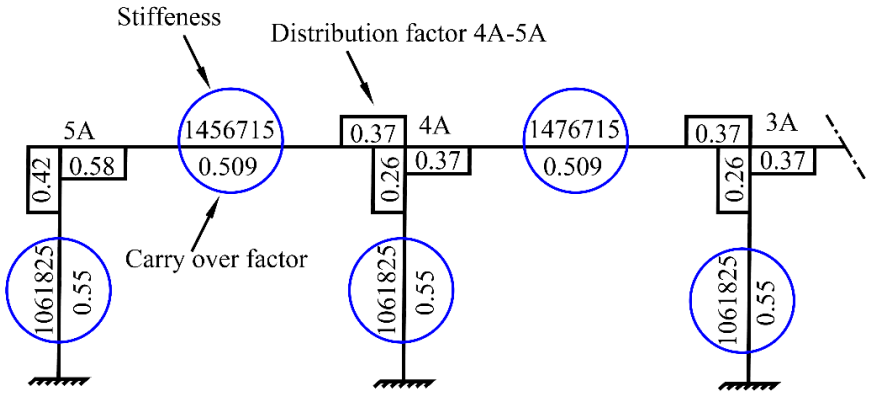

Figure A.4 – Stiffness, carry over, and distribution factors

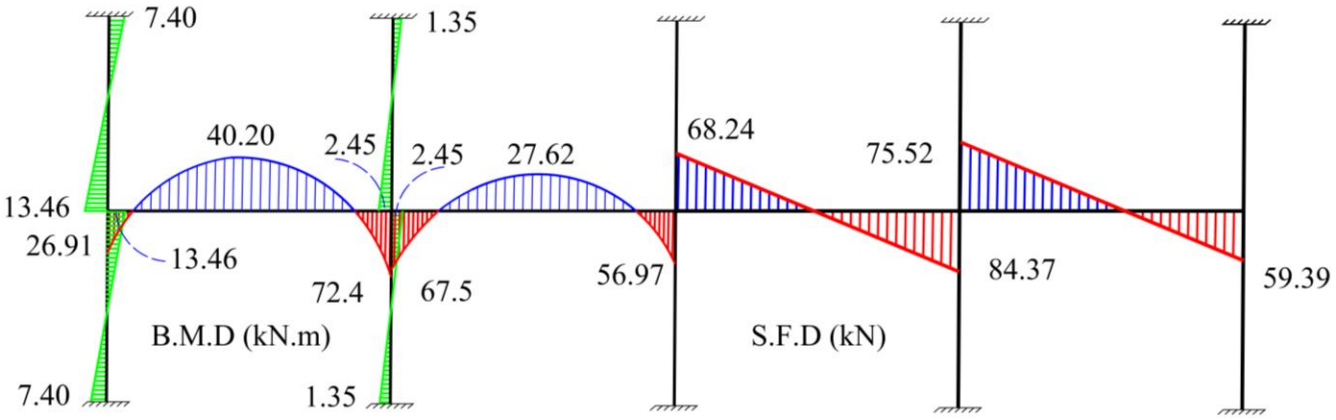

Figure A.5 – Moment and shear diagrams from equivalent frame analysis along line A

- **Distribution of Frame Moments**

The moment distribution for column and field strips in the longitudinal direction are listed in Table A.6.

Table A.6 – Distribution of frame moments

Joint	5	4		3		
Moment	26.91	40.20	72.4	67.5	27.62	56.97
Moment in column strip						
Percentage (%)	100	60	70-90	70-90	55-65	70-90
Moment (kN.m)	26.91	24.12	50.68-65.16	47.25 -60.75	15.19 -17.95	39.88-51.27
Moments in field strip (half middle strip)						
Percentage (%)	0	40	30-10	30-10	45-35	30-10
Moment (kN.m)	0	16.08	21.72 -7.24	20.25 -6.75	12.43 -9.67	17.1-5.7

1.3. Flexural Design of Test Specimen

1.3.1 Material Properties

- Concrete Properties
  - f_c' = 35 MPa $\lambda = 1$ ϕ_c = 1 Ec $= 4500\sqrt{f_c'} = 26622$ MPa
  - $\alpha_1 = 0.85 - 0.0015\ f_c' = 0.798$ $\beta_1 = 0.97 - 0.0025\ f_c' = 0.883$

- Reinforcement Properties
  - GFRP Bent Bars N0.20 (A_f = 285 mm^2; f_{frpu} =1210 MPa; E_{frp} = 53 GPa; ε_{frpu} = 0.0228)
  - GFRP Straight Bars No.20 (A_f = 285 mm^2; f_{frpu} =1334 MPa; E_{frp} = 64.9 GPa; ε_{frpu}= 0.0206)
  - GFRP Straight Bars No.15 (A_f = 199 mm^2; f_{frpu} =1323 MPa; E_{frp} = 64.8 GPa; ε_{frpu}= 0.0204)

1.3.2 Test connections without shear reinforcement

Reinforcement perpendicular to the Free Edge

According to clause 13.10.3 in CSA A23.3-14, The width of the column strip equals 2500mm, while the total factored negative moment transferred to the exterior columns is resisted by the reinforcement placed in the band width (b_b). The bottom reinforcement placed in the connection refers to negative moment reinforcing bars. The reinforcement in the band width (b_b) was calculated as follows

M_r =33.37 kN.m (Table A.2)

$b_b = c + 3t_s = 300 + 3\,(200) = 900$ mm

$$d_x = t_s - \text{cover} - \frac{d_b}{2} = 200 - 21 - \frac{19}{2} = 169.5 \text{ mm}$$

$$M_r = \alpha_1\,\beta_1\,\emptyset_c\,f_c'\,c\,b\left(d_x - \frac{\beta_1 c}{2}\right)$$

$33.37 \times 10^6 = 0.798 \times 0.883 \times 1 \times 35 \times c \times 900\,(169.5 - 0.5 \times 0.883\,c)$

$9799\,c^2 - 3762217\,c + 33.37 \times 10^6 = 0 \rightarrow c = 9.1$ mm

$$\varepsilon_{frp} = \varepsilon_{cu}\left(\frac{d_x}{c} - 1\right) = 0.0035\left(\frac{169.5}{9.1} - 1\right) = 0.062$$

$$f_{frp} = E_{frp} \times \varepsilon_{frp} = 53000 \times 0.062 = 3286 \text{ MPa} \gg f_{frp_u} = 1210 \text{ MPa}$$

$$\rightarrow \text{Try } A_{frp_{min}}$$

The minimum area of reinforcement shall be used in each of the two orthogonal directions in slabs according to clause 8.4.2.3 in CSA S806-12 given by

$$A_{frp_{min}} = Max\left[0.0025A_g, \frac{400\,A_g}{E_f}\right] = Max\left[0.0025\,(900\times 200), \frac{400\,(200\times 900)}{53000}\right]$$
$$= 1358\,mm^2$$

From equilibrium, we can get ε_{frp}

$$C = T$$

$$\alpha_1\ \emptyset_c\,\beta_1\,f_c'\ c\,b = \emptyset_{frp}\,A_{frp}\ E_{frp}\,\varepsilon_{frp}$$

$$0.798\times 1\times\ 0.883\times 35\times\ c\times\ 900 = 1\times 1358\times 53000\times 0.0035\left(\frac{169.5}{c}-1\right)$$

$$22196\,c^2 + 251909\,c - 42698576 = 0\ \rightarrow\ c = 38.6\ \text{mm}$$

$$\varepsilon_{frp} = \varepsilon_{cu}\left(\frac{d_x}{c}-1\right) = 0.0035\left(\frac{169.5}{38.6}-1\right) = 0.0118$$

$$\therefore f_{frp} = E_{frp}\,\varepsilon_{frp} = 53000\times 0.0118 = 625.4\ \text{MPa} < f_{frpu} = 1210\ \text{MPa ok ...}$$

$$M_r = \alpha_1\,\emptyset_c\,\beta_1\,f_c'\ c\,b\left(d_x - \frac{\beta_1\,c}{2}\right)$$

$$M_r = 0.798\times 1\times 0.883\times 35\times 38.6\times 900\left(169.5 - \frac{0.883\times 38.6}{2}\right) = 130.62\ \text{kN.m}$$

No. of bars = 1358 / 285 = 4.76 ∴ use 5 GFRP bent bars No.20 ($A_{f_{act}} = 5\times 285 = 1425\ \text{mm}^2$)

$$\text{Spacing (s)} = \frac{\text{Width}}{\text{No. of bars}} = \frac{900}{5} = 180\ \text{mm}$$

$$\rho_{frp_x} = \frac{A_{frp}}{d_x\ b} = \frac{5\times 285}{169.5\times 900} = 0.0093$$ (Flexural reinforcement ratio ⊥ free edge)

$$\rho_{frpb} = \alpha_1\,\beta_1\frac{\emptyset_c}{\emptyset_{frp}}\frac{f_c'}{f_{frpu}}\left(\frac{\varepsilon_{cu}}{\varepsilon_{cu}+\varepsilon_{frpu}}\right) = 0.798\times 0.883\times\frac{1.00}{1.00}\times\frac{35}{1210}.\left(\frac{0.0035}{0.0035+0.023}\right) = 0.0027$$

$$\therefore \rho_{frp} > \rho_{frpb}\ \text{(Compression Failure)}$$

The minimum flexure reinforcement can be used for in the rest parts of the column strip

$$\frac{A_{frp_{min}}}{m} = \max\left[0.0025A_g, \frac{400\,A_g}{E_f}\right] = \max\left[(0.0025\times(1000\times 200), \frac{400\times(200\times 1000)}{53000}\right] = 1509\frac{mm^2}{m}$$

No. of bars/ m = 1509/ 285 = 5.29/ m ∴ use 6 GFRP bent bars No.20 ($A_{f_{act}} = 6 \times 285 = 1710$ mm^2)

$S_{max} = \min \text{ of } (3t_s, 300 \text{ mm}) = \text{mim of } (600 \text{ mm or } 300 \text{ mm}) \rightarrow S_{max} = 300 \text{ mm}$

$$\text{Spacing } /m = \frac{1000}{6} = 167 \text{ mm}$$

Serviceability limit state

The modulus of elasticity of FRP bars, E_f, is lower than that of steel, E_s, the higher strength cannot be fully utilized in reinforced concrete structures. Hence, the design is mainly to control deflection and crack width. In addition, the stress in the FRP reinforcement must be checked against allowable service limit state stresses. The stress in the FRP reinforcement and crack width were checked according to CSA S806-12 as follows

Service moment due to sustained service loads

The fixed end moment (M_{FEM}) due to the sustained load

$$(M_{FEM})_s = 0.084\, w_s\, l_2\, l_1^2 = 0.084 \times 8.2 \times 5 \times 5^2 = 86.1 \text{ kN.m}$$

The moment to be transferred at the edge column equals

$$M_s = 86.1 \times \frac{33.37}{113.93} = 25.22 \text{ kN.m}$$

Check maximum stress under service load according

$$f_{frp_s} = \frac{M_s}{A_{frp}\, j\, d_x} \leq 0.25\, f_{frpu}$$

where

$M_s = 25.22$ kN.m

$$\rho_{frp} = 0.0093, n_{frp} = \frac{E_f}{E_c} = \frac{53000}{26622} = 1.99$$

$$k = \sqrt{(\rho_{frp}\, n_{frp})^2 + 2\, \rho_{frp} n_{frp}} - \rho_{frp} n_{frp}$$

$$k = \sqrt{(0.0093 \times 1.99)^2 + 2 \times 0.0093 \times 1.99} - 0.0093 \times 1.99 = 0.175$$

$$j = 1 - \frac{k}{3} = 1 - \frac{0.175}{3} = 0.942$$

$$\therefore f_{frp_s} = \frac{25.22 \times 10^6}{5 \times 285 \times 0.941 \times 169.5} = 110.96 \text{ MPa} \leq 0.25\, f_{frpu} = 302.5 \text{ MPa}$$

Check crack width parameter

The crack width parameter was checked based on the CSA S806-12. Clause 8.1.1.3 specifies that, when the maximum strain in FRP tension reinforcement under full-service loads exceeds 0.0015, cross-sections of maximum positive and negative moment shall be so proportioned that the quantity, z, given by

$$\mathrm{z} = k_b \frac{E_s}{E_F} f_{frp_{service}} (d_c A)^{\frac{1}{3}} \not< 45000 \frac{\mathrm{N}}{\mathrm{mm}}$$

where

$$\mathrm{d_c} = 21 + 0.5(19) = 30.5\mathrm{mm}$$

$$\mathrm{A} = \frac{2\,\mathrm{b}\,\mathrm{d_c}}{\text{No. of bars}} = \frac{2 \times 900 \times 30.5}{5} = 10980 \text{ mm}^2$$

$$\therefore \mathrm{z} = k_b \frac{E_s}{E_F} f_{frp_s} (d_c A)^{\frac{1}{3}}$$

$$\mathrm{z} = 1.2 \times \frac{200000}{53000} \times 110.96 \times (30.5 \times 10980)^{\frac{1}{3}} = 34892 \frac{\mathrm{N}}{\mathrm{mm}} < 45000 \frac{\mathrm{N}}{\mathrm{mm}} \quad \text{ok ....}$$

∴ Place one GFRP bent bar No.20 @180 mm in the banded width and one GFRP bent bar No.20 No.20 @ 167 mm for the rest of the connection.

Reinforcement Parallel to the Free Edge

The width of the column strip equals 1400 mm. while, clause 13.11.2.7 in CSA A23.3-14 specifies that one-third of the total factored negative moment at least transferred to the interior columns is resisted by the reinforcement placed in the band width (b_b). The reinforcement in the band width (b_b) was calculated as follows

Total factored -ve moment = 56.97 **(**Table A.4**)**

$\therefore \mathrm{M_r} = \frac{1}{3} \times 56.97 = 18.99$ kN. m

$b_b = c + 1.5\ t_s = 300 + 1.5\ (200) = 600$ mm

$d_y = t_s - \text{cover} - 1.5\ d_b = 200 - 21 - 1.5(19) = 150.5$ mm

$$M_r = \alpha_1\ \beta_1\ \emptyset_c\ f_c'\ c\ b\left(d_y - \frac{\beta_1\ c}{2}\right)$$

$18.99 \times 10^6 = 0.798 \times 0.883 \times 1 \times 35 \times c \times 600\ (150.5 - 0.5 \times 0.883\ c)$

$6533\ c^2 - 2226996\ c + 18.99 \times 10^6 = 0 \rightarrow c = 8.75$ mm

$$\varepsilon_{frp} = \varepsilon_{cu}\left(\frac{d_y}{c} - 1\right) = 0.0035\left(\frac{150.5}{8.75} - 1\right) = 0.0567$$

$$f_f = E_f \times \varepsilon_{frp} = 64900 \times 0.0567 = 3680 \text{ MPa} \gg f_{frp_u} = 1334 \text{ MPa} \rightarrow \text{Try } A_{frp_{min}}$$

$$A_{frp_{min}} = \max\left[0.0025 A_g, \frac{400}{E_f} A_g\right] = \max\left[0.0025\ (600 \times 200), \frac{400 \times (600 \times 200)}{64900}\right]$$

$$= 740\ mm^2$$

From equilibrium, we can get ε_{frp}

$\mathrm{C} = \mathrm{T}$

$$\alpha_1\ \beta_1\ \emptyset_c\ f_c'\ c\ b = \emptyset_{frp}\ A_{frp}\ E_{frp}\ \varepsilon_{frp}$$

$$0.798 \times 0.883 \times 1 \times 35 \times c \times 600 = 1 \times 740 \times 64900 \times 0.0035\left(\frac{150.5}{c} - 1\right)$$

$$14797.31\ c^2 + 168091\ c - 25297695.5 = 0 \rightarrow c = 36.06 \text{ mm}$$

$$\varepsilon_{frp} = \varepsilon_{cu}\left(\frac{d_y}{c} - 1\right) = 0.0035\left(\frac{150.5}{36.06} - 1\right) = 0.0111$$

$$\therefore f_{frp} = E_{frp}\ \varepsilon_{frp} = 64900 \times 0.0111 = 720.39 \text{ MPa} < f_{frpu} = 1334 \text{ MPa}$$

$$M_r = \alpha_1\ \beta_1\ \emptyset_c\ f_c'\ c\ b\left(d_y - \frac{\beta_1\ c}{2}\right)$$

$M_r = 0.798 \times 0.883 \times 1 \times 35 \times 36.06 \times 600\left(150.5 - \frac{0.883 \times 36.06}{2}\right) = 71.81\ \text{kN.m} > 18.13\ \text{kN.m}$

No. of bars = 740 / 285 = 2.6 ∴ use 3 GFRP straight bars No.20 ($A_{f_{act}} = 3 \times 285 = 855\ \text{mm}^2$)

$$\text{Spacing (s)} = \frac{\text{Width}}{\text{No. of bars}} = \frac{600}{3} = 200\ \text{mm}$$

$\rho_{frp} = \frac{A_{frp}}{d_y\ \text{b}} = \frac{3 \times 285}{150.5 \times 600} = 0.00947$ (Flexural reinforcement ratio // free edge)

$\rho_{frpb} = \alpha_1\ \beta_1 \frac{\emptyset_c}{\emptyset_{frp}} \frac{f_c'}{f_{frpu}}\left(\frac{\varepsilon_{cu}}{\varepsilon_{cu} + \varepsilon_{frpu}}\right) = 0.798 \times 0.883 \times \frac{1.00}{1.00} \times \frac{35}{1334} \times \left(\frac{0.0035}{0.0035 + 0.021}\right) = 0.00264$

$$\therefore \rho_{frp} > \rho_{frpb}\ \text{(Compression Failure)}$$

The minimum flexure reinforcement can be used for in the rest parts of the column strip

$\frac{\text{A}_{\text{frp}_{min}}}{m} = \max\left[0.0025 A_g, \frac{400\ A_g}{E_f}\right] = \max\left[(0.0025 \times (1000 \times 200), \frac{400 \times (200 \times 1000)}{64900}\right] = 1233 \frac{\text{mm}^2}{m}$

No. of bars /m = 1233/ 285 = 4.3 /m ∴ use 5 GFRP straight bars No.20 ($A_{f_{act}} = 5 \times 285 = 1425\ \text{mm}^2$)

$\text{S}_{\max} = 300\ \text{mm}$ $\qquad$ $\text{Spacing}/m = \frac{1000}{5} = 200\ \text{mm}$

Serviceability limit state

The stress in the FRP reinforcement must be checked against allowable service limit state stresses. The stress in the FRP reinforcement and crack width was checked according to CSA S806-12 as follows

Service moment due to sustained service loads

The fixed end moment (M_{FEM}) due to the sustained load

$(\text{M}_{\text{FEM}})_s = 0.0842\ w_s\ l_2\ l_1^2 = 0.0842 \times 8.2 \times 2.65 \times 5^2 = 45.74\ \text{kN.m}$

The service moment transferred to the interior column equals

$$\text{M}_\text{s} = \frac{1}{3}\left[45.74 \times \frac{56.97}{60.52}\right] = 14.35\ \text{kN}$$

Check maximum stress under service load according

$$f_{frp_s} = \frac{M_s}{A_{frp}\, j\, d_y} \leq 0.25\, f_{frpu}$$

where

$$\mathrm{M_s} = 14.35 \text{ kN.m}$$

$$\rho_{frp} = 0.00947\,, n_{frp} = \frac{E_f}{E_c} = \frac{64900}{26622} = 2.44$$

$$k = \sqrt{\left(\rho_{frp}\, n_{frp}\right)^2 + 2\,\rho_{frp} n_{frp}} - \rho_{frp} n_{frp}$$

$$k = \sqrt{(0.00947 \times 2.44)^2 + 2 \times 0.00947 \times 2.44} - 0.00947 \times 2.44 = 0.193$$

$$j = 1 - \frac{k}{3} = 1 - \frac{0.193}{3} = 0.936$$

$$\therefore f_{frp_s} = \frac{14.35 \text{ x } 10^6}{3 \times 285 \times 0.936 \times 150.5} = 119.14 \text{ MPa} \leq 0.25\, f_{frpu} = 333.5 \text{ MPa}$$

Check crack width parameter

$$\mathrm{z} = k_b \frac{E_s}{E_F} f_{frp_s} (d_c A)^{\frac{1}{3}} \not< 45000 \frac{\mathrm{N}}{\mathrm{mm}}$$

where

$$\mathrm{d_c} = 21 + 1.5(19) = 49.5 \text{ mm}$$

$$\mathrm{A} = \frac{2\,\mathrm{b}\,\mathrm{d_c}}{\text{No. of bars}} = \frac{2 \times 600 \times 49.5}{3} = 19800 \text{ mm}^2$$

$$\therefore \mathrm{z} = 1.2 \times \frac{200000}{64900} \times 119.14 \times (49.5 \times 19800)^{\frac{1}{3}} = 43764 \frac{\mathrm{N}}{\mathrm{mm}} < 45000 \frac{\mathrm{N}}{\mathrm{mm}} \quad ok \ldots.$$

Place one GFRP straight bar No.20 @200 mm in the banded width as well as in the rest of the connection.

1.3.4 Top Reinforcement

The top flexural reinforcement bars passing through the column core were provided to satisfy structural integrity requirement and connecting the slab to the column on all faces (CSA A23.3-14). Similarly, two longitudinal bottom bars passing through column core. This slightly changed the designed flexural reinforcement ratio and spacing in both orthogonal directions. The final rienforcement details of test connections without shear reinforcement are shown in Figure 3

(chapter 4). The flexural reinforcement ratios for test connections without shear reinforcement within banded widths in both directions can be calculated as follows

Average Bottom flexural reinforcement ratios

$$\rho_{frp_x} = \frac{A_{frp}}{d_x \text{ b}} = \frac{6 \times 285}{169.5 \times 900} = 0.0112 \qquad \rho_{frp_y} = \frac{A_{frp}}{d_y \text{ b}} = \frac{3 \times 285}{150.5 \times 600}$$

$$= 0.0095$$

$$\rho_{frp_{avg}} = \frac{0.0112 + 0.0095}{2} = 0.0104$$

Average Top flexural reinforcement ratios

$$\rho_{frp_x} = \frac{A_{frp}}{d_x \text{ b}} = \frac{2 \times 199}{171.05 \times 900} = 0.0026 \qquad \rho_{frp_y} = \frac{A_{frp}}{d_y \text{ b}} = \frac{2 \times 199}{155.15 \times 600} = 0.0043$$

$$\rho_{frp_{avg}} = \frac{0.0026 + 0.0043}{2} = 0.0034$$

1.3.5 Test Connections with Shear Reinforcement

The test connections with shear reinforcement were designed to have high amounts of flexural and transverse reinforcement such that punching-shear failure would be expected to occur prior flexural failure. That would allow for measuring the shear-strength contribution of the GFRP stirrups and for the shear-reinforcement system to achieve its maximum strength and deformation capacity. The flexural reinforcement ratio of slabs with shear reinforcement approximately increased by 50% than connections without shear reinforcement. The final rienforcement details of test connections without shear reinforcement are shown in Figure 5.3 (chapter 4). In addition, the shear stirrups enclosed the top and bottom flexural reinforcement and one longitudinal bar passed at each stirrup corner in test connections with shear reinforcement. That was to provide enough anchorage for the vertical branch of the stirrup and to be more effective. The flexural reinforcement ratios for test connections without shear reinforcement within banded widths in both directions were calculated as follows

Average Bottom flexural reinforcement ratios

$$\rho_{frp_x} = \frac{A_{frp}}{d_x \text{ b}} = \frac{8 \times 285}{169.5 \times 900} = 0.015 \qquad \rho_{frp_y} = \frac{A_{frp}}{d_y \text{ b}} = \frac{5 \times 285}{150.5 \times 600} = 0.016$$

$$\rho_{frp_{avg}} = \frac{0.015 + 0.016}{2} = 0.0155$$

Average Top flexural reinforcement ratios

$$\rho_{frp_x} = \frac{A_{frp}}{d_x \text{ b}} = \frac{4 \times 199}{171.05 \times 900} = 0.0052 \qquad \rho_{frp_y} = \frac{A_{frp}}{d_y \text{ b}} = \frac{4 \times 199}{186.95 \times 600} = 0.0071$$

$$\rho_{frp_{avg}} = \frac{0.0052 + 0.0071}{2} = 0.0062$$

1.4 Punching Shear Capacity Predictions

The following part outlines the calculation procedure used to predict the punching shear capacity predictions of specimens S-N-0.3 (steel specimen), G-N-0.3 (NSC specimen), G-H-0.3 (HSC connection), G-CS-1.75d (connection with shear stirrups). The punching shear capacity of the five additional connections were predicted using similar procedures in accordance with the type of connection. The punching-shear capacities of the tested edge slab-column connections without shear reinforcement were predicted using available equations in FRP codes and guides namely ACI 440.1R-15, CSA S806-12, and JSCE-97. The predictions from these equations were compared against the experimental results to evaluate their reliability in predicting punching shear capacity of tested connections. The critical shear section for slabs without shear reinforcement is located at *d*/2 from the column faces according to the previously mentioned FRP codes and guides (refer to Figure A.6 a). on the other hand, CSA S806-12 and ACI 440.1R-15 lack provisions for estimating the ultimate capacity of FRPRC two-way slabs with FRP shear reinforcement. The punching-shear capacities of the tested edge slab-column connections with shear reinforcement were predicted using the modified ACI 440.1R-15 and CSA S806-12 punching-shear equations as presented and discussed in chapter 4.

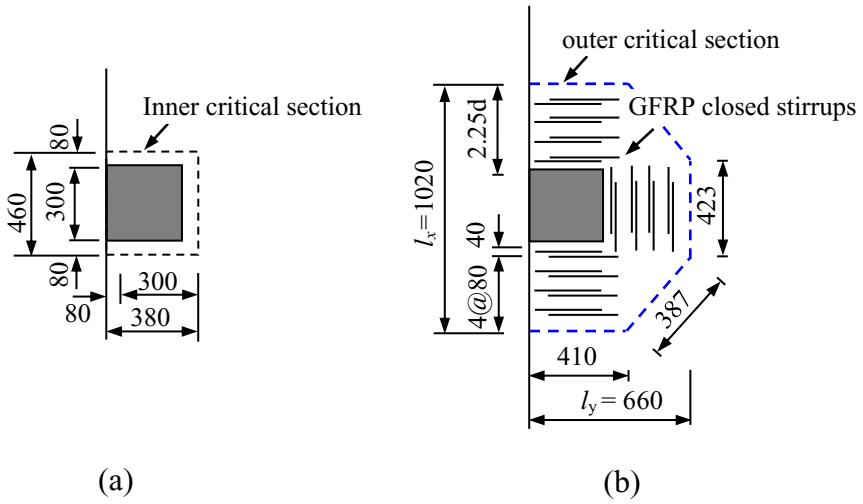

Figure A.6 – Critical section properties (a) Connections without shear stirrups (b) Connection G-CS-1.75d with shear stirrups

1.4.1. Connection S-N-0.3

1.4.1.1 Material and Critical Section Properties

- Concrete Properties
  - f_c' = 39.2 MPa λ = 1 ϕ_c = 1
- Reinforcement Properties
  - Bent and straight Steel Bars 20M (A_s = 300 mm^2; f_y = 460 MPa; E_s = 200 GPa; ε_y = 0.23)
  - Straight Steel Bars 15M (A_s = 198 mm^2; f_y = 440 MPa; E_s = 198 GPa; ε_y = 0.22)
  - E_{avg} = 200 GPa (Average elastic modulus in both orthogonal directions)
- Average Bottom flexural reinforcement ratios

$$\rho_{frp_x} = \frac{A_{frp}}{d_x\ \mathrm{b}} = \frac{6 \times 300}{170 \times 900} = 0.0118 \qquad \rho_{frp_y} = \frac{A_{frp}}{d_y\ \mathrm{b}} = \frac{3 \times 300}{150 \times 600} = 0.010$$

$$\rho_{frp_{avg}} = \frac{0.0118 + 0.01}{2} = 0.0109$$

- Average Top flexural reinforcement ratios

$$\rho_{frp_x} = \frac{A_{frp}}{d_x\ \mathrm{b}} = \frac{2 \times 200}{172 \times 900} = 0.00258 \qquad \rho_{frp_y} = \frac{A_{frp}}{d_y\ \mathrm{b}} = \frac{2 \times 200}{156 \times 600} = 0.00427$$

$$\rho_{frp_{avg}} = \frac{0.00258 + 0.00427}{2} = 0.0034$$

- Critical Section Properties
  - $d_{avg} = \frac{1}{2}\left(d_x + d_y\right) = \frac{1}{2}\,(170 + 150) = 160$ mm
  - $b_o = 2\,b_1 + b_2 = 2 \times (300 + 80) + (300 + 160) = 1220\ mm$
  - $C_{AB} = \frac{\Sigma\, A\, y}{A} = \frac{2(380 \times 160)(380/2)}{2(380 \times 160) + (460 \times 160)} = 118.36$ mm (Distance y is measured from AB)
  - (J_c) is the effective polar moment of inertia for the critical shear section like the polar moment of inertia. It is used to account for torsions and shears on the faces of the shear perimeter.

$$J_c = 2\left(\frac{d_{avg}\,{b_1}^3}{3} + \frac{b_1 d^3}{12}\right) - b_o\,d_{avg}\,{c_{AB}}^2$$

$$= 2\left(\frac{160 \text{ x } 380^3}{3} + \frac{380 \text{ x } 160^3}{12}\right) - 1220 \times 160 \times 118.36^2$$

$$= 3377822076.5 \text{ mm}^4$$

  - Fraction of moment transferred by shear $(\gamma_v) = 1 - \frac{1}{1 + \left(\frac{2}{3}\right)\sqrt{\frac{b_1}{b_2}}} = 1 - \frac{1}{1 + \left(\frac{2}{3}\right)\sqrt{\frac{380}{460}}} =$ 0.377
  - Moment-to-shear ratio about the centroid of the shear perimeter

$$\frac{M_0}{V_{test}} = \frac{M_u}{V_{test}} - \left[\frac{c_1}{2} - \left(c_{AB} - \frac{d}{2}\right)\right] = 300 - (150 - (118.36 - 80) = 188.36 \text{ mm}$$

$$\beta_c = \frac{\text{long side of the column}}{\text{short side of the column}} = \frac{300}{300} = 1$$

1.4.1.2 Punching Shear Capacity

- Punching shear stress from testing

$$v_{test} = V_{test}\left(\frac{1}{b_{o;0.5d}\ d} + \frac{\gamma_v\,(M_O/V_u)}{J_c}\ C_{AB}\right)$$

$$= 359.40 \times 10^3\left(\frac{1}{1220 \times 160} + \frac{0.377 \times 188.36}{3377822076.5} \times 118.36\right) = 2.73 \text{ MPa}$$

- CSA A23.3-14

The punching shear strength (v_c) was calculated based on the CSA A23.3-14. The punching shear strength (v_c) is the least value of the following equations

$$v_c = \text{min of} \begin{cases} \left(0.19 + \dfrac{\alpha_s\, d}{b_{o;0.5d}}\right) \lambda\, \phi_c \left(f_c^{'}\right)^{\frac{1}{2}} \\ 0.19 \left(1 + \dfrac{2}{\beta_c}\right) \lambda\, \phi_c \left(f_c^{'}\right)^{\frac{1}{2}} \\ 0.38\, \lambda\, \phi_c \left(f_c^{'}\right)^{\frac{1}{2}} \end{cases}$$

where α_s is a factor equals 4 for interior columns, 3 for edge columns, 2 for corner columns; $b_{o,0.5d}$ is the perimeter of the critical section for slabs at a distance $d/2$ from the column face (mm); and β_c the ratio of long side to short side of the concentrated load or reaction area.

$$v_c = \left(0.19 + \frac{\alpha_s\, d}{b_{o;0.5d}}\right) \lambda\, \phi_c \left(f_c^{'}\right)^{\frac{1}{2}} = \left(0.19 + \frac{3 \times 160}{1220}\right) \times 1 \times 1 \times (39.2)^{\frac{1}{2}} = 3.65 \text{ MPa}$$

$$v_c = 0.19 \left(1 + \frac{2}{\beta_c}\right) \lambda\, \phi_c \left(f_c^{'}\right)^{\frac{1}{2}} = 0.19 \left(1 + \frac{2}{1}\right) \times 1 \times 1 \times (39.2)^{\frac{1}{2}} = 3.57 \text{ MPa}$$

$$v_c = 0.38\, \lambda\, \phi_c \left(f_c^{'}\right)^{\frac{1}{2}} = 0.38 \times 1 \times 1 \times (39.2)^{\frac{1}{2}} = 2.38 \text{ MPa} \ldots \text{(governs)}$$

$$V_{pred} = \frac{v_c}{\left(\dfrac{1}{b_{o;0.5d}\, d} + \dfrac{\gamma_v\, (M_O/V_u)}{J_c}\, C_{AB}\right)} = \frac{2.38 \times 10^{-3}}{\left(\dfrac{1}{1220 \times 160} + \dfrac{0.377 \times 188.36}{3377822076.5} \times 118.36\right)}$$

$$= 312.69 \text{ kN}$$

$$V_{test} \,/\, V_{pred} = 359.40/312.69 = 1.14$$

- ACI 318-14

The punching-shear strength provided by concrete (v_c) for two-way slabs reinforced with steel bars was calculated based based on the ACI 318-14. The punching shear strength (v_c) is the least value of the following equations

$$v_c = \text{min of} \begin{cases} 0.083\left(2 + \dfrac{\alpha_s\, d}{b_{o;0.5d}}\right)\lambda\,(f_c')^{\frac{1}{2}} \\ 0.083\left(2 + \dfrac{4}{\beta_c}\right)\lambda\,(f_c')^{\frac{1}{2}} \\ 0.32\,\lambda\,(f_c')^{\frac{1}{2}} \end{cases}$$

where α_s is a factor equals 40 for interior columns, 30 for edge columns, 20 for corner columns

$$v_c = 0.083\left(2 + \frac{\alpha_s\, d}{b_{o;0.5d}}\right)\lambda\,(f_c')^{\frac{1}{2}} = 0.083\left(2 + \frac{30\times160}{1220}\right)\times 1 \times (39.2)^{\frac{1}{2}} = 3.08 \text{ MPa}$$

$$v_c = 0.083\left(2 + \frac{4}{\beta_c}\right)\lambda\,(f_c')^{\frac{1}{2}} = 0.083\left(2 + \frac{4}{1}\right)\times 1 \times (39.2)^{\frac{1}{2}} = 3.11 \text{ MPa}$$

$$v_c = 0.32\,\lambda\,(f_c')^{\frac{1}{2}} = 0.38 \times 1 \times (39.2)^{\frac{1}{2}} = 2 \text{ MPa ... (governs)}$$

$$V_{pred} = \frac{v_c}{\left(\dfrac{1}{b_{o;0.5d}\ d} + \dfrac{\gamma_v\,(M_O/V_u)}{J_c}\ C_{AB}\right)} = \frac{2\times10^{-3}}{\left(\dfrac{1}{1220\times160} + \dfrac{0.377\times188.36}{3377822076.5}\times118.36\right)}$$

$$= 262.77 \text{ kN}$$

$$V_{test}\ /\ V_{pred} = 359.40/262.77 = 1.37$$

- JSCE-97

According to JSCE-97, The punching shear strength (v_c) for steel and FRP-RC slabs was calculated as follows

$$v_c = \beta_d\,\beta_p\,\beta_r\,f_{pcd}/\gamma_b$$

where $\beta_d = (1000/d)^{0.25}; \beta_p = (100\rho_f E_f/E_S)^{\frac{1}{3}} \leq 1.5$ is a factor to consider the difference in the elastic modulus between FRP and steel; $\beta_r = 1 + 1/(1 + 0.25\,u_o/d); f_{pcd} = 0.2\sqrt{f_c'} \leq 1.2$; u_o is the perimeter of reaction area of supporting column; E_f is the elastic modulus of FRP tensile reinforcement; E_s is the elastic modulus of steel reinforcement (assumed to be 200 GPa); and ρ_f is average values for reinforcement ratio in both directions; γ_b is a partial factor of safety equal to 1.3 or 1.5 for concrete strengths below and above 50 MPa, respectively, that was set to 1.0 to get an un factored prediction of capacity; f_c' is cylinder concrete compressive strength (MPa), and d is the effective slab depth (mm).

$\beta_d = (1000/160)^{0.25} = 1.58 \leq 1.5 \rightarrow \beta_d = 1.5$

$\beta_p = (100 \times 0.0109 \times (200/200))^{\frac{1}{3}} = 1.03 \leq 1.5\ ok..$

$\beta_r = 1 + 1/(1 + 0.25\ (((2 \times 300) + 300)/160)\ ) = 1.42$

$f_{pcd} = 0.2\sqrt{39.2} = 1.25 \leq 1.2 \rightarrow f_{pcd} = 1.2$

$v_c = \beta_d\ \beta_p\ \beta_r\ f_{pcd}/\gamma_b = (1.5 \times 1.03 \times 1.42 \times 1.2)/1 = 2.63$ MPa

$$V_{pred} = \frac{v_c}{\left(\frac{1}{b_{o;0.5d}\ d} + \frac{\gamma_v\ (M_O/V_u)}{J_c}\ C_{AB}\right)} = \frac{1.73 \times 10^{-3}}{\left(\frac{1}{1220 \times 160} + \frac{0.377 \times 188.36}{3377822076.5} \times 118.36\right)}$$

$= 345.54$ kN

$V_{test}\ /\ V_{pred} = 359.40/345.54 = 1.04$

1.4.2. Connection G-N-0.3

1.4.2.1 Material and Critical Section Properties

- Concrete Properties
  - f_c' = 37.1 MPa λ = 1 ϕ_c = 1
- Critical Section Properties

All test connections had the same column dimensions and effective depth. Hence, the critical section properties are the same. However, the *M/V* ratio at the centroid of the critical section (M_o/V) is different because the test connections subjected to different *M/V* ratios of 0.3 and 0.6 m.

- $d_{avg} = \frac{1}{2}\left(d_x + d_y\right) = \frac{1}{2}\ (169.5 + 150.5) = 160$ mm
- $b_o = 2\ b_1 + b_2 = 2 \times 380 + 460 = 1220\ mm$
- $C_{AB} = \frac{\Sigma\ A\ y}{A} = \frac{2(380 \times 160)(380\ /2)}{2(380 \times 160) + (460 \times 160)} = 118.36$ mm
- $J_c = 2\left(\frac{d_{avg}\ {b_1}^3}{3} + \frac{b_1 d^3}{12}\right) - b_o\ d_{avg}\ {c_{AB}}^2$

$$= 2\left(\frac{160 \text{ x } 380^3}{3} + \frac{380 \text{ x } 160^3}{12}\right) - 1220 \times 160 \times 118.36^2$$

$$= 3377822076.5 \text{ mm}^4$$

- Fraction of moment transferred by shear $(\gamma_v) = 1 - \frac{1}{1+\left(\frac{2}{3}\right)\sqrt{\frac{b_1}{b_2}}} = 1 - \frac{1}{1+\left(\frac{2}{3}\right)\sqrt{\frac{380}{460}}} =$ 0.377
- $\frac{M_0}{V_{test}} = \frac{M_{test}}{V_{test}} - \left[\frac{c_1}{2} - \left(c_{AB} - \frac{d}{2}\right)\right] = 300 - (150 - (118.36 - 80) = 188.36$ mm

- Reinforcement Properties
  - GFRP Bent Bars N0.20 (A_f = 285 mm^2; f_{frpu} =1210 MPa; E_{frp} = 53 GPa; ε_{frpu} = 0.0228)
  - GFRP Straight Bars No.20 (A_f = 285 mm^2; f_{frpu} =1334 MPa; E_{frp} = 64.9 GPa; ε_{frpu}= 0.0206)
  - $E_{avg} = \frac{E_{frp} \times b_2 + 2 \times E_{frp} \times b_1}{b_o} = \frac{53 \times 460 + 2 \times 64.9 \times 380}{1220} = 60.410$ GPa
  - $\rho_{frp_{avg}} = 0.0104$

1.4.2.2 Punching Shear Capacity

- Punching shear stress from testing

$$v_{test} = V_{test}\left(\frac{1}{b_{o;0.5d}\ d} + \frac{\gamma_v\ (M_O/V_u)}{J_c}\ C_{AB}\right)$$

$$= 259.86 \times 10^3\left(\frac{1}{1220 \times 160} + \frac{0.377 \times 188.36}{3377822076.5} \times 118.36\right) = 1.98 \text{ MPa}$$

- CSA S806-12

The punching shear strength (v_c) was calculated based on the CSA S806-12. The punching shear strength (v_c) is the least value of the following equations, which are essentially the CSA A23.3-14 equations with modifications to account for FRP bars instead of steel.

$$v_c = \text{min of} \begin{cases} 0.147\left(0.19 + \dfrac{\alpha_s\, d}{b_{o;0.5d}}\right)\lambda\, \phi_c \left(E_f\, \rho_f\, f_c^{'}\right)^{\frac{1}{3}} \\ 0.028\left(1 + \dfrac{2}{\beta_c}\right)\lambda\, \phi_c \left(E_f\, \rho_f f_c^{'}\right)^{\frac{1}{3}} \\ 0.056\, \lambda\, \phi_c \left(E_f\ \rho_f\, f_c^{'}\right)^{\frac{1}{3}} \end{cases}$$

where ρ_f is the FRP reinforcement ratio; α_s is a factor equals 4 for interior columns, 3 for edge columns, 2 for corner columns; $b_{o,0.5d}$ is the perimeter of the critical section for slabs at a distance $d/2$ from the column face (mm); and β_c the ratio of long side to short side of the concentrated load or reaction area.

$$v_c = 0.147\left(0.19 + \frac{3 \times 160}{1220}\right) \times 1 \times 1 \times (60410 \times 0.0104 \times 37.1)^{\frac{1}{3}} = 2.45\text{Mpa}$$

$$v_c = 0.028\left(1 + \frac{2}{1}\right) \times 1 \times 1 \times (60410 \times 0.0104 \times 37.1)^{\frac{1}{3}} = 2.4\ \text{MPa}$$

$$v_c = 0.056 \times 1 \times 1 \times (60410 \times 0.0104 \times 37.1)^{\frac{1}{3}} = 1.6\ \text{MPa} \ldots (\text{governs})$$

$$V_{pred} = \frac{v_c}{\left(\dfrac{1}{b_{o;0.5d}\ d} + \dfrac{\gamma_v\ (M_O/V_u)}{J_c}\ C_{AB}\right)} = \frac{1.6 \times 10^{-3}}{\left(\dfrac{1}{1220 \times 160} + \dfrac{0.377 \times 188.36}{3377822076.5} \times 118.36\right)}$$

$$= 210.11\ \text{kN}$$

$$V_{test}\ /\ V_{pred} = 259.86/210.11 = 1.24$$

- ACI 440.1R-15

The punching-shear stress provided by concrete (v_c) for two-way slabs reinforced with FRP bars or grids is simply the ACI 318-14. The shear strength (v_c) equation for steel modified by the factor ([5/2] k) accounts for the axial stiffness of the FRP reinforcement through the neutral-axis-depth term (kd). The punching shear strength (v_c) was calculated based on the ACI 440.1R-15 as follows

$$v_c = \frac{4}{5}\, k\, \sqrt{f_c'}$$

where: $k = \sqrt{2\rho_f\, n_f + (\rho_f\, n_f)^2} - \rho_f n_f$; n_f is the modular ratio (E_f/E_C) ; $E_f = 4700\sqrt{f_c'}$

$$n_f = 60410/4700\ \sqrt{37.1} = 2.11$$

$$k = \sqrt{2 \times 0.0104 \times 2.11 + (0.0104 \times 2.11)^2} - 0.0104 \times 2.11 = 0.189$$

$$v_c = \frac{4}{5} \times 0.189 \times \sqrt{37.1} = 0.92\ \text{MPa}$$

$$V_{pred} = \frac{v_c}{\left(\frac{1}{b_{o;0.5d}\ d} + \frac{\gamma_v\ (M_O/V_u)}{J_c}\ C_{AB}\right)} = \frac{0.92 \times 10^{-3}}{\left(\frac{1}{1220 \times 160} + \frac{0.377 \times 188.36}{3377822076.5} \times 118.36\right)}$$

$$= 120.78 \text{ kN}$$

$$V_{test}\ /\ V_{pred} = 259.86/120.78 = 2.15$$

- JSCE -97

$$v_c = \beta_d\ \beta_p\ \beta_r\ f_{pcd}/\gamma_b$$

$$\beta_d = (1000/160)^{0.25} = 1.58 \leq 1.5 \rightarrow \beta_d = 1.5$$

$$\beta_p = (100 \times 0.0104 \times (60.410/200))^{\frac{1}{3}} = 0.68 \leq 1.5\ ok..$$

$$\beta_r = 1 + \frac{1}{1 + 0.25\ \left(\frac{(2 \times 300) + 300}{160}\right)} = 1.42$$

$$f_{pcd} = 0.2\sqrt{37.1} = 1.22 \leq 1.2 \rightarrow f_{pcd} = 1.2$$

$$v_c = (1.5 \times 0.68 \times 1.42 \times 1.2)/1 = 1.73 \text{ MPa}$$

$$V_{pred} = \frac{v_c}{\left(\frac{1}{b_{o;0.5d}\ d} + \frac{\gamma_v\ (M_O/V_u)}{J_c}\ C_{AB}\right)} = \frac{1.73 \times 10^{-3}}{\left(\frac{1}{1220 \times 160} + \frac{0.377 \times 188.36}{3377822076.5} \times 118.36\right)}$$

$$= 227.52 \text{ kN}$$

$$V_{test}\ /\ V_{pred} = 259.86/227.52 = 1.14$$

1.4.3. Connection G-H-0.3

1.4.3.1 Material and Critical Section Properties

- Concrete Properties
  - f_c' = 85.8 MPa λ = 1 ϕ_c= 1
- Critical Section Properties

  $d_{avg} = 160$ mm
  - $b_o = 2\ b_1 + b_2 = 1220\ mm$
  - $C_{AB} = \frac{\Sigma\ A\ y}{A} = 118.36$ mm
  - $J_c = 2\left(\frac{d_{avg}\ {b_1}^3}{3} + \frac{b_1 d^3}{12}\right) - b_o\ d_{avg}\ {c_{AB}}^2 = 3377822076.5$ mm^4

- Fraction of moment transferred by shear $(\gamma_v) = 1 - \frac{1}{1+\left(\frac{2}{3}\right)\sqrt{\frac{b_1}{b_2}}} = 0.377$
- $\frac{M_0}{V_{test}} = \frac{M_{test}}{V_{test}} - \left[\frac{c_1}{2} - \left(c_{AB} - \frac{d}{2}\right)\right] = 300 - (150 - (118.36 - 80) = 188.36$ mm

- Reinforcement Properties
  - GFRP Bent Bars N0.20 (A_f = 285 mm^2; f_{frpu} =1210 MPa; E_{frp} = 53 GPa; ε_{frpu} = 0.0228)
  - GFRP Straight Bars No.20 (A_f = 285 mm^2; f_{frpu} =1334 MPa; E_{frp} = 64.9 GPa; ε_{frpu}= 0.0206)
  - $E_{avg} = 60.410$ GPa $\quad \rho_{frp_{avg}} = 0.0104$

1.4.3.2 Punching Shear Capacity

- Punching shear stress from testing

$$v_{test} = V_{test}\left(\frac{1}{b_{o;0.5d}\ d} + \frac{\gamma_v\ (M_O/V_u)}{J_c}\ C_{AB}\right)$$

$$= 305.5 \times 10^3\left(\frac{1}{1220 \times 160} + \frac{0.377 \times 188.36}{3377822076.5} \times 118.36\right) = 2.33 \text{ MPa}$$

- CSA S806-12

$$v_c = \text{min of} \begin{cases} 0.147\left(0.19 + \frac{\alpha_s\ d}{b_{o;0.5d}}\right)\lambda\ \phi_c\left(E_f\ \rho_f\ f_c^{'}\right)^{\frac{1}{3}} \\ 0.028\left(1 + \frac{2}{\beta_c}\right)\lambda\ \phi_c\left(E_f\ \rho_f f_c^{'}\right)^{\frac{1}{3}} \\ 0.056\ \lambda\ \phi_c\left(E_f\ \ \rho_f\ f_c^{'}\right)^{\frac{1}{3}} \end{cases}$$

$$v_c = 0.147\left(0.19 + \frac{3 \times 160}{1220}\right) \times 1\ \times\ 1\ \times (60410 \times 0.0104 \times 60\ )^{\frac{1}{3}} = 2.88 \text{ MPa}$$

$$v_c = 0.028\left(1 + \frac{2}{1}\right) \times 1 \times 1 \times (60410 \times 0.0104 \times 60\ )^{\frac{1}{3}} = 2.82 \text{ MPa}$$

$$v_c = 0.056 \times 1 \times 1 \times (60410 \times 0.0104 \times 60\ )^{\frac{1}{3}} = 1.88 \text{ MPa ... (governs)}$$

$$V_{pred} = \frac{v_c}{\left(\frac{1}{b_{o;0.5d}\ d} + \frac{\gamma_v\ (M_O/V_u)}{J_c}\ C_{AB}\right)} = \frac{1.88 \times 10^{-3}}{\left(\frac{1}{1220 \times 160} + \frac{0.377 \times 188.36}{3377822076.5} \times 118.36\right)}$$

$$= 246.63 \text{ kN}$$

$$V_{test}\ /\ V_{pred} = 305.5/246.63 = 1.24$$

- ACI 440.1R-15

$$v_c = \frac{4}{5}\, k\, \sqrt{f_c'}$$

where: $k = \sqrt{2\rho_f\, n_f + (\rho_f\, n_f)^2} - \rho_f n_f$; n_f is the modular ratio (E_f/E_C) ; $E_f = 4700\sqrt{f_c'}$

$$n_f = 60410/4700\,\sqrt{85.8} = 1.39$$

$$k = \sqrt{2 \times 0.0104 \times 1.39 + (0.0104 \times 1.39)^2} - 0.0104 \times 1.39 = 0.156$$

$$v_c = \frac{4}{5} \times 0.156 \times \sqrt{85.8} = 1.16 \text{ MPa}$$

$$V_{pred} = \frac{v_c}{\left(\frac{1}{b_{o;0.5d}\, d} + \frac{\gamma_v\, (M_O/V_u)}{J_c}\, C_{AB}\right)} = \frac{1.16 \times 10^{-3}}{\left(\frac{1}{1220 \times 160} + \frac{0.377 \times 188.36}{3377822076.5} \times 118.36\right)}$$

$$= 151.91 \text{ kN}$$

$$V_{test}\,/\,V_{pred} = 305.5/151.91 = 2.01$$

- JSCE-97

$$v_c = \beta_d\, \beta_p\, \beta_r\, f_{pcd}/\gamma_b$$

$$\beta_d = (1000/d)^{0.25} = (1000/160)^{0.25} = 1.58 \le 1.5 \;\rightarrow\; \beta_d = 1.5$$

$$\beta_p = (100\rho_f E_f/E_S)^{\frac{1}{3}} = (100 \times 0.0104 \times (60.410/200))^{\frac{1}{3}} = 0.68 \le 1.5\; ok..$$

$$\beta_r = 1 + 1/(1 + 0.25\, u_o/d) = 1 + \frac{1}{1 + 0.25\,\left(\frac{(2 \times 300) + 300}{160}\right)} = 1.42$$

$$f_{pcd} = 0.2\sqrt{f_c'} = 0.2\sqrt{85.8} = 1.85 \le 1.2 \;\rightarrow f_{pcd} = 1.2$$

$$v_c = \beta_d\, \beta_p\, \beta_r\, f_{pcd}/\gamma_b = (1.5 \times 0.68 \times 1.42 \times 1.2)/1 = 1.73 \text{ MPa}$$

$$V_{pred} = \frac{v_c}{\left(\frac{1}{b_{o;0.5d}\, d} + \frac{\gamma_v\, (M_O/V_u)}{J_c}\, C_{AB}\right)} = \frac{1.73 \times 10^{-3}}{\left(\frac{1}{1220 \times 160} + \frac{0.377 \times 188.36}{3377822076.5} \times 118.36\right)}$$

$$= 227.51 \text{ kN}$$

$$V_{test}\,/\,V_{pred} = 305.5/227.51 = 1.34$$

1.4.4. Connection G-CS-1.75d

1.4.4.1 Material and Critical Section Properties

- Concrete Properties
  - f_c' = 47.6 MPa λ = 1 ϕ_c = 1

Critical Section Properties

The critical shear section should be checked located at *d*/2 from the column faces and at d/2 from the outermost shear reinforcement (2.25d from the column faces) inside and outside the shear-reinforced zone, respectively.

Critical Section Properties at d/2 from the column faces

- $d_{avg} = 160$ mm
- $b_o = 2\,b_1 + b_2 = 1220\,mm$
- $C_{AB} = \frac{\Sigma\, A\, y}{A} = 118.36$ mm
- $J_c = 2\left(\frac{d_{avg}\, {b_1}^3}{3} + \frac{b_1 d^3}{12}\right) - b_o\, d_{avg}\, {c_{AB}}^2 = 3377822076.5$ mm^4
- Fraction of moment transferred by shear $(\gamma_v) = 1 - \frac{1}{1+\left(\frac{2}{3}\right)\sqrt{\frac{b_1}{b_2}}} = 0.377$
- $\frac{M_0}{V_{test}} = \frac{M_{test}}{V_{test}} - \left[\frac{c_1}{2} - \left(c_{AB} - \frac{d}{2}\right)\right] = 310 - (150 - (118.36 - 80) = 198.36$ mm

Critical Section Properties at 2.25d from the column faces

The properties of the outer critical shear perimeter cannot be calculated using the expressions for the critical shear perimeter shown in Figure A.6. The properties of the outer critical shear perimeter were calculated based on the expressions developed El-gabry and Ghali (1996) for such sections as follows

- Perimeter of the outer critical section
  Lengths of shear perimeter sides $l_1 = 410$ mm , $l_2 = 387$ mm, $l_3 = 423$ mm
  $b_o = 2(l_1 + l_2) + l_3 = 2(410 + 387) + 423 = 2017$ mm
- Centroid of the outer critical section (*x*)

$$x = \frac{2\left[l_1\left(l_x - \frac{l_1}{2}\right) + l_2\frac{(l_x - l_1)}{2}\right]}{b_o}$$

$$= \frac{2\left[410\left(660 - \frac{410}{2}\right) + 387\frac{(660 - 410)}{2}\right]}{2015} = 232.94\text{mm}$$

- Polar moment of inertia of the outer critical section

$$J_c = d\left[l_3 x^2 + \frac{{l_1}^3}{6} + 2l_1(l_x - 0.5l_1 - x)^2 + \frac{l_2(l_x - l_1)^2}{6} + 2l_2\left(x - \frac{l_x - l_1}{2}\right)^2\right]$$

$$J_c = 160\left[423 \times 232.94^2 + \frac{412^3}{6} + 2 \times 410\,(660 - 0.5 \times 410 - 232.94)^2 + \right.$$

$$\left.\frac{387(660-410)^2}{6} + 2 \times 387 \times \left(232.94 - \frac{660-410}{2}\right)^2\right] = 14032318151\text{mm}^4$$

- Fraction of moment transferred by shear at the centroid of the outer critical section

$$(\gamma_v) = 1 - \frac{1}{1 + \left(\frac{2}{3}\right)\sqrt{\frac{l_x}{l_y} - 0.2}} = 1 - \frac{1}{1 + \left(\frac{2}{3}\right)\sqrt{\frac{660}{1020} - 0.2}} = 0.31$$

- $\frac{\mathrm{M}_0}{V_{test}} = \frac{M_{test}}{V_{test}} - \left[l_x - x - \frac{\mathrm{c}_1}{2}\right] = 310 - (660 - 232.94 - 150) = 32.94$ mm

- <u>Reinforcement Properties</u>
  - <u>GFRP Bent Bars N0.20</u> (A_f = 285 mm^2; f_{frpu} =1210 MPa; E_{frp} = 53 GPa; ε_{frpu} = 0.0228)
  - <u>GFRP Straight Bars No.20</u> (A_f = 285 mm^2; f_{frpu} =1334 MPa; E_{frp} = 64.9 GPa; ε_{frpu}= 0.0206)
  - $E_{avg} = 60.410$ GPa $\quad \rho_{frp_{avg}} = 0.0155$
  - <u>GFRP Closed stirrups No.10</u> (A_f = 71 mm^2; f_{frpu} = 967 MPa; E_{frp} = 45.7 GPa; ε_{frpu}= 0.0212)

1.4.4.2. Punching Shear Capacity

- <u>Punching shear stress from testing</u>

$$v_{test,in} = V_{test}\left(\frac{1}{b_{o;0.5d}\ d} + \frac{\gamma_v\,(M_o/V_u)}{J_c}\ C_{AB}\right)$$

$$= 370 \times 10^3\left(\frac{1}{1220 \times 160} + \frac{0.377 \times 198.36}{3377822076.5} \times 118.36\right) = 2.87\text{ MPa}$$

$$v_{test,out} = V_{test}\left(\frac{1}{b_{o;2.25d}\ d} + \frac{\gamma_v\ (M_o/V_u)}{J_c}\ x\right)$$

$$= 370 \times 10^3\left(\frac{1}{2015 \times 160} + \frac{0.31 \times 32.94}{14032318151} \times 232.94\right) = 1.21 \text{ MPa}$$

- Shear capacity using Modified code provisions

Within the shear reinforced zone, the factored shear strength, computed as (v_c + v_s), where vc and v_s are the summations of concrete and shear-reinforcement contributions to the shear strength inside the punching zone. To date, CSA S806-12 and ACI 440.1R-15 lack provisions for estimating the ultimate capacity of FRPRC two-way slabs with FRP shear reinforcement. Hence, the punching shear strength for connections with shear reinforcement was calculated based on the proposed design provisions which is extension to CSA S806-12 and ACI 440.1R-15 to account for FRP stirrups as shear reinforcement.

- Proposed design provisions for CSA S806-12

$$v_{c\ inside} = v_{c\ outside} = 0.028\lambda\phi_c\left(E_f\rho_f f_c'\right)^{\frac{1}{3}}$$

$$v_{fv} = \frac{\phi_f A_{fv}(0.005E_{fv})}{b_0 S_{fv}}$$

$$v_{in,pred.} = v_{c\ inside} + v_{fv} = 0.99 + 2 = 2.99 \text{ MPa} \quad , v_{out,pred.} = v_{c\ outside} = 0.99 \text{ MPa}$$

$$V_{in,pred.} = \frac{v_{in,pred.}}{\left(\frac{1}{b_{o;0.5d}\ d} + \frac{\gamma_v\ (M_o/V_u)}{J_c}\ C_{AB}\right)} = \frac{2.99 \times 10^{-3}}{\left(\frac{1}{1220 \times 160} + \frac{0.377 \times 198.36}{3377822076.5} \times 118.36\right)} = 386 \text{ kN}$$

$$V_{out,pred.} = \frac{v_{out,pred.}}{\left(\frac{1}{b_{o;2.25d}\ d} + \frac{\gamma_v\ (M_o/V_u)}{J_c}\ C_{AB}\right)} = \frac{0.99 \times 10^{-3}}{\left(\frac{1}{2015 \times 160} + \frac{0.31 \times 33.3}{14032318151} \times 233.29\right)}$$

$$= 303 \text{ kN}$$

$$V_{test}\ /\ V_{pred} = 370/303 = 1.22$$

The proposed provision for CSA S806-12 gave good predictions and expectations for failure localization within or outside the shear-reinforced zone with respect to the experimental test results for slabs with FRP stirrups as shear reinforcement.

- Proposed design provisions for ACI440.1R-15

$$v_{c\ inside} = v_{c_{outside}} = \frac{2}{5}k\sqrt{f_c'}$$

$$v_{fv} = \frac{\phi_f A_{fv}(0.004E_{fv})}{b_0 S_{fv}}$$

$$n_f = 60410/4700\sqrt{47.6} = 1.86$$

$$k = \sqrt{2 \times 0.0155 \times 1.86 + (0.0155 \times 1.86)^2} - 0.0155 \times 1.86 = 0.21$$

$$v_{c\,inside} = v_{c_{outside}} = \frac{2}{5} \times 0.21 \times \sqrt{47.6} = 0.59 \text{ MPa}$$

$$v_{fv} = \frac{1\times(12\times71)\times(0.004\times45700)}{1220\times80} = 1.6 \text{ MPa}$$

$$v_{in,pred.} = v_{c\,inside} + v_{fv} = 0.59 + 1.6 = 2.19 \text{ MPa} \quad , v_{out,pred.} = v_{c\,outside} = 0.588 \text{ MPa}$$

$$V_{in,pred.} = \frac{v_{in,pred.}}{\left(\frac{1}{b_{o;0.5d}\ d} + \frac{\gamma_v\ (M_o/V_u)}{J_c}\ C_{AB}\right)} = \frac{2.19 \times 10^{-3}}{\left(\frac{1}{1220 \times 160} + \frac{0.377 \times 198.36}{3377822076.5} \times 118.36\right)} = 282 \text{ kN}$$

$$V_{out,pred.} = \frac{v_{out,pred.}}{\left(\frac{1}{b_{o;2.25d}\ d} + \frac{\gamma_v\ (M_o/V_u)}{J_c}\ C_{AB}\right)} = \frac{0.59 \times 10^{-3}}{\left(\frac{1}{2015 \times 160} + \frac{0.31 \times 33.3}{14032318151} \times 233.29\right)}$$

$$= 180 \text{ kN}$$

$$V_{test} / V_{pred} = 370/180 = 2.06$$